PORT of vancouver | Vancouver Fraser Port Authority

Vessel Noise Correlation Study – Phase 2

ECHO Program Summary

This study was undertaken by the Vancouver Fraser Port Authority's Enhancing Cetacean Habitat and Observation (ECHO) Program, as an extension of the Vessel Noise Correlation Study completed in May 2020. The Phase 1 study (using data from 2015-2018) looked at the statistical correlations between vessel operational and design characteristics and vessel underwater radiated noise levels in order to assess the power of these parameters at predicting noise levels. In Phase 2, the study expanded to include data collected by the Boundary Pass underwater listening station between 2018-2020.

What questions was the study trying to answer?

Phase 2 of the vessel noise correlations study investigated the following questions within the three main tasks:

- **Task 1:** Does the Phase 1 model accurately predict underwater noise levels for new data, and does inclusion of additional data improve or alter the model?
- **Task 2:** Does more detailed operational and design data, obtained for a subset of vessels, explain additional variation in underwater radiated noise?
- **Task 3:** What is the variation in underwater radiated noise levels for multiple passes of the same vessel?

Who conducted the project?

To address these research questions, the Vancouver Fraser Port Authority retained a team led by JASCO Applied Sciences (Canada) Ltd., which included ERM, a consulting firm with technical expertise in statistical treatment of environmental data, and a noise control engineer from Acentech.

What methods were used?

The project used data from multiple sources to investigate correlations between vessel underwater radiated noise levels, design characteristics and operating conditions for six major commercial vessel categories: bulker/general cargo carriers, container ships; large passenger/cruise ships; tankers; tugboats; and vehicle carriers. The data sources used for the Phase 2 correlation analysis included, but was not limited to: underwater radiated noise levels from the ECHO Program database; general vessel characteristics from Lloyd's List Intelligence (LLI); actual vessel draft from the Pacific Pilotage Authority (PPA); Existing Vessel Design Index (EVDI) and greenhouse gas (GHG) emissions data from RightShip; and design and operational data from volunteer vessel operators.

- **Task 1:** The additional data were used to validate the statistical model developed in Phase 1. The statistical model was then updated using both the Phase 1 and Phase 2 datasets.
- **Task 2:** A number of vessel operators provided additional design and operational details (focusing on propeller data, shipboard machinery, vessel operational data and hull features) for 29 container ships and 72 bulkers. Statistical methods were used to test if the variability in underwater radiated noise that could not be accounted for in the Task 1 statistical model, could be improved with additional vessel design and operational data. Due to the small sample size and limited variability in key design characteristics, Task 2 results should be considered with caution.
- **Task 3:** Four vessels with a high number of repeat underwater radiated noise level measurements, ranging from 17 to 33 passes per vessel, were selected for detailed review of fine scale noise spectra and in-depth analysis of trends. An acoustic dual-band RPM (rotations per minute) analysis was also completed to add estimated RPM measurement to the data collected in Task 1 and 2.

What were the key findings?

- The statistical model developed in Phase 1 of this study showed a consistent ability to predict the underwater radiated noise levels from vessels captured in the Phase 2 data set.
- Similar to Phase 1, the updated Phase 2 statistical model was able to explain between 25% and 50% of the variance in the underwater radiated noise level measurements. The standard deviation of the variability, unexplained by the model was 5.1 dB averaged over vessel categories and frequency bands.
- Vessel speed over water and actual vessel draft remained the most influential predictors of vessel underwater radiated noise levels in all six vessel categories. Vessel RPM was also positively correlated to underwater noise emissions
- For bulkers and tankers, vessel age was related to underwater radiated noise levels (i.e. older vessels were louder) but was not a significant predictor for container ships, tugs, cruise vessels or vehicle carriers.
- In the Task 2 analysis, reduced underwater radiated noise levels were seen for bulkers that incorporated a rudder bulb, resiliently mounted generators, resiliently mounted engines, or roll stabilizing fins.
- Propeller blade count showed statistical correlations, but the results varied with frequency and vessel category. Other propeller data including pitch, skew, diameter, and rake, showed no correlation with vessel radiated noise levels for either bulkers or container ships included in the Task 2 analysis.
- For repeat passes of the same vessel, all vessels exhibited a positive trend of increasing underwater radiated noise levels with increased speed through water. Actual draft, cargo weight, slip ratio and drift angle were also found to be significantly correlated to vessel underwater radiated noise, although these relationships differed for each of the four vessels included in the detailed Task 3 analysis.
- Analysis of repeat measurements of the same vessel indicated that a single vessel could show significant variation in underwater radiated noise level (in this study between 2.9 and 6.0 dB at a 95% prediction interval), even under the same operational conditions.
- Narrow band spectrum analysis was able to identify tonal frequencies related to blade rate cavitation, engine firing rate and potential propeller singing as notable contributors to underwater radiated noise at low frequencies.
- The spectra of two of the four vessels selected for detailed analysis showed a significant hump, measured up to 30 dB above baseline estimates, between 160 Hz and 400 Hz. Analysis indicated that this was most likely due to singing propellers.

Conclusions and next steps

The updated Phase 2 statistical model confirmed that vessel size, speed through water, and vessel draft remain the strongest correlators to underwater radiated noise, and that propeller RPM may also be strong indicator. The updated statistical model provides an important tool for predicting underwater radiated noise levels by vessel category, using readily available vessel design and operational characteristics.

The variability of the model was such that 95% of vessel measurements included in the study exhibited underwater radiated noise levels that averaged within approximately 10 dB of the model prediction. The variability of underwater radiated noise levels for repeat passes of the same vessel, even under the same operating conditions was approximately 3 to 6 dB. These results highlight the challenges associated with precise measurement and prediction of vessel underwater radiated noise levels and indicate areas of further study to explain this variability.

Future phases of the vessel noise correlations study may seek to further investigate the variability in underwater radiated noise levels with detailed information of the vessel's real time operating conditions. Additionally, integration of vessel underwater radiated nose level datasets collected by others may be used to further test the predictive power of the updated statistical model.

ECHO Vessel Noise Correlations Phase 2 Study

Final Report

Submitted to:
Krista Trounce
Vancouver Fraser Port Authority ECHO Program
Contract: 19-0071(02)

Authors:
Alexander O. MacGillivray[1]
Joanna Zhao[2]
Michael A. Bahtiarian[3]
Joshua N. Dolman[1]
Jorge E. Quijano[1]
Héloïse Frouin-Mouy[1]
Laurie Ainsworth[2]

30 December 2020

P001475-002
Document 02283
Version 1.0

[1]JASCO Applied Sciences (Canada) Ltd
Suite 2305, 4464 Markham St.
Victoria, BC V8Z 7X8 Canada
Tel: +1-250-483-3300
Fax: +1-250-483-3301
www.jasco.com

[2]ERM Consultants Canada Ltd.
1111 West Hastings St.
Vancouver, BC V6E 2J3 Canada
Tel: +1-604-689-9460
Fax: +1-604-687-4277
www.erm.com

[3]Acentech
33 Moulton St.
Cambridge, MA 02138 USA
www.acentech.com

Suggested citation:

MacGillivray, A.O., J. Zhao, M.A. Bahtiarian, J.N. Dolman, J.E. Quijano, H. Frouin-Mouy, and L. Ainsworth. 2020. *ECHO Vessel Noise Correlations Phase 2 Study: Final Report*. Document 02283, Version 1.0. Technical report by JASCO Applied Sciences, ERM Consultants Canada, and Acentech for Vancouver Fraser Port Authority ECHO Program.

Disclaimer:

The results presented herein are relevant within the specific context described in this report. They could be misinterpreted if not considered in the light of all the information contained in this report. Accordingly, if information from this report is used in documents released to the public or to regulatory bodies, such documents must clearly cite the original report, which shall be made readily available to the recipients in integral and unedited form.

Contents

Figures

Tables

List of Annexes

Note: Annexes contain information that is confidential to the Vancouver Fraser Port Authority and its customers. They are not provided as publicly available documents.

1. Introduction

The objective of the Vessel Noise Correlation Study is to investigate how vessel design characteristics and operational parameters correlate with underwater radiated noise. This report covers Phase 2 of the study, which expands upon Phase 1 (MacGillivray et al. 2020), by performing statistical analysis of additional source level data collected at the Transport Canada Underwater Listening Station (ULS) in Boundary Pass. The Phase 1 study used statistical methods to investigate correlations of vessel noise with design characteristics and operational parameters, using the source level data sets collected between September 2015 and April 2018 in Strait of Georgia (on the ECHO ULS) and in Haro Strait (during the 2017 voluntary slowdown trial).

Phase 2 sought to use the Boundary Pass source level data set to validate statistical models developed during Phase 1 and to extend the analysis to investigate the effects of additional vessel design and operational parameters not considered in Phase 1. This research project was carried out jointly by JASCO Applied Sciences, ERM Consultants Canada, and Acentech for the Vancouver Fraser Port Authority's (VFPA's) Enhancing Cetacean Habitat and Observation (ECHO) Program.

Phase 2 of the project is split into the following three tasks:

- Task 1 (Section 2) involved using the Boundary Pass data set, from August 2018 to January 2020, to validate and improve upon the functional regression model that was developed during Phase 1 for predicting noise levels from vessel design characteristics and operational parameters. The new Boundary Pass data set consists of 6295 measurements of 2111 unique vessels, measured on acoustic hydrophone recorders deployed between the international shipping lanes.
- Task 2 (Section 3) involved analyzing source levels for a subset of vessels from the Phases 1 and 2 data sets, for which new information was available, to investigate noise correlations using additional design parameters not available during Phase 1. New design parameters were obtained from vessel operators by VFPA for 100 vessels, including bulkers, container ships, and general cargo vessels. New parameters included design details of the propellers and operational data from the vessel logs.
- Task 3 (Section 4) involved analyzing in detail the source level measurements of single vessels with many repeat passes. The objective of this analysis was to evaluate correlations of noise with operational parameters and to quantify variance of repeat measurements for ships of opportunity. This analysis studied four individual vessels all having many repeat measurements with high data quality. Analysis of narrowband vessel spectra (1 and 0.125 Hz resolution, provided by JASCO) was employed to identify individual component noise sources. Operational parameters considered in this analysis included speed through water, actual draft, drift angle, cargo load, and propeller RPM.

This report provides detailed methods, results, and conclusions for each of the three tasks.

1.1. Dataset Overview

This project utilized data from four different databases to investigate correlations between vessel noise emissions, design characteristics, and operating conditions (Figure 1). Additional data on selected vessels in the ECHO database were voluntarily provided by some vessel operators (see Sections 3 and 4). This research project was limited to commercial vessels in the following six categories:

- Bulker carriers and general cargo vessels,
- Container vessels,
- Cruise vessels (i.e., passenger vessels greater than 100 m length, excluding ferries)
- Tankers
- Tugs
- Vehicle carriers

Each measurement in the ECHO database was matched to records from the Lloyds List Intelligence (LLI), Existing Vessel Design Index (EVDI), and Pacific Pilotage Authority (PPA) databases based on the International Maritime Organization (IMO) number, whenever possible. The IMO number is a 7-digit code that uniquely identifies large cargo vessels (>300 gross tons) and large passenger vessels (>100 gross tons). In cases where a IMO number was unavailable, or was recorded incorrectly, records were instead matched on the basis of the vessel's Maritime Mobile Service Identity (MMSI) number or by vessel name. IMO numbers, MMSI numbers, and vessel names in the ECHO database were obtained from the Automated Information System (AIS), as broadcast at the time of measurement. Data from all four databases were merged into a single vessel noise database for subsequent analysis. Appendix A.1 provides descriptions of all the variables captured in the merged vessel noise databases from Phases 1 and 2.

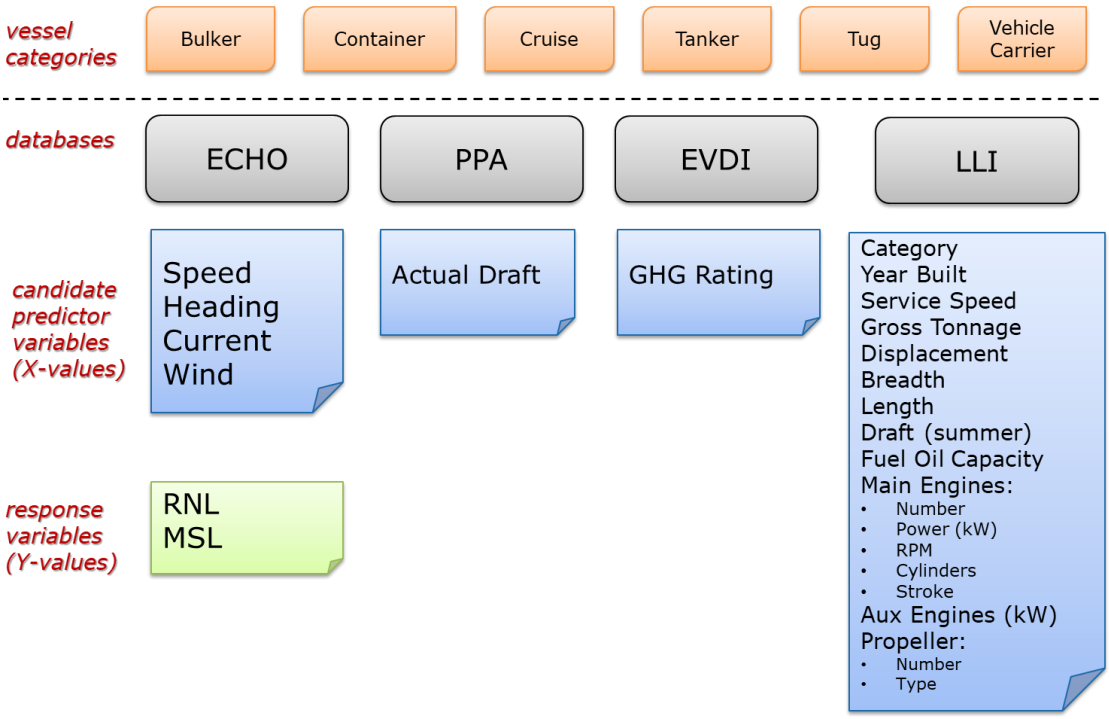

Figure 1. Diagram of databases utilized in the present study. Blue boxes contain predictors variables, and green box contains response variables. ECHO = Enhancing Cetacean Habitat and Observation Program vessel noise database includes the source level measurements and measurement conditions (including wind and currents). PPA = Pacific Pilotage Authority transit logs provide records of actual vessel draft at the time of transit, as recorded by on-duty pilots. EVDI = Existing Vessel Design Index database: contains greenhouse gas (GHG) emissions data and emissions ratings from RightShip. LLI = Lloyd's List Intelligence database: contains those vessel design characteristics identified by the ATC that were available from Lloyd's Register of Shipping.

1.2. Boundary Pass (Phase 2) Data Set: August 2018 to January 2020

Source level measurements for the Phase 2 study were collected on Autonomous Multichannel Acoustic Recorder (AMAR) systems deployed off the east coast of Saturna Island, at the location of the Transport Canada Underwater Listening Station (ULS) in Boundary Pass, but before the cabled station was installed (Figure 2). Source level data were analyzed using JASCO's ShipSound system and the data set included measurements of multiple commercial vessel types, identified through correlation of acoustic measurements to the automated identification system (AIS) (by Maritime Mobile Service Identity (MMSI) or International Maritime Organization (IMO) number).

The ECHO database includes each vessel's Radiated Noise Level (RNL)[1], Monopole Source Level (MSL), closest point of approach (CPA) to the station, speed, and other key parameters. Table 1 provides a summary of the numbers of accepted source level measurements from Boundary Pass during the study period. Throughout this report, the newer Boundary Pass measurements from August 2018 to January 2020 are referred to as the 'Phase 2' data set. The older Strait of Georgia ULS and Haro Strait slowdown trial measurements (September 2015 to April 2018) are referred to as the 'Phase 1' data set.

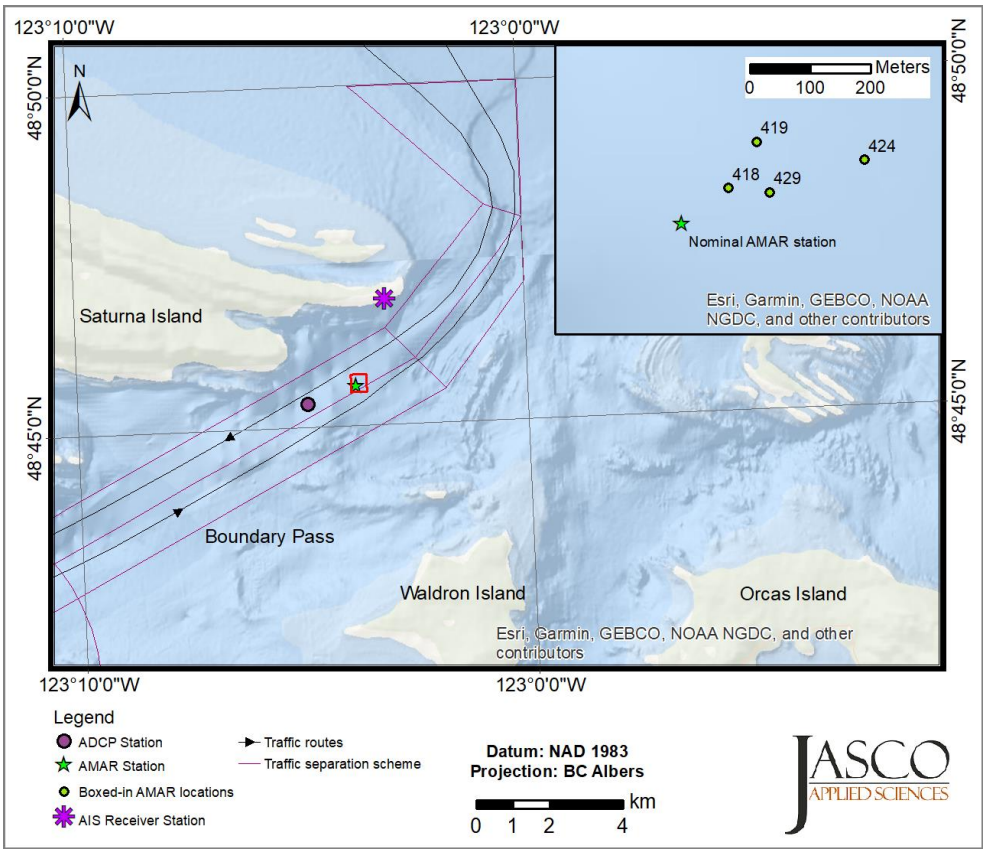

Figure 2. Location of the Boundary Pass hydrophone recorders and Acoustic Doppler Current Profiler (ADCP).

Table 1. Summary, by category, of vessel source level measurements collected in the Phase 2 data set (Boundary Pass) during the period August 2018 to January 2020.

Category	Accepted measurements	Unique vessels
Bulker & General cargo	3221	1436
Container	1591	257
Cruise	115	37
Tanker	329	140
Tug	496	77
Vehicle Carrier	543	164
Total	**6295**	**2111**

[1] RNL was measured approximately to ANSI S12.64 standard (ANSI/ASA S12.64/Part 1 2009).

2. Task 1: Functional Regression Model Validation

The objective of Task 1 was to use the Phase 2 (Boundary Pass) source level data set to first test, then update, the statistical model that was developed during the Phase 1 study. As in Phase 1, the intent was to use the ECHO source level database to identify those design and operational parameters that have the greatest influence on underwater radiated noise from marine shipping in six broad vessel categories. Statistical models developed under Task 1 reveal the broad trends of vessel source levels with design and operational parameters in the ECHO database.

2.1. Methods

2.1.1. Source Levels

Two types of vessel source levels are stored in the ECHO database: Radiated Noise Level (RNL) and Monopole Source Level (MSL). RNL is equal to the measured sound pressure level (SPL), scaled according to the distance between a sound source and the hydrophone (i.e., using the spherical spreading propagation method of $20 \times \mathrm{Log}_{10}(R)$). MSL is equal to the measured sound pressure level scaled according to a numerical acoustic propagation loss (PL) model that accounts for the effect of the local environment on sound propagation (i.e., sea-surface reflection, water column refraction and absorption, and bottom loss). RNL and MSL were previously calculated by ShipSound, which is the automated software system that is used on the ULS for measuring vessel source levels. The methods used by ShipSound for calculating vessel source levels are described in the Phase 1 report (MacGillivray et al. 2020). RNL and MSL measurements, in decidecade frequency bands, were available for the 10 to 63,000 Hz frequency range (Figure 3).

The source level calculation methods applied by ShipSound were identical between the Phase 1 and Phase 2 data sets, except in one respect: the method for calculating the monopole source depth changed following the second set of AMAR deployments, after March 2019. Prior to this date (and for the entirety of the Phase 1 data set), the source depth was calculated as 50% of the AIS draft. Following this date (and for most of the Phase 2 data set), the method for calculating the source depth was changed to 70% of the AIS draft, for consistency with the newly published ISO 17208-2:2019 measurement standard (ISO 2019). This systematic change in source depth could affect the correlation analysis, and so we applied a frequency-dependent adjustment to the Phase 2 MSL values to make them consistent with a source depth of 50% of actual draft for all measurements. The adjustment was based on formula A.19 from the ISO 17208-2:2019 ship noise measurement standard. It was not necessary to apply a similar adjustment to the RNL values because they are not dependent on source depth.

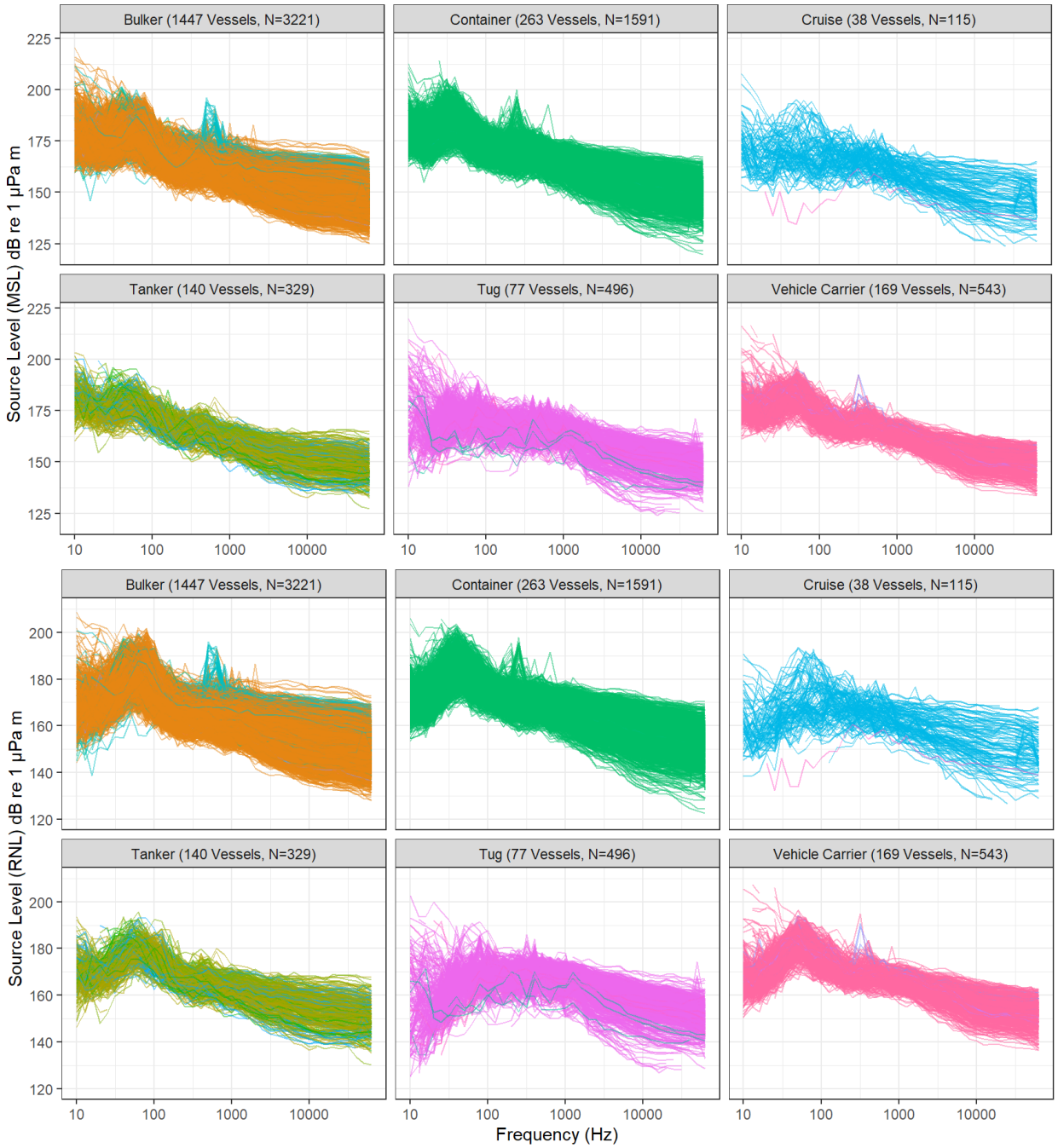

Figure 3. Plot of decidecade (top) Monopole Source Level (MSL) and (bottom) Radiated Noise Level (RNL) versus frequency from the Boundary Pass source level database (each profile represents a unique measurement). Different colour profiles reflect different vessel sub-types in the LLI database (i.e., according to VESSEL.TYPE.LLI). See Annex 1.

2.1.2. Data Conditioning

Each measurement in the Phase 2 data set was matched to records from the LLI, EVDI, and PPA databases, to obtain the same predictor variables for design and operational parameters used in the Phase 1 study (MacGillivray et al. 2020). This involved removing erroneous and duplicate records to correct misclassified vessels, and calculating derived quantities required for subsequent statistical analysis. A graphical analysis was carried out to explore relationships between source levels and predictors, and to identify outliers. Records from these databases were combined into a merged database (R data format) and spreadsheet (Excel format) for subsequent statistical analysis. The reader is referred to the Phase 1 report (MacGillivray et al. 2020) for a detailed description of the database merging procedure and the covariates employed for Task 1.

The merged database contained missing (NA) values where information for a specified predictor was unavailable in the LLI, PPA, or EVDI databases. The percentage of missing data was calculated for each of the candidate predictors, for each vessel category (Figure 4). Source levels were treated as missing (NA) when ShipSound determined that background noise levels were within 3 dB of received signal levels during a vessel measurement (Figure 5). Source levels for some cruise ships in the 16–50 kHz range were contaminated by sonar-like signals, which may originate from ultrasonic anti-fouling devices on these vessels (Angadi et al. 2020). Data in frequency bands affected by this issue were flagged as missing data (i.e., value set to NA), because these signals are unrelated to the general design characteristics of the vessels. Tugs had the most missing source level data, because they are generally smaller and quieter than the larger cargo vessels. Missingness was generally greatest at the lowest and highest frequencies for all vessel categories

Imputation was used to estimate missing data from known data values for similar measurements. Imputation is typically required when applying multi-variate statistical methods, because incomplete cases (i.e., measurements with missing data on at least one variable) may not otherwise be used. Imputation of the variables in the Phase 2 data set was carried out following the same methods described in the Phase 1 report (MacGillivray et al. 2020).

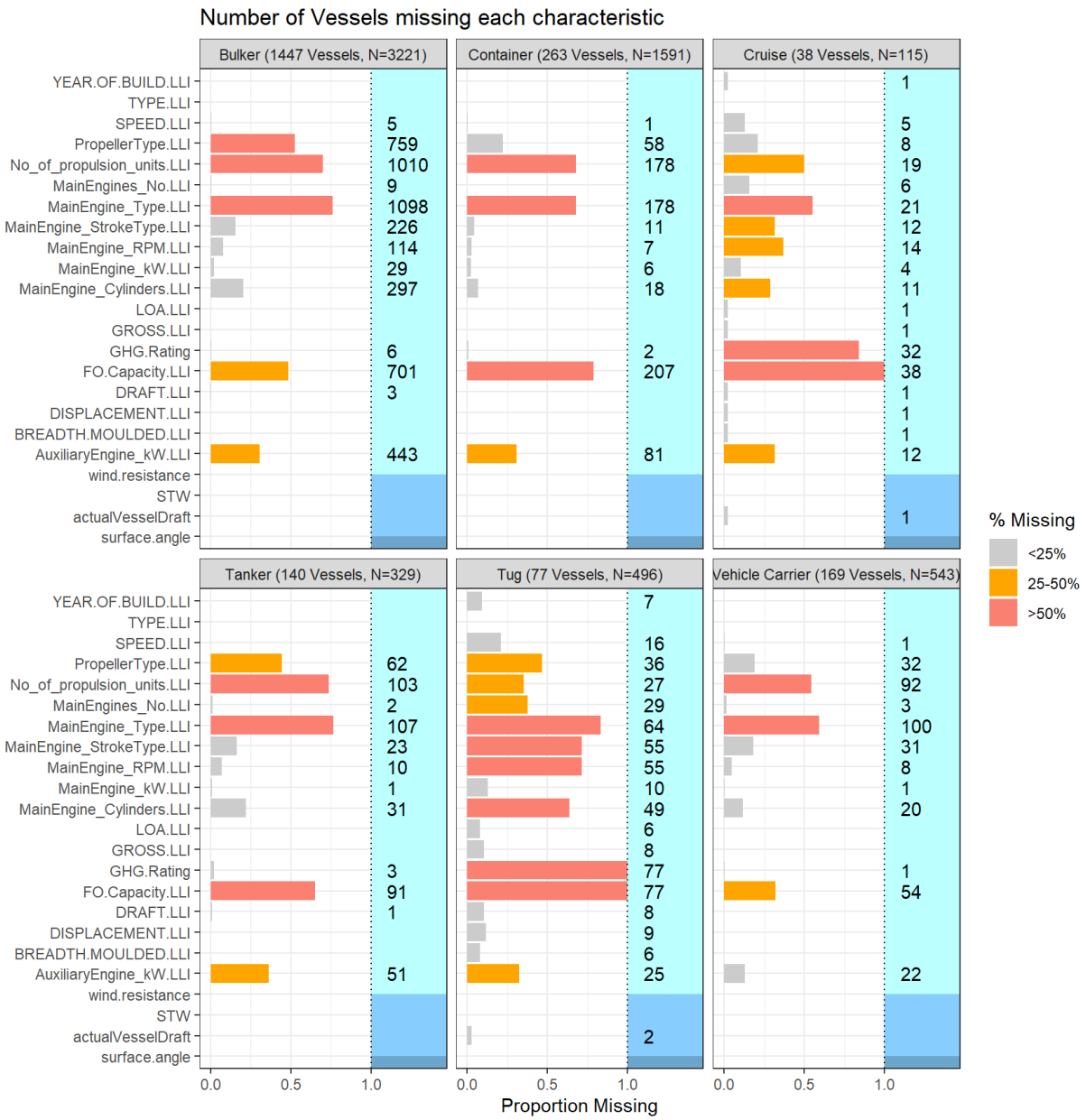

Figure 4. Missingness of predictor variables in the Phase 2 (Boundary Pass) data set, by vessel category. The horizontal bars indicate the fraction of missing data. The numbers to the right of the bars indicate the total number of missing values.

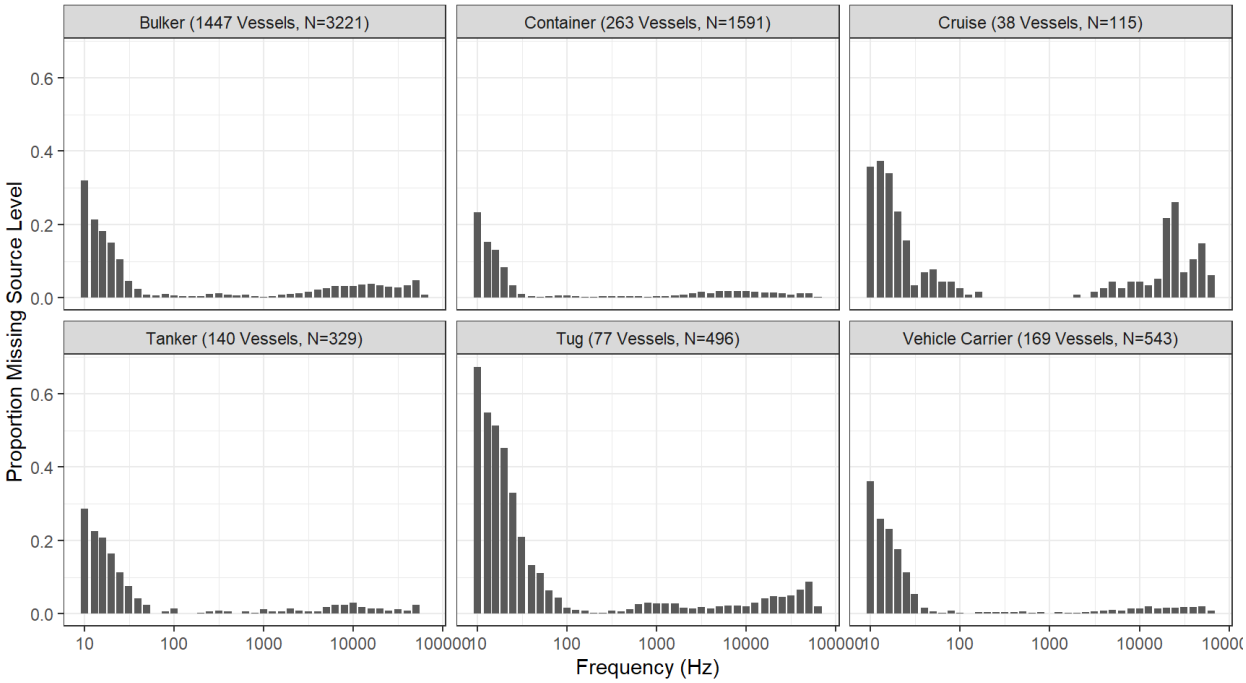

Figure 5. Missingness of Monopole Source Level (MSL) and Radiated Noise Level (RNL) data, in decidecade bands. Note that missingness of RNL and MSL data was identical because it was calculated from the same hydrophone measurements.

Many vessels in the Phase 2 data set had more than one measurement, with 90 vessels having 10 or more measurements (Figure 6). It was most common for vessels to be measured twice in the Phase 2 data set, due to the fact the Boundary Pass recorders captured vessels on both their inbound and outbound trips from the Port of Vancouver. In the Phase 1 data set, it was more common for vessels to be measured once, as the Strait of Georgia ULS only captured vessels on the inbound traffic lane. There appeared to be systematic differences in the loading conditions between inbound and outbound trips by some types of vessels (see Section 2.2.1). Thus, it is expected that the Phase 2 data set included a greater range of loading conditions for cargo vessels.

Repeat measurements are valuable when they capture the same vessel under different operating conditions but, when vessels are sampled unequally, repeat measurements can also introduce bias toward the most frequently sampled vessels. To balance these competing effects, repeat vessel measurements were randomly subsampled (without replacement) so that they were included only when operating conditions were substantially different. Subsampling was applied the Phase 2 data set following the same procedures described in the Phase 1 report (MacGillivray et al. 2020).

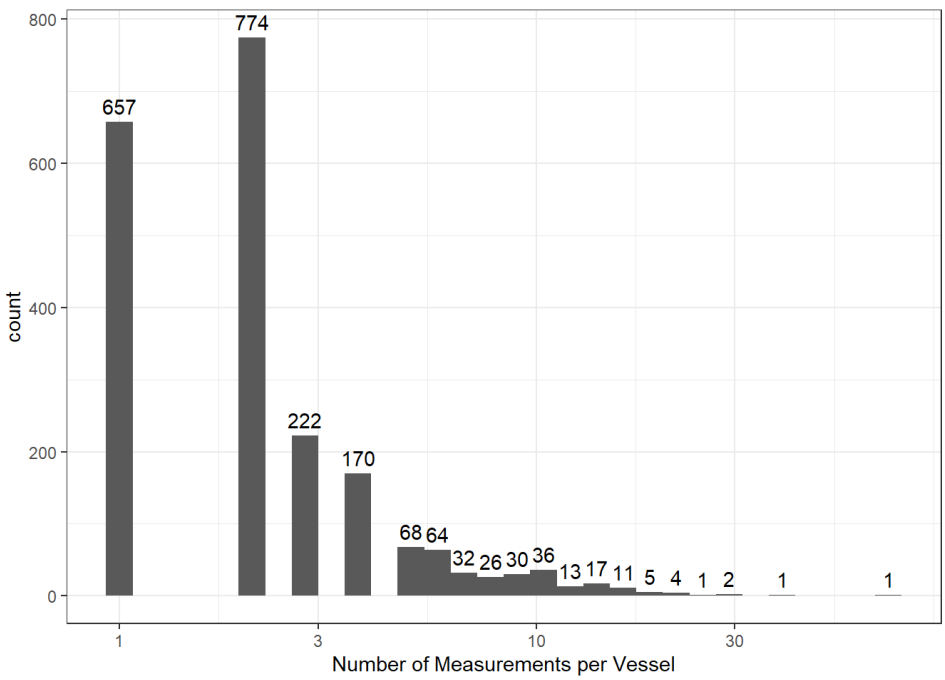

Figure 6. Histogram of number of repeat measurements per vessel for the Phase 2 data set (all categories).Physical models were used to capture the effect of water currents, wind, and source-receiver geometry on measured source levels. Meteorological data for Boundary Pass were obtained from the weather station at East Point lighthouse, approximately 3 km from the hydrophones (Environment Canada 2020). Ocean current data for the Boundary Pass data set were obtained from an Acoustic Current Doppler Profiler (ADCP) deployed 1.4 km from the hydrophones (Figure 2). Speed through water, wind resistance, and surface angle were calculated for each measurement following the same methods described in the Phase 1 report (MacGillivray et al. 2020). In addition, the lateral movement of each vessel due to wind and ocean currents (drift.angle) was calculated from the difference between the vessel heading and its course over ground (Figure 7). The new drift angle predictor was calculated for the Phases 1 and 2 data sets.

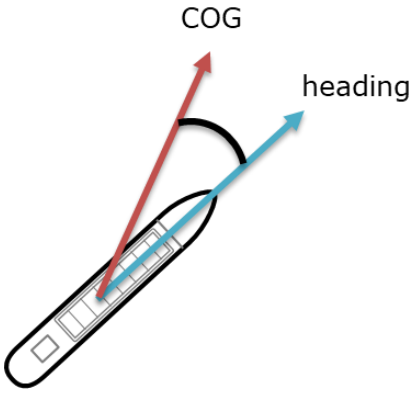

Figure 7. Calculation of drift angle from the difference of course over ground (COG) and vessel heading, as reported by Automated Identification System (AIS).

2.1.3. Exploratory Analysis

As in the Phase 1 study, bivariate scatter plots, density plots, and correlation matrix plots were used to investigate relationships between pairs of variables (source levels and predictors). To simplify exploratory analysis of the source level data, decade band source levels (RNL and MSL) were calculated for the following three frequency ranges:

- 10–100 Hz;
- 100–1000 Hz; and
- 1000–10,000 Hz.

Decade band source levels were calculated by summing the decidecade band RNL and MSL source factors inside these three frequency ranges (with appropriate weighting at the band edges where the decidecade bands partially overlapped two decade bands).

Histograms and density plots (smoothed histograms) were used to assess the distributions of numerical variables. Correlation matrix plots were created to show correlation coefficients between pairs of (numerical) variables. The correlation coefficient, r, is a dimensionless number, in the range $-1 < r < 1$, that indicates the strength of linear correlation between two variables. Positive r-values indicate a positive relationship between two parameters and negative r-values indicate a negative relationship between two parameters. Standard statistical thresholds for correlation values are as follows:

- Strong correlation: $|r| \geq 0.8$;
- Moderate correlation: $0.8 > |r| \geq 0.5$; and
- Weak correlation: $|r| \leq 0.5$.

When pairs of predictor variables are strongly correlated (i.e., when they are linearly dependent), it is often necessary to drop one of the predictors from a multiple regression model because the effects of those predictors cannot easily be separated from one another and may lead to numerical instability and inaccurate regression estimates. A correlation matrix analysis was used to identify correlated predictor variables and to determine which sets of independent predictors should be retained for the multiple-predictor statistical model.

2.1.4. Functional Regression Model Validation

Functional regression analysis is an extension of standard regression analysis. For each observation, the outcome variable value (or predictor variable values) can be a functional curve rather than a single number. This is a useful method for assessing source level data because it allows the simultaneous assessment of the relationship between predictor variables and noise emissions at all frequencies simultaneously. This approach avoids the need to run multiple regression analysis on noise levels separately for all the individual frequency bands. During the Phase 1 study, a multiple-predictor functional regression model was developed to analyze the statistical relationship between vessel design characteristics (as predictors) and vessel source levels (as outcome variables).

One of the main objectives of Phase 2 was to test the validity of the multiple-predictor functional regression model developed during the Phase 1 study. To test the model, a graphical analysis was first carried out to assess how the relationships between noise levels and vessel design characteristics differed between the Phase 1 and Phase 2 data sets. Next, the Phase 2 (Boundary Pass) design characteristics and operational parameters were fed into the Phase 1 model to see how well it reproduced the Phase 2 measurements. The prediction error was quantified by comparing distributions of the model residuals with the Phase 1 results. The residual analysis was used to assess how differences in vessel design characteristics and operating parameters impacted the model fit and to identify potential improvements to the model.

2.1.5. Functional Regression Model Update

As a last step, an updated functional regression model was developed, using the combined Phases 1 and 2 data sets as input. The validation task resulted in an updated functional regression model with the following modifications:

- The auxiliary engine power (AuxiliaryEngine_kW.LLI) was removed from the set of model predictors, due to inconsistencies in the way that this variable was reported by LLI (in the Phase 1 data set, this parameter was not reported but rather estimated based solely on gross tonnage and vessel type—see Section 2.2.3). In the updated functional regression model, the relationship between auxiliary engine power and radiated noise could not be investigated using the combined data sets.
- The vessel age at time of measurement (vessel_age) was added to the set of model predictors, to ascertain whether length of time in service was correlated with noise emissions. This was taken to be the whole-number difference between the year of build of the vessel (YEAR.OF.BUILD.LLI) and the year when the noise measurement was obtained.
- Combined vessel category groupings (Container & Vehicle Carrier, Bulker & Tanker) were split apart, and distinct models were created for each of the four individual vessel categories. The updated functional regression model was therefore applied to each category separately (each with frequency-dependent coefficients for MSL and RNL).

During development of the statistical models in the Phase 1 study, Containers were grouped with Vehicle Carriers and Bulkers were grouped with Tankers, based on commonalities in their design and source level characteristics. These groupings were selected using principal component analysis and expert knowledge regarding the design and operating conditions of these types of vessels. These categories were subsequently split in the present study, to see whether the increased sample size from Phase 2 could be used to resolve category-specific noise correlation trends.

In addition to these changes, the signal-to-noise ratio (SNR) threshold was increased for the Phase 2 data set only, at 25 Hz and below (50 Hz and below for tugs), to cull outlying measurements that were contaminated by current-induced flow noise. A review of the Phase 2 data indicated that the highly variable flow-noise contamination was responsible for some increased outliers at very low frequencies in the Boundary Pass measurements (see Section 2.2.3). To ameliorate this issue, MSL and RNL values in the 10–20 Hz bands were set to NA if they had SNR less than 8 dB (the ShipSound default is 3 dB, consistent with ANSI S12.64 and ISO 17208-1). This increased overall missingness in these bands from 23.1% to 37.4% but reduced the influence of outlying measurements at low frequencies on the functional regression model.

The functional regression model captures the effect of multiple predictors on frequency-dependent source levels. Results are summarized using the coefficient of determination (r^2) and frequency-dependent slope coefficient ($\beta(f)$, where f = frequency) between multiple predictors and decidecade source level measurements.

2.2. Results

2.2.1. Exploratory Analysis

A range of operational and measurement conditions were sampled for each vessel category in the Phase 2 data set (Figures 8 and 9). Compared to the Phase 1 data set, the distributions of speed through water (STW) values in the Container and Vehicle Carrier categories were narrower, due to the higher speed targets for the ECHO Program seasonal slowdown in Haro Strait and Boundary Pass for these categories in 2018 and 2019 (14.5 knots), as compared to Haro Strait in 2017 (11 knots). The distributions of the vessel drafts (actualVesselDraft) in the Bulker and Tanker categories appeared to be wider, and more heavily weighted toward deeper drafts, than in the Phase 1 data set. This is likely because more heavily-laden outbound vessels were sampled in these categories in Boundary Pass

(Figure 10). The ranges of operational conditions sampled in the Phase 2 data set were otherwise very similar to the Phase 1 data set.

Annex 1 provides detailed results of the exploratory analysis, including correlation plots and density plots for all vessel categories.

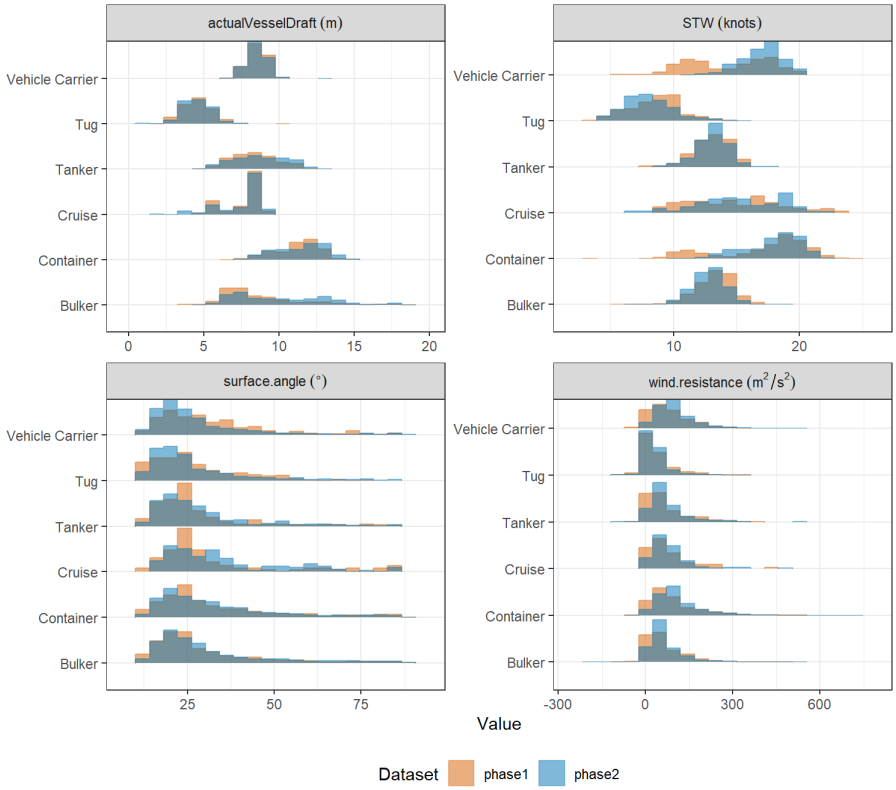

Figure 8. Histograms of operational variables for the Phases 1 and 2 data sets. The heights of the bars indicate the relative number of samples at each x value.

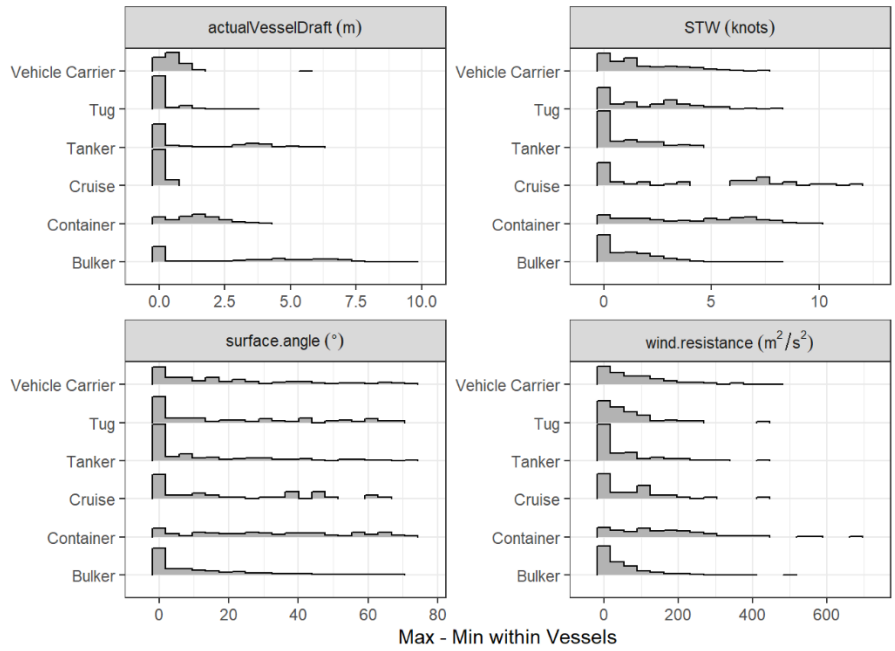

Figure 9. Histograms of the ranges (max-min) of operational variables for individual vessels for the Phase 2 data set.

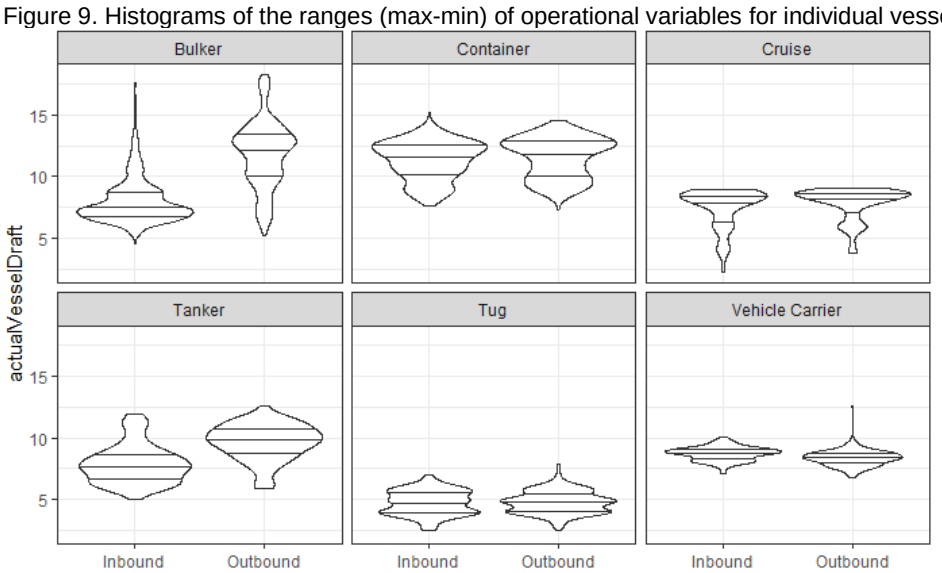

Figure 10. Violin plots comparing the drafts of inbound (heading <180) and outbound (heading ≥180) vessels in the Phase 2 (Boundary Pass) data set. The width of the swath shows the smoothed distribution of the data and the horizontal lines show the 25th, 50th, and 75th percentiles of the data. Outbound vessels have significantly greater drafts in the Bulker and Tanker categories.

Correlation matrix plots were used to identify strong correlations between pairs of variables (both predictors and decade-band source levels) in the Phase 2 data set. As in Phase 1, most variables were subjected to a logarithmic transformation before computing the correlation coefficient. The log-transformed variables were as follows:

- speed through water (STW);
- gross tonnage (GROSS.LLI);
- summer draft (DRAFT.LLI);
- length overall (LOA.LLI);

- design speed (SPEED.LLI);
- displacement (DISPLACEMENT.LLI);
- breadth (BREADTH.LLI);
- main engine power (MainEngine_kW.LLI); and
- main engine RPM (MainEngine_RPM.LLI).

The remaining variables were preserved in linear units for the correlation analysis. Figure 11 shows the correlation matrix for the Bulker category. The first three rows or columns of the correlation matrix can be used to visually identify correlations between RNL and the predictor variables. Subsequent rows and columns can be used to visually identify correlations between pairs of predictors. Larger circles with darker shading indicate strong positive or negative relationships and colour indicates the direction of the relationship, with blue positive and red negative. Appendix B.1 provides Phase 2 correlation matrix plots for all vessel categories.

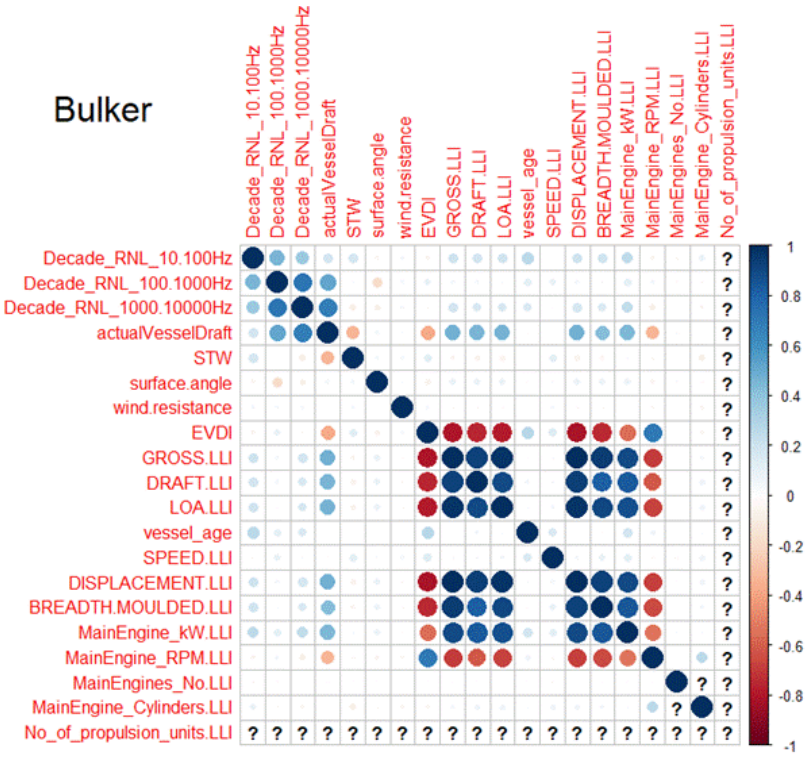

Figure 11. Correlation matrix plot, showing correlations between pairs of variables for the Bulker category, from the Phase 2 (Boundary Pass) data set. The size and colour of the circles indicate the strength and magnitude of the correlation (blue = positive, red = negative, correlations along the diagonal are r=1). The "?" indicates where the correlation cannot be computed between two variables (usually due to missing values, but sometimes due to a variable having a constant value).

2.2.2. Data Set Comparisons: Phase 1 versus Phase 2

A comparison of source level data from Phases 1 and 2 showed that vessel noise profiles from the two data sets were very similar, except that measured source levels for Containers and Vehicle Carriers were slightly higher, on average, in Phase 2. This difference is attributable to the higher average speed of these vessel categories in Boundary Pass, primarily due to the following reasons:

1. During the ECHO Program seasonal slowdown, speed targets for Containers and Vehicle Carriers were increased in 2018-2019, as discussed in previous section.

2. Vehicle carriers transit more slowly in the Strait of Georgia (Phase 1 data set), where they generally start to reduce speed before their turn into the Fraser River navigation channels (see, e.g., Figure 67 in JASCO Applied Sciences and SMRU Consulting (2020)).

Speed is the most influential factor determining vessel source levels, as demonstrated during Phase 1, hence the observed differences in the mean source levels.

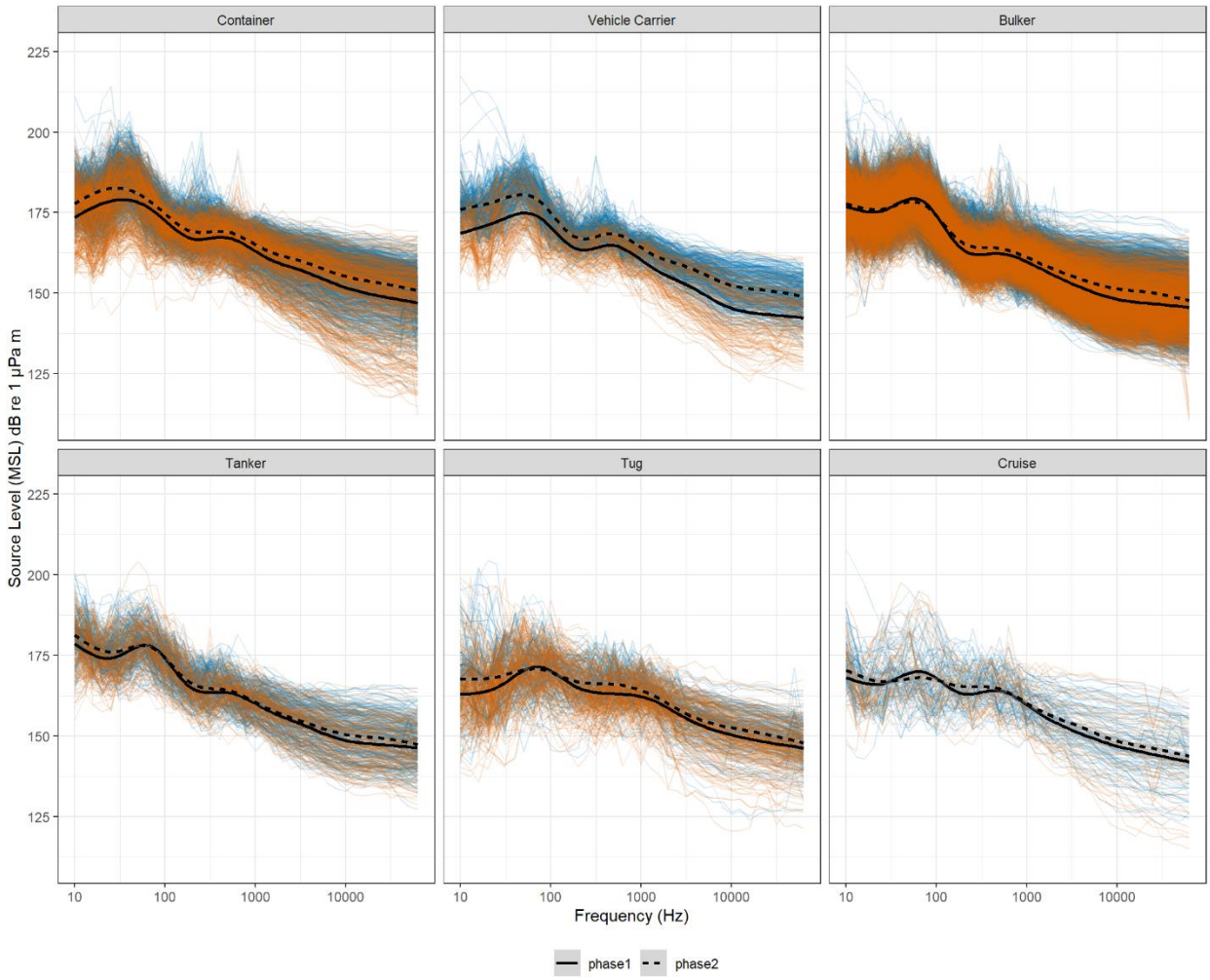

Figure 12. Comparison of MSL versus frequency profiles from the Phases 1 and 2 data sets (orange = Phase 1, blue = Phase 2). Solid line is median Phase 1 data and dashed line is median Phase 2 data.

Phase 1 and 2 showed similar, but not identical correlations between source levels and predictor variables (Figure 13, Appendix B.2). Differences in the univariate correlations do not necessarily reflect differences in the underlying trends in the data sets, however, as correlations can be affected by sampling effects (i.e., if the range of the data is different between data sets). For example, speed-related correlations were generally weaker in the Phase 2 data set, which is attributable to the narrower range of speeds sampled in Boundary Pass (discussed above). Surface angle correlations were also weaker in the Phase 2 data set, which is likely attributable to site-specific differences in sound propagation conditions (i.e., due to differences in bathymetry and seabed composition). EVDI correlations for Containers and Vehicle Carriers appeared to be stronger in the Phase 2 data set, but this was once again attributable to speed differences, as trends for these categories were very similar to Phase 1 after adjusting measured source levels for STW and actual draft at the time of measurement (see Section 2.2.5).

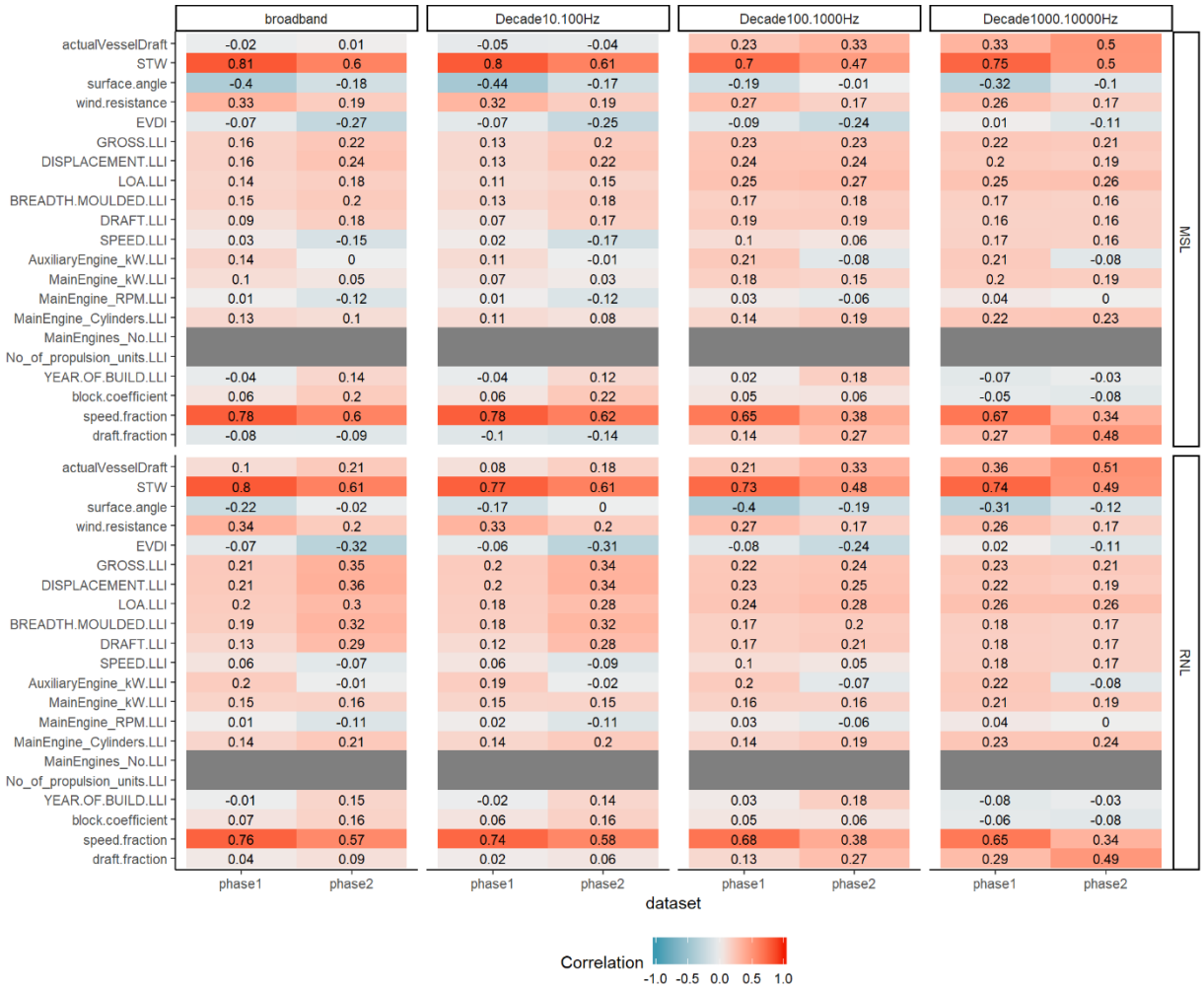

Figure 13. Comparisons of Phases 1 and 2 correlations between vessel characteristics and source levels (MSL and RNL) for the Container category. Columns show the correlation coefficient (−1 < r < 1) with broadband and decade-band source levels. Top rows show MSL correlations and bottom rows show RNL correlations. The colours indicate the strength and magnitude of the correlation (blue = positive, red = negative). Greyed out boxes represent no variation in vessel characteristic to compute any correlation.

One important difference identified during review of the univariate correlations was a significant difference in the distribution of auxiliary engine power values (AuxiliaryEngine_kW.LLI) in the Phase 2 data set, particularly for the Container and Vehicle Carrier categories (Figure 14). Investigation into this discrepancy revealed that auxiliary engine power as provided in the Phase 1 data set was not reported but rather calculated based solely on gross tonnage and vessel type, whereas auxiliary engine power, as provided in the Phase 2 data set was reported. Since this design parameter was not reported in a consistent fashion in the LLI database, and in Phase 1 was a derived parameter based solely on other variables, it was excluded from subsequent statistical analysis and removed from the functional regression model. No similar issues were identified for the remaining design parameters reported by LLI[2]. Annex 2 provides detailed results of the data set comparisons.

[2] Displacement tonnage (Displacement.LLI) was also found to be a calculated parameter, in both the Phase 1 and Phase 2 datasets, but it was not employed as a predictor in the statistical model and therefore would not affect the model validation.

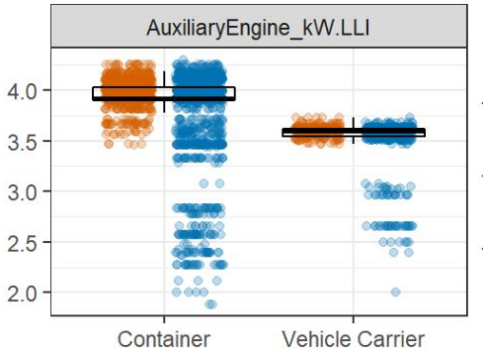

Figure 14. Dot plot of auxiliary engine power (log transformed) from the Phase 1 (orange) and Phase 2 (blue) data sets, as reported by Lloyd's List for Containers and Vehicle Carriers. In the Phase 1 data set, this parameter is not reported but rather calculated based solely on gross tonnage and vessel type. Random horizontal jitter has been added to the dots to separate them and improve clarity.

2.2.3. Phase 1 Functional Regression Model Validation

Testing of the Phase 1 model showed that it was able to reliably predict frequency-dependent source levels in the Phase 2 data set (Figure 15), to within the expected margin of error. The error tolerance of the Phase 1 model was quantified using residuals (observed – predicted). The residuals from fitting the Phase 1 model to the Phase 2 data had similar distributions to those of the original residuals from the Phase 1 data (Figure 16). The MSL predictions were slightly better than the RNL predictions (i.e., with lower rms error), which is attributable to the fact that MSL more accurately accounts for the influence of the measurement location on measured noise emissions (i.e., due to differences in bathymetry, geoacoustics, and measurement geometry at the different sites). Annex 3 shows detailed results of the model validation task for all vessel categories.

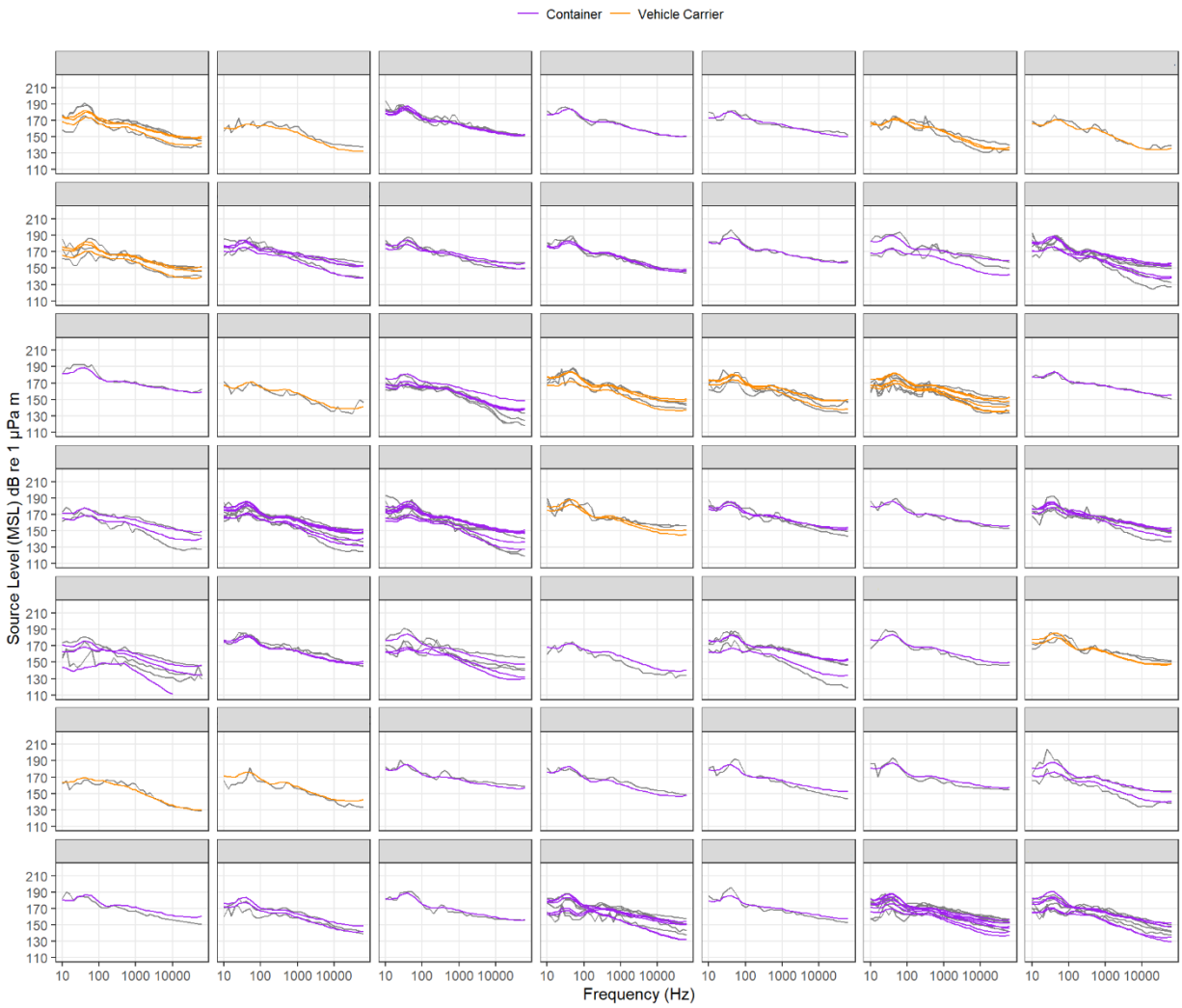

Figure 15. Comparison of measured (gray) and predicted (orange, purple) source levels (MSL) for Phase 2 measurements of Containers and Vehicle Carriers using the Phase 1 functional regression model. Vessel identities have been anonymized for reporting purposes. Panels show multiple measurements and model predictions for a single vessel.

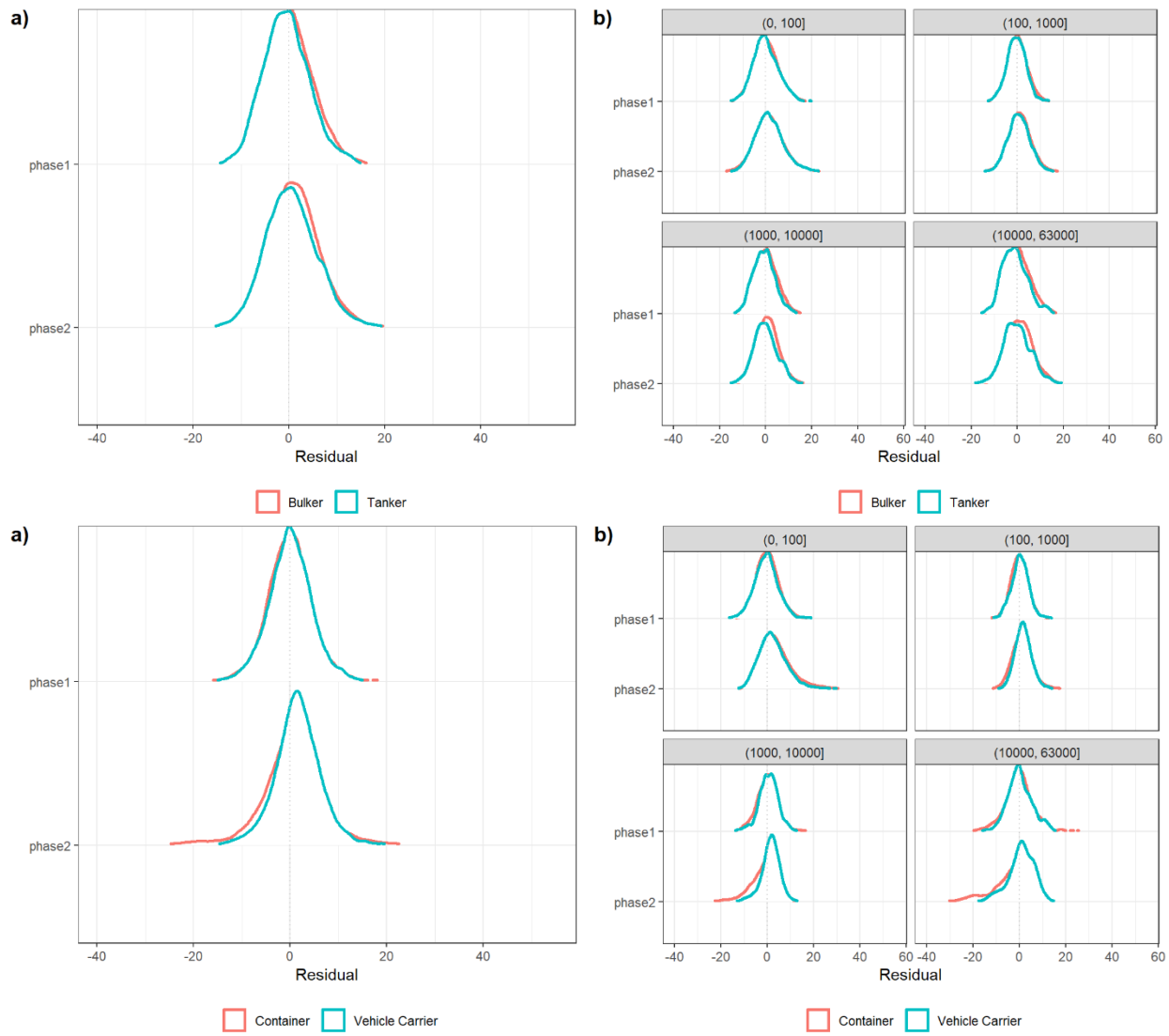

Figure 16. Distributions of MSL model residuals for the Phase 1 model applied to the Phases 1 and 2 data sets for Bulkers and Tankers (top) and Containers and Vehicle Carriers (bottom). Left panels (a) show overall residuals in all decidecade bands and right panels (b) show residuals for decidecade bands in specified frequency ranges.

Although the average of the Phase 2 residuals remained close to zero, there were more extreme outliers in two cases: at the upper tail of the 10–100 Hz frequency range (all categories) and at the lower tail of the 1000-63000 Hz frequency range (mainly for Containers and Vehicle Carriers). The lower-tail outliers were due to changes in the way that auxiliary engine power (AuxiliaryEngine_kW.LLI) was reported by LLI in the Phase 2 data set, as discussed in the previous section. The range of this predictor was much greater in the Phase 2 data set, particularly for Containers and Vehicle Carriers (see Figure 14). Therefore, applying the regression coefficients for this predictor sometimes yielded source levels that had significant errors when compared to the measured data. As a result, the auxiliary engine power trend from the Phase 1 model was determined to be invalid, as it was derived from a calculated dependent variable.

The upper-tail outliers in the 10–100 Hz range were attributed to imperfect removal of flow noise by ShipSound from some measurements in the Phase 2 data set. Water currents during running tides are, on average, approximately 50% faster in Boundary Pass (Phase 2 data set) than in Strait of Georgia (Phase 1 data set) and this generated more low-frequency vibration that was picked up by the hydrophones. Furthermore, the AMAR moorings in Boundary Pass, with their integrated buoyancy, were believed to be more susceptible to vortex shedding than the bottom-mounted ULS frames in the Strait of

Georgia[3]. A manual review of 36 measurements randomly sampled from the top 5th percentile of the Phase 2 data set showed that non-stationary flow noise was not always removed by the automated noise subtraction algorithm in ShipSound (Figure 17). Thus, the low-frequency outliers reflected a systematic issue with some of the Boundary Pass measurements, associated with the measurement site, rather than a shortcoming in the Phase 1 model. To address this issue, the SNR rejection threshold was manually increased for low-frequency bands in the Phase 2 data set to suppress the outliers (see Section 2.1.5). Nonetheless, these outliers are a small fraction of the data and testing during development of the updated functional regression model (next section) showed that they do not significantly affect the correlation analysis or resulting regression models.

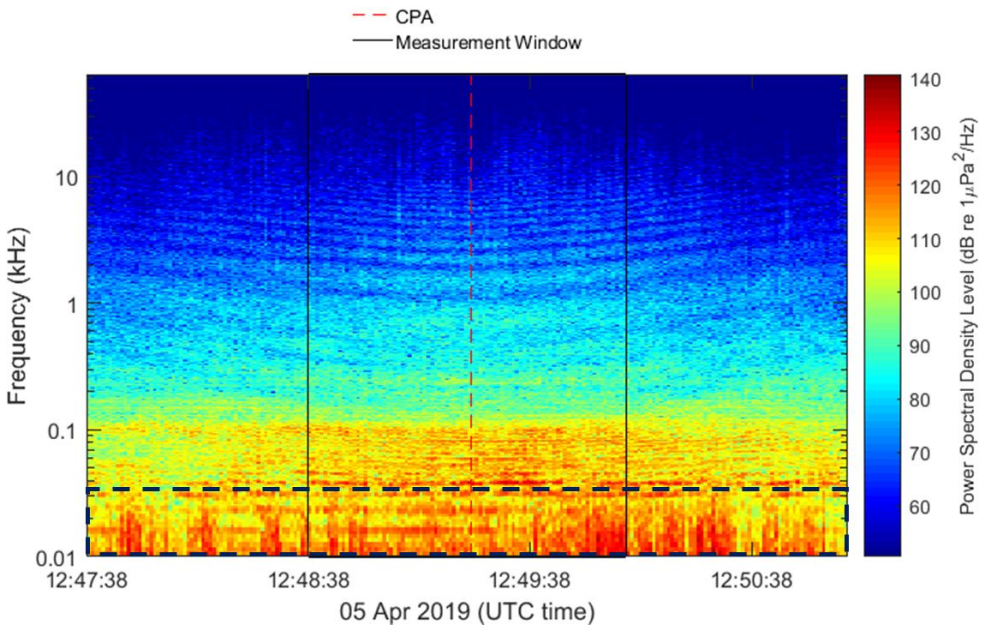

Figure 17. Example of ShipSound measurement contaminated by intermittent low-frequency flow noise below 30 Hz (dashed box). The flow noise in this example was not successfully removed by ShipSound because it was not constant throughout the measurement period.

[3] Vibration noise below 100 Hz is substantially reduced in measurements on the cabled ULS deployed in May 2020 in Boundary Pass at the same site as the AMAR moorings.

2.2.4. Updated Functional Regression Model

After the data set comparisons and validation tasks were completed, the functional regression model was updated using the combined Phases 1 and 2 data sets. As discussed in Section 2.1.5, the updated statistical model dropped the auxiliary engine power, added the vessel age, and split the combined vessel categories into separate groups. Confidence intervals, coefficients of determination, and influence plots were created for the updated functional regression model, following the methods of the Phase 1 study (see figures in Appendix C). Additional analysis details of the updated functional regression model are provided in Annex 4.

Depending on the frequency band and the vessel category, the updated functional regression model was generally able to explain 25-50% of the variance in the observed source level measurements in the ECHO data sets (see Appendix C.1). This was reflected by the fact that the model was able to accurately reproduce the broad-scale features of vessel noise profiles, but not the fine-scale features of the profiles (Figure 18). The fine-scale features—particularly the narrow-band spikes—were not reproduced by the model because they do not follow a predictable trend between different vessels. These features are believed to be responsible for most of the residual mismatch between observations and predictions that was unexplained by the updated functional regression model.

Figure 18. Comparison of measured (gray) and predicted (orange) source levels (MSL) for anonymized Phase 2 measurements of Containers using updated functional regression model. Panels show multiple measurements and model predictions for a single vessel.

In order to better understand the changes that resulted from incorporating the Phase 2 data set into the model, comparison plots of the regression coefficient functions (i.e., the frequency-dependent trends, $\beta(f)$, between predictors and source levels) were generated for the two input data sets (Figures 19 to 22). These plots show how the regression coefficient functions changed from the original gray fit to the colored fits for the model based on the combined Phases 1 and 2 data sets. The plots also show how the regression coefficient functions changed when the combined vessel categories were split apart (i.e., for Bulkers & Tankers and Containers & Vehicle Carriers).

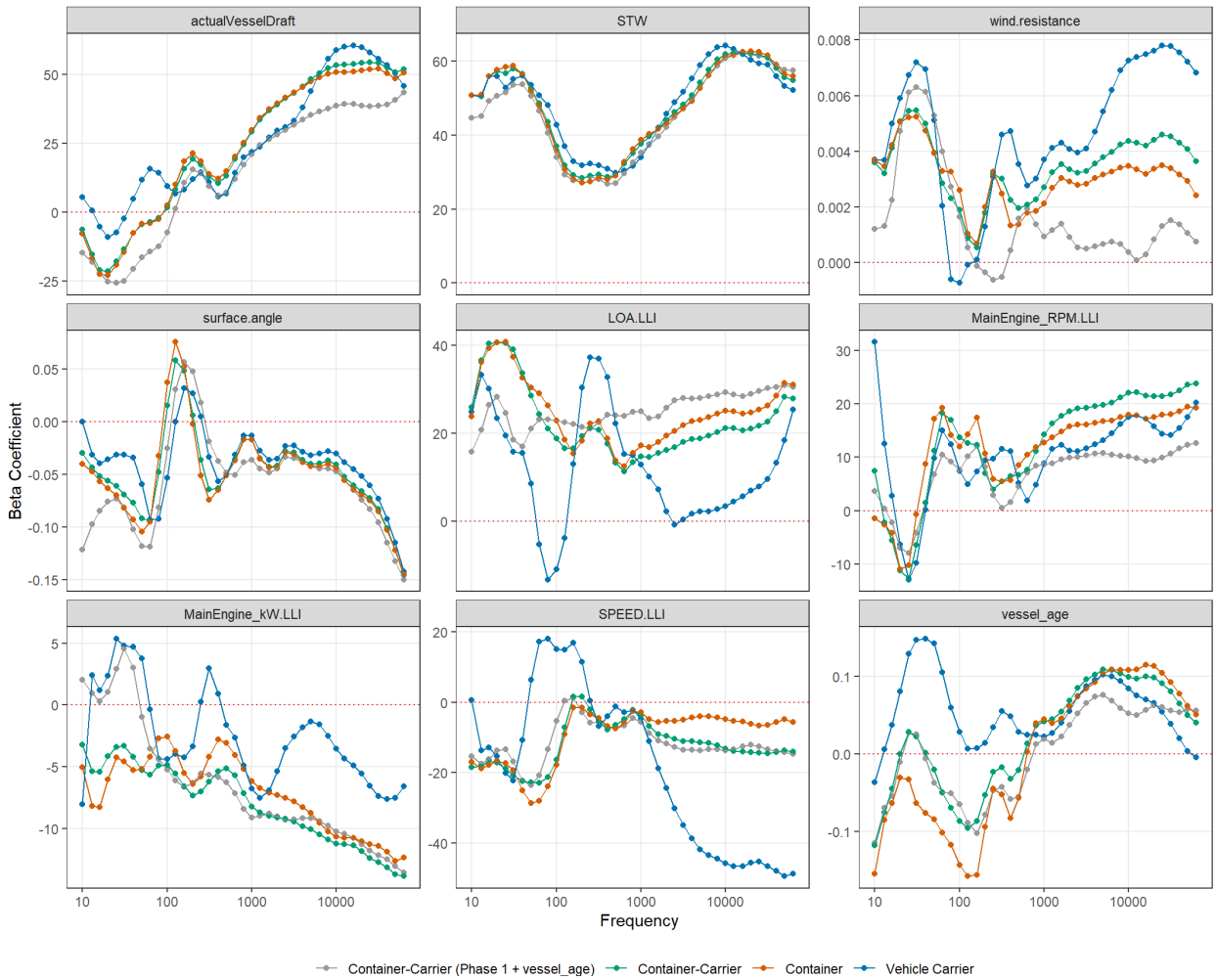

Figure 19. Containers and Vehicle Carriers: Monopole Source Level (MSL) regression coefficient functions $\beta(f)$ (i.e., frequency-dependent slope coefficients) versus log(frequency) for all predictors. The four lines in each panel correspond to the regression coefficient functions obtained using four different data sets: Phase 1 Containers and Vehicle Carriers (gray), Phases 1 and 2 Containers and Vehicle Carriers (green), Phases 1 and 2 Containers only (orange), and Phases 1 and 2 Vehicle Carriers only (blue).

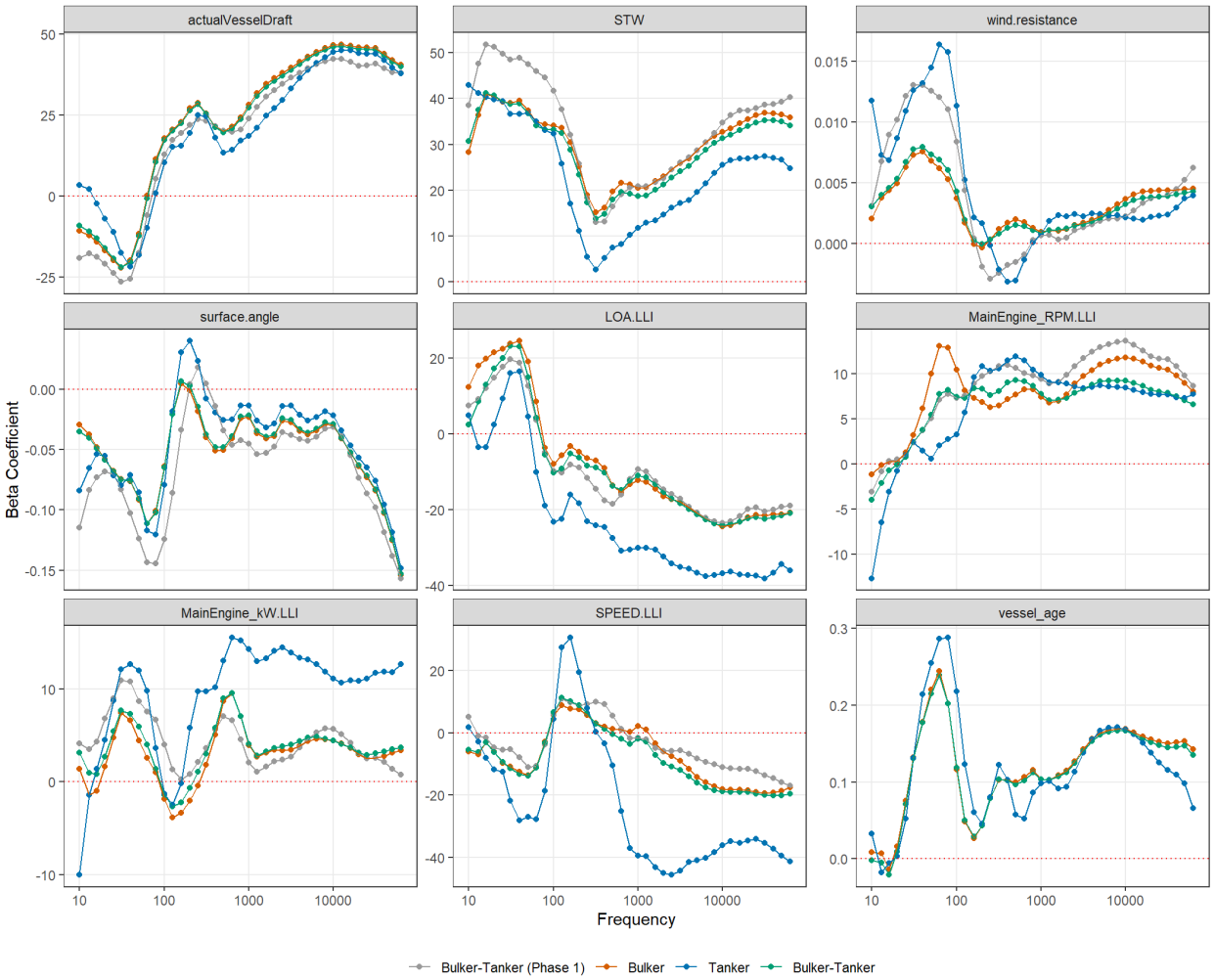

Figure 20. Bulkers and Tankers: Monopole Source Level (MSL) regression coefficient functions $\beta(f)$ (i.e., frequency-dependent slope coefficients) versus log(frequency) for all predictors. The four lines in each panel correspond to regression coefficient functions obtained using four different data sets: Phase 1 Bulkers and Tankers (gray), Phases 1 and 2 Bulkers and Tankers (green), Phases 1 and 2 Bulkers only (orange), and Phases 1 and 2 Tankers only (blue).

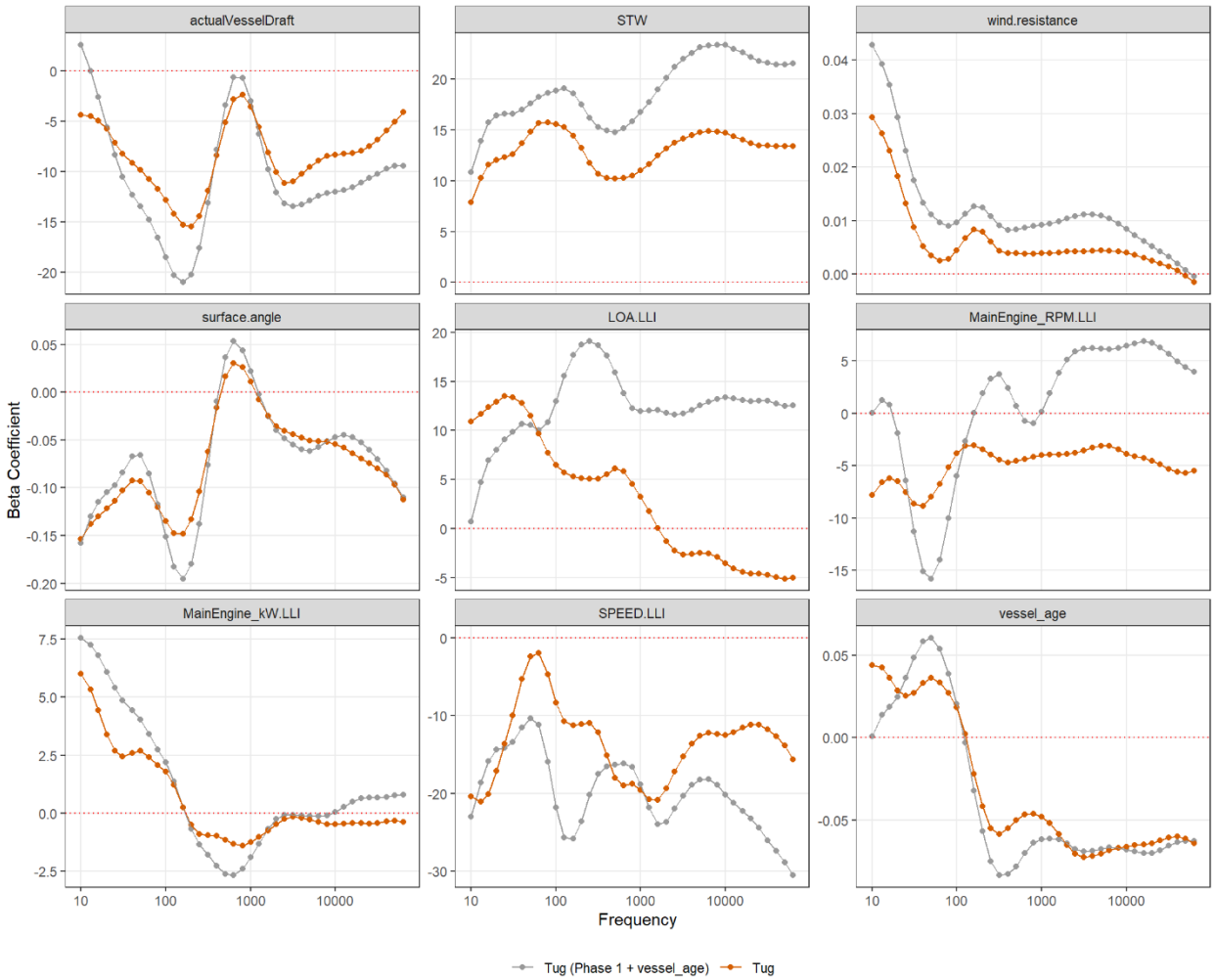

Figure 21. Tugs: Monopole Source Level (MSL) regression coefficient functions $\beta(f)$ (i.e., frequency-dependent slope coefficients) versus log(frequency) for all predictors. The two lines in each panel correspond to regression coefficient functions obtained using the two different data sets: Phase 1 (gray), Phases 1 and 2 (orange).

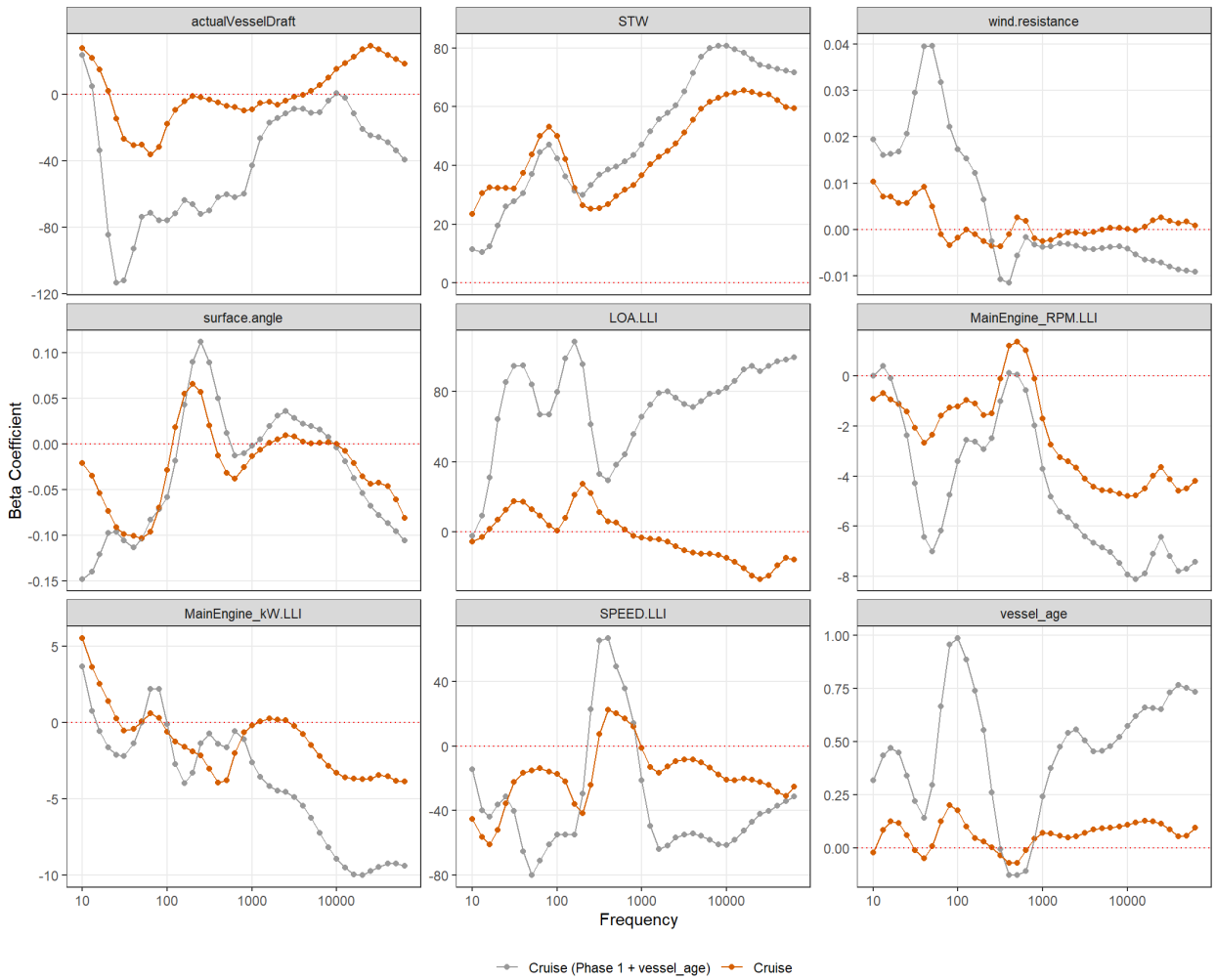

Figure 22. Cruise vessels: Monopole Source Level (MSL) regression coefficient functions $\beta(f)$ (i.e., frequency-dependent slope coefficients) versus log(frequency) for all predictors. The two lines in each panel correspond to regressions function obtained using the two different data sets: Phase 1 (gray), Phases 1 and 2 (orange).

For all vessel categories, regression coefficient functions for speed through water and actual draft (the two most influential parameters) changed very little with the addition of the Phase 2 data set. Larger differences were observed in the regression coefficient functions for design characteristics, but only for some categories. Regression coefficient functions were largely unchanged for Bulkers and Containers, the two categories with the most measurements, which indicates that their trends were generally consistent between the Phases 1 and 2 data sets. The largest changes in the regression coefficient functions were observed for Tugs and Cruise vessels. This is not unsurprising, given that these two categories had the smallest number of samples and the greatest fraction of missing predictors in both the Phase 1 and 2 data sets. Nonetheless, datasets for Tugs and Cruise vessels remain sparse and thus the derived trends with design characteristics remain uncertain in most instances (see discussion in Section 2.3).

When Vehicle Carriers were split from Containers (see Figure 19), their regression coefficient functions were much less significant for vessel length (LOA.LLI) and engine power (MainEngine_kW.LLI). Furthermore, their regression coefficient functions exhibited different frequency-dependent trends for design speed (SPEED.LLI) and vessel age (vessel_age). These differences appear to be due, in part, to the fact that Vehicle Carriers have a narrower range of design characteristics than Containers and thus their correlations are weaker and more uncertain (see discussion in Section 2.3, and influence plots in Appendix C.3.6). When Tankers were split from Bulkers (see Figure 20) their regression coefficient

functions had a greater magnitude for three design characteristics: vessel length (LOA.LLI), design speed (SPEED.LLI), and engine power (MainEngine_kW.LLI). This appears to indicate that Tankers, as a group, exhibit stronger trends of noise emissions with design characteristics than Bulkers, though their frequency-dependent trends remain similar nonetheless.

The unexplained variability in the updated functional regression model (i.e., due to the fine-scale frequency-dependent features discussed above) was quantified by calculating the standard deviations of the model residuals in different frequency ranges (Table 2). The model residuals are simply the differences between the measured and predicted source levels. The standard deviation of the residuals is therefore a measure of the uncertainty (or prediction error) of the model. The standard deviation of the updated Phase 1 and 2 model residuals ranged from 3.3 to 8.0 dB, with a mean value of 5.1 dB when averaged across vessel category and frequency range (Table 2).

Table 2. Standard deviations (decibels) of model residuals from the updated functional regression model built on the Phases 1 and 2 data sets.

Frequency range (Hz)	Bulker	Container	Cruise	Tanker	Tugs	Vehicle Carrier
Standard deviation (MSL)						
$0 < f \leq 100$	5.3	5.5	6.8	5.5	6.2	4.7
$100 < f \leq 1000$	4.5	4.5	5.1	4.8	5.7	3.6
$1000 < f \leq 10{,}000$	4.3	3.9	5.0	4.2	5.6	3.6
$10{,}000 < f \leq 63{,}000$	5.4	4.7	6.9	5.1	7.8	5.2
Standard deviation (RNL)						
$0 < f \leq 100$	5.3	5.5	6.7	5.6	6.2	4.7
$100 < f \leq 1000$	4.4	4.4	5.0	4.7	5.6	3.6
$1000 < f \leq 10{,}000$	4.0	3.6	4.7	3.9	5.2	3.3
$10{,}000 < f \leq 63{,}000$	5.4	4.6	6.7	5.2	8.0	5.1

2.2.5. Correlations with Greenhouse Gas Emissions

A graphical analysis was used to investigate whether the weak trends between vessel noise emissions and greenhouse gas (GHG) emissions, observed during the Phase 1 study, changed after addition of the Phase 2 data set. Emissions data from RightShip were available in terms of two different variables:

- EVDI (Existing Vessel Design Index): equal to the rate of CO_2 emissions of a vessel, in grams per gross tonnage, per nautical mile travelled. A higher value represents higher intensity of emissions.
- GHG.Rating: a letter grade scale (A-G) ranking the CO_2 efficiency of a vessel relative to its size and class cohort. The scale indicates the number of standard deviations from the mean score for a vessel class. A is the best, G the worst, and D is the centre.

GHG ratings were only available for cargo vessels, so tugs and cruise vessels were excluded from this analysis. Following the methodology described in the Phase1 report, graphical comparisons were performed using decade band RNL, after adjusting for speed through water and actual vessel draft using the updated functional regression model. A small number of EVDI values over 30 were treated as outliers and discarded from the Bulker category.

Addition of the Phase 2 data resulted in very similar trends to the Phase 1 study, although the inclusion of more data increased the significance of the trends in some instances (Table 3). The findings of this analysis were as follows:

- Containers and Vehicle Carriers still exhibited a weak trend of decreasing RNL with increasing EVDI (i.e., higher intensity of CO_2 emissions) in the 10–100 Hz and 100–1000 Hz bands. The RNL trend in the 1000–10000 Hz band was increasing for Vehicle Carriers and slightly decreasing for Containers with increasing EVDI. As before, no clear trends were evident in the GHG rating data.
- Bulkers and Tankers still exhibited a trend of increasing RNL with increasing EVDI in the 100–1000 Hz and 1000–10000 Hz bands. The RNL trend in the 10–100 Hz band was nearly flat for Tankers and slightly increasing for Bulkers with increasing EVDI. A trend was still evident in the GHG rating data, with A-grade vessels generally having lower RNL than F-grade vessels.

As was noted in the Phase 1 study, these trends are likely driven by differences in relative GHG emissions between large and small vessels, and the tendency of GHG ratings to improve with increasing vessel size in each group. Trends plots for the GHG noise correlations are provided in Appendix D.

Table 3. Best-fit trend line parameters of adjusted RNL versus EVDI data as determined by linear regression analysis. The coefficient of determination (r^2) is a number in the range 0–1 that indicates the strength of correlation between RNL and EVDI (0 = no correlation, 1 = perfect correlation). Asterisks indicate the significance level of the slope (* = $p < .05$, ** = $p < .01$, *** = $p < .001$). Values without an asterisk are not statistically significant (i.e., $p \geq .05$).

Decade band	Slope of adjusted RNL versus EVDI (†) (dB/g[CO_2] GT^{-1} nmi^{-1})	Coefficient of determination (r^2)
Bulkers		
10–100 Hz	0.219***	0.00630
100–1000 Hz	0.536***	0.0541
1000–10000 Hz	0.656***	0.0710
Containers		
10–100 Hz	-0.467***	0.121
100–1000 Hz	-0.256***	0.0716
1000–10000 Hz	-0.112***	0.00813
Tankers		
10–100 Hz	0.0927	0.00293
100–1000 Hz	0.881***	0.313
1000–10000 Hz	0.659***	0.106
Vehicle Carriers		
10–100 Hz	-0.0583	0.00235
100–1000 Hz	-0.172***	0.0492
1000–10000 Hz	0.192***	0.422

(†) Note that the trends listed in Table 7 of the Phase 1 report were mistakenly inverted—i.e., the slopes were for EVDI versus RNL, rather than RNL versus EVDI. The slope values given here are for RNL versus EVDI, as originally intended.

2.3. Discussion

As in the Phase 1 study, the updated functional regression model showed that operational parameters (speed through water and actual draft) were the most influential predictors of source levels for all vessel categories. Furthermore, the explanatory power of the model (i.e., the coefficient of determination, r^2) was largest for those vessel categories in which vessels were measured while operating under a wide range of speed and draft conditions. This explains why the r^2 values for the updated functional regression model were greatest for the Container and Vehicle Carrier categories (r^2 ~ 50%) and lowest for the Tug category

(r^2 < 25%). Surface angle and wind resistance had a minor influence on source levels, but these parameters are only included to control for variations in measurement conditions. As in the Phase 1 study, the design characteristics were generally less influential on vessel source levels than the operational parameters.

The updated functional regression model was used to rank the influence of the different design characteristics for each vessel category (Table 4). Rankings were not provided for the Cruise category because the observed trends remained statistically insignificant, despite the increased sample size (see Appendix C.2.3). Similarly, rankings were not provided for Vehicle Carriers because, once these vessels were split from Containers, their design characteristics did not exhibit a sufficient range of variation to demonstrate clear trends (see Appendix C.3.6). For the remaining four vessel categories, the updated functional regression model indicated very similar trends to the Phase 1 study, but with some minor differences as follows:

- For Bulkers, the category with the greatest number of measurements, length overall and main engine design RPM remained the two most influential design characteristics. However, the newly-added vessel age characteristic was also observed to be associated with increased noise; older Bulkers tended to have uniformly higher source levels than newer Bulkers. Main engine power and design speed did not appear to have a significant influence in this category.
- For Containers, length overall, main engine power, and design speed remained the most influential design characteristics (after auxiliary engine power was removed). Main engine design RPM no longer appeared to be influential, after the split with Vehicle Carriers, and vessel age did not appear to be significant for this category.
- For Tankers, which were previously grouped with Bulkers, length overall and engine design RPM remained the two most influential design characteristics. However, after the split with Bulkers, main engine power and design speed also appeared to be influential for Tankers. As with Bulkers, older Tankers tended to have higher source levels, but the range of variation with age was smaller because vessels in this category also tended to be newer.
- For Tugs, main engine design RPM was the only design parameter that appeared to have a clearly significant trend with source levels, in the updated functional regression model. Other design characteristics (length overall included) had weak correlations with Tug source levels and their regression coefficient functions were not clearly significant over a wide range of frequencies. Thus, design characteristics for Tugs continue to be difficult to associate with underwater noise emissions, despite the increased number of measurements from the Phase 2 data set.

As discussed in the Phase 1 report, it is important to note that the statistical methods employed in Task 1 only had the ability to examine correlation, not causation. This analysis was also limited by the sampling methods inherent to the data set, which was collected from ships of opportunity calling at the Port of Vancouver (i.e., not in a fashion that controlled for design parameters and operating conditions).

Table 4. Ranking of design parameters, based on a qualitative review of the updated functional multiple regression model. Arrows indicate direction of association with Radiated Noise Level (RNL) and frequency dependence: ↑ = positive, ↓ = negative, ↑↓ = positive at low frequency and negative at high frequency, ↓↑ = negative at low frequency and positive at high frequency, – = negligible. For example, SPEED.LLI (↓) for Containers indicates that RNL decreases as design speed increases. Grayed out parameters did not appear to have a significant correlation with RNL, based on the confidence intervals of the regression coefficient functions (see Appendix C.2). The Vehicle Carriers group sampled a range of design parameters that was too narrow to rank their influence (see Appendix C.3.6). Cruise vessels did not appear to exhibit significant trends with any design parameter (see Appendix C.2.3).

Ranking	Bulkers	Containers	Tankers	Tugs
Highest ↕ Lowest	LOA.LLI (↑↓)	LOA.LLI (↑)	LOA.LLI (↑↓)	MainEngine_RPM.LLI (↓)
	MainEngine_RPM.LLI (↑)	MainEngine_kW.LLI (↓)	MainEngine_RPM.LLI (↑)	SPEED.LLI (–)
	vessel_age.LLI (↑)	SPEED.LLI (↓)	MainEngine_kW.LLI (↑)	LOA.LLI (–)
	MainEngine_kW.LLI (–)	MainEngine_RPM.LLI (–)	SPEED.LLI (↓)	MainEngine_kW.LLI (–)
	SPEED.LLI (–)	vessel_age.LLI (–)	vessel_age.LLI (↑)	vessel_age.LLI (–)

3. Task 2: Investigation of Additional Design and Operational Parameters

The objective of Task 2 was to investigate noise correlations using additional data on design and operational parameters that were not available in the Phase 1 study. The additional information used in this analysis was provided by regional vessel operators for a subset of vessels in the full ECHO source level database (from September 2015 to January 2020). Results from Task 2 indicate directions for future study, further hypotheses to be tested, and design characteristics to be included for future model updates and developments.

3.1. Methods

3.1.1. Data Conditioning

Additional design and operational data were provided by five different vessel operators for a total of 99 unique vessels. The additional data included detailed information on propeller design, shipboard machinery, vessel operations, and hull-features potentially affecting the propeller wake field. Not all information was available for all vessels, but a manual review identified 26 variables from this set that had a sufficient range and number of samples to include in the Task 2 analysis. Appendix A.2 provides a table listing all the new variables considered in Task 2, as well as the number of vessels and measurements associated with each. Additional data were provided for 72 Bulkers and 27 Containers, which altogether accounted for 610 measurements in the ECHO database. Source levels were extracted for this subset of the ECHO data set and joined to a table containing the additional variables. This subset was then scrutinized for residual trends in noise emissions that were not explained by the updated statistical model developed in Task 1.

3.1.2. Residuals Analysis

The 26 additional variables were analyzed by examining trends in the residual differences between observed and predicted source levels from the updated functional regression statistical model The relationships between the additional variables and the residuals were explored to determine if any of the new variables may provide additional predictive power. That is, this analysis examined residual trends in the measured source levels that could not be attributed to the 9 predictors included in the updated functional regression model completed in Task 1 (see Section 2.2.4). The residuals from the updated functional regression model are the differences between the measured and predicted source levels in decidecade bands and can be either positive or negative:

$$\mathrm{e}(f) = \mathrm{L}(f) - \hat{L}(f) \tag{1}$$

where *e* is the residual difference (dB) between the measured source level L and predicted source level $\hat{L}$ in decidecade frequency band *f* (*L* may refer to either RNL or MSL, in this case). Trends in the residuals may indicate that a difference in a specific variable is associated with changes in underwater radiated noise emissions that, for the dataset subset examined, would improve the model.

The original set of design characteristics and operating parameters from Task 1 was used to create model predictions for the subset of vessels in Task 2 (i.e., to calculate $\hat{L}(\mathrm{f})$ values). Residuals were calculated separately for Bulkers and Containers, as these two categories had distinct sets of beta coefficients in the updated functional regression model. The residuals were then calculated and plotted against the new design characteristics to highlight variables that may be correlated with vessel noise emissions, after accounting for the effects of the original 9 predictor variables. Trends in the residuals may help explain variability not captured in the updated functional regression model.

Different vessels in the Task 2 data set had different numbers of repeat measurements: for example, 15 vessels had only one measurement, whereas 5 vessels had over 25 measurements. The uneven sampling could potentially bias the observed trends, therefore a subsampling procedure was applied to the Task 2 data set to reduce the potential for certain highly-sampled vessels to skew the results. The subsampling procedure was the same as was applied to the Task 1 dataset, whereby a maximum of 8 measurements per vessel were included in the Task 2 analysis, with repeat measurements only included when they represented different speed, draft, and wind conditions (see 2.5.1 in MacGillivray et al. (2020) for details). The subsampling procedure retained 341 measurements of the 610 total measurements available for the Task 2 vessel subset (Figure 23). Three different random subsamples of the data were reviewed, to verify that the observed trends were not sampling artefacts.

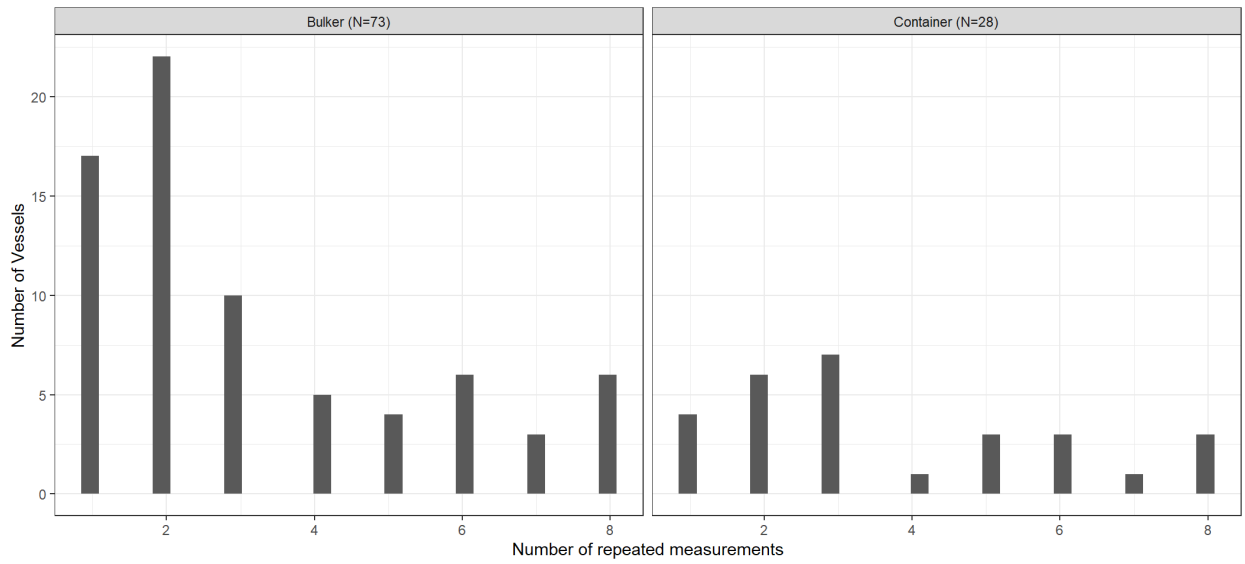

Figure 23. Histogram showing of number of repeat vessel measurements included in the Task 2 analysis, after subsampling.

Exploratory graphical analysis included scatter plots to examine numerical variables and box-and-whisker plots to examine categorical variables. The residuals were grouped into four frequency ranges, as follows, to examine frequency-dependent trends:

- 10 Hz ≤ f ≤ 100 Hz
- 100 Hz < f ≤ 1000 Hz
- 1000 Hz < f ≤ 10,000 Hz
- 10,000 Hz < f ≤ 63,000 Hz

Plots were manually reviewed to identify potential trends or patterns in the data.

3.2. Results

The sections below highlight variables which the manual review identified as possessing a clear visual relationship with the residual source levels. Variables that are not discussed below either did not exhibit a clear trend or possessed too few samples to attribute any statistical significance to the observed trends. Annex 5 provides plots of the residuals for all 26 additional variables captured in the Task 2 data set. Note that, in the plots below, residuals are plotted for all decidecade bands encompassed by each of the four frequency ranges indicated above (i.e., so the number of points is equal to the number of measurements times the number of decidecade bands above background level).

3.2.1. Bulkers

Several notable trends were observed in the residual source level data for design characteristics of Bulkers:

- Residual source levels for 5 Bulkers with installed fins were consistently lower than residual source levels for 60 Bulkers without installed fins, at frequencies above 100 Hz (median MSL difference 2.6–3.8 dB; Figure 24). Fins are hydrofoils protruding from the hull and are designed to reduce the effect of vessel roll, though different designs are in use (e.g., active versus passive stabilizers). This result should be interpreted with caution, as it is based on measurements of a small number of vessels. More investigation would be needed to confirm whether this design characteristic is related to underwater noise.
- Residual source levels for 16 Bulkers without a bulbous bow were consistently lower than residual source levels for 56 Bulkers with a bulbous bow, at frequencies above 100 Hz (median MSL difference 1.1–2.8 dB; Figure 25). This result is surprising, as bulbous bows are intended to smooth the vessel wake and might thus be expected to reduce cavitation.
- Residual source levels for 15 Bulkers with a rudder bulb were consistently lower than residual source levels for 52 Bulkers without a rudder bulb, at frequencies above 100 Hz (median MSL difference 1.8–3.9 dB; Figure 26). Rudder bulbs are designed to reduce turbulence in the wake of the propeller, and therefore may be expected to reduce cavitation noise from a vessel.
- Residual source levels for 11 Bulkers with five propeller blades were consistently lower than residual source levels for 60 Bulkers with four propeller blades, in the 10-100 frequency range (median MSL difference 1.5 dB; Figure 27). Ross (1987) reported that the number of propeller blades can influence underwater radiated vessel noise in two distinct yet opposite ways. The first way is that the pressure gradient produced by a passing propeller blade induces oscillating forces on the vessel hull, and the magnitude of these forces decreases as the number of propeller blades increases. These pressure oscillations are concentrated at low frequencies (typically below 100 Hz) and are radiated by the hull as low-frequency tonal noise at the blade rate and its harmonics (see Glossary). As the number of blades increases the magnitude of the blade-rate noise decreases even as the frequency of the oscillation increases. The second way that underwater radiated noise is influenced by blade count is due to propeller cavitation. Noise from propeller cavitation increases with the area of the cavitating surface, and this type of noise generally increases with the number of blades. Cavitation noise is broadband (i.e., present at nearly all frequencies) but tends to dominate the vessel spectrum at higher frequencies where tonal noise sources are less prominent (i.e., above several hundred Hz). The correlation seen for the Bulkers is consistent with the first way, discussed above, whereby propellers with greater numbers of blades generate lower levels of noise below 100 Hz. due to tonals at the blade rate and its harmonics. There does not appear to have been a correlation between blade count and noise above 100 Hz for Bulkers (but see Section 3.2.2, for Containers).
- Residual source levels for 17 Bulkers with boss cap fins were slightly higher than residual source levels for 50 Bulkers without boss cap fins, in the 10-10,000 Hz frequency range (median MSL difference 0.7-1.4 dB; Figure 28). This result is surprising, as boss cap fins are designed to reduce hub vortex cavitation, although it should be noted the magnitude of the observed difference is somewhat marginal
- Residual source levels for 46 Bulkers with resiliently mounted generators were consistently lower, at all frequencies, than residual source levels for 7 vessels without resiliently mounted generators (median MSL difference 0.4-1.6 dB; Figure 29). Larger differences were observed at higher frequencies, which is surprising, as resilient mountings are mainly expected to reduce vibration noise at machine-vibration frequencies (below a few hundred Hz) and not at higher frequencies above 1 kHz where cavitation tends to dominate. Given the small sample size, this result must be interpreted with caution.
- Residual source levels for 9 Bulkers with resiliently mounted engines were lower than residual source levels for 39 vessels without resiliently mounted engines, below 100 Hz (median MSL difference 1.5 dB; Figure 29). While frequencies above 1000 Hz appeared to exhibit the opposite trend, they are not

expected be influenced by resilient mounting of machinery. The differences in high frequencies may, therefore, be due to an unrelated phenomenon. Again, given the small sample size, this result must be interpreted with caution.

Two notable trends were observed in the residual source level data for operational characteristics of Bulkers:

- Residual source levels for 40 Bulkers were clearly increasing with engine RPM over the entire frequency range (Figure 31). Note that this is the actual engine RPM, as logged by the vessel operator near the time of measurement, which is not to be confused with the nominal design RPM (from Lloyds List) or the acoustically detected RPM (as noted in Section 4.1.2). Engine RPM is directly related to shaft rate and propeller tip speed for direct-drive vessels (as most Bulkers are), so the trend with underwater noise is as expected. However, it is interesting to note that the trend of the residuals is in addition to the speed through water trend predicted by the updated functional regression model. This indicates that there appears to be an additional component of noise associated with engine RPM (and thus shaft RPM) that is not accounted for in the updated functional regression model. It is possible that this residual difference is indirectly related to the propeller slip, though there was insufficient slip ratio data for Bulkers to confirm whether this was the case. Propeller slip is typically expressed as a slip ratio which is calculated as the percent difference between actual and idealized movement of the propeller through water, based on the speed of advance of the propeller.
- Residual source levels for 40 Bulkers showed a trend of increasing source level with increasing vessel trim (fore draft – aft draft) between -2.5 and +2.5 m, over the entire frequency range (Figure 32). This suggests that vessels that are trimmed to stern (i.e., with negative pitch) may generate less underwater radiated noise.

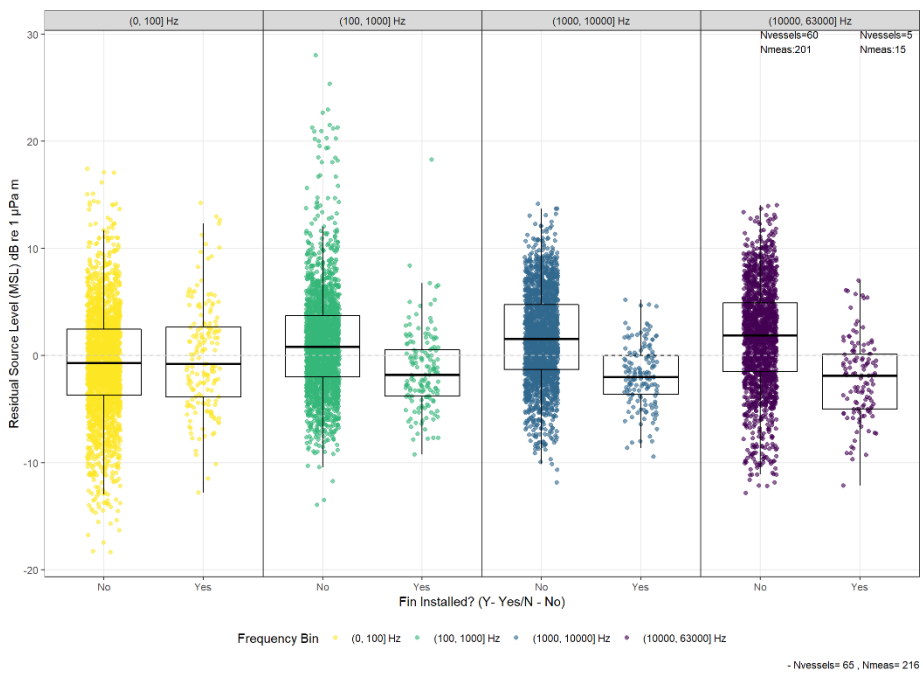

Figure 24. Box-and-whisker plots of residuals (MSL) from the updated functional regression model for Bulkers with and without installed fins for 4 frequency ranges. Points are plotted for all decidecade bands encompassed by the indicated frequency range. The plot annotation indicates the number of vessels and number of measurements in the two different groups.

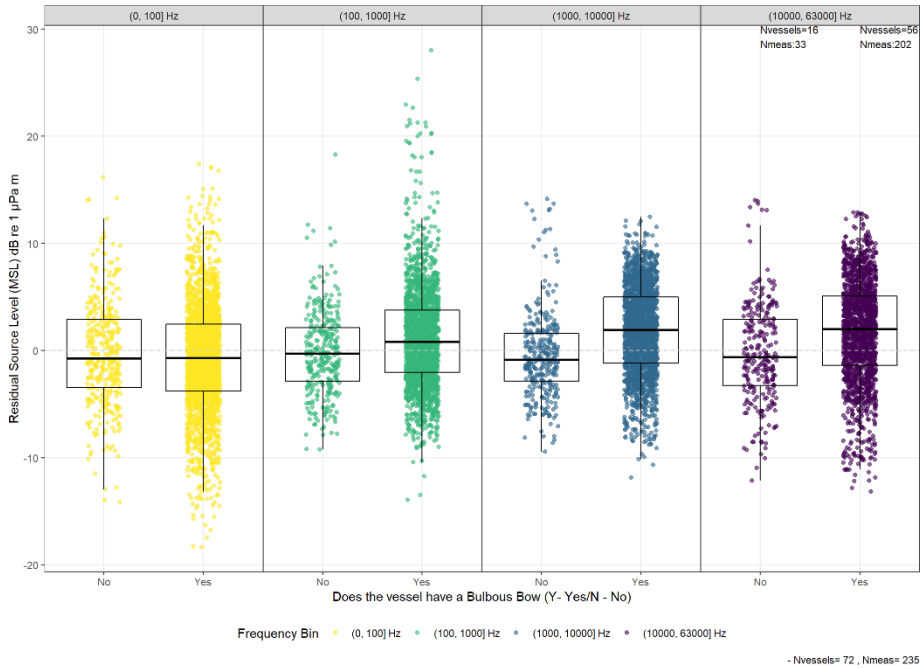

Figure 25. Box-and-whisker plots of residuals (MSL) from the updated functional regression model for Bulkers with and without a bulbous now for 4 frequency ranges. Points are plotted for all decidecade bands encompassed by the indicated frequency range. The plot annotation indicates the number of vessels and number of measurements in the two different groups.

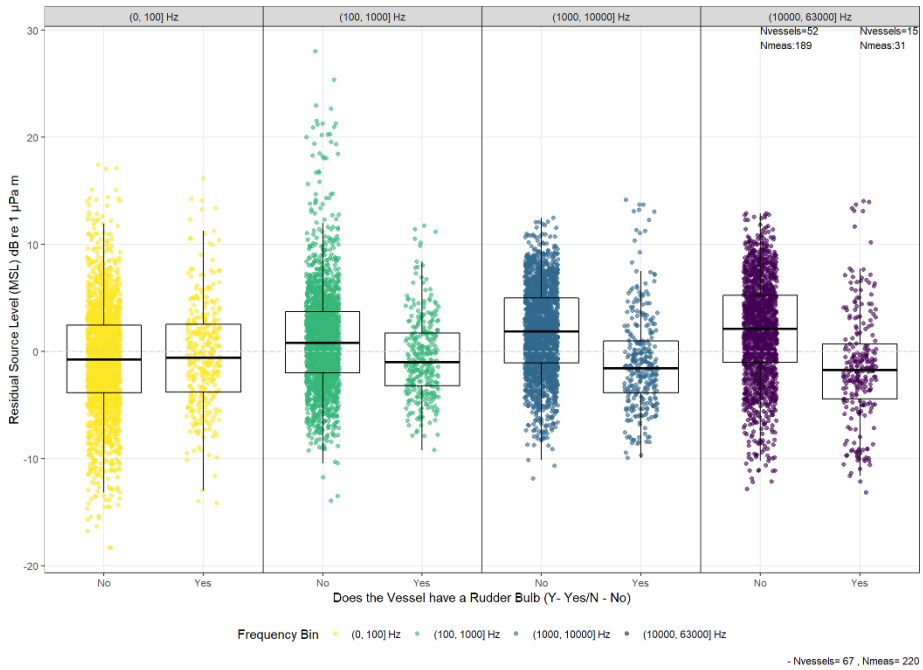

Figure 26. Box-and-whisker plots of residuals (MSL) from the updated functional regression model for Bulkers with and without a rudder bulb for 4 frequency ranges. Points are plotted for all decidecade bands encompassed by the indicated frequency range. The plot annotation indicates the number of vessels and number of measurements in the two different groups.

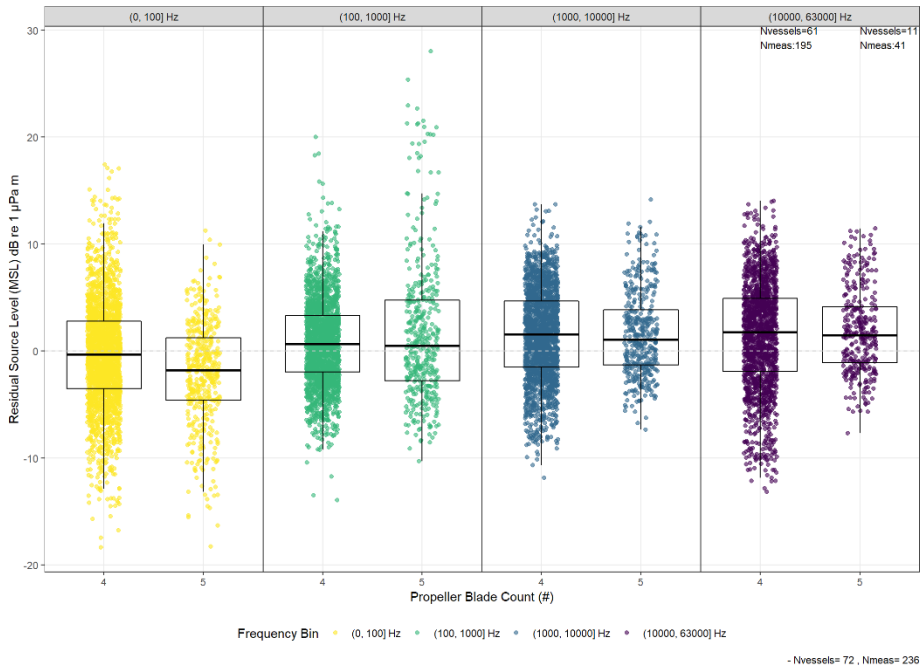

Figure 27. Box-and-whisker plots of residuals (MSL) from the updated functional regression model for Bulkers with four and five propeller blades, in 4 frequency ranges. Points are plotted for all decidecade bands encompassed by the indicated frequency range. The plot annotation indicates the number of vessels and number of measurements in the different groups.

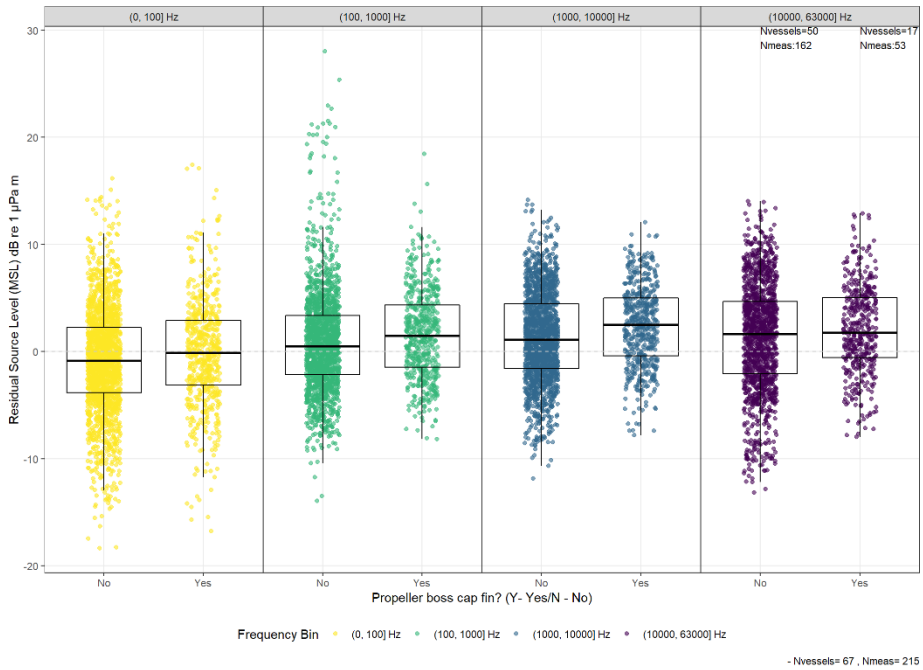

Figure 28. Box-and-whisker plots of residuals (MSL) from the updated functional regression model for Bulkers with and without boss cap fins, in 4 frequency ranges. Points are plotted for all decidecade bands encompassed by the indicated frequency range. The plot annotation indicates the number of vessels and number of measurements in the different groups.

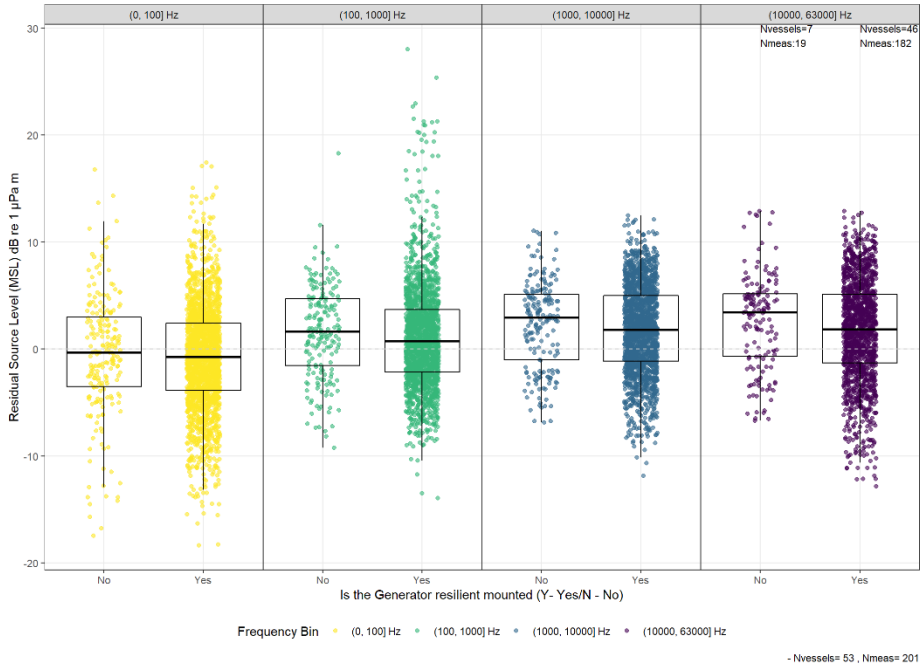

Figure 29. Box-and-whisker plots of residuals (MSL) from the updated functional regression model for Bulkers with and without resiliently-mounted generators, in 4 frequency ranges. Points are plotted for all decidecade bands encompassed by the indicated frequency range. The plot annotation indicates the number of vessels and number of measurements in the different groups.

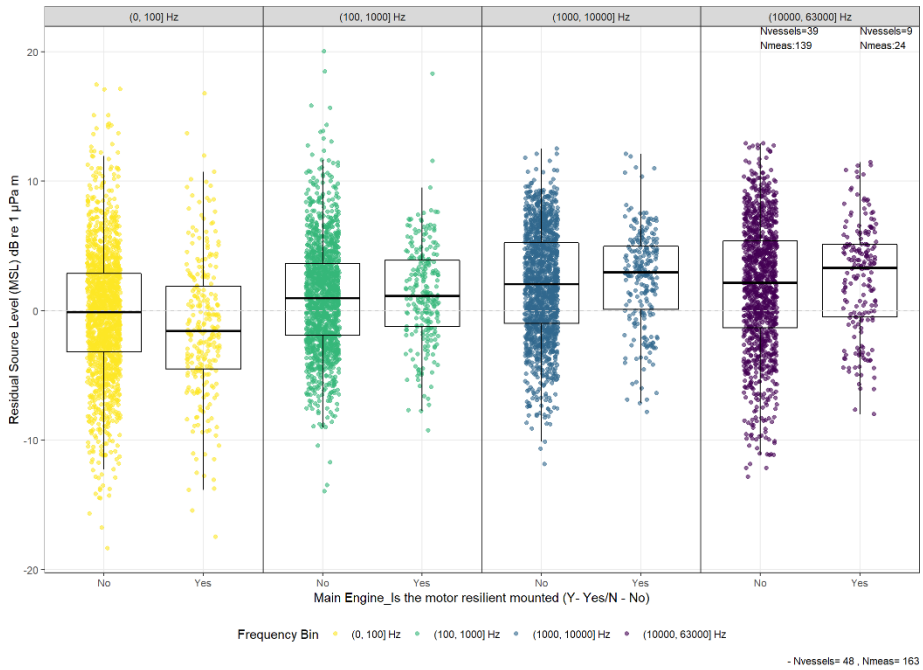

Figure 30. Box-and-whisker plots of residuals (MSL) from the updated functional regression model for Bulkers with and without resiliently-mounted engines, in 4 frequency ranges. Points are plotted for all decidecade bands encompassed by the indicated frequency range. The plot annotation indicates the number of vessels and number of measurements in the different groups.

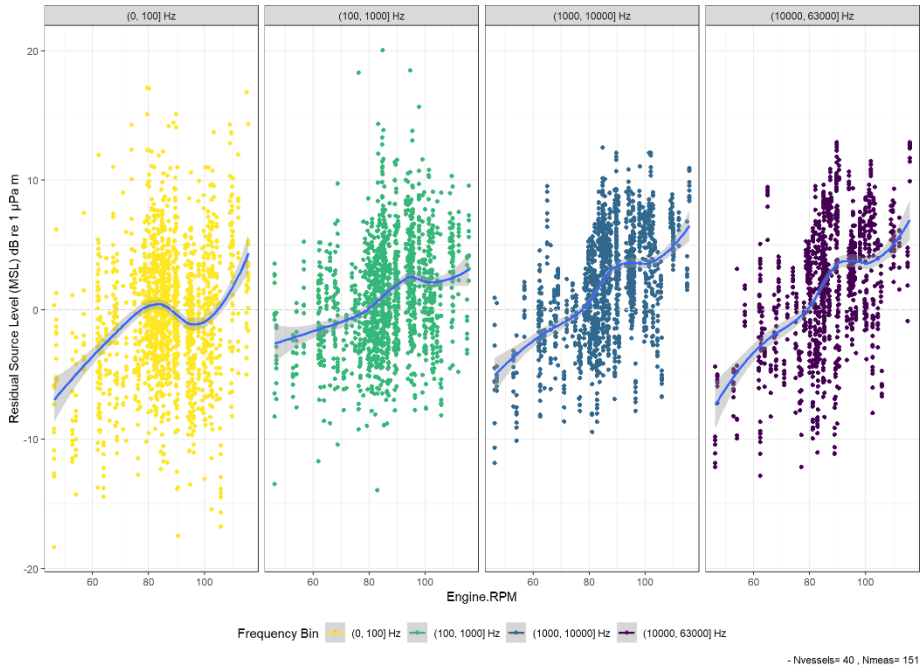

Figure 31. Scatter plots of residuals (MSL) from the updated functional regression model for Bulkers versus logged engine RPM (40 vessels total, 150 measurements). Points are plotted for all decidecade bands encompassed by the indicated frequency range. Spline curve shows smoothed trend of data with 95% confidence interval.

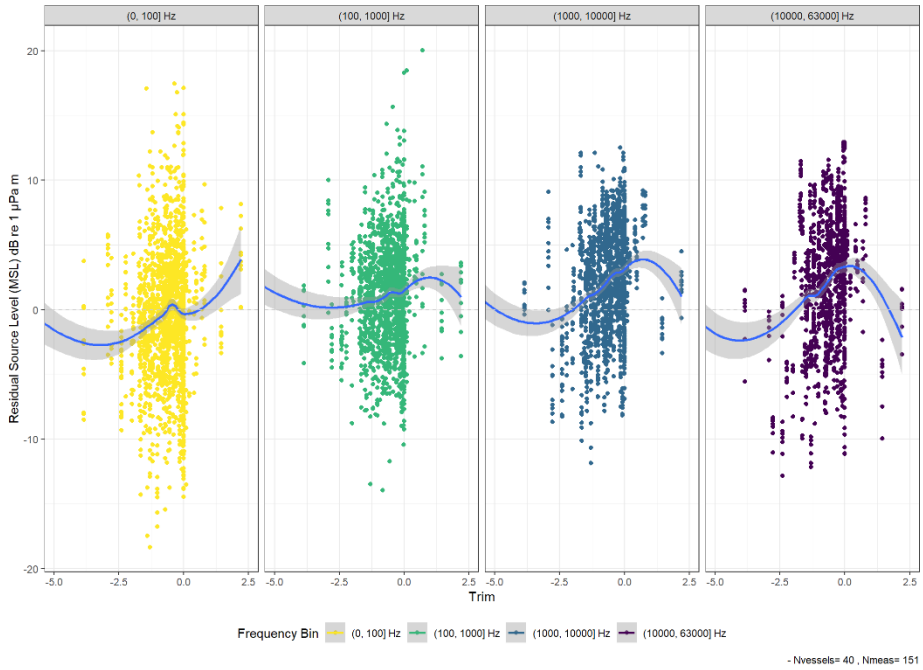

Figure 32. Scatter plots of residuals (MSL) from the updated functional regression model for Bulkers versus trim (fore draft – aft draft, in m) (40 vessels total, 150 measurements). Points are plotted for all decidecade bands encompassed by the indicated frequency range. Spline curve shows smoothed trend of data with 95% confidence interval. The spline trends at the lower and upper extremities of the X axis are fitted to sparse data and may therefore be unreliable.

3.2.2. Containers

One notable trend was observed in the residual source level data for design characteristics of Containers:

- Residual source levels for 16 container vessels with five propeller blades were lower than residual source levels for 10 Containers with six propeller blades, above 100 Hz (median MSL difference 0.8-2.6 dB; Figure 33). Note that four-bladed propellers had only one measurement, which was considered too few to evaluate. This result is consistent with the observation reported by Ross (1987) that propellers with more blades are expected to produce more broadband cavitation noise, which is dominant at higher frequencies (in this case, above 100 Hz). This is because propellers with more blades typically have a greater cavitating surface area. Note that blade-rate tonal noise (below 100 Hz) is expected to decrease as the number of propeller blades increases, but this does not appear to have been the case for Containers (but see Section 3.2.1 for Bulkers).

A few notable trends were observed in the residual source level data for operational characteristics of Containers:

- Residual source levels for 28 Containers showed a trend of increasing source level with increasing drift angle (see Section 2.1.2), over the entire frequency range (Figure 34). It is interesting to note that a similarly clear trend was not observed for Bulkers (the observed range of drift angles for Bulkers was approximately the same as for Containers). One possible explanation for this difference is that Container vessels (when loaded) present a greater cross-sectional area above the waterline, so they may therefore experience more air resistance to cross wind and to headwinds when crabbing.
- Residual source levels for 26 Containers showed a slight trend of increasing source level with increasing slip ratio, between -20-40% (with a possible inflection near 10%), over the entire frequency range (Figure 35). Slip ratio is the percent difference between actual and idealized speed of advance of the propeller. This quantity is not straightforward to interpret, however, as it was understood to be calculated over a period of hours as reported by the vessel operators and thus does not necessarily reflect vessel operations during the precise time of measurement.
- Residual source levels for 28 container vessels showed a trend of increasing source level with increasing engine RPM, over the entire frequency range (Figure 36). Note that this is the actual engine RPM, which is not to be confused with the nominal design RPM or the acoustically detected RPM (see previous section). The observed trend appears to be consistent with Bulkers, though the slope is not as pronounced. It is possible that this residual difference is indirectly related to the propeller slip: the correlation coefficient between engine RPM and slip ratio for the Container measurements was $r = 0.56$, which is moderately strong.

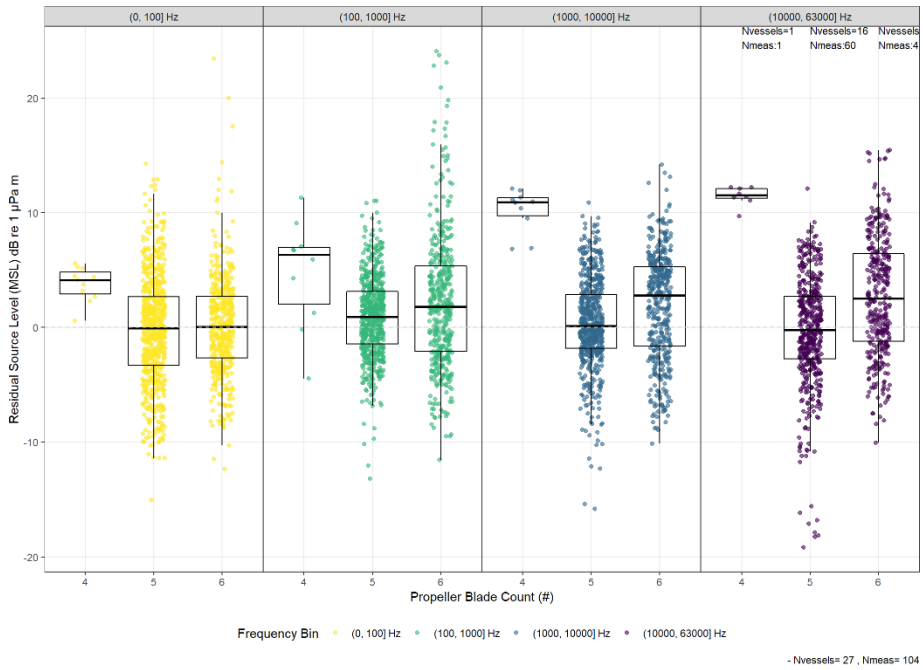

Figure 33. Box-and-whisker plots of residuals (MSL) from the updated functional regression model for Containers versus number of propellers, in 4 frequency ranges. Points are plotted for all decidecade bands encompassed by the indicated frequency range. The plot annotation indicates the number of vessels and number of measurements in the different groups.

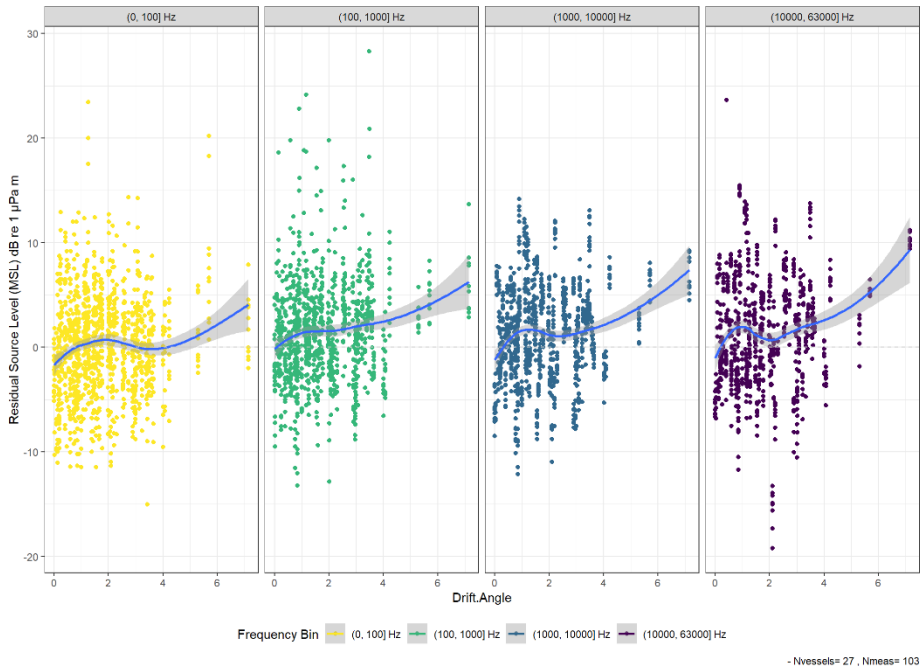

Figure 34. Scatter plots of residuals (MSL) from the updated functional regression model for Containers versus absolute drift angle (deg) (28 vessels total, 104 measurements). Points are plotted for all decidecade bands encompassed by the indicated frequency range. Spline curve shows smoothed trend of data with 95% confidence interval.

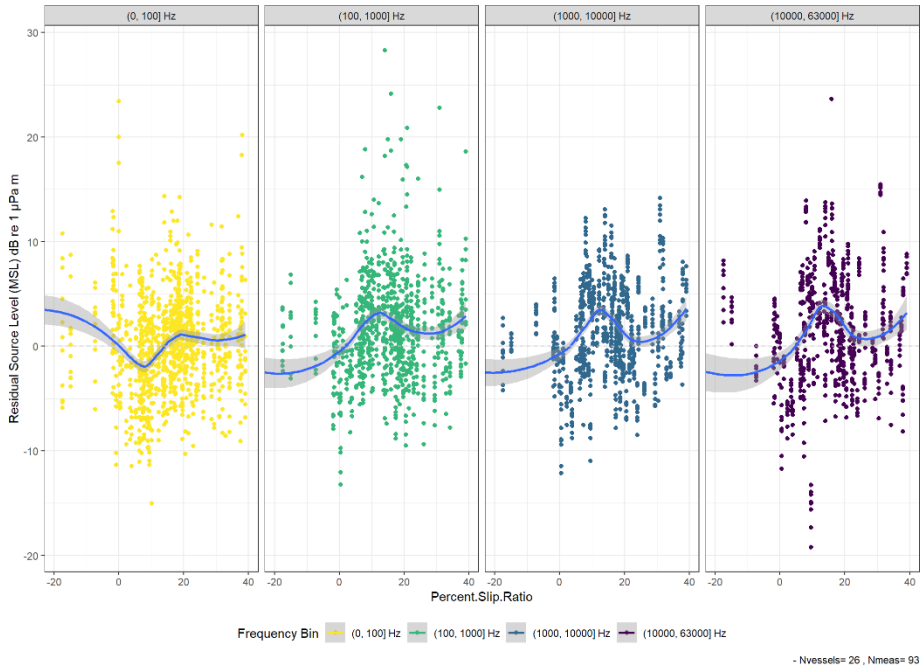

Figure 35. Scatter plots of residuals (MSL) from the updated functional regression model for Containers versus slip ratio (%) (26 vessels total, 93 measurements). Points are plotted for all decidecade bands encompassed by the indicated frequency range. Spline curve shows smoothed trend of data with 95% confidence interval.

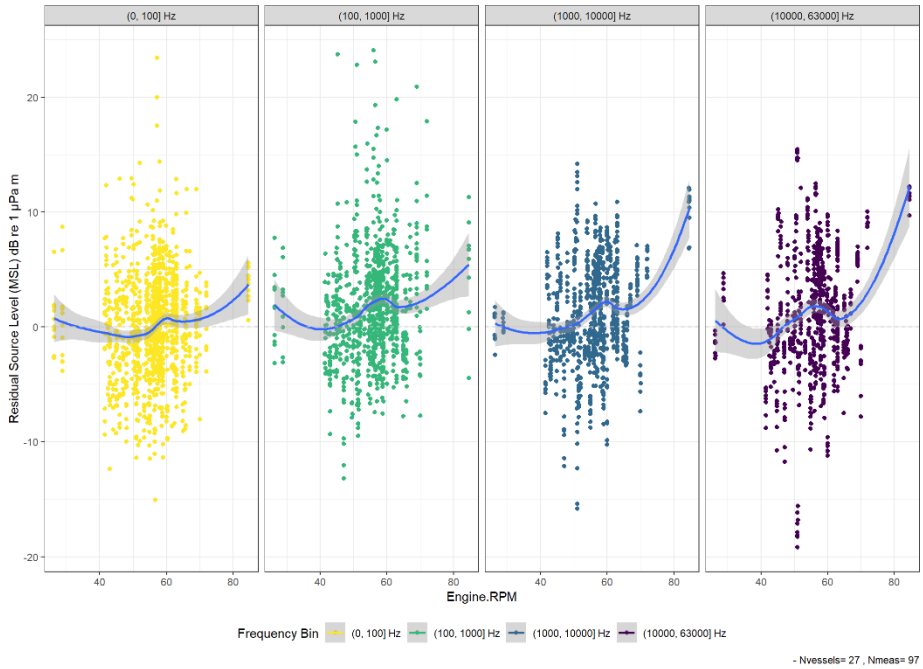

Figure 36. Scatter plots of residuals (MSL) from the updated functional regression model for Containers versus engine RPM (28 vessels total, 98 measurements). Points are plotted for all decidecade bands encompassed by the indicated frequency range. Spline curve shows smoothed trend of data with 95% confidence interval.

3.3. Discussion

Analysis of residual source levels for a subset of Bulkers identified five design characteristics that were associated with lower underwater radiated noise levels: rudder bulbs, more propeller blades (five versus four), resilient mounting of engines, resilient mountings of generators, and installed fins. Rudder bulbs were associated with lower residual noise levels above 100 Hz, which is consistent with the expectation that this characteristic would smooth the propeller wake field, thus reducing cavitation. Five propeller blades were associated with lower residual noise levels, below 100 Hz, than four propeller blades. This is consistent with the result, reported by Ross (1987), that propellers with more blades are expected to generate less hull vibration and thereby less interior and exterior noise at the blade rate (and its harmonics). Although resiliently mounted generators and main engines were both associated with lower noise levels, as expected, it is unclear why these two characteristics exhibited different frequency trends (this may have been related to small sample sizes). Installed fins were associated with lower residual noise levels above 100 Hz, but the significance of this result was unclear, given that only five Bulkers with fins were analyzed. More investigation would be needed to determine whether this was a spurious correlation. The analysis also identified two design characteristics that were associated with higher residual source levels for Bulkers: bulbous bows and boss cap fins. This result was surprising, as both these technologies are intended to improve the uniformity of the vessel wake and might therefore be expected to reduce cavitation noise.

Analysis of residual source levels for a subset of Containers found that fewer propeller blades (five versus six) were associated with lower underwater radiated noise levels above 100 Hz. This was consistent with the result reported by Ross (1987) that propellers with more blades generate more cavitation noise, due to the greater area of the cavitating surface. The residuals analysis found no other notable trends in the design characteristics for Containers. This was mainly because many of the characteristics that exhibited trends for Bulkers (installed fins, bulbous bow, rudder bulb, boss cap) could not be evaluated for Containers due to lack of variation in their designs.

While trends of radiated noise with number of propeller blades appeared to be somewhat contradictory between Bulkers (with fewer blades being noisier below 100 Hz) and Containers (with more blades being noisier above 100 Hz), it is significant that these trends were observed in different frequency ranges with different noise generating mechanisms (i.e., narrow-band blade rate noise versus broadband cavitation noise). This may point to other differences in design characteristics that influence how underwater radiated noise is generated. For example, increased tip clearance (i.e., increased distance between the propeller tip and the vessel hull) is also expected to reduce blade rate noise below 100 Hz, and this characteristic may be different between Bulkers and Containers. Similarly, operating drafts tend to be larger for Container vessels than Bulkers (see Figure 8), which may increase cavitation inception speed.

Somewhat surprisingly, none of the design characteristics describing the geometry of the propellers (skew, diameter, rake, and pitch), appeared to exhibit notable trends with residual underwater noise emissions for Bulkers or Containers.

The primary operational characteristic associated with higher residual noise emissions was increased engine RPM (i.e., actual RPM, not to be confused with design RPM). This trend was consistent for both Bulkers and Containers, though less pronounced for Container vessels. Other operating parameters that were associated with higher residual noise emissions were forward trim (for Bulkers), higher drift angle (for Containers but not Bulkers), and higher slip ratio (for Containers). The available data on operating conditions were somewhat limited, however, and not necessarily consistent between vessels.

It should be emphasized that the trends identified in the Task 2 analysis are based on a more limited subset of the ECHO data, and so the selected measurements may not reflect the data set as a whole. The observed trends are, in many instances, based on a small number vessels and may also be influenced by confounding factors (e.g., common sets of design characteristics between similar vessels), which could not be controlled for by applying the updated functional regression model. Results from Task 2 should be interpreted as indicating directions for more detailed investigation and for future hypothesis testing.

4. Task 3: Analysis of Repeat Single-Vessel Measurements

The objective of Task 3 was to perform detailed analysis of repeat source level measurements for a selected group of four well-sampled vessels. The purpose of this analysis was to identify sources of radiated noise, using spectrum analysis, and to analyze trends with operational parameters using statistical methods. Results from Task 3 highlight vessel-specific trends and quantify uncertainties associated with repeat vessel measurements in the ECHO database.

4.1. Methods

4.1.1. Selected Vessels

Detailed analysis of noise emissions data was carried out for four individual vessels with a relatively large number of repeat measurements in the Phases 1 and 2 data sets. These vessels were selected from a shortlist of frequent callers to the Port of Vancouver and their identities have been anonymized for reporting purposes (Table 5). Additional design details and operational logs for the selected vessels were provided by their owners and operators. The purpose of this analysis was to analyze trends of individual vessel source levels with logged operating characteristics, and to quantify the variability in measured source levels that were observed during repeated passes under similar operating conditions.

Table 5. Design characteristics of anonymized vessels selected for detailed analysis. All vessels employed 2-stroke diesel engines with direct-drive, fixed-pitch, and single-screw propulsion (i.e., no gearbox).

Anonymized name	Year built	Measurements	Length (m)	Prop diameter (m)	Blade count	Nominal RPM	Summer draft (m)	Main engine (kW)	Number of cylinders	Bulbous bow
Bulk Carrier A	2014	33	209	6.2	4	102	12.8	8110	6	No
Container Ship A	2010	17	335	8.9	6	91	14.6	57200	10	Yes
Gen. Cargo Vessel A	1992	19	185	6.8	4	105	12.2	10200	5	Yes
Gen. Cargo Vessel B	2002	29	200	6.8	5	105	12.5	13736	5	Yes

4.1.2. Dual-band RPM analysis

To provide additional data on vessel operating characteristics for the correlation analysis, JASCO's dual-band shaft rate (i.e., propeller RPM) detector was run on the Task 3 vessel measurements. This detector analyzes the acoustic signature of a vessel, using a dual-band method, to estimate the shaft rate at the time of measurement (Quijano et al. 2020). It is known that the spectrum of a transiting vessel exhibits harmonic (narrowband) peaks at specific frequencies. These peaks can be related to the rotatory speed of mechanical components such as propellers, shaft, engines, and onboard generators (Arveson and Vendittis 2000, McKenna et al. 2012, Gassmann et al. 2017). In addition, the generation of cavitation at the tip of the propellers results in the high frequency noise, which can be analyzed by Detection of Envelope Modulation on Noise (DEMON) methods (Chung et al. 2011, Pollara et al. 2017). JASCO's detector employs a dual-band method that analyzes both low-frequency tonals in the 0–40 Hz band, and modulation of the DEMON spectrum in the 10–30 kHz band, to obtain an estimate of shaft-rate RPM. Validation of JASCO's dual-band detector, using pilot logged RPM data from the 2019 ECHO slowdown, demonstrated that the estimation algorithm yielded a 74−91% success rate (depending on vessel category) when calculating shaft rates with a maximum estimation error of 20% (Quijano et al. 2020).

4.1.3. Source level trend analysis

Univariate trends of RNL versus speed through water were analyzed in terms of a power law model (Ross 1987) of the following form, which was fit to the data:

$$\mathrm{RNL} = C_v \times 10\log_{10}\left(\frac{v}{v_{\mathrm{ref}}}\right) + \mathrm{RNL}_{\mathrm{ref}} \tag{2}$$

where, C_v is the slope of increase in RNL with speed through water (v, measured in knots) and, $\mathrm{RNL}_{\mathrm{ref}}$ (dB re 1 µPa m) is the RNL at the reference speed through water (v_{ref}). Measurements of post-World-War-II shipping, reported by Ross, suggested a power-law coefficient in the range C_v = 5–6. Subsequent measurements during the 2017 ECHO slowdown trial reported broadband coefficients for deep-sea commercial vessels in the range 3.1-8.1 (MacGillivray et al. 2019). For this study, best-fit values of C_v are calculated from repeated vessel measurements (i.e., no prior value of C_v is assumed). Speed through water measurements were also compared to estimated shaft-rate RPM for the selected vessels.

4.1.4. Correlation Analysis

Correlations between operational variables and frequency-dependent noise emissions were calculated for the four selected vessels. Specifically, the univariate correlation coefficient, r, was calculated between each operational variable and decidecade band RNL. The correlation coefficient is described in more detail in Section 2.1.3. Correlations with RNL were analyzed for the following operational variables:

- Speed through water (log transformed)
- Shaft-rate RPM (log transformed)
- Actual draft (log transformed)
- Drift angle (absolute value)
- Trim (fore draft – aft draft)
- Cargo weight (tonnes)
- Ballast weight (tonnes)
- Slip ratio (percentage, averaged over a 1-4 hour period; see Glossary)

Of these eight variables, only the first four were available for every vessel. Data for the latter four variables were provided by the vessel operators and were therefore only available in some instances.

4.1.5. Multiple Linear Regression Analysis

Guided by the correlation analysis, a multiple linear regression analysis was used to determine relationships between these operational variables and broadband RNL for the selected vessels. Multiple linear regression analysis is used to model trends between a response variable (broadband RNL, in this case) and multiple simultaneous predictor variables (the operational variables, in this case). While many different sets of predictor variables are possible, not every combination of variables produces a statistically significant result. The significance of the trend with a particular variable may be assessed using a p-value, with a threshold of significance taken to be $p < 0.05$. Multiple linear regression models were built in a stepwise-additive fashion, by adding predictors one at a time (starting with those having the largest r values from the correlation analysis) and retaining only parameters that yielded a statistically significant relationship with broadband RNL.

For the selected vessels, the RNL values used in the multiple linear regression were adjusted for wind speed and surface angle, at time of measurement, using the updated functional regression model developed in Task 1 (Section 2.2.4). This was done to control the broadband RNL for differences in measurement conditions (the resulting adjustments were small, generally less than 1 dB in magnitude).

Note that RNL, rather than MSL, was used for the correlation and multiple linear regression analyses because it is insensitive to the choice of monopole source depth, and therefore better reflects changes in radiated noise associated with changes in actual vessel draft (see discussion in Section 4.1 of MacGillivray et al. (2020)).

4.1.6. Fine-scale Spectrum Analysis

JASCO has access to raw spectral data from the ShipSound measurements, as calculated directly from pressure waveforms recorded on the ULS hydrophones. The ShipSound system provided fine-scale frequency vs. underwater sound levels using Fast Fourier Transform (FFT) algorithm which is a much more granular frequency transform than the decidecade bands. Using FFT methods, ShipSound produced two different Power Spectral Density (PSD) data sets. The first data set was PSD with 1 Hz resolution in the frequency range of 1 to 64,000 Hz (64,000 lines). The second data set had finer resolution of 0.125 Hz in the frequency range of 0.125 to 500 Hz (4,000 lines).

These data sets were provided for a multiple individual measurement runs for each ship given in Table 5. The FFT data for each vessel was graphed and examined for spectral conditions. The expected and usual tones examined include: rotation rate (RR), blade rate (BR), firing rate (FR) and their harmonics. The determination of each discrete frequency tone is given in the Equations below.:

$$\mathrm{n} \times R\mathrm{R} = (n)(N)/60\ \mathrm{Hz}\,, \tag{3}$$

$$\mathrm{n} \times B\mathrm{R} = (n)(N)(b)/60\ \mathrm{Hz}\,, \text{and} \tag{4}$$

$$\mathrm{n} \times F\mathrm{R} = (n)(N)(c)/\big((s)(60)\big)\ \mathrm{Hz}\,, \tag{5}$$

where n is a whole number integer (1, 2, 3, 4…) related to the respective harmonic; N is engine speed (RPM); b is the number of propeller blades (per shaft); c is the number of cylinders in main engines; and s is the main engine stroke (= 2 or 4)[4].

The frequencies for primary rotation rate (1xRR), blade rate (1xBR) and firing range (1xFR) were computed using the shaft-rate as determined using the dual-band RPM detector described in Section 4.1.2. Both the standard resolution and high-resolution data were manually examined for each of the runs for each of the four ships.

Typical and unique sound spectra are reported in Section 4.2.4. Manual methods for determining engine speed were compared with the ShipSound dual-band RPM detector. Unique spectra and their causation were investigated and discussed. Along with the fine-scale data, wave files were also evaluated audibly.

4.2. Results

4.2.1. Source Level Measurements

The broadband RNL and MSL for the four selected vessels are summarized in a box-and-whisker plot of all accepted measurements, before controlling for vessel speed or environmental conditions at the times of the measurements (Figure 37). Table 6 shows the RNL and MSL summary statistics associated with the box-and-whisker plots. There is a considerable difference between the measured source levels of these particular vessels, with 10.4 dB range in median RNL between vessels (12.6 dB range in MSL).

Source levels were plotted in decidecade bands, to determine how noise emissions for the selected vessels varied with frequency (Figures 38 and 39). All four vessels exhibited a broadband noise hump below 100 Hz, but the two vessels with highest source levels (General Cargo A and Container Ship A) both had prominent narrow-band peaks in the 100-1000 Hz range. Furthermore, the frequencies of these narrowband peaks appear to increase with vessel speed (i.e., they appear shifted to the right in

[4] All main engines for the ships evaluated are 2 stroke engines.

Figures 38 and 39, at higher STW). These peaks are explored more thoroughly in the fine-scale spectrum analysis (Section 4.1.6). Some of the range of variability in Figures 37 to 39 is attributable to changes in operating conditions (e.g., due to speed differences). This variability is explored more thoroughly in the multiple linear regression analysis (Section 4.2.3).

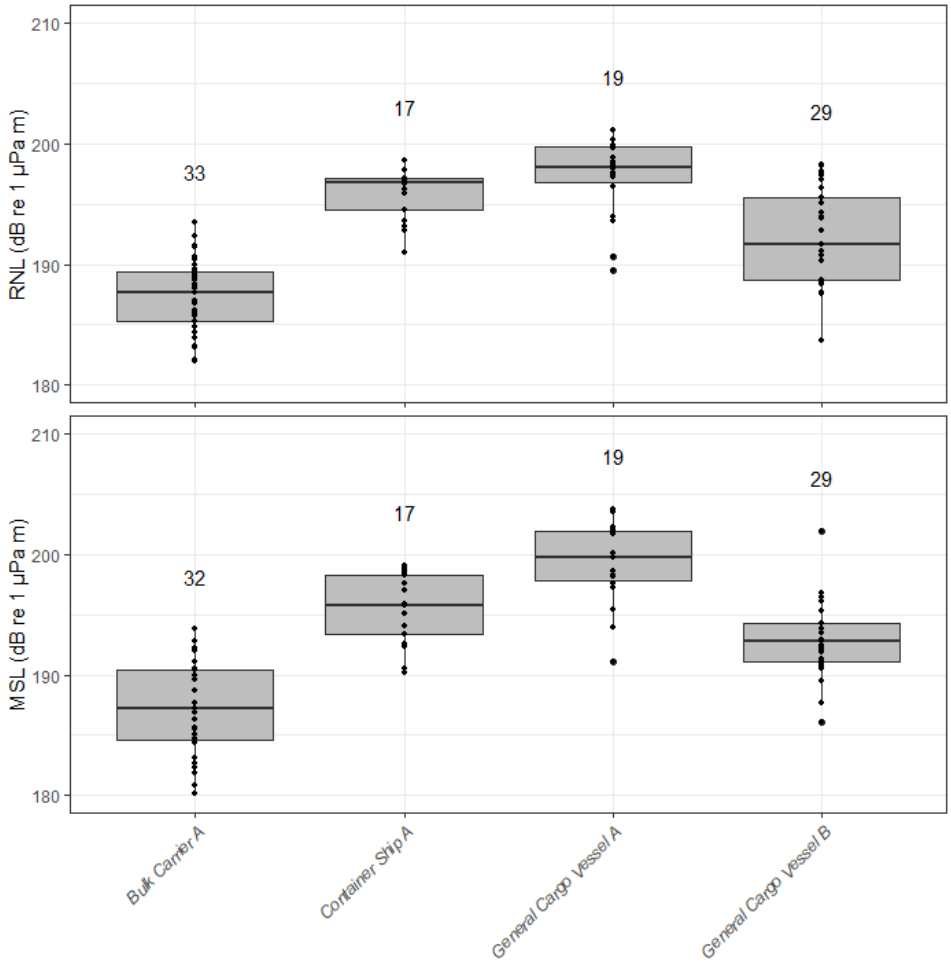

Figure 37. (Top) Radiated noise level (RNL) and (bottom) monopole source level (MSL): Box-and-whisker plot summarizing broadband source level measurements (20 Hz to 64 kHz). Points show individual measurements. The total number of accepted measurements for each vessel is indicated above each box. MSL values for General Cargo Vessel B are clustered in a narrower range than RNL values, due to the greater emphasis that MSL places upon frequencies below 100 Hz, which are less variable for this particular vessel (see Figures 38 and 39).

Table 6. Five-number summary (minimum, lower quartile, median, upper quartile, maximum) of accepted source level measurements for all vessels (RNL and MSL, dB re 1 µPa m).

Statistic	Bulk Carrier A		Container Ship A		General Cargo Vessel A		General Cargo Vessel B	
	RNL	MSL	RNL	MSL	RNL	MSL	RNL	MSL
Maximum	193.4	193.8	198.6	199.0	201.1	203.7	198.3	201.9
Upper quartile	189.3	190.4	197.1	198.2	199.7	201.9	195.6	194.3
Median	187.6	187.2	196.7	195.7	198.0	199.8	191.6	192.7
Lower quartile	185.3	184.3	194.5	193.3	196.8	197.9	188.6	191.0
Minimum	182.0	179.6	190.9	190.1	189.5	191.0	183.7	186.1

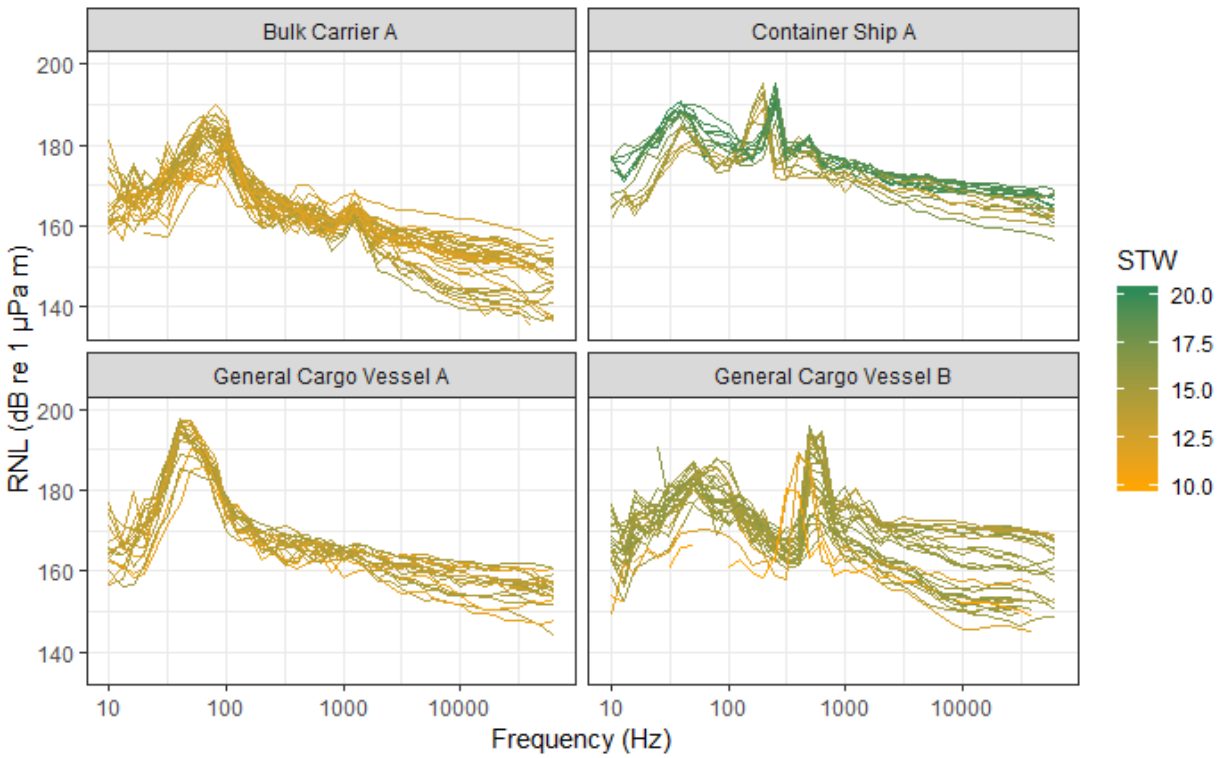

Figure 38. Source level (RNL) versus frequency measurements. Color scale indicates speed at time of measurement.

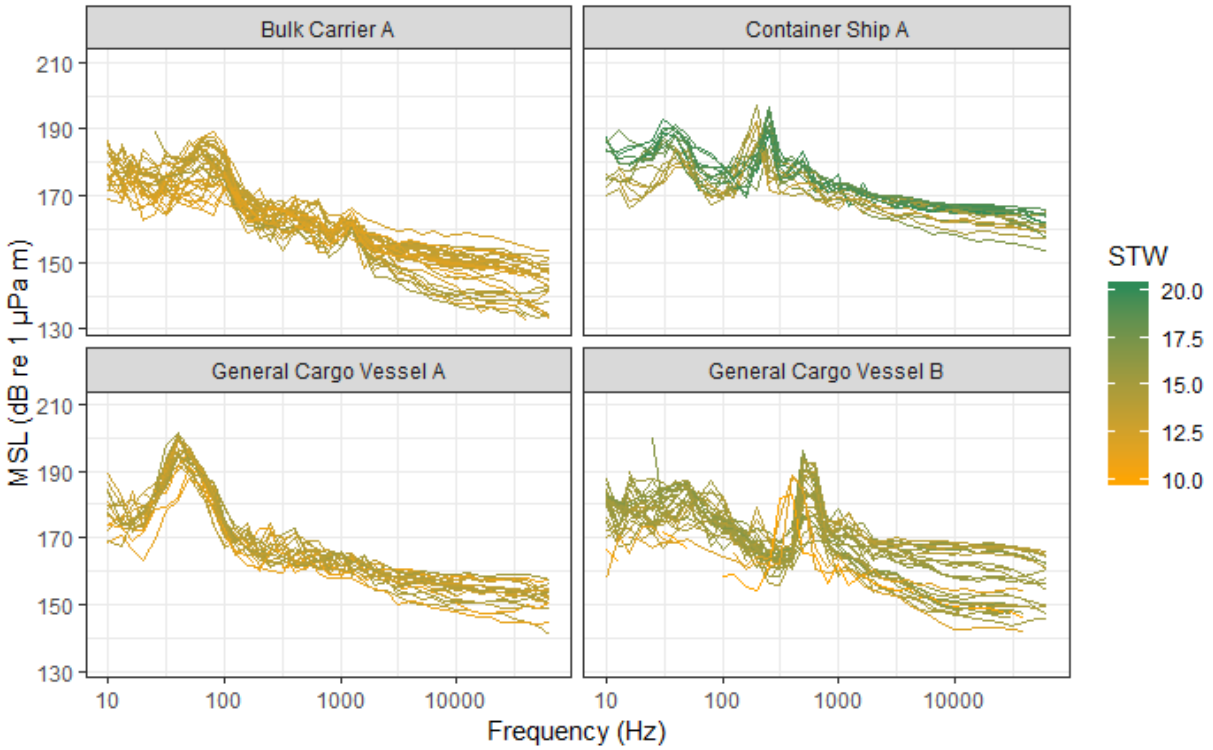

Figure 39. Source level (MSL) versus frequency measurements. Color scale indicates speed at time of measurement.

4.2.2. Vessel Speed and RPM Trend Analysis

A standard trend analysis of RNL with STW (Figure 40) showed that source levels increased with vessel speed in all cases. However, the trend was only statistically significant for two of the four vessels (Table 7), which is attributable to the scatter of the measurements and the influence of other factors, such as draft, on source levels. General Cargo Vessel B, for example, clearly had higher broadband RNL when the actual draft was greater. The residual scatter associated with the draft variations rendered the STW trend not statistically significant for this vessel. Thus, capturing the trends of RNL with operating conditions required consideration of all operational conditions simultaneously (see Section 4.1.4).

A trend analysis of STW with estimated shaft rate showed that the correlation between these two variables was inconsistent between vessels (Figure 41). For example, there was a strong positive correlation between STW and shaft rate RPM for Container Ship A, whereas there was no correlation—or possibly a negative—correlation between these variables for Bulk Carrier A (even when accounting for outliers identified in Section 4.2.5). This is likely because STW depends not only on shaft rate, but also on the drag coefficient of the hull (which changes with draft and trim).

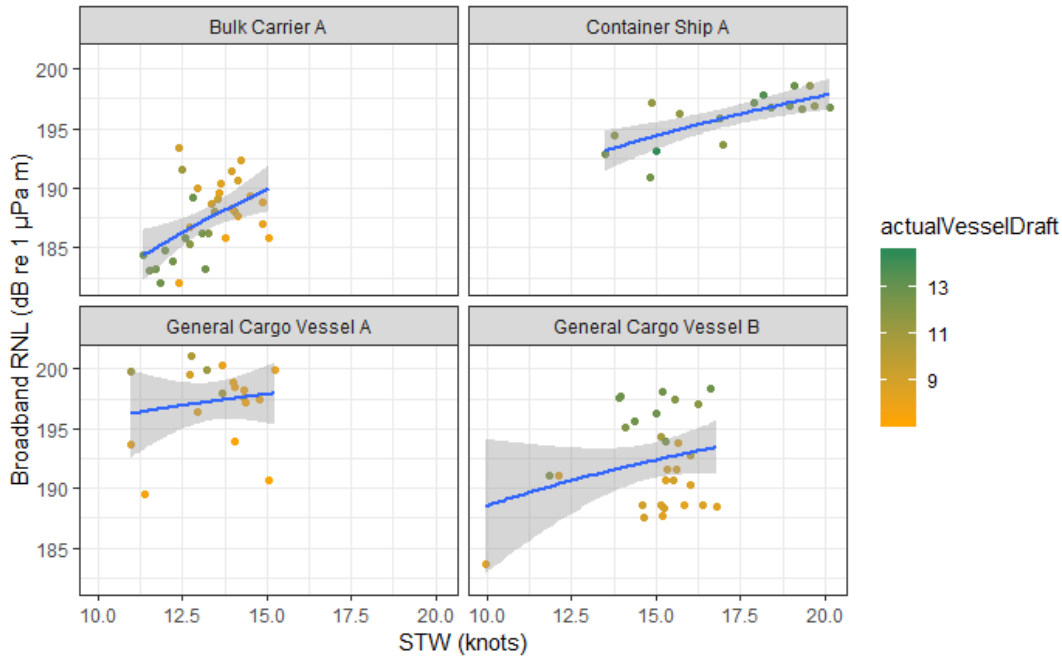

Figure 40. Broadband source level (RNL) versus speed through water for selected vessels. The 95% confidence interval of the trend is shown in gray. Dot color indicates actual vessel draft (m) at time of measurement.

Table 7. Radiated noise level (RNL) versus speed through water: Best-fit trend line parameters as determined by linear regression analysis. C_v is the best-fit slope of trend line, and RNL is the intercept. The coefficient of determination (r^2) indicates the strength of correlation between RNL and speed through water (0 = no correlation, 1 = perfect correlation). Significance indicates whether the observed trend could have occurred by chance with greater than a 5% probability (based on *p*-value).

Vessel	C_v	RNL_{ref} (dB re 1 µPa m)	V_{ref} (knots)	Coef. of determination (r^2)	Significant ($p < 0.05$)
Bulker Carrier A	4.54	181.9	10	0.244	Yes
Container Ship A	2.72	189.6	10	0.520	Yes
General Cargo Vessel A	1.20	195.8	10	0.026	No
General Cargo Vessel B	2.17	188.5	10	0.067	No

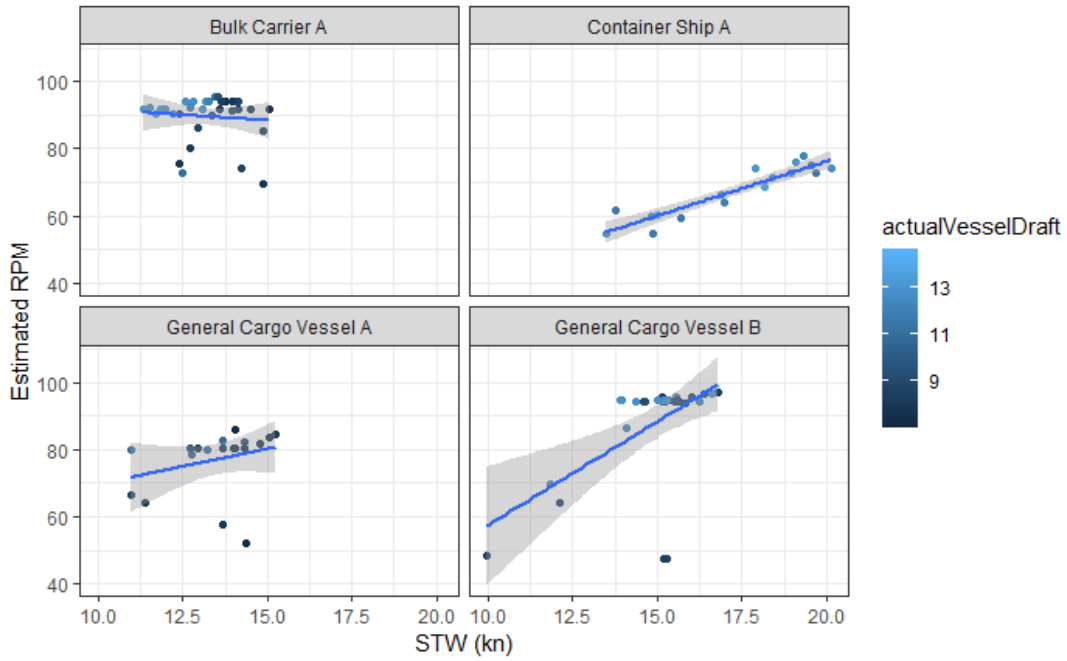

Figure 41. Scatter plot showing trend of estimated shaft-rate RPM, from dual-band RPM detector, versus STW for the selected vessels. Dot color indicates actual draft at time of measurement. A manual analysis flagged a small number of outlier RPM values for Bulker Carrier A and General Cargo Vessel B (see Section 4.2.5).

4.2.3. Correlation and Multiple Linear Regression Analyses

A correlation analysis was used to investigate whether logged operating parameters were associated with increased or decreased noise emissions in specific frequency bands (Figure 42; Appendix E.2). While different vessels exhibited different trends, both Container Ship A and General Cargo Vessel B exhibited a strong negative correlation of RNL with speed (and shaft-rate) at frequencies where narrow-band tonal noise dominated their low-speed spectrum (i.e., corresponding to the spikes between in 160–400 Hz in Figures 38 and 39). This negative correlation is attributed to speed-specific noise generation only present at the lower speed range of these particular vessels, as discussed in the following sections. In general, however, the correlations were not uniform with frequency and different vessels exhibited different correlation patterns. This lack of consistency could be due to differences between vessels though it may also be attributable, in part, to the high probability of spurious correlations caused by relatively small sample sizes ($17 \leq n \leq 33$).

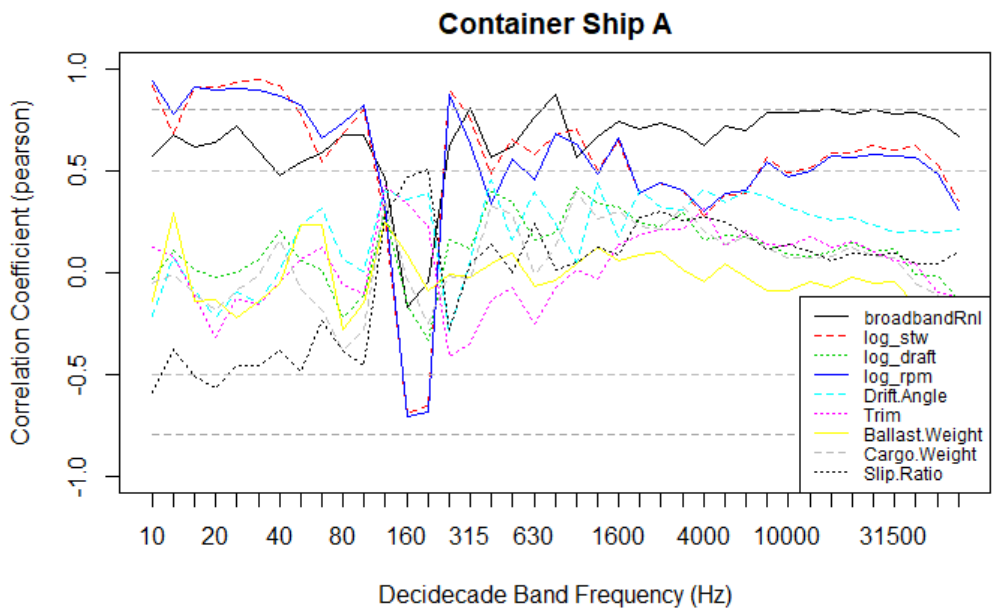

Figure 42. Decidecade band correlations of logged operating parameters with decidecade RNL for Container Ship A. Each line shows the correlation coefficient (*r*) with a single operating parameter versus frequency. Correlation of decidecade band RNL with broadband RNL is also shown for reference. Positive *r*-values indicate that an increase in the parameter was associated with an increase in RNL, whereas a negative *r*-value indicates an increase in the parameter was associated with a decrease in RNL. Dashed horizontal lines indicate standard statistical thresholds for strong ($|r| \geq 0.8$) and moderate ($0.8 > |r| \geq 0.5$) correlations.

Multiple linear regression analysis was used to simultaneously investigate trends between multiple predictors and broadband RNL for each of the selected vessels. Forward step-wise regression was used for model development, as described in Section 4.1.4. A final set of statistically significant predictors were obtained for each vessel (Tables 8 and 9). The final set of model coefficients was different for each vessel, although the number of significant predictors was no more than three. The analyses led to the following results:

- For Bulk Carrier A, the best-fit model had only STW as a significant predictor (Figure 43). It is important to note, however, that draft had a strong negative correlation with STW for this vessel (see Figure 40), and thus STW and draft together were not both significant (draft alone was less significant than STW alone). The r^2 was smallest for this vessel, despite having the greatest number of measurements. This indicates that RNL measurements for this vessel had a large random component, which could not be explained by the available predictor variables.
- For Container Ship A, the best-fit model included shaft-rate RPM, slip ratio, and cargo weight (Figure 44). Shaft rate RPM and slip ratio both had positive trends with RNL. Surprisingly, cargo weight had a negative trend with RNL although this may be because cargo weight was also negatively correlated with STW (see Appendix E.1.1). Draft was not significant, but this may be because the data for this vessel only encompassed a narrow range of drafts (see Figure 41). This was the only vessel where the best-fit model included shaft rate RPM rather than STW, but it is interesting to note that this vessel also had by far the strongest correlation between shaft-rate RPM and STW (see Figure 41).
- For General Cargo Vessel A, which had the fewest measurements, the best-fit model included speed through water and actual draft (Figure 45). This is consistent with the trends identified in the data set as a whole by the Phase 1 study.

- For General Cargo Vessel B, the best-fit model included STW, actual draft, and drift angle. The influence of drift angle was smaller than the other two parameters, but nonetheless significant. The r^2 was greatest for this vessel and it had operational data for the fewest number of predictors.

The fact that these vessels all had different best-fit trends is likely a consequence of the opportunistic sampling inherent to the data sets under consideration. Nonetheless, the strong positive trends of RNL with STW (or a shaft rate strongly correlated with STW, in the case of Container Ship A) is consistent with other measurement studies conducted by the ECHO program (MacGillivray et al. 2019).

Table 8. Coefficients of the final multiple linear regression models for the selected vessels. Asterisks indicate the significance level (* = p < .05, ** = p < .01, *** = p < .001). Dashes indicate that the trend for the specified predictor was not statistically significant (i.e., p ≥ .05). NA indicates that the predictor was not available for the specified vessel.

Vessel	STW (knots)†	Actual Draft (m) †	Estimated RPM†	Absolute Drift Angle (deg)	Slip Ratio	Cargo Weight (tonnes)	Ballast Weight (tonnes)	Trim (m)	Constant Term (dB)
Bulk Carrier A	45.58**	–	–	–	–	–	–	NA	136.2***
Container Ship A	–	–	41.10***	–	16.33*	-8.77×10^{-5}*	–	–	123.5***
General Cargo Vessel A	47.20*	56.64**	–	–	NA	NA	NA	–	92.2**
General Cargo Vessel B	20.13**	41.25***	–	0.91*	NA	NA	NA	NA	126.2***

† A $\log_{10}$ transformation was applied to STW, actual draft, and estimated RPM when performing the multiple linear regression.

Table 9. Statistics for the multiple linear regression models in Table 8. The multiple r^2 is the fraction of the data variance explained by the model. The *p*-value is the probability that the observed trends would occur by chance. The residual standard error is the standard deviation of the model residuals. The *n* value was smaller than the total number of measurements in some instances because of missing values for some predictors (only complete cases could be used in the regression analysis). The 95% prediction interval corresponds to the 95% range of the predicted RNL values (median) and is a measure of the scatter of the data around the observed trend.

Vessel	*n* samples	Multiple r^2	*p*-value	Residual standard error (dB)	95% prediction interval (dB)
Bulk Carrier A	33	0.2684	0.00202	2.52	±5.25
Container Ship A	16	0.7388	0.000821	1.21	±2.91
General Cargo Vessel A	14	0.5761	0.00892	2.52	±6.01
General Cargo Vessel B	29	0.8103	3.538×10^{-9}	1.78	±3.88

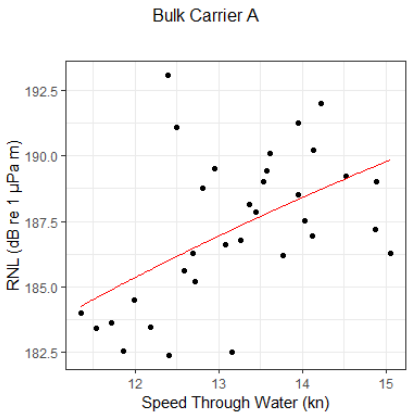

Figure 43. Partial regression plots for Bulk Carrier A derived from a multiple regression analysis (red line), along with the partial residuals (black dots) of the MSL data. In this case, STW was the only significant predictor variable. A steep slope in the multiple regression analysis (red lines) indicates a strong trend between the predictor variable and the RNL

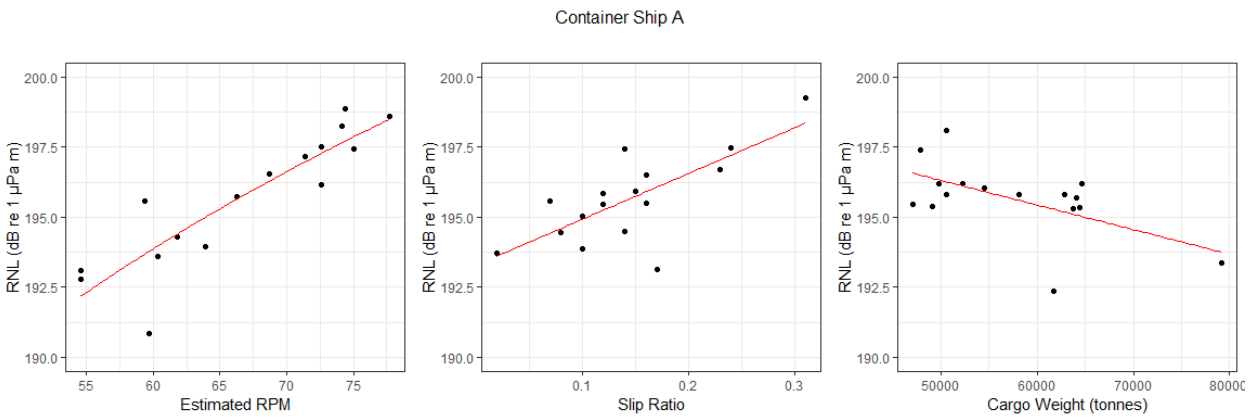

Figure 44. Partial regression plots for Container Ship A derived from a multiple regression analysis (red line), along with the partial residuals (black dots) of the MSL data. A steep slope in the multiple regression analysis (red lines) indicates a strong trend between the predictor variable and the RNL.

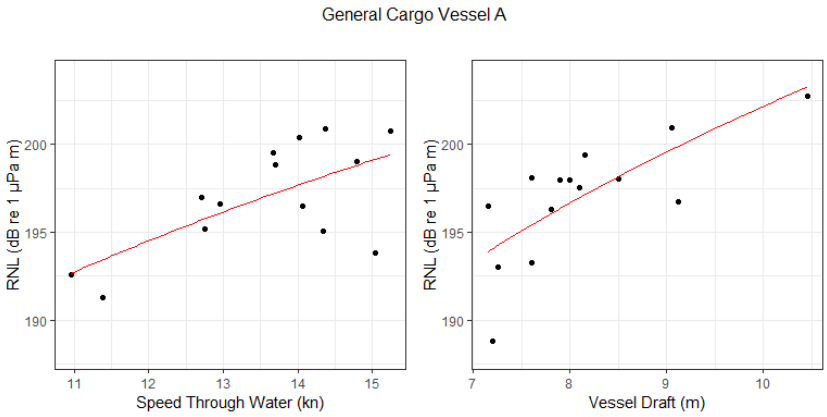

Figure 45. Partial regression plots for General Cargo Vessel A derived from a multiple regression analysis (red line), along with the partial residuals (black dots) of the RNL data. A steep slope in the multiple regression analysis (red lines) indicates a strong trend between the predictor variable and the RNL.

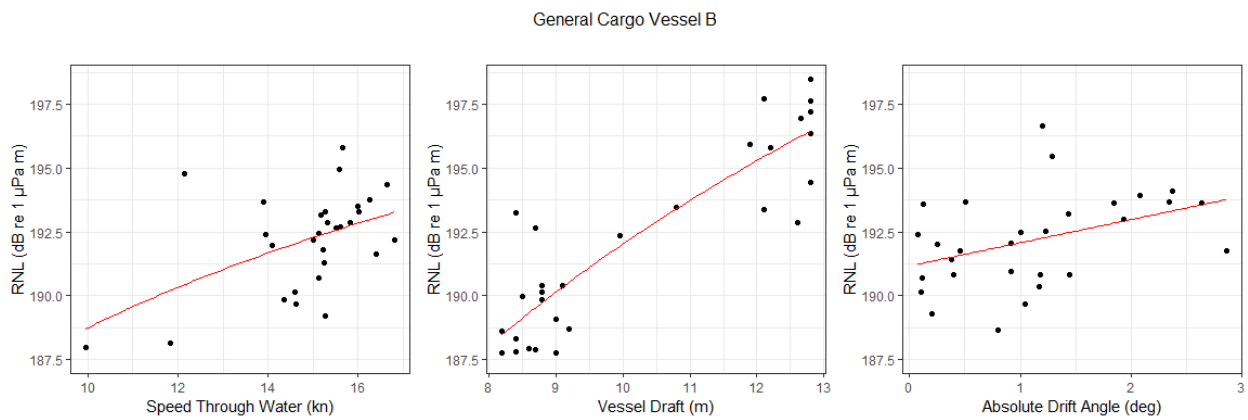

Figure 46. Partial regression plots for General Cargo Vessel B derived from a multiple regression analysis (red line), along with the partial residuals (black dots) of the RNL data. A steep slope in the multiple regression analysis (red lines) indicates a strong trend between the predictor variable and the RNL.

4.2.4. Fine-Scale Spectrum Analysis

Fine-scale spectra were evaluated for multiple runs of each of the four ships given in Table 5. As noted above there were three different underwater sound data sets as a function of frequency. The first is the decidecade data as evaluated above and documented in Figures 39 and 38. The other two were underwater Power Spectral Density (PSD) data in 1 Hz (standard) resolution and 0.125 Hz (high) resolution. These two latter data sets are examined in this section.

One of the elements to evaluate is the contribution of tonal ship sound from two primary sources: the propeller and the main propulsion engine. The propeller produces two types of underwater sound: low frequency tonal sounds and broadband cavitation sound. More specifically, the low frequency tonal sound can be identified in the noise spectrum at the blade rate primary frequency (1 x BR) and its harmonics (n × BR). These frequencies are computed according to Equation (4). The blade rate frequency is a function the number of propeller blades and the engine rotation speed (RPM). The amplitude of the blade rate frequency is a complex acoustic phenomenon dependent on many factors. The reader is directed to references such as Ross (1987) for a more in-depth discussion of the interrelationships. The propeller spectrum is associated with a low frequency hump, noted below, and also higher frequency propeller cavitation. Because there is no specific tonal frequency associated with broadband sounds (i.e., as provided by equations (4) through (6)), they are not so easily attributed to a specific source.

The main propulsion engine also produces two significant sounds both associated with the motion and firing of the diesel engine. Sound occurs at the engine rotation rate (1 × RR) and the cylinder firing rate (1 × FR). Rotation rate frequency is defined in Equation (3) and the firing rate frequency is defined in Equation (5). Ross (1987) points out that one of the primary diesel engine sounds is piston slap which occurs at rotation rate and firing rate frequencies. For any of the vessels' data sets, the rotation rate (1 x RR) and firing rate (1 x FR) will induce tonal sounds along with their harmonics (n x RR and n x FR). However, when there are significant defects (bent shaft, engine misfire) you can see extreme levels of such tonal sounds. Finally, tonal sound and harmonics can be generated by any other mechanical devices within the vessel, such as pumps, bearings, air compressors, and fans whose frequencies were not examined within this study.

Table 10 provides a computation of the forcing frequencies mentioned above at the nominal engine speed. However, each vessel's measurement run has an associated engine rotation speed, evaluated using the dual-band RPM analysis described in section 4.1.2, which is the speed used in computation of the forcing frequencies for this evaluation.

There are other sources of tonal sound from a ship including: mechanical unbalance, electromagnetic forces, gears noise, bearing noise, and vortex shedding. Unbalance sound would occur at the primary rotation rate (1 × RR) frequency. Electromagnetic sound occurs at the electrical line frequencies and harmonics: 60, 120 and 180 Hz. Tonal sound from gearboxes is usually at the gear-mesh frequency (rotation rate time the number of gears on that shaft). Since all of the vessels evaluated utilized a direct-drive, low-frequency diesel engine without a reduction gearbox, this noise type was not present in this evaluation. Tonal sound from bearings is possible and can be computed using equations provided in Harris (1991), given the details of the bearing type and internal geometry. Lastly, vortex shedding is a type of flow noise resulting in tonal sound. It occurs when there is a coincidence between structural resonances and the Strouhal Frequency (F_S) which is a function of appendage speed through the water and cross-sectional thickness as given in Ross (1987).

Table 10. Nominal ship forcing frequencies, as calculated from Equations (3)-(5).

Anonymized Name	Bulk Carrier A	Gen. Cargo Vessel A	Gen. Cargo Vessel B	Container Ship A
Nominal RPM	102	105	105	91
1 x RR, Hz	*1.7*	*1.8*	*1.8*	*1.5*
Blade Count	**4**	**4**	**5**	**6**
1 x BR, Hz	*6.8*	*7.0*	*8.8*	*9.1*
2 x BR, Hz	*13.6*	*14.0*	*17.5*	*18.2*
No. Cylinders	**6**	**5**	**5**	**10**
Stroke	**2**	**2**	**2**	**2**
1 x FR, Hz	*10.2*	*8.8*	*8.8*	*15.2*
2 x FR, Hz	*20.4*	*17.6*	*17.6*	*30.4*

The standard and high-resolution spectrum data for each of the four vessels given in Table 5 was evaluated and observations regarding interesting spectral characteristics are as follows.

4.2.4.1. Bulk Carrier A

Figure 47 shows three spectra from this vessel (Series 1, 2 & 3)[5] measured between February and September 2016. The ship speed through water ranged between 12.4 and 14 knots with engine speed determined using the dual-band RPM detector between 90 and 94 rpm. The figure is zoomed into a frequency range of 0–50 Hz as the original data set was from 0–500 Hz. At an average speed of 92 rpm, the blade rate with a 4 bladed propeller is 6.1 Hz. The firing rate with a 6 cylinder engine is 9.2 Hz. The primary blade rate and firing rate frequencies are identified in Figure 47. Each tone shows slight variation between the three sets of data. Rotation rate (1 x RR) is 1.5 Hz and the signal at that frequency is relatively low and muddled. However, harmonics of rotation rate, which include both blade rate (4 × RR) and firing rate (6 × RR) among others, are clearly marked in figures 34 and 35. Also, this data shows a 10 dB higher sound level from first harmonic of firing rate than the first harmonic of blade rate. The highest single forcing frequency is the 5th harmonic of blade rate (5 × BR) which is the same exact frequency for all three series. The 6th harmonic of blade rate coincides with the 4th harmonic of firing rate, yet that forcing frequency is not distinguishable for this vessel[6].

Figure 48 shows one sample spectra (Series 31) out to the full frequency range of 500 Hz. It was measured on November 3, 2019. The spectra clearly show multiple blade rate harmonics (2 × BR, 4 × BR and 10 × BR). It also shows the sixth firing rate harmonics (6 x FR) among other rotation rate harmonics

[5] A series refers to the spectrum from a single (anonymized) PSD versus frequency measurement, as identified in the figures in this section.
[6] Such an occurrence may indicate a phase cancelation of the two tonal sounds, but such an occurrence would be random and unusual.

which are clearly identifiable in this spectrum. The second blade rate harmonic (2 × BR) has the largest signal-to-noise ratio and the forcing frequencies in the 50 to 60 Hz low-frequency hump are the highest in amplitude.

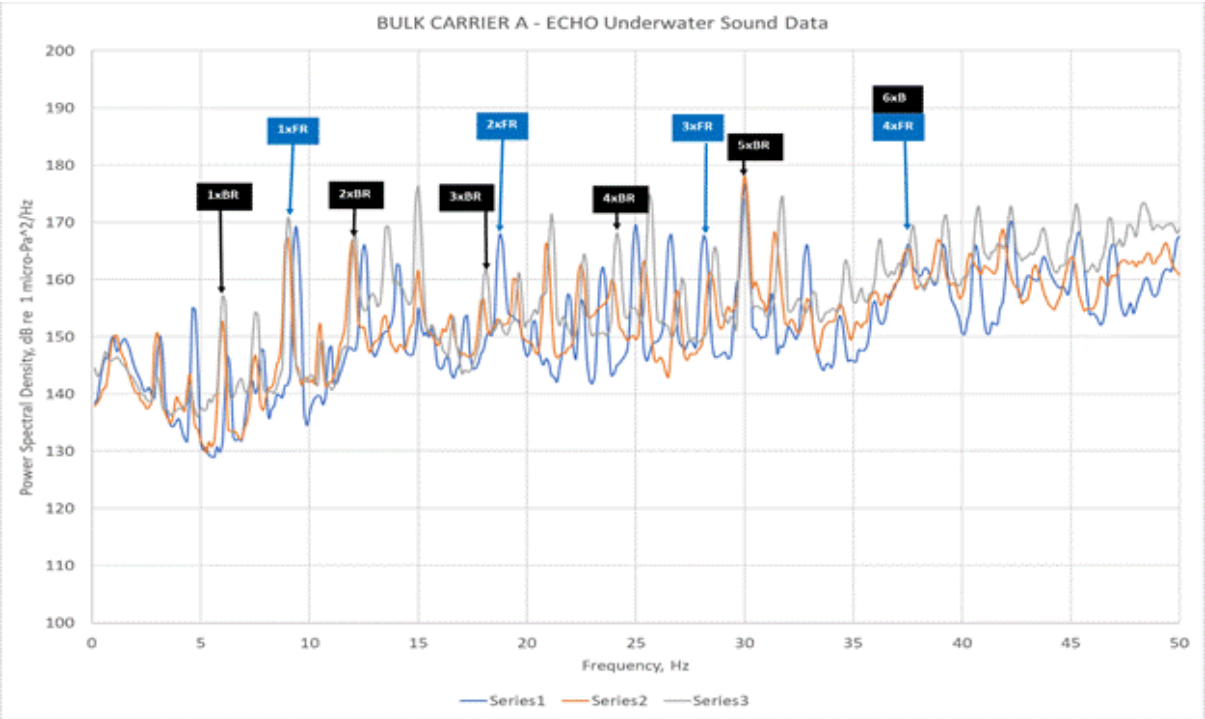

Figure 47. Bulk Carrier A - High Resolution PSD data showing both blade rate and firing rate harmonics.

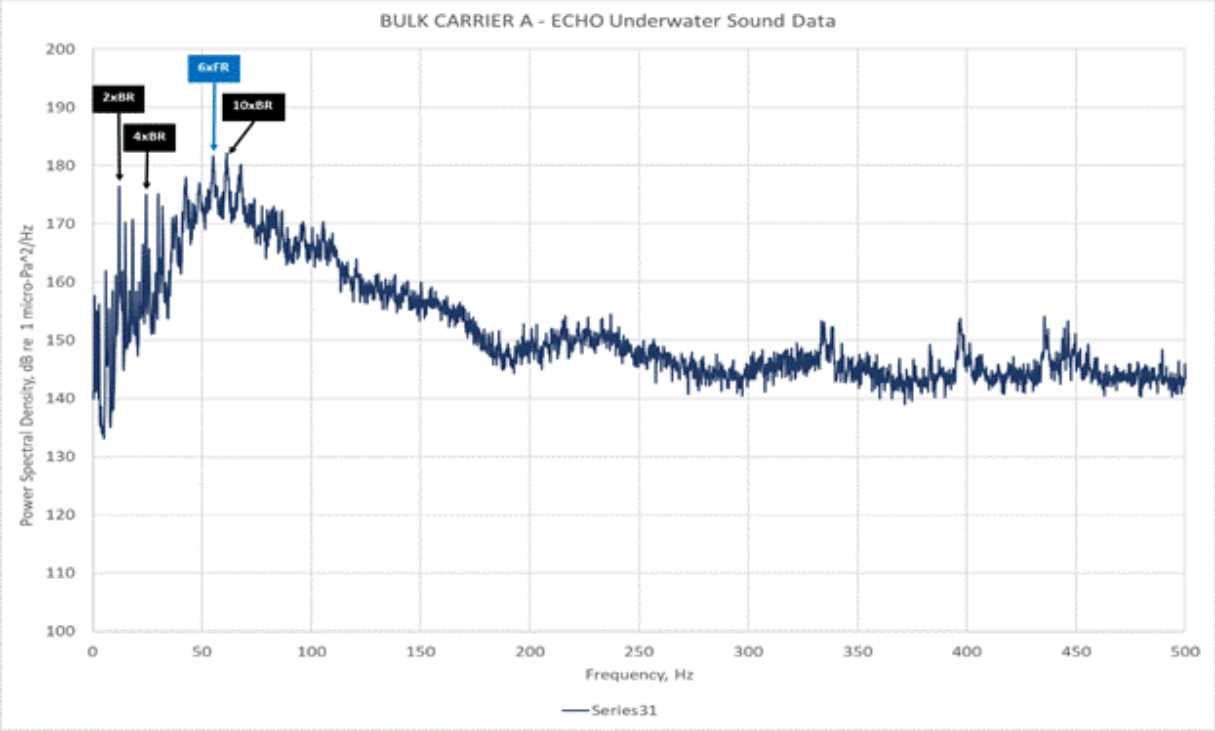

Figure 48. Bulk Carrier A - High Resolution PSD data showing blade rate and firing rate forcing frequencies

4.2.4.2. General Cargo Vessel A

This vessel's spectra demonstrate a situation similar to Bulk Carrier A. The spectrum in green (Series 6) was measured on November 19, 2018 and the spectrum in blue (Series 7) was measured just three days later, on November 21, 2018. General Cargo Vessel A, Figure 49 shows a 25 dB increase in sound at the firing rate frequency (1 x FR) as opposed to the 10 dB increase in sound seen at the firing rate harmonic (1 x FR) seen in Bulk Carrier A. The dual-band RPM detector determined the engine speed to be 80.4 RPM, but this is consistent if the engine speed was actually 90 RPM. This is a difference of 12.5% which is within error margin of the RPM estimation (see Section 4.2.5).

Figure 49 shows very clearly the low frequency, broadband hump of acoustic energy characteristic of many cargo vessels below 100 Hz. In the case of General Cargo Vessel A, the broadband hump is shown to be centered at 40 Hz. A review of all nineteen spectra associated with General Cargo Vessel A show the same 40 Hz hump. The sound spectrum greater than 100 Hz is mostly flat and toneless. Figure 50 shows the full frequency spectrum for the same data sets and continued toneless spectra out to 20,000 Hz.

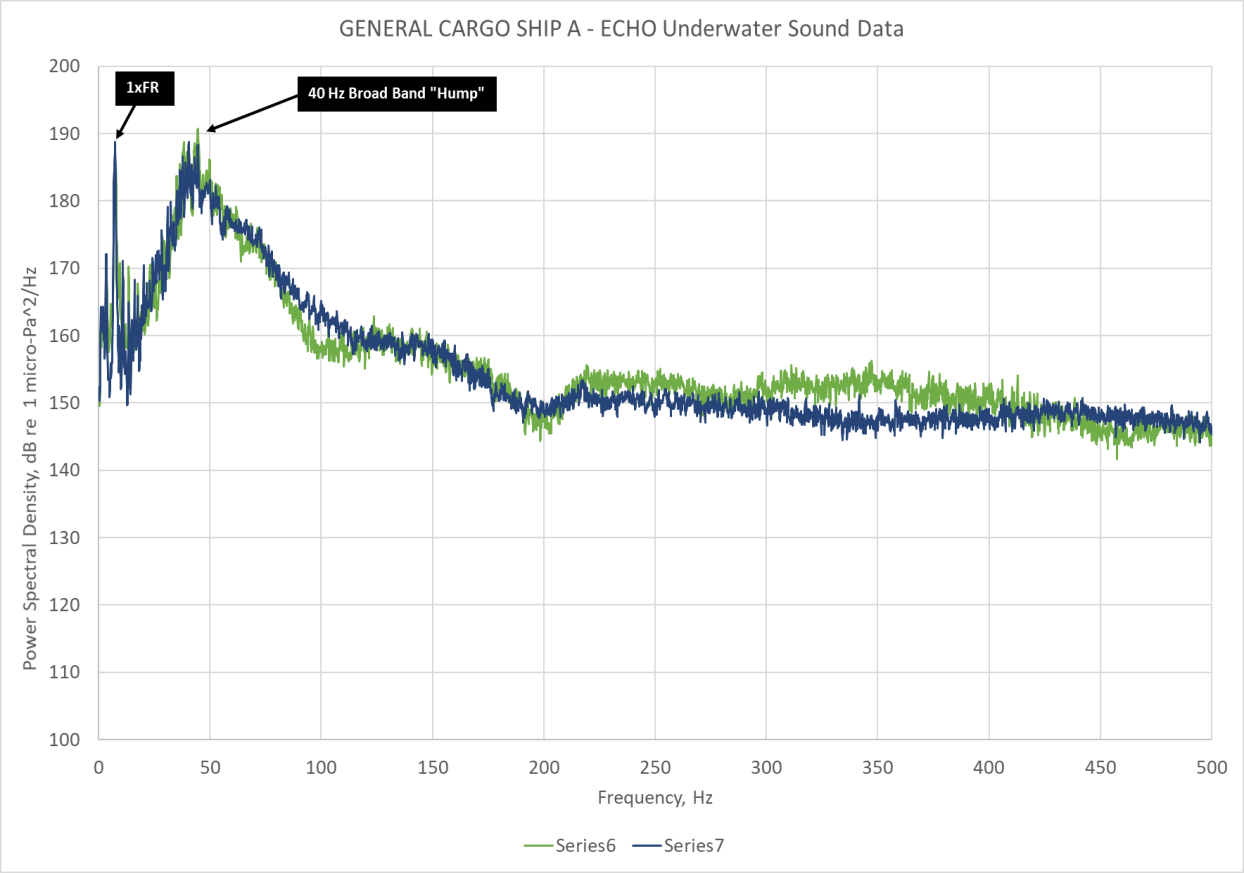

Figure 49. General Cargo A - High Resolution PSD data showing firing rate and broadband hump below 100 Hz.

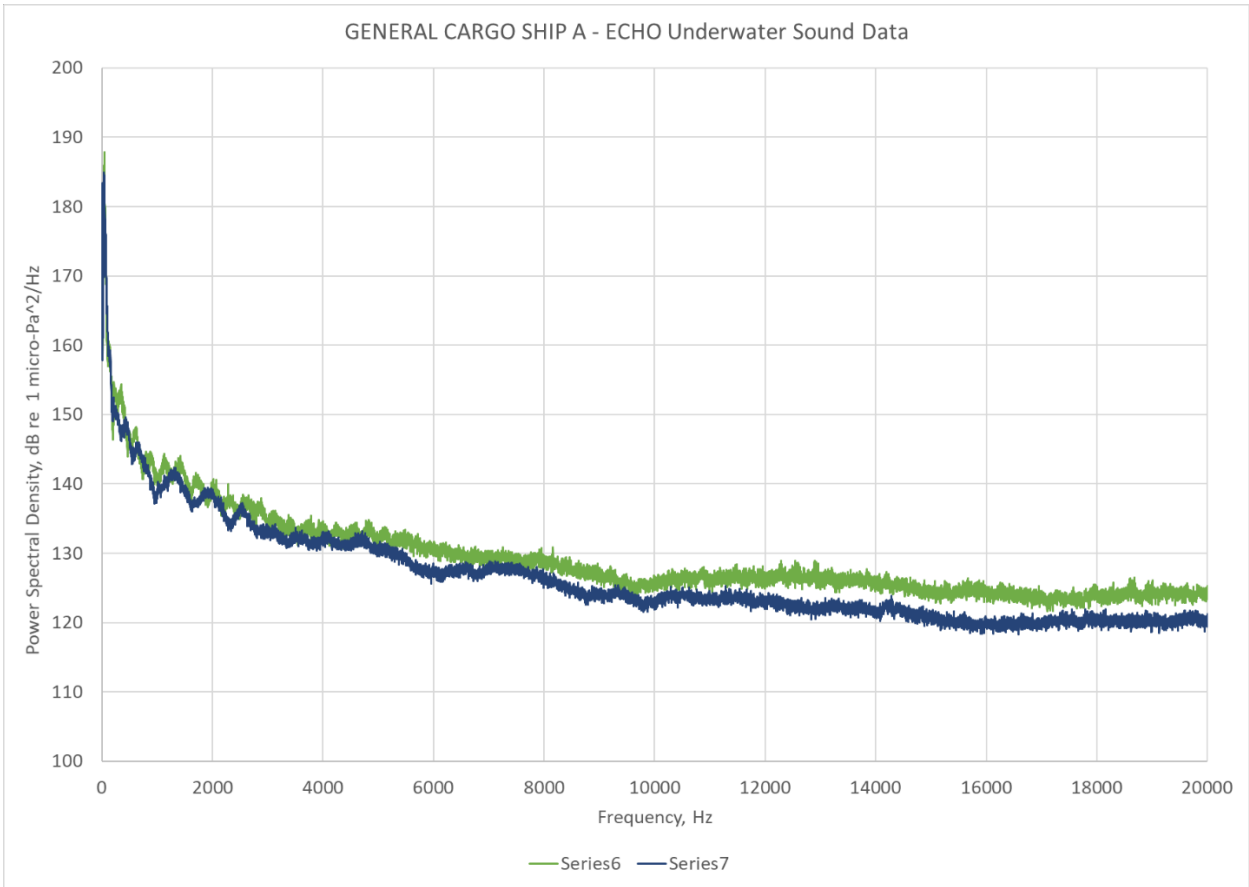

Figure 50. General Cargo A – Standard Resolution PSD data showing flat and toneless spectra.

4.2.4.3. General Cargo Vessel B

General Cargo Vessel B's spectra display extreme characteristics and a unique situation with respect to the blade rate and firing rate frequencies. General Cargo Vessel B has 5 propeller blades and 5 main engine cylinders as given in Table 5. This results in the vessel's blade rate and firing rating frequencies being equivalent.

Figure 51 shows three data sets from August 12, 2017 (Series 8), October 1, 2017 (Series 11), and November 2, 2018 (Series 18). The 1 × BR/FR tone is shown to be 20 dB higher for Series 18 than Series 8 or 11. Series 18 has the highest BR/FR tone of the 29 measurements.

Figure 51 also shows numerous tones above 100 Hz. There are two very sharp tones at 119 and 179 Hz. The source of these tones are likely harmonics from the electrical generation systems, which should be produced at 120 and 180 Hz. More notably, Figure 51 shows a combination of broadband and tonal sound centered at 285, 349/358 (dual peak) 445, and 483 Hz. The first three peaks are observed in Series 11 data set. The 349/358 and 445 Hz peaks are observed in Series 8. The Series 18 spectra only shows the 483 Hz peak. Further, these features generate 20 to 30 dB increases in the vessel's underwater noise at the noted frequencies. The standard frequency data shows toneless spectra at frequencies beyond 2,000 Hz.

These broadband peaks may be the result of a singing propeller blade. A singling propeller is a term used to describe trailing edge vortex shedding from the propeller that incites resonance in the propeller blade tip. General Cargo Vessel B has one propeller with five blades. It seems unlikely that five propeller blades will produce five widely different frequencies. Another source of some of these tones may be a shaft bearing defect. A short discussion on these two acoustic phenomena is given in Section 4.3.

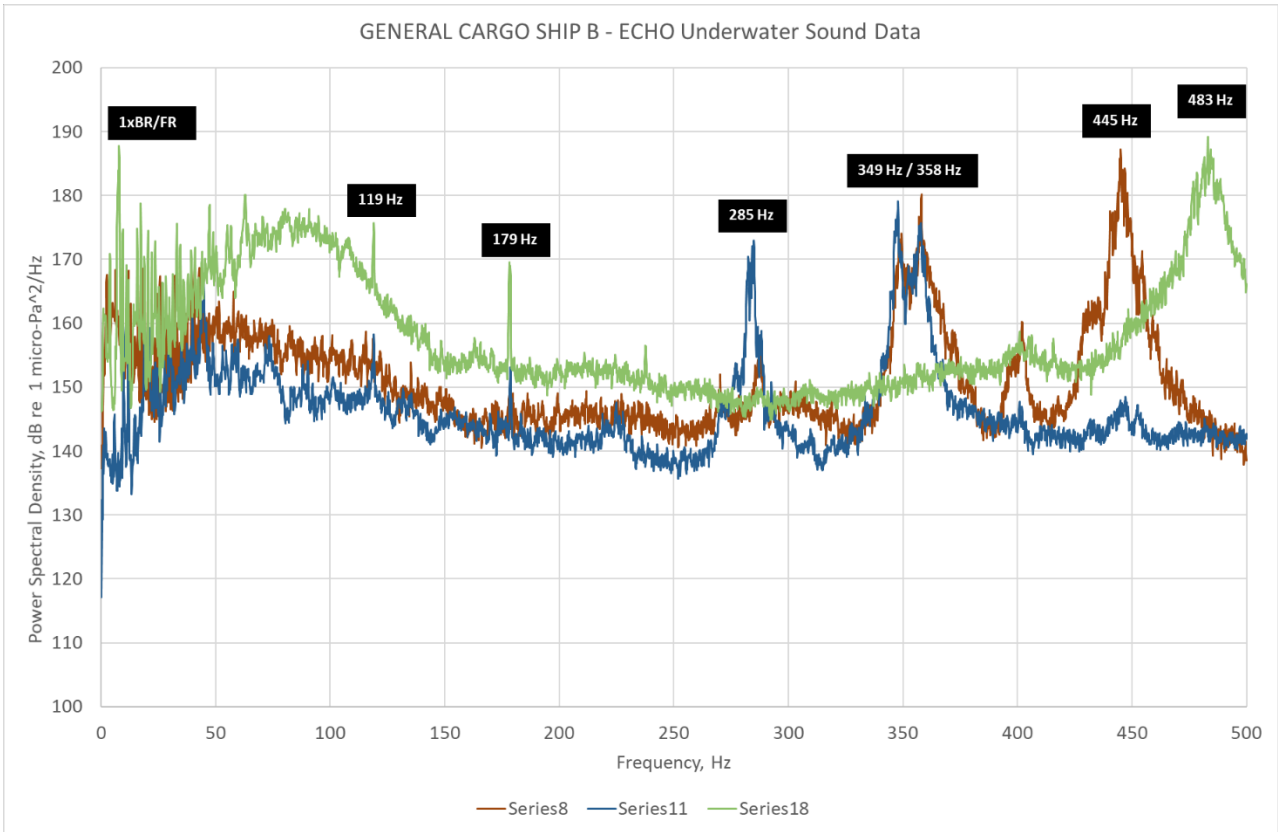

Figure 51. General Cargo B – High Resolution PSD data showing multiple tones.

4.2.4.4. Container Ship A

Container Ship A has spectra somewhat similar to General Cargo Vessel B and unique from other ships. Figure 52 shows three data sets with three different spectra. The first data set (Series 1) was measured on September 14, 2018 and exhibits a 30 dB peak centered at 232 Hz. Eleven of the other seventeen data sets display the same spectral characteristics. Series 10 measured on August 12, 2019 exhibits a 30 dB peak centered at 183 Hz. Series 11 was measured just 3 days later on August 15, 2019 and exhibits only 20 dB peaks at both 183 and 232 Hz.

The notable difference between Series 1 and Series 10 is speed. The events with the 183 Hz peak were present at vessel speeds through water which ranged from 14 to 16 knots (55-62 engine RPM). The events with the 232 Hz peak were present when the vessel had speeds through water that ranged from 17 to 20 knots (64 to 78 engine RPM). Series 11 which displayed both peaks had a vessel speed of 15 knots at 60 RPM. These characteristics point strongly to singing from either two different propeller blades or two different resonant modes of vibration within a single blade.

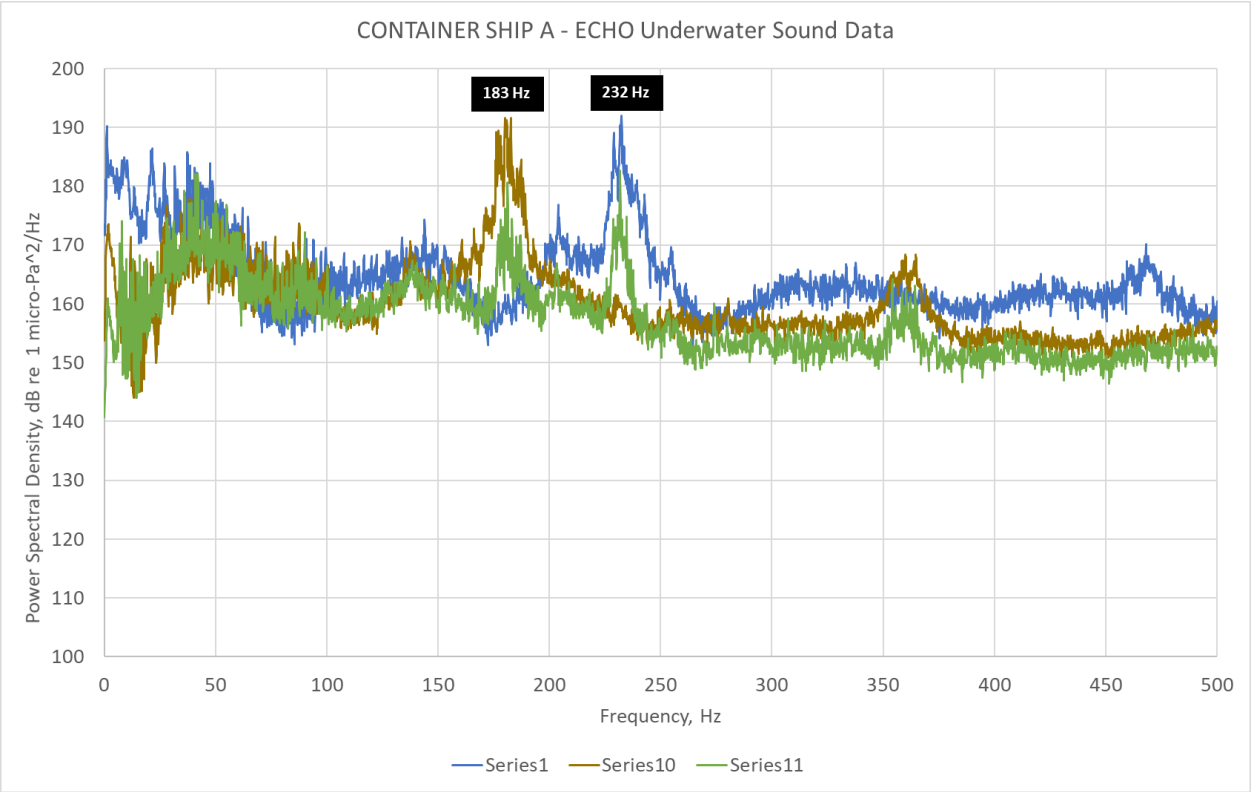

Figure 52. Container Ship A – High Resolution PSD data showing two broad peaks with dominant tonal frequencies identified.

4.2.5. Manual versus Automated RPM Estimation

All four ships were examined for the presence of three major ship generated forcing frequencies: (1) rotation rate, (2) blade rate and (3) firing rate. The determination of each forcing frequency and its harmonics are described in Section 4.1.6. Identification of each of these forcing frequencies for all four vessels is provided in the spectra analysis in section 4.2.4.1 to 4.2.4.4 above. These frequencies can be used to effectively determine the ship engine operating speed. This process can be done manually by visual inspection of PSD graphs or via software which is the methodology behind the dual-band RPM detector described in Section 4.1.2.

Using the manual PSD inspection method, the engine speed from the dual-band RPM detector was compared to manual computation (Figure 53). Two methods were used for the manual computation. One was to find a single significant tonal peak and calculate the engine speed, after properly identifying what engine order (or harmonic) the peak represents. The second method is to determine the difference between two successive peaks, both assumed to be rotation rate orders, (i.e., harmonics *n* and *n*+1) and use the frequency separation to determine the rotational rate. Figure 53 shows that the multiple peak method is much better at correlating to the estimated shaft rate. The single peak method provides a higher engine speed than determined by the dual-band RPM detector. The average difference between the manual and automated methods was 6%. There were three outliers in the data with differences as large as 50%, shown in Figure 53. The source of estimation error for the outliers in Figure 40 are unknown at this time.

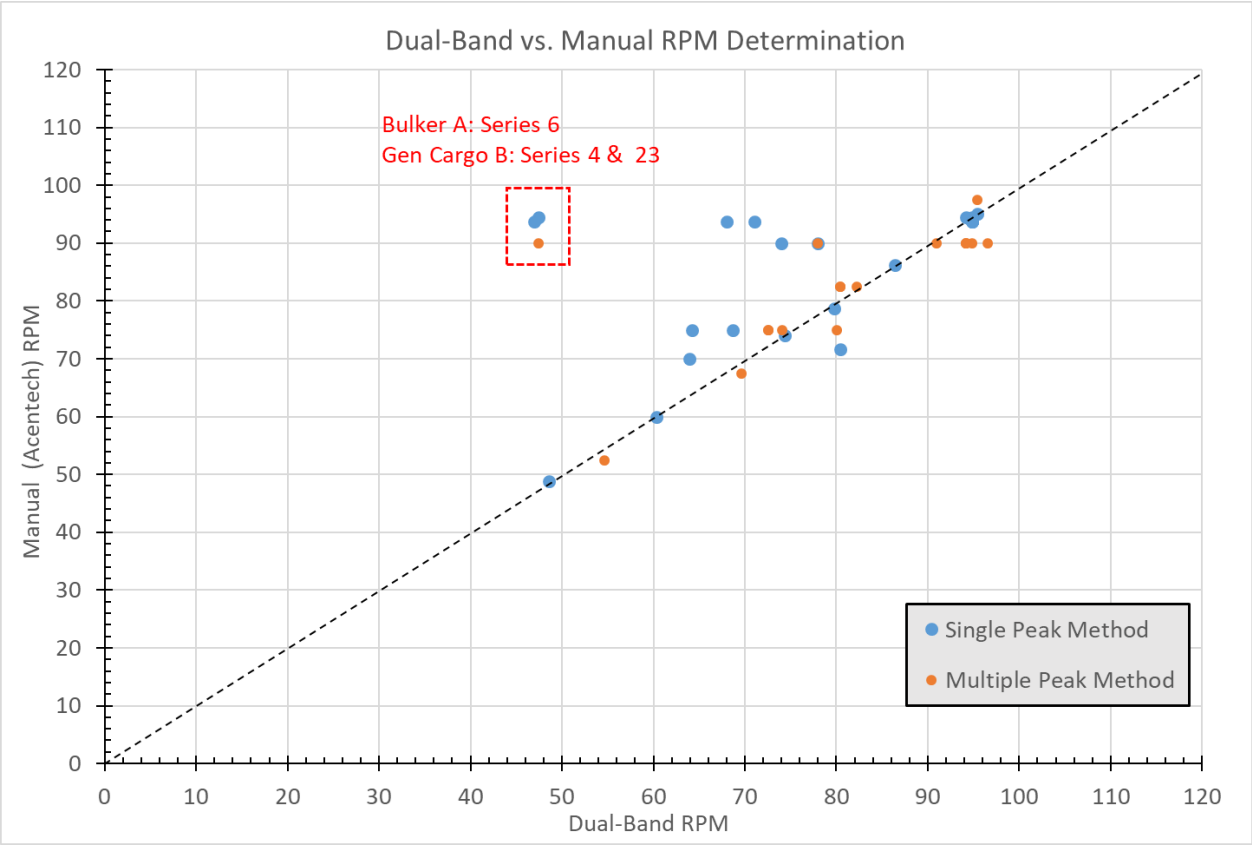

Figure 53. Dual-band RPM detector (automated) vs. manual engine RPM determination. The vessels and event series are identified for outlier data.

4.3. Discussion

4.3.1. Measurement Error and Uncertainties

The multiple linear regression analysis for the four selected vessels showed that the 95% prediction interval of the RNL trends was in the range ±2.9 to 6.0 dB (see Table 9). This means that, even after accounting for changes in RNL due to operating and measurement conditions, measurements of broadband RNL for the selected vessels was only repeatable to within an uncertainty of ±2.9 to 6.0 dB, 95% of the time. Some of the residual uncertainty is no doubt a consequence of the opportunistic nature of the sampling inherent to the ECHO data sets. Controlled measurement trials (i.e., following procedures published by standards bodies or registration societies) would be expected to yield more repeatable source level measurements. However, this also shows that any ranking of vessel noise emissions based on the ECHO data sets should account for the uncertainty inherent to the measurement procedures.

4.3.2. Spectrum Measurements

The review of the four vessels identified an acoustic feature characteristic common to cargo vessels. This is the low frequency broadband hump, below 100 Hz. This feature was prominent in the spectra of Bulk Carrier A and General Cargo Vessel A. It was less prominent in the spectra of General Cargo Vessel B and Container Ship A. For Bulk Carrier A the hump, when present, was centered around 80 Hz. Some measurement events did not show this hump characteristic. For General Cargo Vessel A, the hump was highly pronounced and centered at 40 Hz. Nearly all the measurement events showed this hump

characteristic. This feature is also readily identified in the decidecade data as shown in Figures 38 and 39.

This low frequency hump acoustic phenomena was described in Arveson and Vendittis (2000) and is attributed to cavitation. Arveson and Vendittis (2000) found 5 dB higher levels on the starboard side and attributed this to vortex shedding radiation relative to propeller configuration. Blake et al. (1988) defines the peak of the hump as frequency f_m and equates that to the following expression:

$$f_m = \frac{95}{C}\sqrt{\frac{\rho_o}{P}} \tag{6}$$

where, C is chord length at 90% propeller blade radius, ρ_0 is water density, and P is the ambient hydrostatic pressure.

A distinctive spectral feature was identified for two of the four selected vessels: Container Ship A and General Cargo Vessels B. These vessels were selected, in part, for their unique sound characteristics and it is not likely that half of all merchant ships have similar acoustic conditions. Both vessels have similar acoustic output, very high tonal energy with broad peaks, as discussed above. The cause of this high tonal output is theorized to be due to a singing propeller or (less likely) noise related to a faulty main shaft bearing. It is interesting to note that similar narrowband tones were observed in measurements of container vessels in Santa Barbara Channel by McKenna et al. (2013). The authors of the Santa Barbara Channel study indicated that these types of narrowband tones were present in approximately 10% of the vessels in their data set.

As given in Harris (1991) bearing noise occurs at non-integer orders of shaft operating speed. As the shaft speed changes the bearing frequency should follow linearly. The frequency of bearing faults will also depend on bearing type and physical attributes of the bearing. Thus, correctly identifying sounds as being generated by bearings requires detailed design information which was not available during this study. It is considered however, that bearing noise should display much finer peaks than found in the spectra for both vessels. Most importantly there was no indication of linear variation of engine speed with the center frequency of the peaks. Thus, it seems unlikely that these tones are the result of bearing noise.

According to Ross (1987), a signing propeller blade occurs when the Strouhal Frequency (F_S) or vortex shedding frequency equals a resonant mode of vibration for the propeller blade. F_S is a function of the linear speed that the propeller blade leading edge moves through the water and the cross-sectional width of the leading edge. Confirmation of the blade singing phenomenon requires detailed design information about a vessel's propeller. However, once the condition of singing occurs, the frequency (F_S) does not change with changes in a vessel's speed through the water or engine rotation speed. This fact points toward propeller singing as the likely cause of the strong peaks above 100 Hz descripted in section 4.2.4.3 and 4.2.4.4 for Container Ship A and General Cargo Vessel B, respectively.

5. Summary and Conclusions

The primary objective of Phase 2 of the ECHO Vessel Noise Correlations study was to improve upon the statistical significance and understanding of trends identified in Phase 1, through inclusion of approximately 17 months of new source level data from Boundary Pass. The objectives and findings of the three main tasks from the Phase 2 study may be summarized as follows:

Task 1. Functional Regression Model Validation

The objective of Task 1 was to use source level data from the Boundary Pass AMARs, from August 2018 to January 2020, first to test the statistical model from Phase 1, and then to update the model using the new data set. An initial exploratory analysis of the Boundary Pass (Phase 2) data set showed that distributions of some variables, such as speed and draft, were different due to changes in vessel operating conditions at the new ULS location. Furthermore, one of the vessel design characteristics (auxiliary engine power) was found to be reported in an inconsistent fashion by Lloyds List in the new data set. Nonetheless, validation testing showed that the Phase 1 model performed well on the Boundary Pass data set, as distributions of the residual errors in predicted source levels were consistent overall between the old and new data sets. Some minor outliers below 100 Hz were attributed to increased flow noise on the Boundary Pass hydrophones, due to the higher currents, and some minor outliers above 1000 Hz were attributed to the aforementioned inconsistencies in reported auxiliary engine power.

Based on the findings of the validation testing, an updated statistical model was created using the entire ECHO source level data set from September 2015 through January 2020. The new model, still based on the functional regression method, discarded auxiliary engine power as a predictor and introduced vessel age as a new predictor (retaining nine predictors in total). Furthermore, combined vessel categories that had been previously grouped together in Phase 1 (Containers & Vehicle Carriers, Bulkers & Tankers) were split apart to take advantage of the larger sample sizes from Boundary Pass.

Vessel speed and actual draft, the two main operational parameters, remained the most influential predictors of vessel source levels in each category. Rankings of influential design characteristics were similar, but not identical, to Phase 1:

- Vessel size (represented via length overall) was ranked as the design parameter with the strongest correlation to underwater radiated noise for Bulkers, Containers, and Tankers.
- Other parameters that were investigated (main engine RPM, main engine power, design speed, and vessel age) had weaker, but nonetheless statistically significant, correlations with underwater radiated noise. These correlations were, however, not generally consistent between vessel categories (see Table 4 for a summary). Differences from Phase 1 were mainly attributable to splitting of the previously combined vessel category groupings.
- Rankings could not be provided for Vehicle Carriers, because their design characteristics did not exhibit a sufficient range of variation after being split from Containers.
- Cruise vessels did not appear to exhibit significant trends with any design parameter, due to lack of sufficient data.

Depending on the frequency band and category, the updated functional regression model was generally able to explain 25-50% of the variance in the observed source level measurements in the ECHO data sets (this was similar to the Phase 1 functional regression model). The standard deviation of the residual model errors was 5.1 dB, when averaged over vessel category and frequency band. Finally, trends with greenhouse gas emissions intensity were weak and largely unchanged from Phase 1.

Task 2. Investigation of Additional Design and Operational Parameters

The objective of Task 2 was to investigate noise correlations using additional data on design and operational parameters that were not available during Phase 1. These additional data were provided by vessel owners and operators for 99 unique vessels (72 Bulkers and 27 Containers) in the ECHO data set. Potentially significant correlations were identified by examining trends in residual differences between

observed and predicted source levels that were unexplained by the updated functional regression model from Task 1.

Analysis of the Bulker data found that rudder bulbs, resiliently mounted generators, resiliently mounted engines and (possibly) installed fins were associated with lower residual source levels, whereas boss cap fins and bulbous bows were associated with higher residual source levels. These same characteristics could not be evaluated for Containers, due to lack of variation in their designs. Trends of residual source levels with number of propeller blades were different between Bulkers and Containers, but this was believed to be due to differences in the associated noise generating mechanisms: for Bulkers, propellers with fewer blades were associated with higher residual source levels, but only below 100 Hz (likely due to tonal blade rate noise); for Containers, propellers with fewer blades were associated with lower residual source levels, but only above 100 Hz (likely due to broadband cavitation noise). Otherwise, no clear trends were associated with other characteristics describing the propeller design (i.e., with skew, diameter, rake, and pitch). Some interesting trends were observed with operational parameters (vessel trim, drift angle, and slip ratio), but available data were somewhat limited. It should be emphasized that the trends identified in the Task 2 analysis were based on a limited subset of the ECHO data set and therefore may not be applicable to the data set as a whole.

Task 3. Analysis of Repeat Single-Vessel Measurements

The objective of Task 3 was to perform detailed analysis of repeat source level measurements, for four different (anonymized) vessels, to identify sources of radiated noise (via spectrum analysis) and to quantify uncertainties associated with repeat measurements. All vessels exhibited a positive trend of increasing broadband source level with speed through water, however the slope of the trend was different for each vessel (with power law coefficients ranging from 1.2-4.5). The measurements also had substantial scatter about the trend. To better control the measurements for changes in operational conditions, multiple linear regression was used to identify the statistical significance of RNL trends with up to eight different operational variables. Only variables that had significant trends with broadband RNL were retained in the multiple regression analysis, and the resulting best-fit models were different for each of the four vessels. The operational variables with significant trends for the four vessels were as follows:

- Bulk Carrier A: speed through water only;
- Container Ship A: shaft-rate RPM (estimated), slip ratio, and cargo weight;
- General Cargo Vessel A: speed through water, and actual draft;
- General Cargo Vessel B: speed through water, actual draft, and drift angle.

After detrending the data for differences in these operational conditions, measured RNL values for these four vessels were found to be repeatable to within an uncertainty of ±2.9–6.0 dB (95% prediction interval, per vessel).

Spectrum analysis identified propeller blade rotation (blade rate), cavitation, propeller singing, and engine firing rate as some of the dominant sources of radiated noise levels for these vessels. Noise levels for two of the vessels (Container Ship A and Cargo Vessel B) were dominated by strong tonal components in the frequency range 160–400 Hz. Furthermore, the frequencies of these tones apparently varied with shaft rate. While the root causes for these high amplitude sounds have not been confirmed, the best theory is a singing propeller for both Container Ship A and General Cargo Vessel B. It is unlikely that the vessel operators know their vessels are producing these sounds. These data show that propeller singing can generate very high levels of sound and increase radiated noise by as much as 30 dB, in the frequency range where it occurs, compared to similar vessels. Thus, eradicating propeller singing from deep-sea cargo vessels may have a substantial impact on lowering underwater sound levels from vessels.

List of Abbreviations and Symbols

ADCP	Acoustic Doppler Current Profiler
AIS	Automated Identification System
AMAR	Autonomous Multichannel Acoustic Recorder
ANSI	American National Standards Institute
ASA	Acoustical Society of America
BR	Blade Rate
CO_2	Carbon Dioxide
COG	Course Over Ground
CPA	Closest Point of Approach
dB	Decibels
DEMON	Detection of Envelope Modulation On Noise
ECHO	Enhancing Cetacean Habitat and Observation
EVDI	Existing Vessel Design Index
f	Frequency
FFT	Fast Fourier Transform
FR	Firing Rate
GHG	Greenhouse Gases
GT	Gross Tonnage
Hz	Hertz
ISO	International Standards Organization
kW	Kilowatts
LLI	Lloyds List International
LOA	Length Overall
MSL	Monopole Source Level
n	Number of measurements
NA	Not Available
PL	Propagation Loss
PPA	Pacific Pilotage Association
PSD	Power Spectrum Density
r^2	Coefficient of Determination
RNL	Radiated Noise Level
RPM	Revolutions Per Minute
RR	Rotation Rate
SNR	Signal-to-Noise Ratio
SPL	Sound Pressure Level
STW	Speed Through Water
ULS	Underwater Listening Station

VFPA	Vancouver Fraser Port Authority
β(f)	Regression coefficient function at frequency f.

Glossary

1/3-octave
One third of an octave. Note: A one-third octave is approximately equal to one decidecade (1/3 oct ≈ 1.003 ddec; ISO 2017).

1/3-octave-band
Frequency band whose bandwidth is one one-third octave. Note: The bandwidth of a one-third octave-band increases with increasing centre frequency.

absorption
The reduction of acoustic pressure amplitude due to acoustic particle motion energy converting to heat in the propagation medium.

Acoustic Current Doppler Profiler (ADCP)
An active sonar system for measuring ocean currents, much like the weather Doppler systems used to map atmospheric winds and rain. It consists of multiple acoustic transducers projecting upwards into the water column. It can measure the currents at many depths, thus providing a profile of the ocean currents.

ambient noise
All-encompassing sound at a given place, usually a composite of sound from many sources near and far (ANSI S1.1-1994 R2004), e.g., shipping vessels, seismic activity, precipitation, sea ice movement, wave action, and biological activity.

automated identification system (AIS)
A radio-based tracking system whereby vessels regularly broadcast their identity, location, speed, heading, dimensions, class, and other information to nearby receivers.

background noise
Total of all sources of interference in a system used for the production, detection, measurement, or recording of a signal, independent of the presence of the signal (ANSI S1.1-1994 R2004). Ambient noise detected, measured, or recorded with a signal is part of the background noise.

bandwidth
The range of frequencies over which a sound occurs. Broadband refers to a source that produces sound over a broad range of frequencies (e.g., seismic airguns, vessels) whereas narrowband sources produce sounds over a narrow frequency range (e.g., sonar) (ANSI/ASA S1.13-2005 R2010).

beta coefficient
The effect of a predictor variable (X) on a response variable (Y), often referred to as the slope of the trend between X and Y for continuous X, estimated using linear regression. See regression coefficient function.

blade rate (BR)
Also called the blade passing rate, this is equal to the rotation rate of the propeller times the number of blades. Vessel tonal noise is typically generated at the blade rate and its harmonics.

box-and-whisker plot
A plot that illustrates the centre, spread, and overall range of data from a visual 5-number summary. The ends of the box are the upper and lower quartiles (25th and 75th percentiles). The horizontal line inside the box is the median (50th percentile). The whiskers and points extend outside the box to the highest and lowest observations, where the points correspond to outlier observations (i.e., observations that fall more than 1.5 × IQR beyond the upper and lower quartiles, where IQR is the interquartile range).

broadband sound level
The total sound pressure level measured over a specified frequency range. If the frequency range is unspecified, it refers to the entire measured frequency range.

cavitation
A rapid formation and collapse of vapor cavities (i.e., bubbles or voids) in water, most often caused by a rapid change in pressure. Fast-spinning vessel propellers typically cause cavitation, which creates a lot of noise.

coefficient of determination (r^2)
A dimensionless number, in the range 0–1, that indicates the strength of correlation between two variables (0 = no correlation, 1 = perfect correlation). This is also the fraction of the data variance explained by a statistical model.

correlation coefficient
A dimensionless number, r, in the range $-1 < r < 1$, that indicates the strength of linear correlation between two variables. Positive r-values indicate a positive relationship between two parameters and negative r-values indicate a negative relationship between two parameters.

decade
Logarithmic frequency interval whose upper bound is ten times larger than its lower bound (ISO 2006).

decidecade
One tenth of a decade (ISO 2017). Note: An alternative name for decidecade (symbol ddec) is “one-tenth decade”. A decidecade is approximately equal to one third of an octave (1 ddec ≈ 0.3322 oct) and for this reason is sometimes referred to as a “one-third octave”.

decidecade band
Frequency band whose bandwidth is one decidecade. Note: The bandwidth of a decidecade band increases with increasing centre frequency.

decibel (dB)
One-tenth of a bel. Unit of level when the base of the logarithm is the tenth root of ten, and the quantities concerned are proportional to power (ANSI S1.1-1994 R2004).

Detection of Envelope Modulation on Noise (DEMON)
A method for acoustically calculating the rotation rate of a vessel's propeller by analyzing the modulation of its cavitation noise spectrum.

EVDI
Existing Vessel Design Index.

far-field
The zone where, to an observer, sound originating from an array of sources (or a spatially distributed source) appears to radiate from a single point. The distance to the acoustic far-field increases with frequency.

fast Fourier transform (FFT)
A computationally efficiently algorithm for computing the discrete Fourier transform.

firing rate (FR)
Also called the cylinder firing rate, this is the rate at which the pistons fire in a reciprocating engine. Vessel noise is typically generated at the firing rate and its harmonics.

functional regression
A type of linear regression that assumes the response variable is a smoothly varying function of some variable *f* (i.e. frequency). Each observation in functional regression consists of a curve *y*(*f*), whereas in linear regression each observation corresponds to a single response value y.

frequency
The rate of oscillation of a periodic function measured in cycles-per-unit-time. The reciprocal of the period. Unit: hertz (Hz). Symbol: *f*. 1 Hz is equal to 1 cycle per second.

harmonic
A sinusoidal sound component that has a frequency that is an integer multiple of the frequency of a sound to which it is related. For example, the second harmonic of a sound has a frequency that is double the fundamental frequency of the sound.

hertz (Hz)
A unit of frequency defined as one cycle per second.

hydrophone
An underwater sound pressure transducer. A passive electronic device for recording or listening to underwater sound.

imputation
The process whereby missing data associated with an observation or measurement is estimated based on known data values for similar measurements.

linear regression
A statistical method that quantifies the relationship between a dependent variable and one or more explanatory variables. Linear regression involving more than one explanatory variable is referred to as multiple linear regression.

LLI
Lloyd List International

mean-square sound pressure spectral density
Distribution as a function of frequency of the mean-square sound pressure per unit bandwidth (usually 1 Hz) of a sound having a continuous spectrum (ANSI S1.1-1994 R2004). Unit: $\mu Pa^2/Hz$.

median
The 50th percentile of a statistical distribution.

monopole source level (MSL)
A source level that has been calculated using an acoustic model that accounts for the effect of the sea-surface and seabed on sound propagation, assuming a point-like (monopole) sound source. See related term: radiated noise level.

octave
The interval between a sound and another sound with double or half the frequency. For example, one octave above 200 Hz is 400 Hz, and one octave below 200 Hz is 100 Hz.

parabolic equation method
A computationally efficient solution to the acoustic wave equation that is used to model propagation loss. The parabolic equation approximation omits effects of back-scattered sound, simplifying the computation of propagation loss. The effect of back-scattered sound is negligible for most ocean-acoustic propagation problems.

point source
A source that radiates sound as if from a single point (ANSI S1.1-1994 R2004).

power spectrum density
Generic term, formally defined as power in W/Hz, but sometimes loosely used to refer to the spectral density of other parameters such as square pressure or time-integrated square pressure.

PPA
Pacific Pilotage Authority

pressure, acoustic
The deviation from the ambient hydrostatic pressure caused by a sound wave. Also called overpressure. Unit: pascal (Pa). Symbol: *p*.

pressure, hydrostatic
The pressure at any given depth in a static liquid that is the result of the weight of the liquid acting on a unit area at that depth, plus any pressure acting on the surface of the liquid. Unit: pascal (Pa).

principal components analysis (PCA)
PCA is a commonly used data reduction and interpretation technique. It takes high dimensional data (many variables) and projects them onto a smaller, more manageable space for analysis and visualization.

propagation loss (PL)
The decibel reduction in sound level between two stated points that results from sound spreading away from an acoustic source subject to the influence of the surrounding environment. Also referred to as transmission loss.

radiated noise level (RNL)
A source level that has been calculated assuming sound pressure decays geometrically with distance from the source, with no influence of the sea-surface and seabed. See related term: monopole source level.

received level (RL)
The sound level measured (or that would be measured) at a defined location.

regression coefficient function ($\beta(f)$)
A smooth function describing the frequency-dependent slope of the trend between a continuous predictor variable (X) and a response variable (Y), as estimated using functional regression.

slip ratio
The percent difference between actual and idealized speed of advance of a propeller through water.

sound
A time-varying pressure disturbance generated by mechanical vibration waves travelling through a fluid medium such as air or water.

sound pressure level (SPL)
The decibel ratio of the time-mean-square sound pressure, in a stated frequency band, to the square of the reference sound pressure (ANSI S1.1-1994 R2004).

For sound in water, the reference sound pressure is one micropascal (p_0 = 1 µPa) and the unit for SPL is dB re 1 µPa^2:

$$L_p = 10\log_{10}\left({p^2}/{p_0^2}\right) = 20\log_{10}\left({p}/{p_0}\right)$$

Unless otherwise stated, SPL refers to the decibel level of the root-mean-square (rms) sound pressure.

source level (SL)
The sound level measured in the far-field and scaled back to a standard reference distance of 1 metre from the acoustic centre of the source. Unit: dB re 1 µPa·m (pressure level) or dB re 1 µPa^2·s·m (exposure level).

spectral density level
The decibel level (10·log$_{10}$) of the spectral density of a given parameter such as SPL or SEL, for which the units are dB re 1 µPa^2/Hz and dB re 1 µPa^2·s/Hz, respectively.

spectrum
An acoustic signal represented in terms of its power, energy, mean-square sound pressure, or sound exposure distribution with frequency.

speed over ground (SOG)
The speed of a vessel relative to the surface of the earth.

speed through water (STW)
The speed of a vessel relative to the water.

tonal
A sharp peak in the noise spectrum, centred at specific frequency. The frequency of a tonal may be tied to the reciprocating or rotation rate of a specific piece of machinery, or to one of its resulting harmonics.

ULS
Underwater Listening Station.

VFPA
Vancouver Fraser Port Authority.

Literature Cited

[ISO] International Organization for Standardization. 2006. *ISO 80000-3:2006 Quantities and units – Part 3: Space and time*. https://www.iso.org/standard/31888.html.

[ISO] International Organization for Standardization. 2017. *ISO 18405:2017. Underwater acoustics – Terminology*. Geneva. https://www.iso.org/standard/62406.html.

[ISO] International Organization for Standardization. 2019. *ISO 17208-2:2019. Underwater acoustics – Quantities and procedures for description and measurement of underwater sound from ships – Part 1: Requirements for precision measurements in deep water used for comparison purposes*. https://www.iso.org/standard/62409.html.

Angadi, K., J. Wood, J. Turner, K. Palmer, and D. Tollit. 2020. *Burrard Inlet Underwater Noise Characterization: 2019 Final Report*. Technical report by SMRU Consulting North America for Vancouver Fraser Port Authority ECHO Program.

ANSI S1.1-1994. R2004. *American National Standard: Acoustical Terminology*. American National Standards Institute and Acoustical Society of America, NY, USA. https://webstore.ansi.org/Standards/ASA/ANSIS11994R2004.

ANSI/ASA S1.13-2005. R2010. *American National Standard: Measurement of Sound Pressure Levels in Air*. American National Standards Institute and Acoustical Society of America, NY, USA. https://webstore.ansi.org/Standards/ASA/ANSIASAS1132005R2010.

ANSI/ASA S12.64/Part 1. 2009. *American National Standard: Quantities and Procedures for Description and Measurement of Underwater Sound from Ships – Part 1: General Requirements*. American National Standards Institute and Acoustical Society of America, NY, USA. https://webstore.ansi.org/Standards/ASA/ANSIASAS12642009Part.

Arveson, P.T. and D.J. Vendittis. 2000. Radiated noise characteristics of a modern cargo ship. *Journal of the Acoustical Society of America* 107(1): 118-129. https://doi.org/10.1121/1.428344.

Blake, W.K., H. Hemingway, and T. Mathews. 1988. Two Phase Flow Noise. *Proceedings of NoiseCon 88*.

Chung, K.W., A. Sutin, A. Sedunov, and M. Bruno. 2011. DEMON Acoustic Ship Signature Measurements in an Urban Harbor. *Advances in Acoustics and Vibration*: 13. https://doi.org/10.1155/2011/952798.

Environment Canada. 2020. *Marine Weather* (webpage). https://weather.gc.ca/mainmenu/marine_menu_e.html.

Gassmann, M., S.M. Wiggins, and J.A. Hildebrand. 2017. Deep-water measurements of container ship radiated noise signatures and directionality. *Journal of the Acoustical Society of America* 142(3): 1563-1574. https://doi.org/10.1121/1.5001063.

Harris, C.M. 1991. *Handbook of Acoustical Measurements and Noise Control*. McGraw Hill.

JASCO Applied Sciences and SMRU Consulting. 2020. *ECHO Program 2019 Voluntary Vessel Slowdown Hydroacoustic Studies: Final Report*. Document Number 01994, Version 1.0. Technical report by JASCO Applied Sciences and SMRU Consulting for Vancouver Fraser Port Authority.

MacGillivray, A.O., Z. Li, D.E. Hannay, K.B. Trounce, and O. Robinson. 2019. Slowing deep-sea commercial vessels reduces underwater radiated noise. *Journal of the Acoustical Society of America* 146: 340-351. https://doi.org/10.1121/1.5116140.

MacGillivray, A.O., J. Ainsworth, H. Frouin-Mouy, J.N. Dolman, and M.A. Bahtiarian. 2020. *ECHO Vessel Noise Correlations Study: Final Report*. Document Number 02025, Version 2.0. Technical report by JASCO Applied Sciences, ERM, and Acentech for Vancouver Fraser Port Authority ECHO Program.

McKenna, M.F., D. Ross, S.M. Wiggins, and J.A. Hildebrand. 2012. Underwater radiated noise from modern commercial ships. *Journal of the Acoustical Society of America* 131(1): 92-103. https://doi.org/10.1121/1.3664100.

McKenna, M.F., S.M. Wiggins, and J.A. Hildebrand. 2013. Relationship between container ship underwater noise levels and ship design, operational and oceanographic conditions. *Scientific Reports* 3: 1760. https://doi.org/10.1038/srep01760.

Pollara, A., A. Sutin, and H. Salloum. 2017. Modulation of high frequency noise by engine tones of small boats. *Journal of the Acoustical Society of America* 142(1): EL30-EL34. https://doi.org/10.1121/1.4991345.

Quijano, J.E., C.E. Lumsden, Z. Li, and A.O. MacGillivray. 2020. Chapter 4. Vessel RPM Acoustic Validation. *In ECHO Program 2019 Voluntary Vessel Slowdown Hydroacoustic Studies: Final Report*. 01994, Version 1.0. Technical report by JASCO Applied Sciences and SMRU Consulting for Vancouver Fraser Port Authority.

Ross, D. 1987. *Mechanics of Underwater Noise*. Pergamon Press, NY, USA.

Appendix A. Description of Variables in Merged Databases

A.1. Task 1 Database

Table 11. Description of all the variables captured in the merged vessel noise database for Task 1.

Variable	Description	Data source	Variable type	Included in MVA	Units	Notes
measurementId	PortListen ID value for ECHO measurement. Unique for every measurement. Contains deployment ID of measuring station, MMSI of recorded vessel, and datetime of closest approach.	ECHO	Operational	Not Included		
stationId	ID of station where measurement was recorded	ECHO	Method	Not Included		
deploymentId	Deployment ID of hydrophone recorder.	ECHO	Method	Not Included		Unique for every hydrophone deployment
mmsi	Maritime Mobile Service Identity. A nine digit code used by AIS to identify vessels.	ECHO	Design	Not Included		
imo	IMO number. Seven digit number assigned to hull of ship. Generally given to ocean faring ships, so some port tugs do not have IMO numbers.	ECHO	Design	Not Included		
timestampCpa	Date and time of CPA of vessel to hydrophone, according to AIS.	ECHO	Operational	Not Included	Time (UTC)	
timestampAcousticCpa	Date and time of CPA of the vessel to hydrophone as determined by acoustic detector in PortListen.	ECHO	Operational	Not Included	Time (UTC)	
vesselName	Name of vessel.	ECHO	Design	Not Included		
vesselType	Numerical AIS code for vessel type. Codes are specific to vessel class and cargo it carries.	ECHO	Design	Not Included	Double digit code	
jascoVesselClass	Class of vessel, as determined from AIS and MarineTraffic.com, based on JASCO's naming scheme.	ECHO	Design	Not Included		Captured by category
shipLength	Length of vessel, from AIS.	ECHO	Design	Not Included	m	Superseded by Lloyd's
shipBreath	Breadth of vessel, from AIS (note typo in column name).	ECHO	Design	Not Included	m	Superseded by Lloyd's

staticDraught	Static draft of vessel from AIS. This draft of vessel while not underway.	ECHO	Design	Not Included	m	Instead use actualVesselDraft
actualVesselDraft	Actual vessel draft from PPA, AIS, and summer draft, in that order.	ECHO	Operational	Independent	m	
distanceAtCpa	Horizontal distance between vessel and hydrophone at CPA.	ECHO	Method	Not Included	m	Captured by surface.angle
sogMean	Mean speed over ground in measurement window from AIS. This is speed of vessel relative to surface of Earth.	ECHO	Operational	Not Included	knots	Captured by STW
cogMean	Mean course over ground in measurement window from AIS. Heading of vessel relative to earth's surface.	ECHO	Operational	Not Included	degrees	Captured by STW, wind.resistance
rotMean	Mean rate of turn of vessel through water in measurement window from AIS.	ECHO	Operational	Not Included	degrees/min	Limited by measurement QC
trueHeadingMean	Mean heading in measurement window, counterclockwise from True North from AIS.	ECHO	Operational	Not Included	degrees	Captured by STW
STW	Speed through water. Calculated from speed over ground, course over ground, current speed, and current direction. Previously referred to as "sow".	ECHO	Operational	Independent	knots	
qcStatus	Quality Check Status. Every measurement has been subjected to manual review. Invalid measurements may be rejected for various reasons.	ECHO	Method	Not Included		Only accepted measurements to be included in MVA
windSpeed	Wind speed at time of measurement from nearest met station.	ECHO	Operational	Not Included	knots	Captured by wind.resistance
windDirection	Direction of wind at time of measurement from nearest met station.	ECHO	Operational	Not Included	degrees	Captured by wind.resistance
currentSpeed	Speed of water current at time of measurement (measured or predicted, depending on location).	ECHO	Operational	Not Included	knots	Captured by STW
currentDirection	Direction of the water current (measured or predicted, depending on location).	ECHO	Operational	Not Included	degrees	Captured by STW
shaftRate	Rotational rate of vessel's propellers. Estimated based on DEMON algorithm.	ECHO	Operational	Not Included	RPM	Insufficient data
monopoleSourceDepth	Depth of representative monopole source for vessel. Taken to be half active draft of vessel reported over AIS.	ECHO	Operational	Not Included	m	Captured by draft
vesselDwt	Dead weight tonnage from AIS. Measure of weight of cargo ship can carry (not its own weight).	ECHO	Design	Not Included	tons	Superseded by Lloyd's

vesselYearBuilt	Year vessel was built, from AIS.	ECHO	Design	Not Included	years	Superseded by Lloyd's
category	ECHO vessel category.	ECHO	Design	Independent		To be verified against Lloyd's list type (TYPE.LLI)
kDWT	Kilo dead weight tonnage from AIS (DWT/1000).	ECHO	Design	Not Included	kilotons	Superseded by Lloyd's
stw.mps	Speed through water (MKS).	ECHO	Operational	Not Included	m/s	Captured by STW
sogMean.mps	Mean speed over ground (MKS).	ECHO	Operational	Not Included	m/s	Captured by STW
windSpeed.mps	Wind speed (MKS).	ECHO	Operational	Not Included	m/s	Captured by wind.resistance
surface.angle	Depression angle from vessel to hydrophone (calculated). Measured with respect to sea surface.	ECHO	Method	Independent	degrees	
hydrophone.depth	Depth of hydrophone below mean sea level.	ECHO	Method	Not Included	m	Captured by surface.angle
wind.resistance	Resistance on vessel due to wind. Calculated from windspeed, wind direction, speed over ground, and course over ground.	ECHO	Operational	Independent	m^2/s^2	
drift.angle	Difference between trueHeadingMean and cogMean.	ECHO	Operational	Independent		
vessel_age	Difference between timestampCpa and YEAR.OF.BUILD.LLI.	ECHO	Design	Independent	years	
Job.ID.PPA	Pilot job ID from PPA lots. Unique for each trip.	PPA	Operational	Not Included		
Vessel.PPA	Vessel name, according to PPA.	PPA	Design	Not Included		
DWT.PPA	Deadweight tonnage, according to PPA.	PPA	Design	Not Included	tons	Superseded by Lloyd's List
GRT.PPA	Gross tonnage, according to PPA.	PPA	Design	Not Included	tons	Superseded by Lloyd's List
LOA.PPA	Overall Length of vessel, according to PPA.	PPA	Design	Not Included	m	Superseded by Lloyd's List
Beam.PPA	Width at widest point of a vessel, according to PPA.	PPA	Design	Not Included	m	Superseded by Lloyd's List
S.Draft.PPA	Maximum Draft/draught of vessel, according to PPA.	PPA	Operational	Not Included	m	Superseded by Lloyd's List

Actual.Draft.PPA	Actual draft of vessel logged by pilot. Measured by pilot visually or with software.	PPA	Operational	Not Included	m	Not always equal to AIS draft (actualVesselDraft)
Type.PPA	Class of vessel, based on PPA's naming scheme.	PPA	Design	Not Included		To be verified against ECHO type (category)
PILOT_ECHO.PPA	Value stating whether vessel took part in ECHO slowdown trial.	PPA	Operational	Not Included		Not enough data
First.Pilot.StartBW.PPA	Time when pilot on vessel began their bridge watch.	PPA	Operational	Not Included	time (UTC)	
First.Pilot.StopBW.PPA	Time when pilot on vessel completed their bridge watch.	PPA	Operational	Not Included	time (UTC)	
VesselName.EVDI	Vessel name, from ECHO	EVDI	Design	Not Included		
VesselClass.EVDI	Vessel class, from ECHO	EVDI	Design	Not Included		
GHG.Rating	GHG Emissions Rating. Letter grade scale comparing CO_2 efficiency of vessels with similar size and type. Scale indicates number of standard deviations from mean score for vessel class. D is centre.	EVDI	Design	Independent		
EVDI	Existing Vessel Design Index. Measure of ship's CO_2 emissions.	EVDI	Design	Not Included	grams CO_2 per tonne nautical mile	Captured by GHG.Rating
vessel.ID.lloyds	Matching ID number in Lloyd's List database.	LLI	Design	Not Included		
IMO.LLI	IMO, according to Lloyd's List's database.	LLI	Design	Not Included		
MMSI.LLI	MMSI, according to Lloyd's List's database.	LLI	Design	Not Included		
TYPE.LLI	Lloyd's List code signifying vessel type.	LLI	Design	Independent		Subtype of Category
VESSEL.TYPE.LLI	Vessel type, according to Lloyd's List.	LLI	Design	Not Included		Unabbreviated TYPE.LLI
GROSS.LLI	Gross tonnage, according to Lloyd's List.	LLI	Design	Independent	tonnes	
DRAFT.LLI	Maximum Draft of vessel, according to Lloyd's List. Measured at Summer load lines.	LLI	Design	Independent	m	
LOA.LLI	Overall length of vessel, according to Lloyd's List.	LLI	Design	Independent	m	
YEAR.OF.BUILD.LLI	Year vessel was built, from Lloyd's List.	LLI	Design	Independent	years	
HULL.TYPE.LLI	Code signifying type of hull for vessel. Code is only indicated when hull differs from standard mono hull.	LLI	Design	Not Included		Insufficient data (blank entries not significant)

HULL.TYPE.DECODE.LLI	Text explaining HULL.TYPE column code. DS = Double Side, DH = Double Hull, DB = Double Bottom. DS, DB, and DH are typically for tankers.	LLI	Design	Not Included		Insufficient data
HULL.MATERIAL.LLI	Material vessel's hull is made from.	LLI	Design	Not Included		Insufficient data (all steel)
PROPULSION.TYPE.LLI	Type of propulsion used to move vessel.	LLI	Design	Not Included		Insufficient data (all motor, except for two LNG)
FO.Capacity.LLI	Fuel Oil Capacity. Measure of cubic metre capacity of fuel tanks in vessel.	LLI	Design	Independent	m^3	To be determined if 35% non-missing data is sufficient to impute remainder
SPEED.LLI	Maximum speed of vessel, according to Lloyd's List. Speed ship is designed to maintain, at summer load waterline at maximum propeller RPM.	LLI	Design	Independent	knots	May be combined with STW to calculate speed as % MCR
SPEED.TYPE.LLI	Acronyms denoting type of speed measured in SPEED.LLI. AS = Average Speed, DS = Design Speed, SS = Service Speed, and TS = Trial Speed.	LLI	Design	Not Included		Insufficient data
DISPLACEMENT.LLI	Maximum displacement of vessel, according to Lloyd's List. Measured at summer load line.	LLI	Design	Independent	tonnes	
BREADTH.MOULDED.LLI	Maximum breadth of vessel, measured at moulded line of frame.	LLI	Design	Independent	m	
MainEngine_Type.LLI	Engine type. DSE = Diesel Electric, DSL = Diesel, GST = Gas Turbine	LLI	Design	Independent		May only be possible to include for Cruise vessels
Main.Engine_Designer.LLI	Designer of engine installed in vessel.	LLI	Design	Not Included		May be included as independent factor
MainEngine_Designation.LLI	Designation code of engine	LLI	Design	Not Included		May be related to EVDI
MainEngines_No.LLI	Number of main engines in vessel.	LLI	Design	Independent		
MainEngine_kW.LLI	Maximum rated power output of main engines.	LLI	Design	Independent	kilowatts	
MainEngine_RPM.LLI	Maximum rated RPM of main engine.	LLI	Design	Independent		
MainEngine_Cylinders.LLI	Number of cylinders in main engine.	LLI	Design	Independent		
MainEngine_StrokeType.LLI	Number of strokes engine performs.	LLI	Design	Independent		

PropellerType.LLI	The type of propeller. Az = Azimuth Drive, CP = Controllable Pitch, DP = Directional Pitch, FP = Fixed Pitch, RP = Rudder Pitch, Z = Z type	LLI	Design	Independent		
No_of_propulsion_units.LLI	Number of propulsive engines. Corresponds to number of propellers.	LLI	Design	Independent		
AuxiliaryEngine_kW.LLI	Maximum rated power output of the auxiliary engines. This covariate was removed due to inconsistency in how this variable was calculated between Phases 1 and 2 data sets.	LLI	Design	Not Included	kilowatts	
TotalEngine_kW.LLI	Power output of combined main and auxiliary engines.	LLI	Design	Not Included	kilowatts	Equal to sum of Main and Aux engine kW
broadbandMsl	Broadband MSL of vessel measurement (20–63000 Hz).	ECHO	Operational	Dependent	dB re 1 µPa m	
broadbandRnl	Broadband RNL of vessel measurement (20–63000 Hz).	ECHO	Operational	Dependent	dB re 1 µPa m	
RNL_10Hz	RNL for 1/3-octave-band centred at 10 Hz.	ECHO	Operational	Dependent	dB re 1 µPa m	
RNL_13Hz	RNL for 1/3-octave-band centred at 13 Hz.	ECHO	Operational	Dependent	dB re 1 µPa m	
RNL_16Hz	RNL for 1/3-octave-band centred at 16 Hz.	ECHO	Operational	Dependent	dB re 1 µPa m	
RNL_20Hz	RNL for 1/3-octave-band centred at 20 Hz.	ECHO	Operational	Dependent	dB re 1 µPa m	
RNL_25Hz	RNL for 1/3-octave-band centred at 25 Hz.	ECHO	Operational	Dependent	dB re 1 µPa m	
RNL_31Hz	RNL for 1/3-octave-band centred at 31 Hz.	ECHO	Operational	Dependent	dB re 1 µPa m	
RNL_40Hz	RNL for 1/3-octave-band centred at 40 Hz.	ECHO	Operational	Dependent	dB re 1 µPa m	
RNL_50Hz	RNL for 1/3-octave-band centred at 50 Hz.	ECHO	Operational	Dependent	dB re 1 µPa m	
RNL_63Hz	RNL for 1/3-octave-band centred at 63 Hz.	ECHO	Operational	Dependent	dB re 1 µPa m	
RNL_80Hz	RNL for 1/3-octave-band centred at 80 Hz.	ECHO	Operational	Dependent	dB re 1 µPa m	

RNL_100Hz	RNL for 1/3-octave-band centred at 100 Hz.	ECHO	Operational	Dependent	dB re 1 µPa m	
RNL_125Hz	RNL for 1/3-octave-band centred at 125 Hz.	ECHO	Operational	Dependent	dB re 1 µPa m	
RNL_160Hz	Radiated noise level for the 1/3-octave-band centred at 160 Hz.	ECHO	Operational	Dependent	dB re 1 µPa m	
RNL_200Hz	RNL for 1/3-octave-band centred at 200 Hz.	ECHO	Operational	Dependent	dB re 1 µPa m	
RNL_250Hz	RNL for 1/3-octave-band centred at 250 Hz.	ECHO	Operational	Dependent	dB re 1 µPa m	
RNL_315Hz	RNL for 1/3-octave-band centred at 315 Hz.	ECHO	Operational	Dependent	dB re 1 µPa m	
RNL_400Hz	RNL for 1/3-octave-band centred at 400 Hz.	ECHO	Operational	Dependent	dB re 1 µPa m	
RNL_500Hz	RNL for 1/3-octave-band centred at 500 Hz.	ECHO	Operational	Dependent	dB re 1 µPa m	
RNL_630Hz	RNL for 1/3-octave-band centred at 630 Hz.	ECHO	Operational	Dependent	dB re 1 µPa m	
RNL_800Hz	RNL for 1/3-octave-band centred at 800 Hz.	ECHO	Operational	Dependent	dB re 1 µPa m	
RNL_1000Hz	RNL for 1/3-octave-band centred at 1000 Hz.	ECHO	Operational	Dependent	dB re 1 µPa m	
RNL_1250Hz	RNL for 1/3-octave-band centred at 1250 Hz.	ECHO	Operational	Dependent	dB re 1 µPa m	
RNL_1600Hz	RNL for 1/3-octave-band centred at 1600 Hz.	ECHO	Operational	Dependent	dB re 1 µPa m	
RNL_2000Hz	RNL for 1/3-octave-band centred at 2000 Hz.	ECHO	Operational	Dependent	dB re 1 µPa m	
RNL_2500Hz	RNL for 1/3-octave-band centred at 2500 Hz.	ECHO	Operational	Dependent	dB re 1 µPa m	
RNL_3150Hz	RNL for 1/3-octave-band centred at 3150 Hz.	ECHO	Operational	Dependent	dB re 1 µPa m	

RNL_4000Hz	RNL for 1/3-octave-band centred at 4000 Hz.	ECHO	Operational	Dependent	dB re 1 µPa m	
RNL_5000Hz	RNL for 1/3-octave-band centred at 5000 Hz.	ECHO	Operational	Dependent	dB re 1 µPa m	
RNL_6300Hz	RNL for 1/3-octave-band centred at 6300 Hz.	ECHO	Operational	Dependent	dB re 1 µPa m	
RNL_8000Hz	Radiated noise level for the 1/3-octave-band centred at 8000 Hz.	ECHO	Operational	Dependent	dB re 1 µPa m	
RNL_10000Hz	RNL for 1/3-octave-band centred at 10 kHz.	ECHO	Operational	Dependent	dB re 1 µPa m	
RNL_12500Hz	RNL for 1/3-octave-band centred at 1.25 kHz.	ECHO	Operational	Dependent	dB re 1 µPa m	
RNL_16000Hz	RNL for 1/3-octave-band centred at 16 kHz.	ECHO	Operational	Dependent	dB re 1 µPa m	
RNL_20000Hz	RNL for 1/3-octave-band centred at 20 kHz.	ECHO	Operational	Dependent	dB re 1 µPa m	
RNL_25000Hz	RNL for 1/3-octave-band centred at 25 kHz.	ECHO	Operational	Dependent	dB re 1 µPa m	
RNL_31500Hz	RNL for 1/3-octave-band centred at 31 kHz.	ECHO	Operational	Dependent	dB re 1 µPa m	
RNL_40000Hz	RNL for 1/3-octave-band centred at 40 kHz.	ECHO	Operational	Dependent	dB re 1 µPa m	
RNL_50000Hz	RNL for 1/3-octave-band centred at 50 kHz.	ECHO	Operational	Dependent	dB re 1 µPa m	
RNL_63000Hz	RNL for 1/3-octave-band centred at 63 kHz.	ECHO	Operational	Dependent	dB re 1 µPa m	
MSL_10Hz	MSL for 1/3-octave-band centred at 10 Hz.	ECHO	Operational	Dependent	dB re 1 µPa m	
MSL_13Hz	MSL for 1/3-octave-band centred at 13 Hz.	ECHO	Operational	Dependent	dB re 1 µPa m	
MSL_16Hz	MSL for 1/3-octave-band centred at 16 Hz.	ECHO	Operational	Dependent	dB re 1 µPa m	

MSL_20Hz	MSL for 1/3-octave-band centred at 20 Hz.	ECHO	Operational	Dependent	dB re 1 µPa m	
MSL_25Hz	MSL for 1/3-octave-band centred at 25 Hz.	ECHO	Operational	Dependent	dB re 1 µPa m	
MSL_31Hz	MSL for 1/3-octave-band centred at 31 Hz.	ECHO	Operational	Dependent	dB re 1 µPa m	
MSL_40Hz	MSL for 1/3-octave-band centred at 40 Hz.	ECHO	Operational	Dependent	dB re 1 µPa m	
MSL_50Hz	MSL for 1/3-octave-band centred at 50 Hz.	ECHO	Operational	Dependent	dB re 1 µPa m	
MSL_63Hz	MSL for 1/3-octave-band centred at 63 Hz.	ECHO	Operational	Dependent	dB re 1 µPa m	
MSL_80Hz	MSL for 1/3-octave-band centred at 80 Hz.	ECHO	Operational	Dependent	dB re 1 µPa m	
MSL_100Hz	MSL for 1/3-octave-band centred at 100 Hz.	ECHO	Operational	Dependent	dB re 1 µPa m	
MSL_125Hz	MSL for 1/3-octave-band centred at 125 Hz.	ECHO	Operational	Dependent	dB re 1 µPa m	
MSL_160Hz	MSL for 1/3-octave-band centred at 160 Hz.	ECHO	Operational	Dependent	dB re 1 µPa m	
MSL_200Hz	MSL for 1/3-octave-band centred at 200 Hz.	ECHO	Operational	Dependent	dB re 1 µPa m	
MSL_250Hz	MSL for 1/3-octave-band centred at 250 Hz.	ECHO	Operational	Dependent	dB re 1 µPa m	
MSL_315Hz	MSL for 1/3-octave-band centred at 315 Hz.	ECHO	Operational	Dependent	dB re 1 µPa m	
MSL_400Hz	MSL for 1/3-octave-band centred at 400 Hz.	ECHO	Operational	Dependent	dB re 1 µPa m	
MSL_500Hz	MSL for 1/3-octave-band centred at 500 Hz.	ECHO	Operational	Dependent	dB re 1 µPa m	
MSL_630Hz	MSL for 1/3-octave-band centred at 630 Hz.	ECHO	Operational	Dependent	dB re 1 µPa m	

MSL_800Hz	MSL for 1/3-octave-band centred at 800 Hz.	ECHO	Operational	Dependent	dB re 1 µPa m	
MSL_1000Hz	MSL for 1/3-octave-band centred at 1000 Hz.	ECHO	Operational	Dependent	dB re 1 µPa m	
MSL_1250Hz	MSL for 1/3-octave-band centred at 1250 Hz.	ECHO	Operational	Dependent	dB re 1 µPa m	
MSL_1600Hz	MSL for 1/3-octave-band centred at 1600 Hz.	ECHO	Operational	Dependent	dB re 1 µPa m	
MSL_2000Hz	MSL for 1/3-octave-band centred at 2000 Hz.	ECHO	Operational	Dependent	dB re 1 µPa m	
MSL_2500Hz	MSL for 1/3-octave-band centred at 2500 Hz.	ECHO	Operational	Dependent	dB re 1 µPa m	
MSL_3150Hz	MSL for 1/3-octave-band centred at 3150 Hz.	ECHO	Operational	Dependent	dB re 1 µPa m	
MSL_4000Hz	MSL for 1/3-octave-band centred at 4000 Hz.	ECHO	Operational	Dependent	dB re 1 µPa m	
MSL_5000Hz	MSL for 1/3-octave-band centred at 5000 Hz.	ECHO	Operational	Dependent	dB re 1 µPa m	
MSL_6300Hz	MSL for 1/3-octave-band centred at 6300 Hz.	ECHO	Operational	Dependent	dB re 1 µPa m	
MSL_8000Hz	MSL for 1/3-octave-band centred at 8000 Hz.	ECHO	Operational	Dependent	dB re 1 µPa m	
MSL_10000Hz	MSL for 1/3-octave-band centred at 10 kHz.	ECHO	Operational	Dependent	dB re 1 µPa m	
MSL_12500Hz	MSL for 1/3-octave-band centred at 1.25 kHz.	ECHO	Operational	Dependent	dB re 1 µPa m	
MSL_16000Hz	MSL for 1/3-octave-band centred at 16 kHz.	ECHO	Operational	Dependent	dB re 1 µPa m	
MSL_20000Hz	MSL for 1/3-octave-band centred at 20 kHz.	ECHO	Operational	Dependent	dB re 1 µPa m	
MSL_25000Hz	MSL for 1/3-octave-band centred at 25 kHz.	ECHO	Operational	Dependent	dB re 1 µPa m	

MSL_31500Hz	MSL for 1/3-octave-band centred at 31 kHz.	ECHO	Operational	Dependent	dB re 1 µPa m	
MSL_40000Hz	MSL for 1/3-octave-band centred at 40 kHz.	ECHO	Operational	Dependent	dB re 1 µPa m	
MSL_50000Hz	MSL for 1/3-octave-band centred at 50 kHz.	ECHO	Operational	Dependent	dB re 1 µPa m	
MSL_63000Hz	MSL for 1/3-octave-band centred at 63 kHz.	ECHO	Operational	Dependent	dB re 1 µPa m	
Decade_MSL_10.100Hz	MSL for decade band between 10 and 100 Hz.	ECHO	Operational	Not Included	dB re 1 µPa m	Calculated from 1/3-octave-band levels.
Decade_MSL_100.1000Hz	MSL for decade band between 100 and 1000 Hz	ECHO	Operational	Not Included	dB re 1 µPa m	Calculated from 1/3-octave-band levels.
Decade_MSL_1000.10000Hz	MSL for decade band between 1000 and 10000 Hz.	ECHO	Operational	Not Included	dB re 1 µPa m	Calculated from 1/3-octave-band levels.
Decade_RNL_10.100Hz	MSL for decade band between 10 and 100 Hz.	ECHO	Operational	Not Included	dB re 1 µPa m	Calculated from 1/3-octave-band levels.
Decade_RNL_100.1000Hz	MSL for decade band between 100 and 1000 Hz.	ECHO	Operational	Not Included	dB re 1 µPa m	Calculated from 1/3-octave-band levels.
Decade_RNL_1000.10000Hz	MSL for decade band between 1000 and 10000 Hz.	ECHO	Operational	Not Included	dB re 1 µPa m	Calculated from 1/3-octave-band levels.

A.2. Task 2 Database

Table 12. Description of additional design and operational variables considered in the Task 2 residuals analysis, along with the number of unique vessels and measurements associated with each variable.

Variable Name	Description	Unique Vessels: Bulkers	Measurements: Bulkers	Unique Vessels: Containers	Measurements: Containers
Ballast.Weight	Weight of ballast carried by the vessel (tonnes).	1	12	26	96
Block Co-efficient (load condition / summer)	Block co-efficient at summer load condition (tonnes).	55	206	29	116
Cargo.Weight	Weight of cargo carried by the vessel.	1	12	26	96
Does the vessel have a Bulbous Bow (Y- Yes/N - No /U - unknown)	Yes/No column denoting if the bow of the vessel is bulbous.	71	266	29	116
Does the Vessel have a Rudder Bulb (Y- Yes/N - No /U - unknown)	Yes/No column denoting if the rudder of the vessel is bulbous.	66	251	29	116
Drift.Angle	Difference between the direction of the ship's bow and the true direction of travel (deg).	72	263	29	116
Ducts or nozzles installed? (Y- Yes/N - No /U - unknown)	Yes/No column denoting if any ducts or nozzles are installed on the vessel propulsion systems.	68	254	29	116
Engine.RPM	Current RPM of the engine, as measured by vessel operators/computers (RPM).	40	169	28	105
Fin Installed? (Y- Yes/N - No /U - unknown)	Yes/No column denoting if fins are installed on the vessel.	64	247	29	116
Generator_Average Power Rating	Average power rating for all the generators on the vessel (kW).	20	46	0	0
Generator_Nominal RPM	Normal operating RPM for the generators (RPM).	45	149	2	2

Is the Generator resilient mounted (Y- Yes/N - No /U - unknown)	Yes/No/NA column denoting if the generators are on vibration damping mountings.	52	232	3	3
Main Engine_Is the motor resilient mounted (Y- Yes/N - No /U - unknown)	Yes/No/NA column denoting if the main engine is on vibration damping mountings.	47	178	20	98
Measured.Pitch.deg	Measured trim of the vessel by vessel operators/computers. Pitch is also known as the forward/backward tilt of the vessel (deg).	0	0	26	103
Percent.Slip.Ratio	The slip ratio, defined as the percent difference between actual and idealized speed of advance of propeller.	1	12	26	103
Propeller Blade Count (#)	Number of blades on the propeller	71	267	29	116
Propeller boss cap fin? (Y- Yes/N - No /U - unknown)	Yes/No column denoting if any propeller boss cap present on the vessel.	66	242	6	13
Propeller Diameter	As indicated (m)	71	267	29	116
Propeller Hub Diameter	As indicated (m)	46	211	25	93
Propeller Pitch	The distance that a propeller theoretically (i.e. without slip) advances during one revolution (m).	53	214	29	116
Propeller Pitch Angle	Angle between propeller blade and propeller plane of rotation. Calculated from Propeller Pitch (deg).	53	214	29	116
Propeller Rake (absolute)	Absolute value of rake (deg)	24	133	21	82
Propeller Rake	As indicated (deg)	24	133	21	82
Propeller Skew Angle to Shaft Perpendicular	As indicated (deg)	60	224	25	93

TotalElectricPower	Total electric power load generated by the generators, as measured by vessel operators/computers (kW).	13	50	2	2
Trim	Pitch trim of the vessel, calculated from difference of fore and aft drafts (m).	40	165	2	2

Appendix B. Correlation Plots

B.1. Phase 2 Data Set Correlation Matrices

Correlation matrix plots in this appendix show correlations between pairs of variables in different vessel categories for the Phase 2 data set. The coloured circles indicate the strength and magnitude of the correlation (blue = positive, red = negative, correlations along the diagonal are r=1). The "?" indicates where the correlation cannot be computed between two variables (usually due to missing values, but sometimes due to a variable having a constant value). The first three rows and columns of the correlation matrix can be used to visually identify correlations between RNL and the predictor variables. Subsequent rows and columns can be used to visually identify correlations between pairs of predictors.

B.1.1. Bulkers

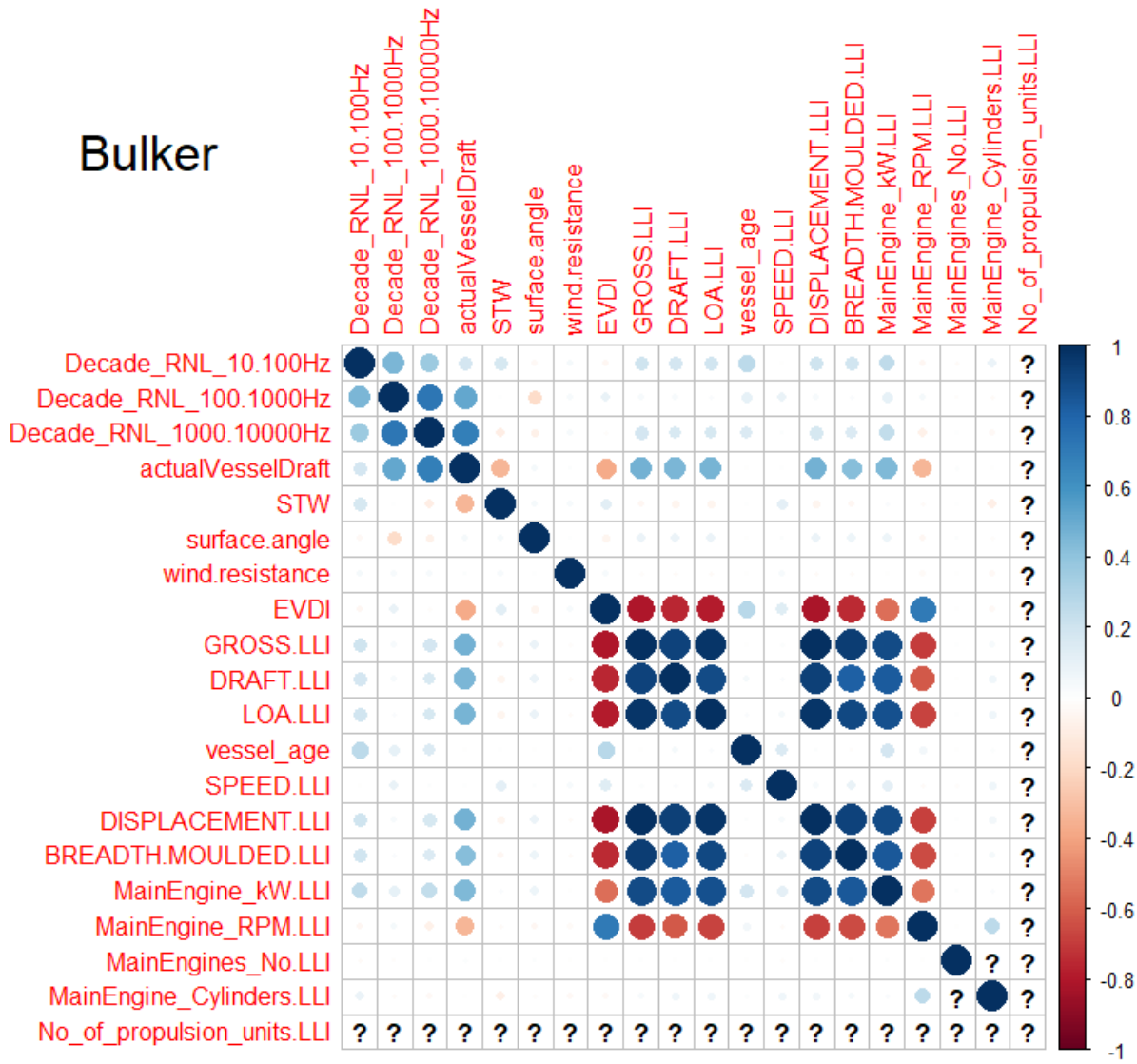

B.1.2. Containers

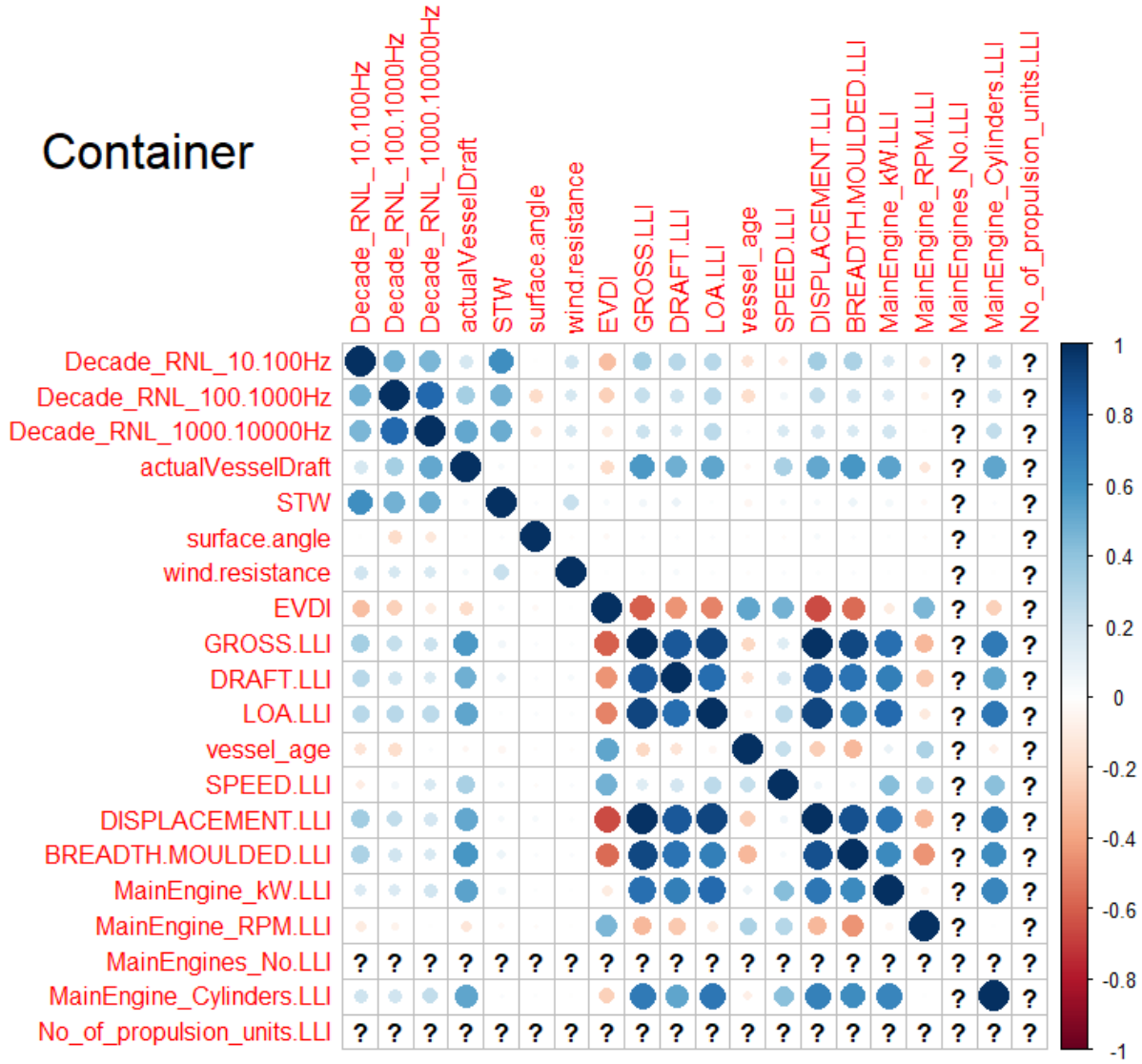

B.1.3. Cruise

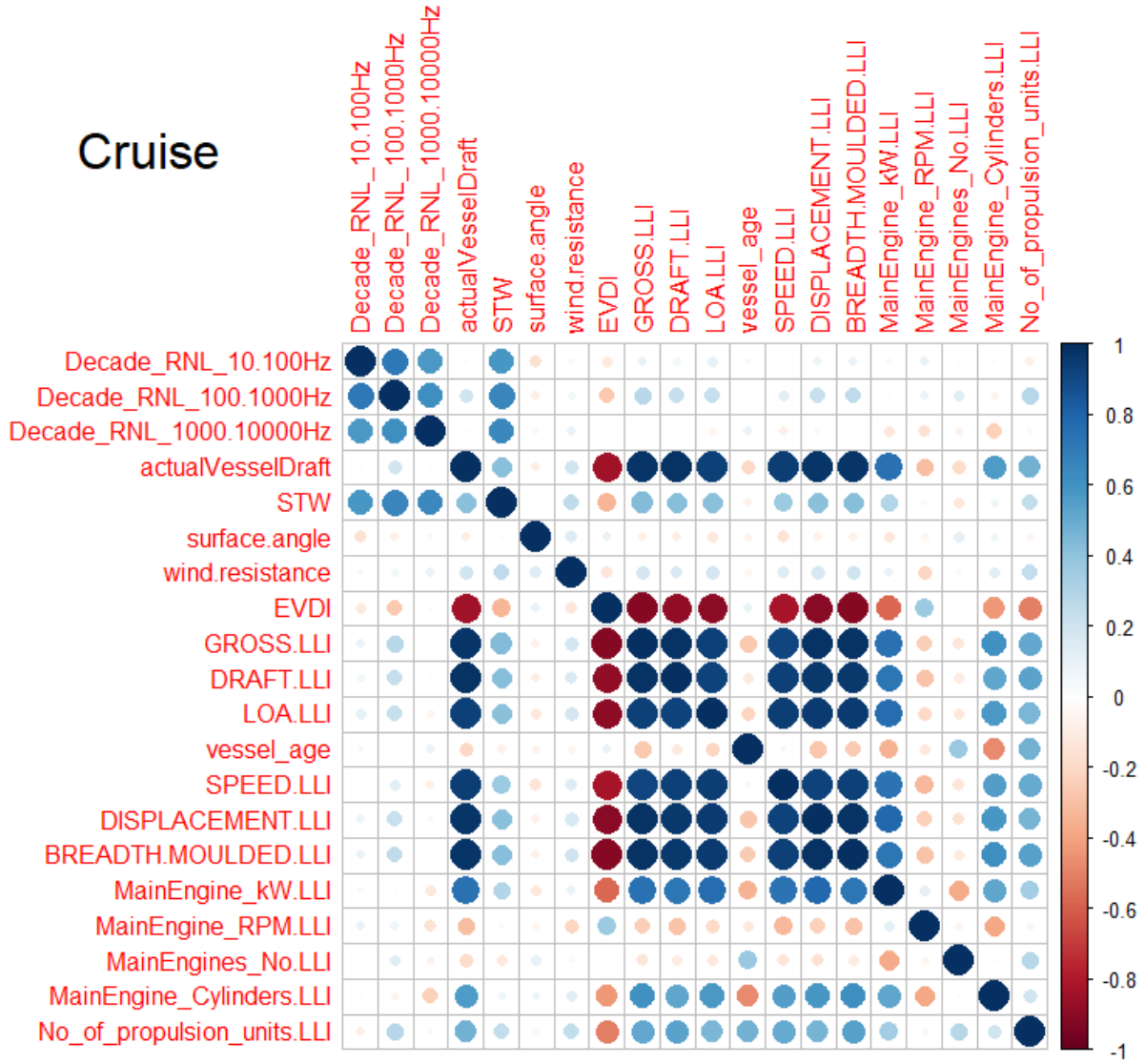
Cruise
Decade_RNL_10.100Hz
Decade_RNL_100.1000Hz
Decade_RNL_1000.10000Hz
actualVesselDraft
STW
surface.angle
wind.resistance
EVDI
GROSS.LLI
DRAFT.LLI
LOA.LLI
vessel_age
SPEED.LLI
DISPLACEMENT.LLI
BREADTH.MOULDED.LLI
MainEngine_kW.LLI
MainEngine_RPM.LLI
MainEngines_No.LLI
MainEngine_Cylinders.LLI
No_of_propulsion_units.LLI
1
0.8
0.6
0.4
0.2
0
-0.2
-0.4
-0.6
-0.8
-1

B.1.4. Tanker

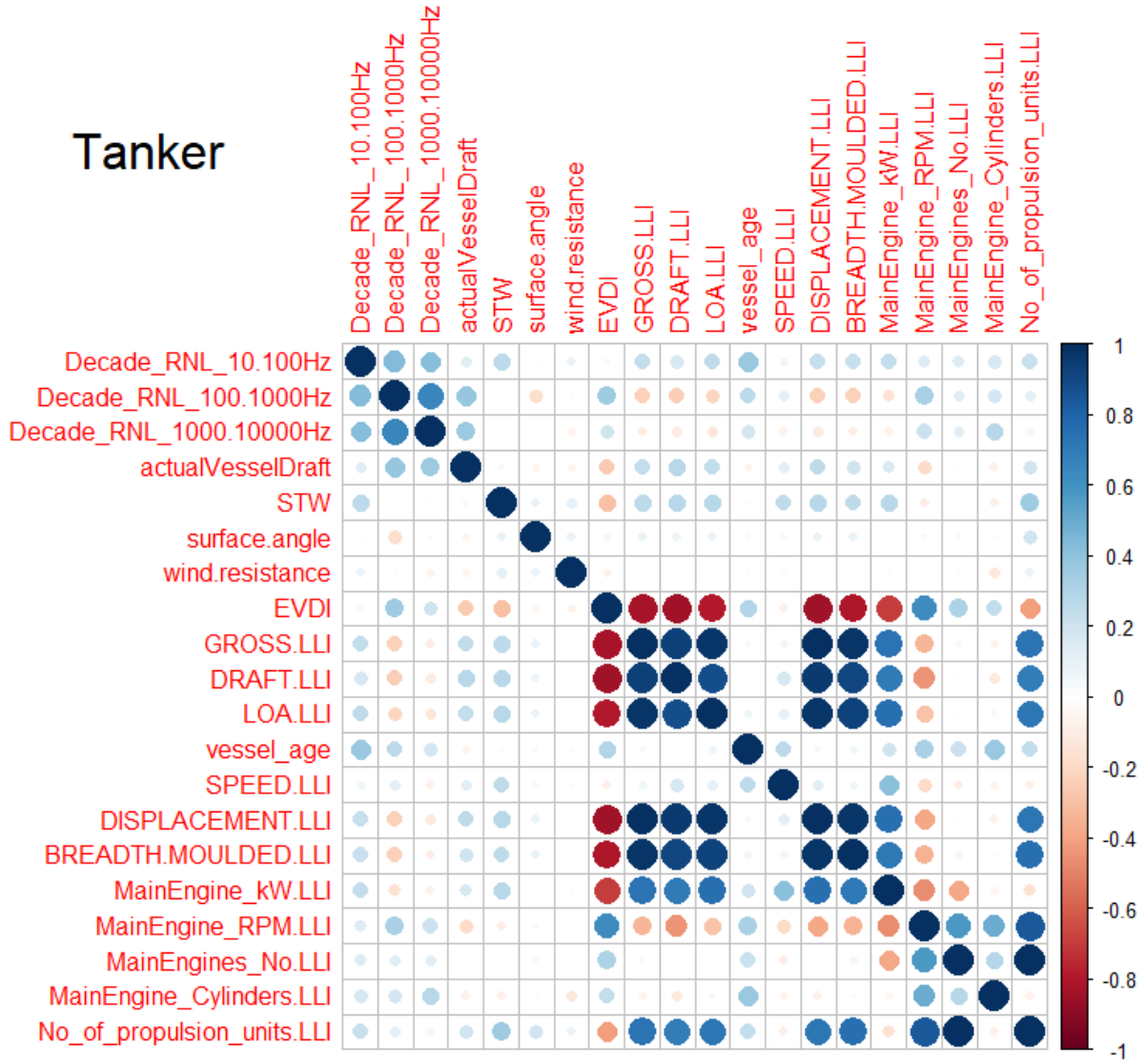
Tanker
Decade_RNL_10.100Hz
Decade_RNL_100.1000Hz
Decade_RNL_1000.10000Hz
actualVesselDraft
STW
surface.angle
wind.resistance
EVDI
GROSS.LLI
DRAFT.LLI
LOA.LLI
vessel_age
SPEED.LLI
DISPLACEMENT.LLI
BREADTH.MOULDED.LLI
MainEngine_kW.LLI
MainEngine_RPM.LLI
MainEngines_No.LLI
MainEngine_Cylinders.LLI
No_of_propulsion_units.LLI
1
0.8
0.6
0.4
0.2
0
-0.2
-0.4
-0.6
-0.8
-1

B.1.5. Tugs

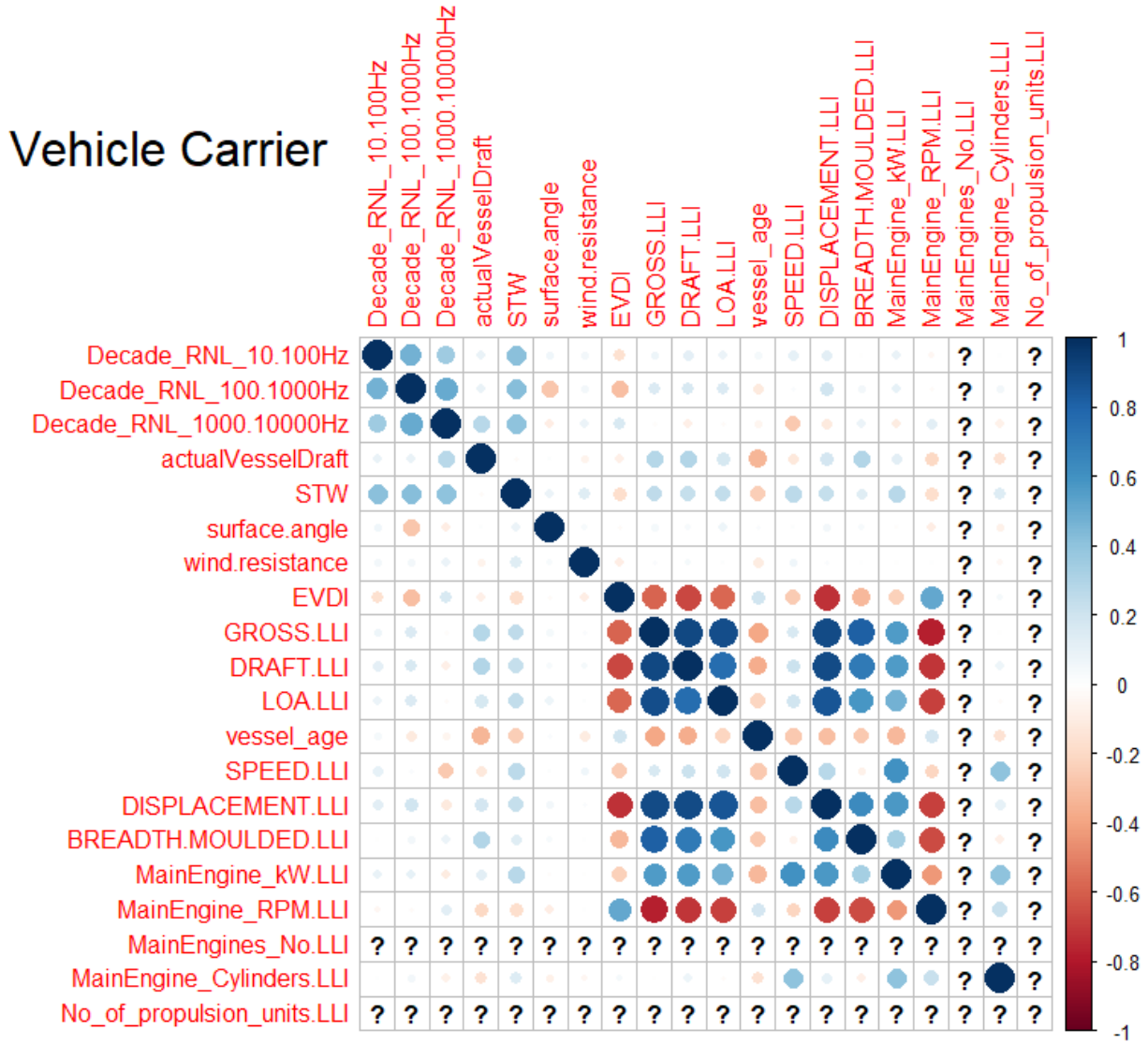
Vehicle Carrier
Decade_RNL_10.100Hz
Decade_RNL_100.1000Hz
Decade_RNL_1000.10000Hz
actualVesselDraft
STW
surface.angle
wind.resistance
EVDI
GROSS.LLI
DRAFT.LLI
LOA.LLI
vessel_age
SPEED.LLI
DISPLACEMENT.LLI
BREADTH.MOULDED.LLI
MainEngine_kW.LLI
MainEngine_RPM.LLI
MainEngines_No.LLI
MainEngine_Cylinders.LLI
No_of_propulsion_units.LLI
1
0.8
0.6
0.4
0.2
0
-0.2
-0.4
-0.6
-0.8
-1

B.1.6. Vehicle Carriers

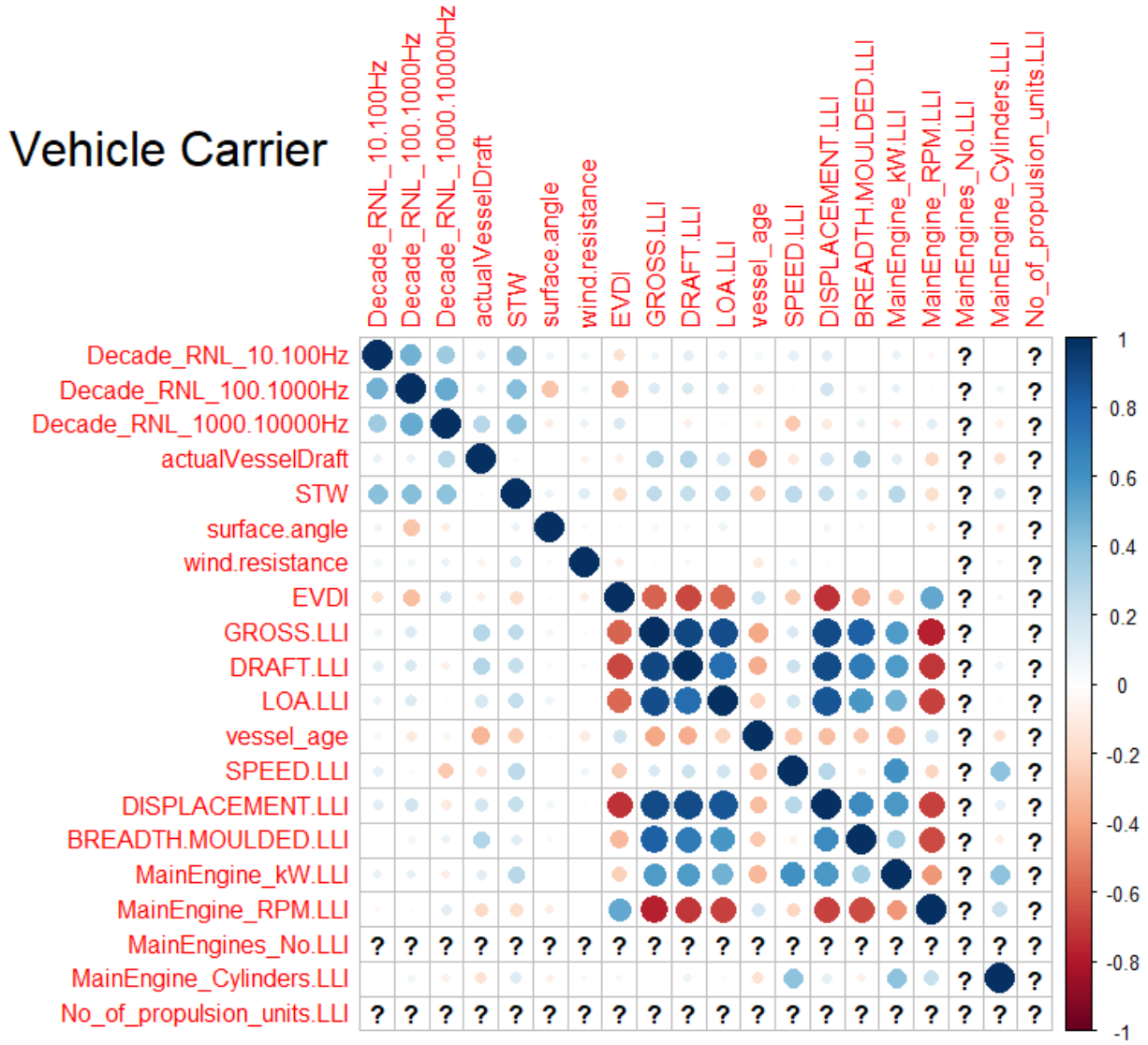

B.2. Correlation Comparisons: Phase 1 versus Phase 2

Plots in this appendix show comparisons of Phases 1 and 2 correlations of vessel characteristics and source levels (MSL and RNL), in different categories. Columns show the correlation coefficient ($-1 < r < 1$) with broadband and decade-band source levels. Top rows show MSL correlations and bottom rows show RNL correlations. The colours indicate the strength and magnitude of the correlation (blue = positive, red = negative). Greyed out boxes represent no variation in vessel characteristic to compute any correlation.

B.2.1. Bulkers

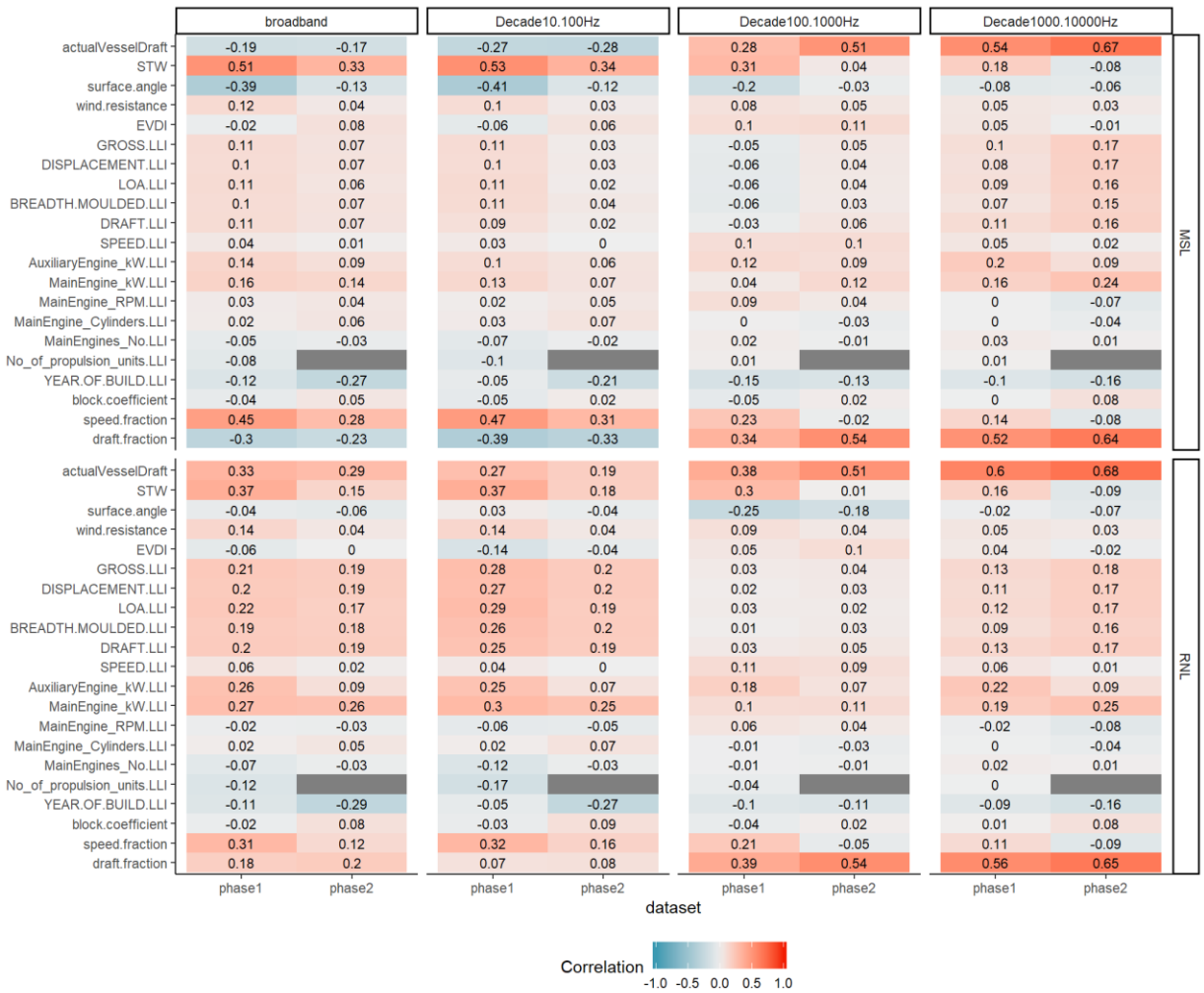

B.2.2. Containers

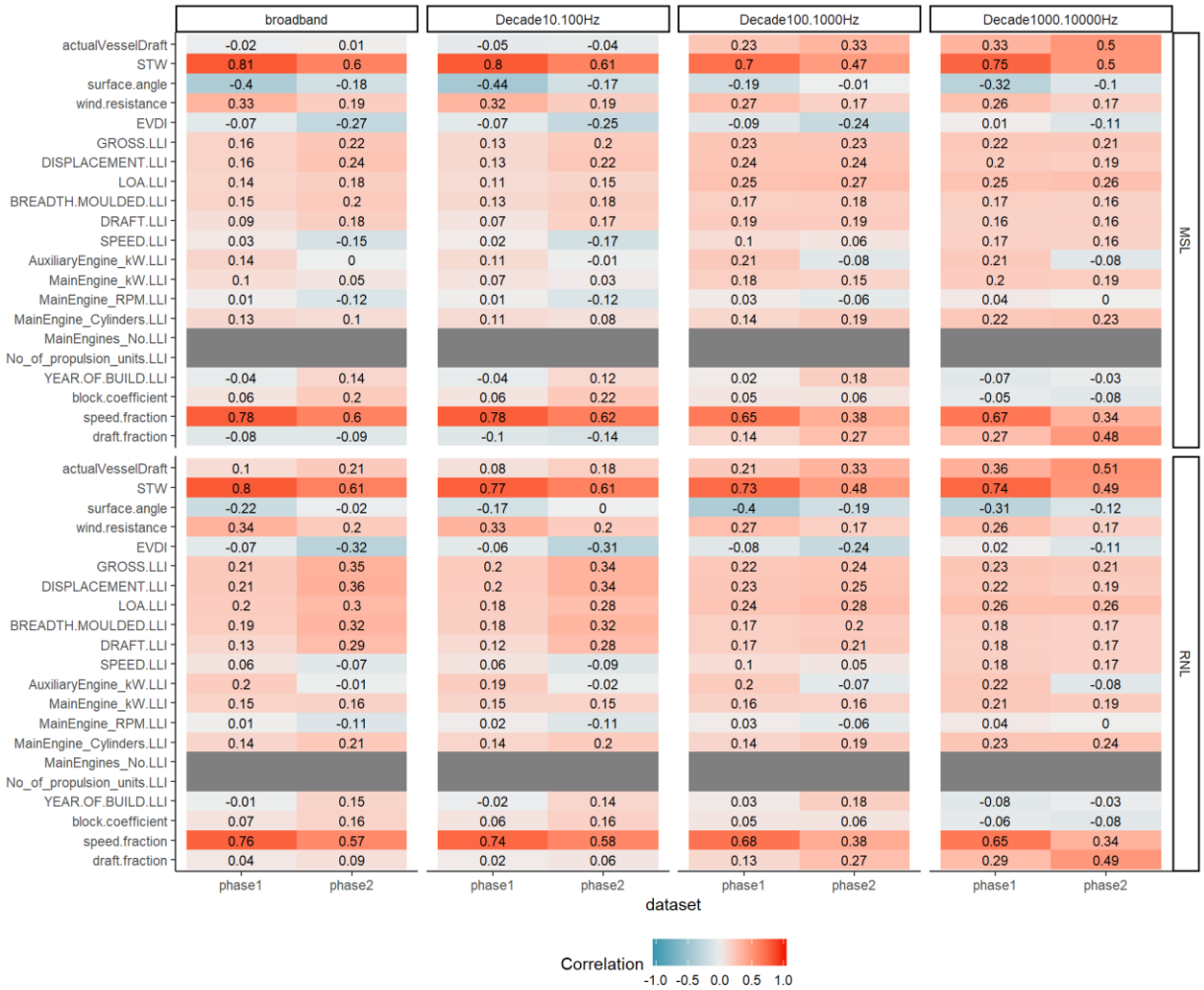

B.2.3. Cruise

	broadband		Decade10.100Hz		Decade100.1000Hz		Decade1000.10000Hz		
	phase1	phase2	phase1	phase2	phase1	phase2	phase1	phase2	
actualVesselDraft	-0.38	-0.02	-0.4	-0.1	-0.27	0.18	-0.12	-0.07	MSL
STW	0.61	0.52	0.5	0.45	0.75	0.66	0.76	0.62	MSL
surface.angle	-0.34	-0.18	-0.43	-0.2	-0.22	-0.04	-0.3	0.02	MSL
wind.resistance	0.21	-0.08	0.21	-0.06	0.18	0.05	0.09	0.08	MSL
EVDI	0.18	-0.07	0.14	-0.04	0.25	-0.23	0.03	0	MSL
GROSS.LLI	-0.31	0.05	-0.31	-0.03	-0.21	0.24	-0.09	-0.07	MSL
DISPLACEMENT.LLI	-0.31	0.03	-0.31	-0.04	-0.22	0.19	-0.1	-0.08	MSL
LOA.LLI	-0.3	0.02	-0.34	-0.03	-0.17	0.2	-0.11	-0.1	MSL
BREADTH.MOULDED.LLI	-0.28	0.03	-0.26	-0.03	-0.23	0.22	-0.07	-0.07	MSL
DRAFT.LLI	-0.38	-0.04	-0.4	-0.11	-0.26	0.15	-0.12	-0.09	MSL
SPEED.LLI	-0.28	-0.09	-0.33	-0.11	-0.13	0.11	-0.04	-0.13	MSL
AuxiliaryEngine_kW.LLI	-0.31	0	-0.31	-0.03	-0.21	0.08	-0.09	0.02	MSL
MainEngine_kW.LLI	-0.3	-0.08	-0.29	-0.07	-0.23	-0.04	-0.23	-0.15	MSL
MainEngine_RPM.LLI	-0.27	-0.04	-0.3	0.01	0.01	0	-0.29	-0.13	MSL
MainEngine_Cylinders.LLI	-0.14	0.04	-0.1	0	-0.26	-0.01	-0.13	-0.19	MSL
MainEngines_No.LLI	0.28	0.08	0.31	0.04	0.22	0.11	-0.02	-0.07	MSL
No_of_propulsion_units.LLI	-0.09	-0.14	-0.03	-0.14	-0.13	0.23	-0.31	-0.01	MSL
YEAR.OF.BUILD.LLI	-0.31	0.07	-0.31	0.01	-0.26	0.02	-0.15	-0.11	MSL
block.coefficient	0.01	0.07	0.13	0.05	-0.15	-0.17	0.01	-0.01	MSL
speed.fraction	0.69	0.58	0.6	0.52	0.74	0.59	0.72	0.71	MSL
draft.fraction	-0.11	-0.1	-0.11	-0.08	-0.15	-0.26	-0.05	0.04	MSL
actualVesselDraft	-0.32	0.12	-0.42	0.03	-0.23	0.2	-0.09	-0.02	RNL
STW	0.68	0.59	0.53	0.58	0.75	0.66	0.76	0.64	RNL
surface.angle	-0.27	-0.08	-0.16	-0.16	-0.32	-0.08	-0.26	0.05	RNL
wind.resistance	0.17	-0.04	0.15	-0.03	0.16	0.06	0.08	0.09	RNL
EVDI	0.17	-0.2	0.15	-0.12	0.23	-0.26	0.02	-0.03	RNL
GROSS.LLI	-0.27	0.19	-0.35	0.08	-0.18	0.26	-0.06	-0.02	RNL
DISPLACEMENT.LLI	-0.28	0.17	-0.35	0.06	-0.19	0.21	-0.07	-0.04	RNL
LOA.LLI	-0.25	0.16	-0.36	0.08	-0.14	0.22	-0.09	-0.06	RNL
BREADTH.MOULDED.LLI	-0.26	0.17	-0.31	0.08	-0.21	0.24	-0.04	-0.02	RNL
DRAFT.LLI	-0.33	0.1	-0.43	0.01	-0.23	0.17	-0.09	-0.05	RNL
SPEED.LLI	-0.23	0.03	-0.36	0	-0.09	0.12	-0.02	-0.09	RNL
AuxiliaryEngine_kW.LLI	-0.27	0.05	-0.35	0	-0.18	0.07	-0.06	0.04	RNL
MainEngine_kW.LLI	-0.28	0.02	-0.33	-0.03	-0.21	-0.03	-0.22	-0.12	RNL
MainEngine_RPM.LLI	-0.23	-0.09	-0.32	-0.05	0	-0.03	-0.28	-0.14	RNL
MainEngine_Cylinders.LLI	-0.12	0.13	-0.1	0.05	-0.23	0.01	-0.13	-0.16	RNL
MainEngines_No.LLI	0.26	0.1	0.29	0.01	0.2	0.13	-0.04	-0.06	RNL
No_of_propulsion_units.LLI	-0.12	-0.04	-0.1	-0.12	-0.14	0.24	-0.32	0.03	RNL
YEAR.OF.BUILD.LLI	-0.33	0.11	-0.34	-0.04	-0.25	-0.01	-0.14	-0.09	RNL
block.coefficient	-0.06	0.05	0.05	-0.08	-0.17	-0.18	0.02	0	RNL
speed.fraction	0.72	0.57	0.64	0.57	0.73	0.58	0.7	0.71	RNL
draft.fraction	-0.07	-0.19	-0.1	-0.14	-0.1	-0.28	-0.04	0	RNL

dataset

Correlation -1.0 -0.5 0.0 0.5 1.0

B.2.4. Tanker

	broadband		Decade10.100Hz		Decade100.1000Hz		Decade1000.10000Hz		
	phase1	phase2	phase1	phase2	phase1	phase2	phase1	phase2	
actualVesselDraft	-0.12	-0.17	-0.08	-0.07	0.08	0.31	0.26	0.32	MSL
STW	0.39	0.24	0.55	0.3	0.05	0.02	0.04	-0.02	MSL
surface.angle	-0.31	-0.1	-0.31	-0.11	-0.21	0	-0.14	-0.02	MSL
wind.resistance	0.25	0.07	0.23	0.03	0.15	-0.03	0.11	-0.07	MSL
EVDI	-0.02	0.05	-0.19	-0.07	0.41	0.4	0.04	0.22	MSL
GROSS.LLI	0.11	0.18	0.22	0.2	-0.33	-0.25	-0.04	-0.11	MSL
DISPLACEMENT.LLI	0.11	0.16	0.22	0.2	-0.33	-0.26	-0.08	-0.13	MSL
LOA.LLI	0.11	0.19	0.19	0.2	-0.33	-0.24	-0.09	-0.15	MSL
BREADTH.MOULDED.LLI	0.11	0.19	0.24	0.21	-0.33	-0.25	-0.09	-0.1	MSL
DRAFT.LLI	0.09	0.12	0.2	0.16	-0.28	-0.25	-0.05	-0.1	MSL
SPEED.LLI	0.14	0	0.29	0.09	0.07	0.07	-0.39	-0.09	MSL
AuxiliaryEngine_kW.LLI	0.08	0.06	0.2	0.11	-0.34	0.14	-0.02	0.07	MSL
MainEngine_kW.LLI	0.18	0.22	0.34	0.23	-0.24	-0.19	-0.11	-0.09	MSL
MainEngine_RPM.LLI	0	0.18	-0.16	0.02	0.33	0.37	0.25	0.22	MSL
MainEngine_Cylinders.LLI	-0.02	0.17	-0.18	0.05	0.35	0.21	0.25	0.25	MSL
MainEngines_No.LLI	-0.02	0.11	-0.05	0.03	-0.01	0.16	-0.02	0.12	MSL
No_of_propulsion_units.LLI	-0.02	0.07	-0.05	0.03	-0.01	0.11	-0.02	0.03	MSL
YEAR.OF.BUILD.LLI	-0.2	-0.39	-0.14	-0.23	-0.18	-0.27	0.01	-0.19	MSL
block.coefficient	0.04	0.12	0.07	0.16	-0.18	-0.16	-0.02	-0.13	MSL
speed.fraction	0.26	0.22	0.3	0.21	-0.01	-0.04	0.33	0.04	MSL
draft.fraction	-0.18	-0.22	-0.26	-0.18	0.32	0.48	0.29	0.38	MSL
actualVesselDraft	0.24	0.19	0.2	0.13	0.24	0.39	0.33	0.37	RNL
STW	0.26	0.19	0.44	0.27	0.05	0	0.04	-0.02	RNL
surface.angle	-0.07	-0.03	0.1	0.02	-0.3	-0.18	-0.09	-0.03	RNL
wind.resistance	0.27	0.07	0.27	0.08	0.14	-0.02	0.12	-0.06	RNL
EVDI	0	0.08	-0.2	-0.03	0.32	0.36	0.01	0.21	RNL
GROSS.LLI	0.13	0.16	0.31	0.25	-0.25	-0.23	-0.01	-0.1	RNL
DISPLACEMENT.LLI	0.12	0.14	0.3	0.23	-0.24	-0.24	-0.05	-0.12	RNL
LOA.LLI	0.13	0.18	0.31	0.26	-0.24	-0.21	-0.06	-0.13	RNL
BREADTH.MOULDED.LLI	0.12	0.15	0.3	0.23	-0.24	-0.24	-0.05	-0.09	RNL
DRAFT.LLI	0.12	0.11	0.27	0.19	-0.2	-0.23	-0.02	-0.09	RNL
SPEED.LLI	0.14	0.04	0.22	0.07	0.11	0.11	-0.38	-0.07	RNL
AuxiliaryEngine_kW.LLI	0.11	0.07	0.29	0.08	-0.23	0.13	0.02	0.07	RNL
MainEngine_kW.LLI	0.16	0.17	0.36	0.24	-0.15	-0.16	-0.08	-0.07	RNL
MainEngine_RPM.LLI	0.1	0.21	-0.03	0.13	0.27	0.32	0.23	0.21	RNL
MainEngine_Cylinders.LLI	0.04	0.18	-0.16	0.14	0.28	0.18	0.22	0.24	RNL
MainEngines_No.LLI	0.05	0.16	0.06	0.13	0.01	0.13	-0.01	0.12	RNL
No_of_propulsion_units.LLI	0.05	0.12	0.06	0.12	0.01	0.08	-0.01	0.03	RNL
YEAR.OF.BUILD.LLI	-0.23	-0.4	-0.19	-0.38	-0.18	-0.26	0.02	-0.19	RNL
block.coefficient	0.03	0.12	0.12	0.21	-0.14	-0.14	0	-0.12	RNL
speed.fraction	0.14	0.15	0.25	0.19	-0.03	-0.08	0.32	0.03	RNL
draft.fraction	0.12	0.11	-0.05	0	0.38	0.53	0.33	0.41	RNL

dataset

Correlation -1.0 -0.5 0.0 0.5 1.0

B.2.5. Tugs

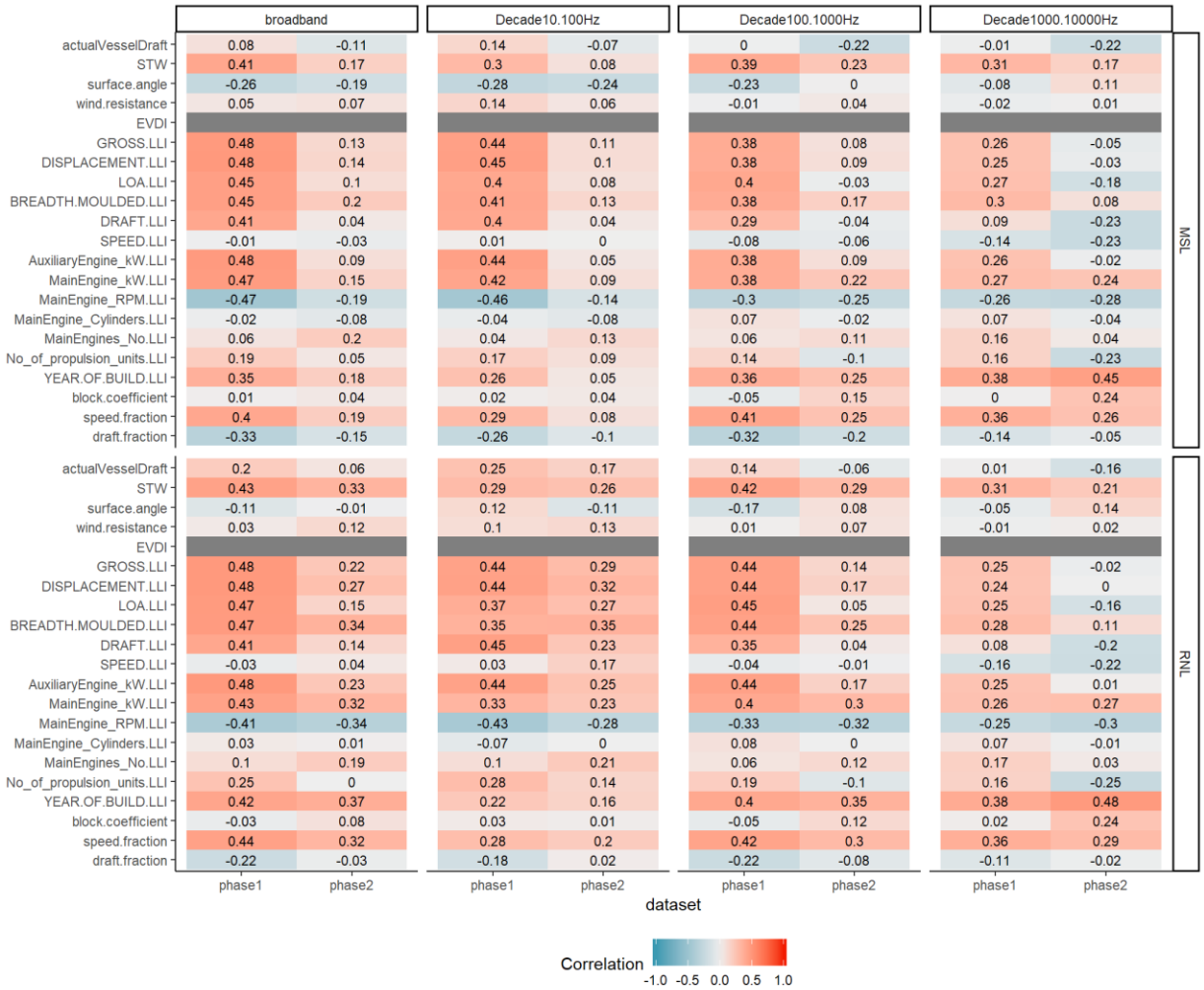
broadband
Decade10.100Hz
Decade100.1000Hz
Decade1000.10000Hz
MSL
RNL
actualVesselDraft
STW
surface.angle
wind.resistance
EVDI
GROSS.LLI
DISPLACEMENT.LLI
LOA.LLI
BREADTH.MOULDED.LLI
DRAFT.LLI
SPEED.LLI
AuxiliaryEngine_kW.LLI
MainEngine_kW.LLI
MainEngine_RPM.LLI
MainEngine_Cylinders.LLI
MainEngines_No.LLI
No_of_propulsion_units.LLI
YEAR.OF.BUILD.LLI
block.coefficient
speed.fraction
draft.fraction
phase1
phase2
dataset
Correlation
-1.0 -0.5 0.0 0.5 1.0

B.2.6. Vehicle Carriers

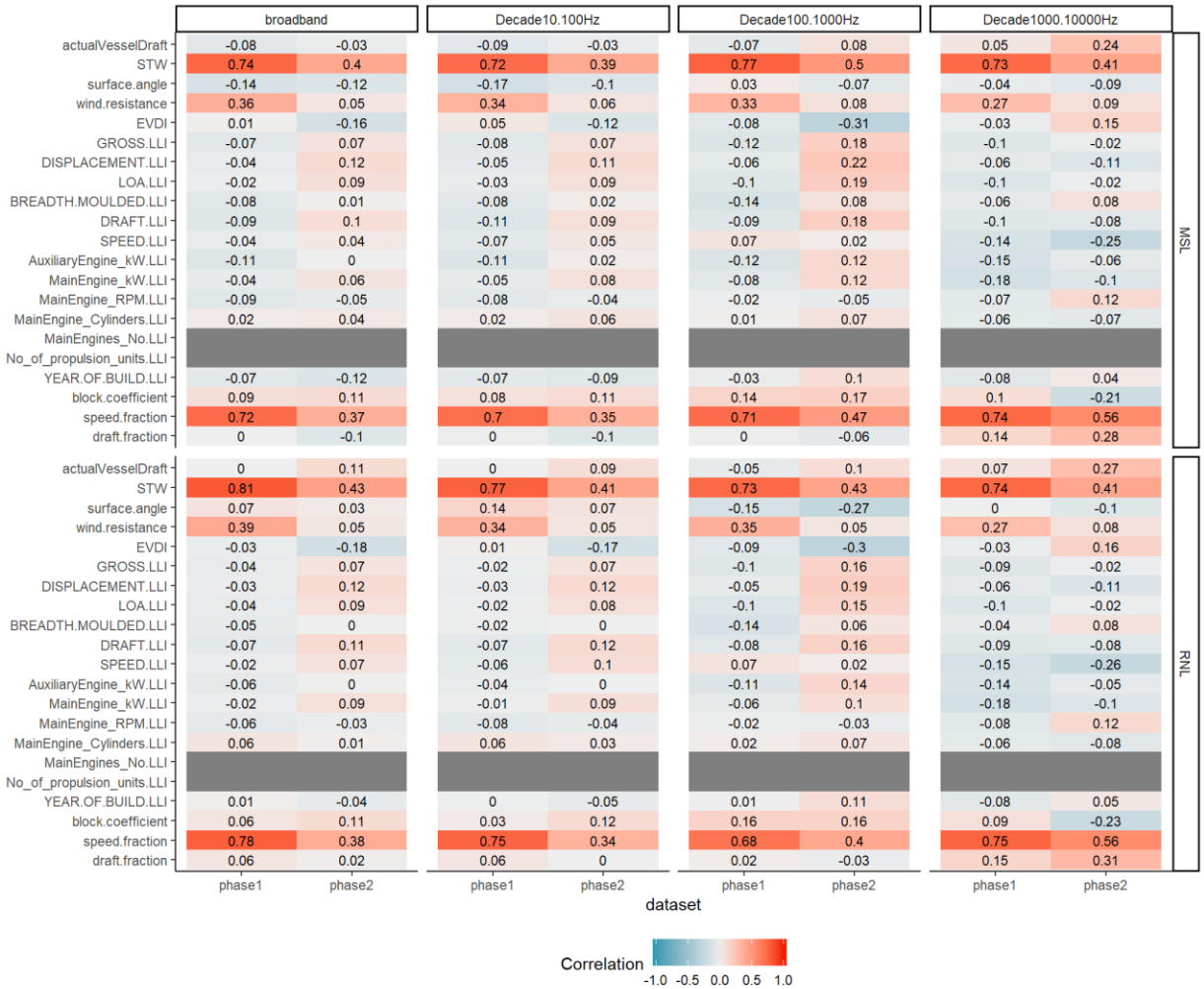

Appendix C. Updated Functional Regression Model

C.1. Coefficients of Determination

Plots in this section show the coefficient of determination (r^2) versus log(frequency) for the updated functional regression model. The coefficient of determination (r^2) is a number in the range 0–1 that indicates the strength of correlation with a response variable, and which indicates the fraction of the source level variability explained by the model in each frequency band. Separate r^2 values are shown for MSL (left) and RNL (right), though the two are very similar.

C.1.1. Bulkers

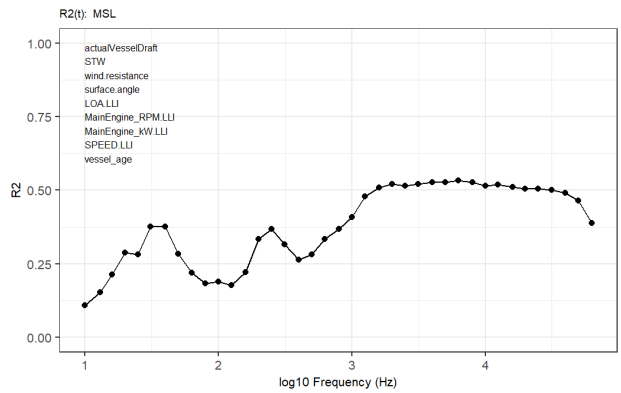

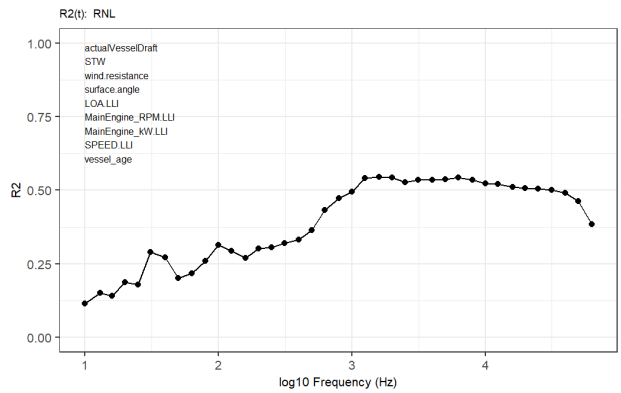

C.1.2. Containers

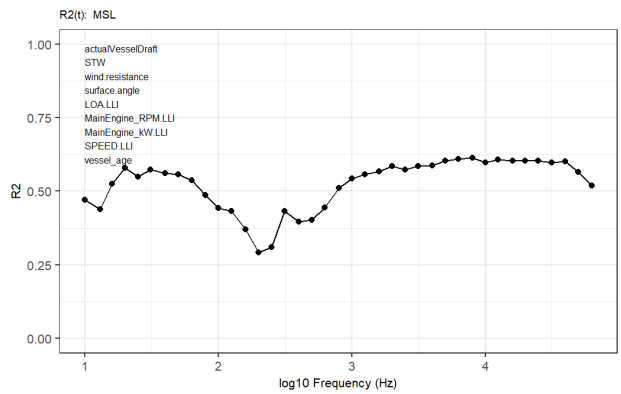

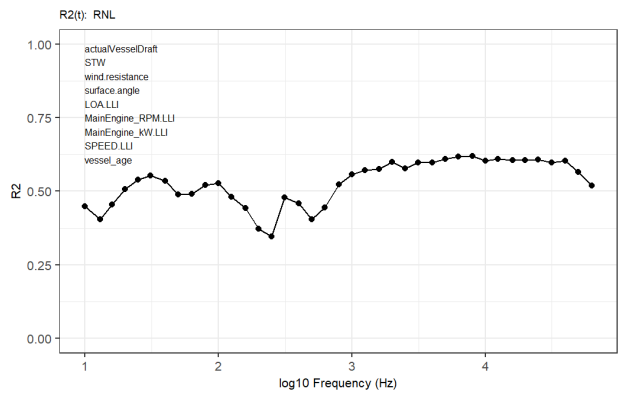

C.1.3. Cruise

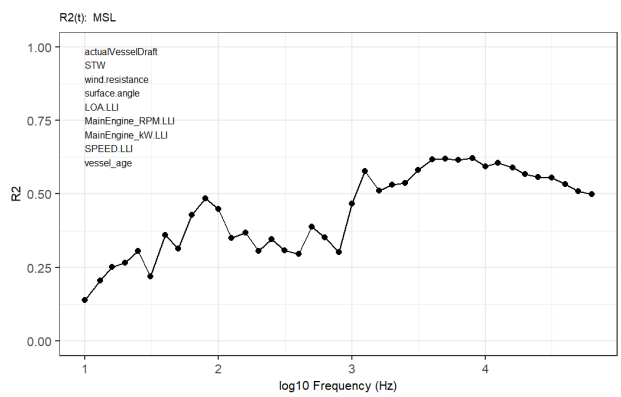

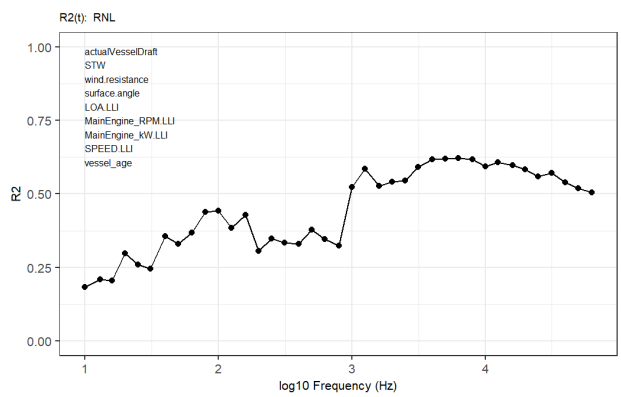

C.1.4. Tanker

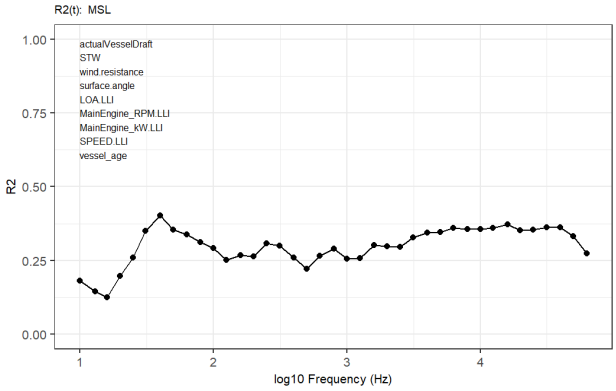

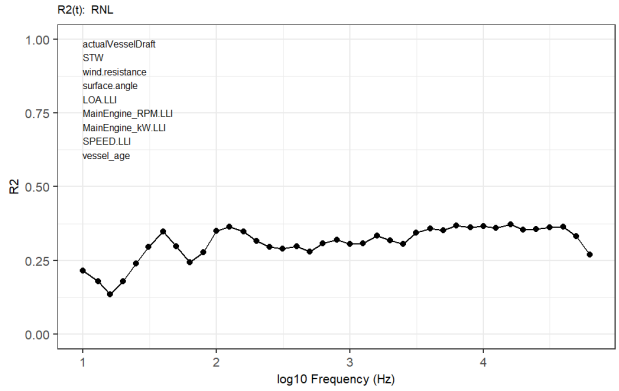

C.1.5. Tugs

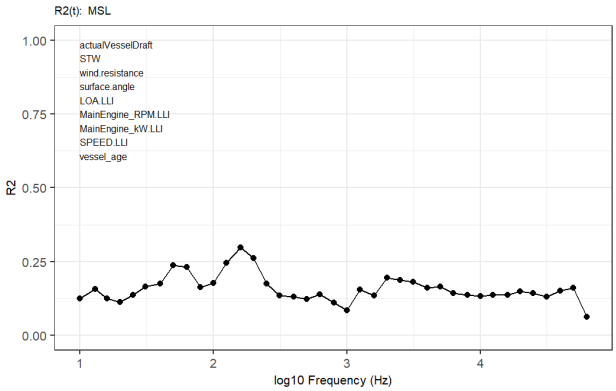

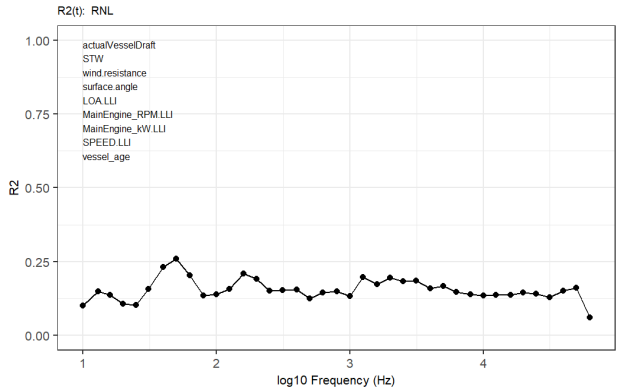

C.1.6. Vehicle Carriers

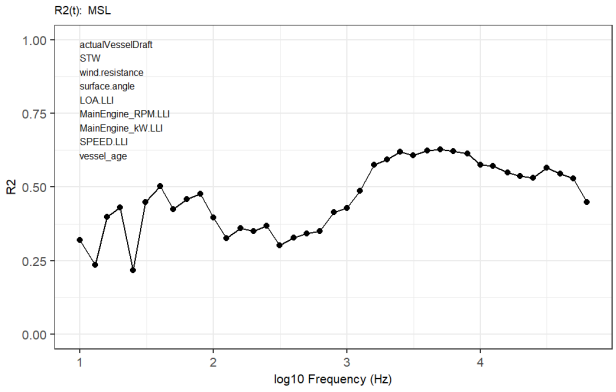

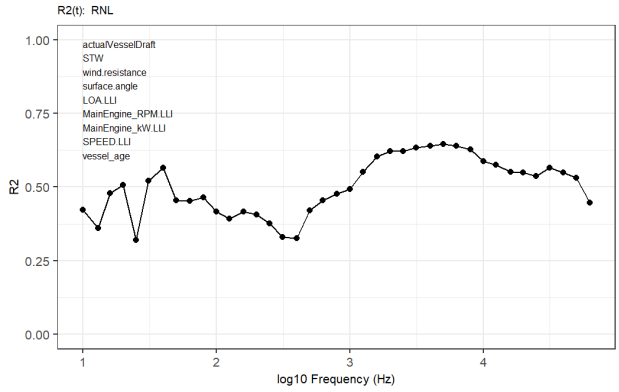

C.2. Beta Coefficients

Plots in this section show the regression coefficient function $\beta(f)$ (i.e., frequency-dependent slope coefficient) versus log(frequency) for each predictor variable. The $\beta(f)$ value at any frequency is equal to the slope of the trend between the predictor value (possibly log transformed) and the source level. The solid line is the estimated regression coefficient function across frequencies and the hatched area is the 95% confidence interval on the estimated regression coefficient function. Positive values of $\beta(f)$ indicate that increasing the predictor was associated with higher source levels, whereas negative values indicate that increasing the predictor was associated with lower source levels.

C.2.1. Bulkers

C.2.1.1. MSL

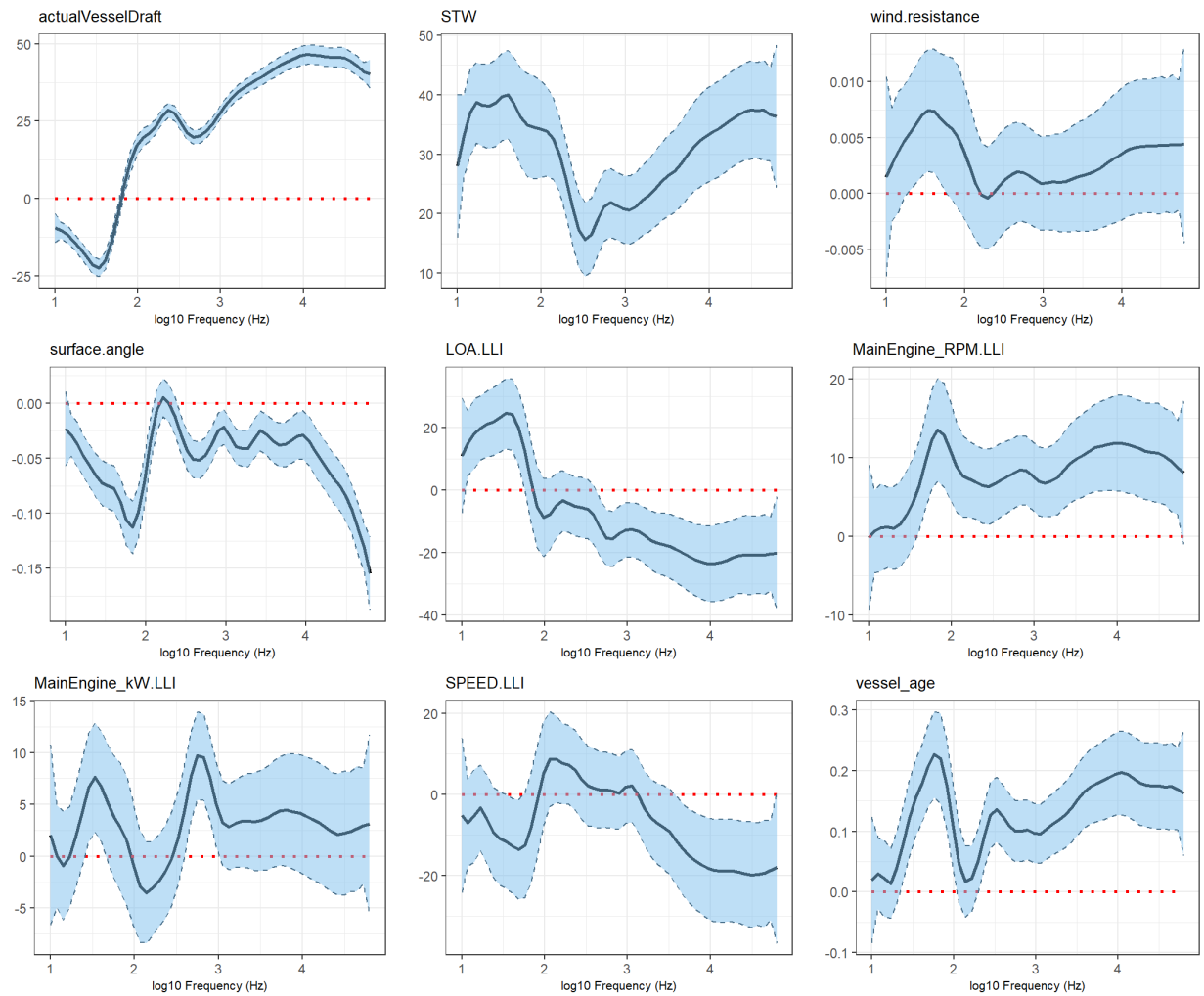

C.2.1.2. RNL

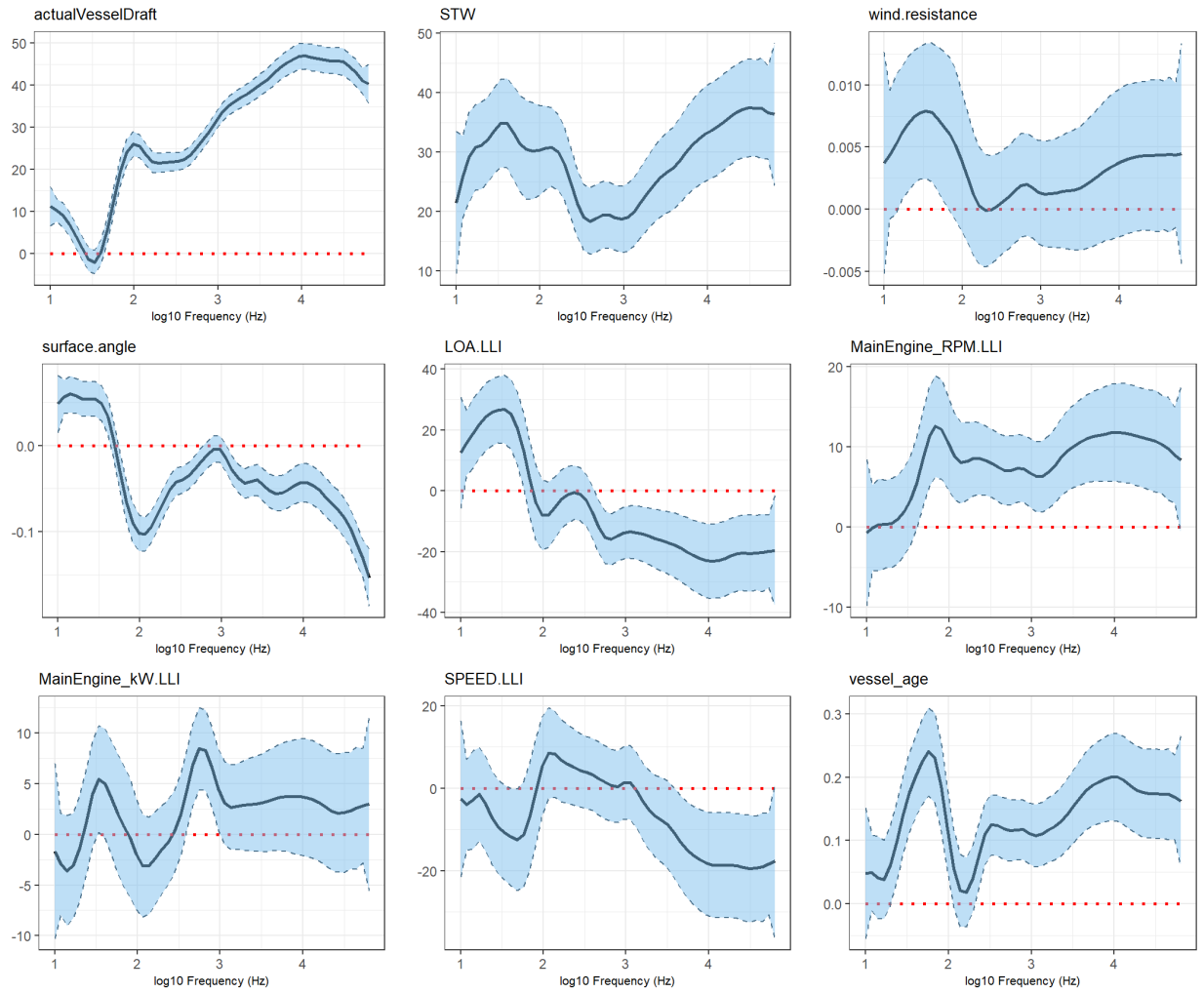
actualVesselDraft
STW
wind.resistance
surface.angle
LOA.LLI
MainEngine_RPM.LLI
MainEngine_kW.LLI
SPEED.LLI
vessel_age
log10 Frequency (Hz)

C.2.2. Containers

C.2.2.1. MSL

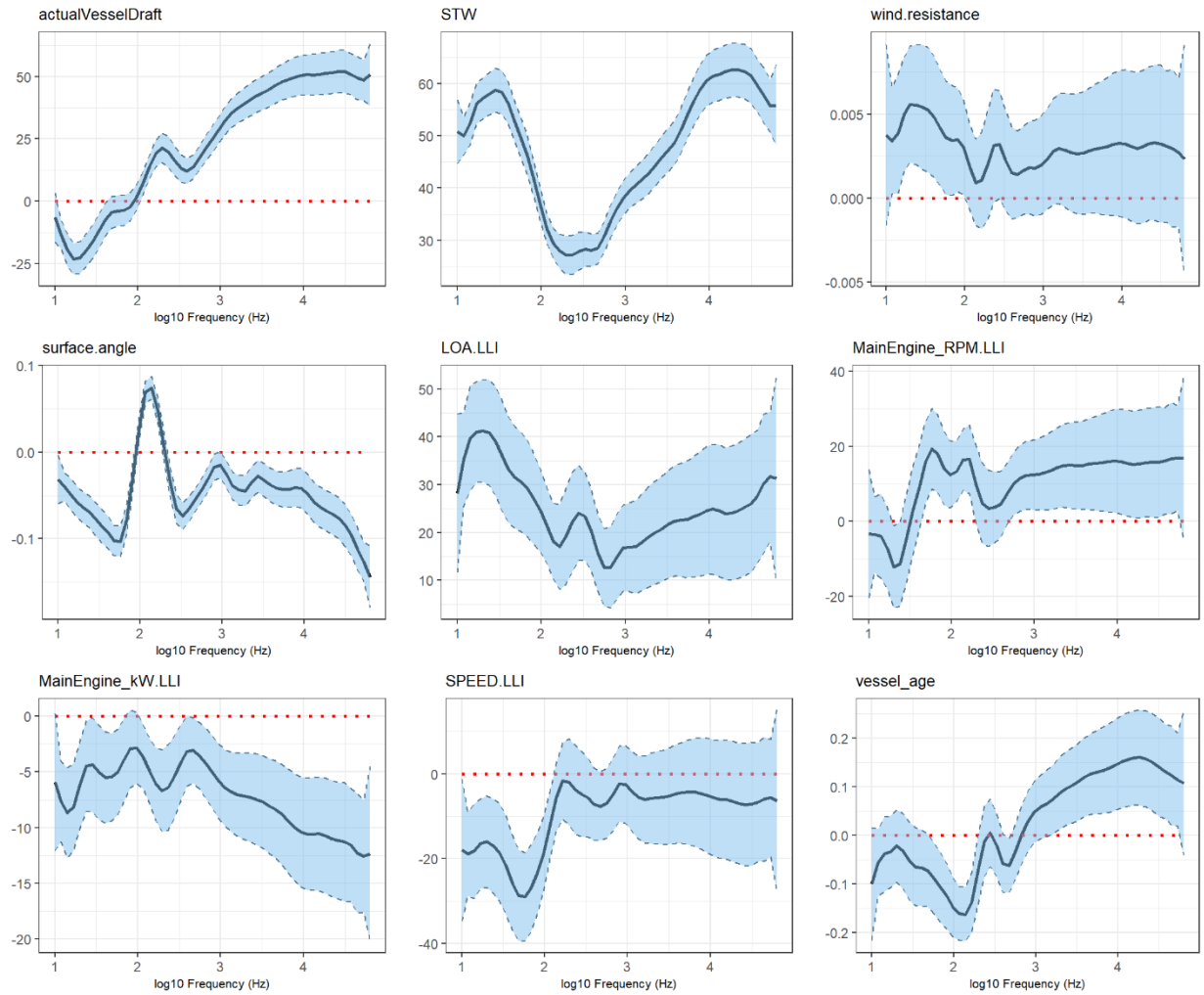

C.2.2.2. RNL

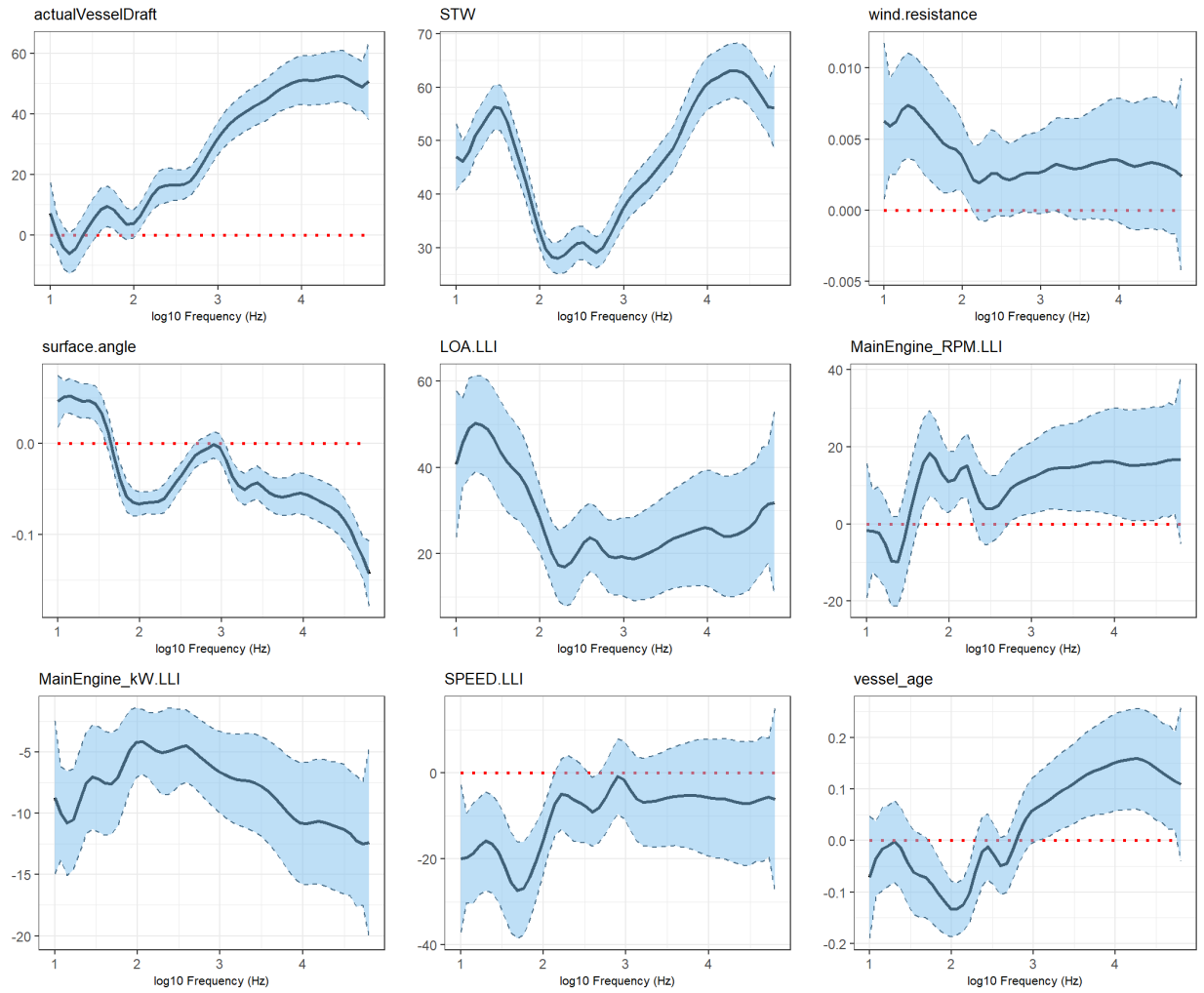
actualVesselDraft
STW
wind.resistance
surface.angle
LOA.LLI
MainEngine_RPM.LLI
MainEngine_kW.LLI
SPEED.LLI
vessel_age
log10 Frequency (Hz)

C.2.3. Cruise

C.2.3.1. MSL

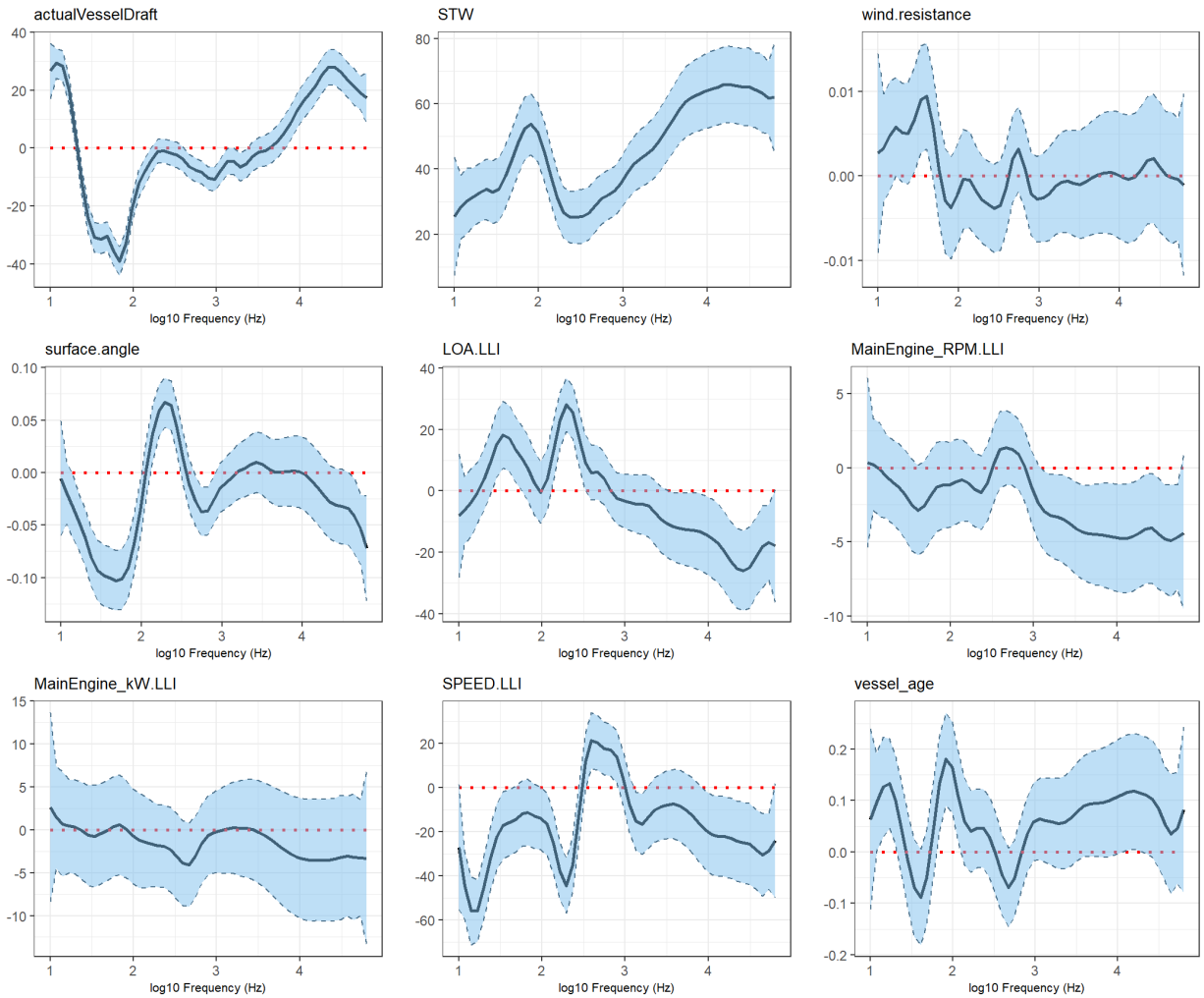

C.2.3.2. RNL

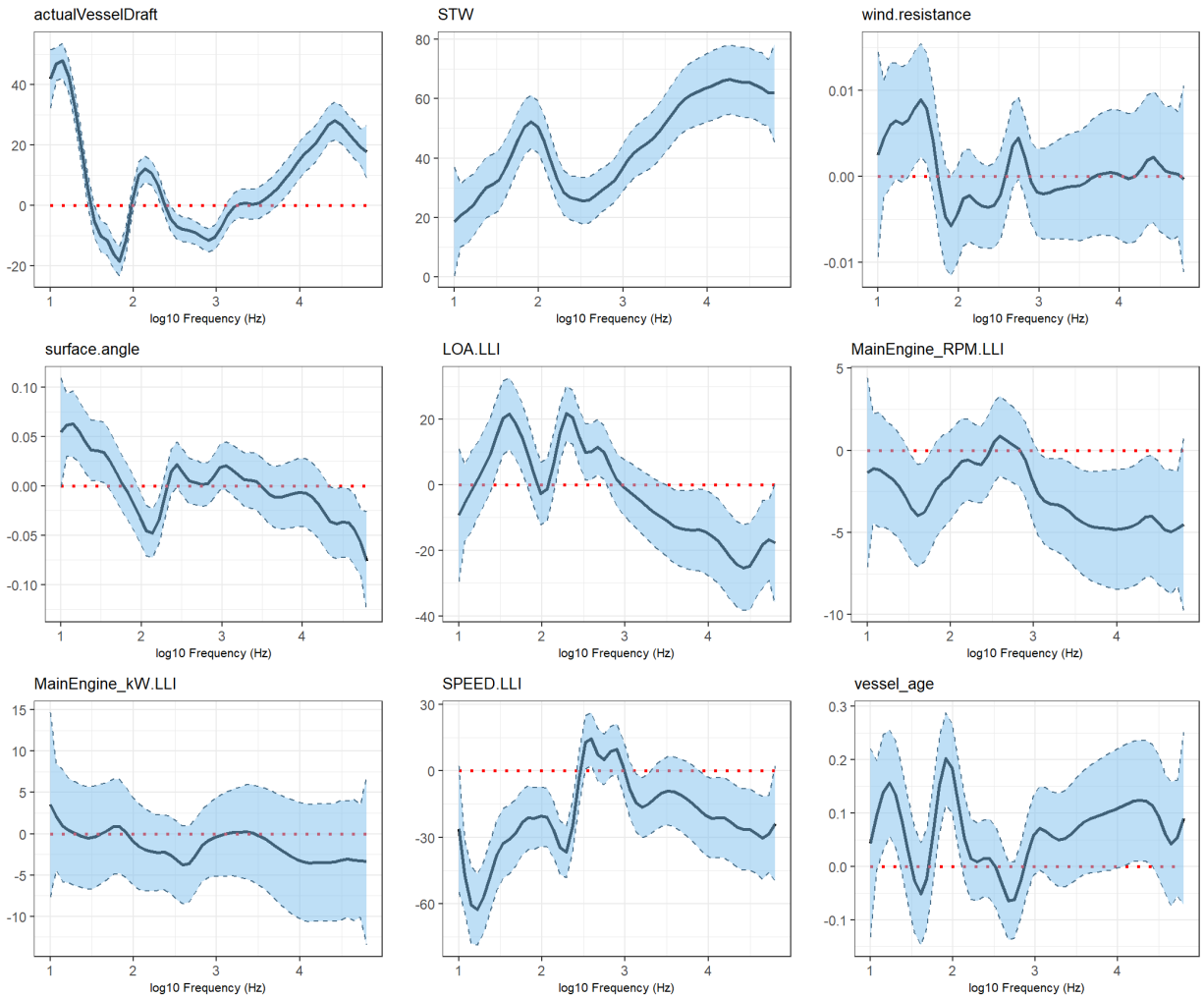
actualVesselDraft
STW
wind.resistance
surface.angle
LOA.LLI
MainEngine_RPM.LLI
MainEngine_kW.LLI
SPEED.LLI
vessel_age
log10 Frequency (Hz)

C.2.4. Tanker

C.2.4.1. MSL

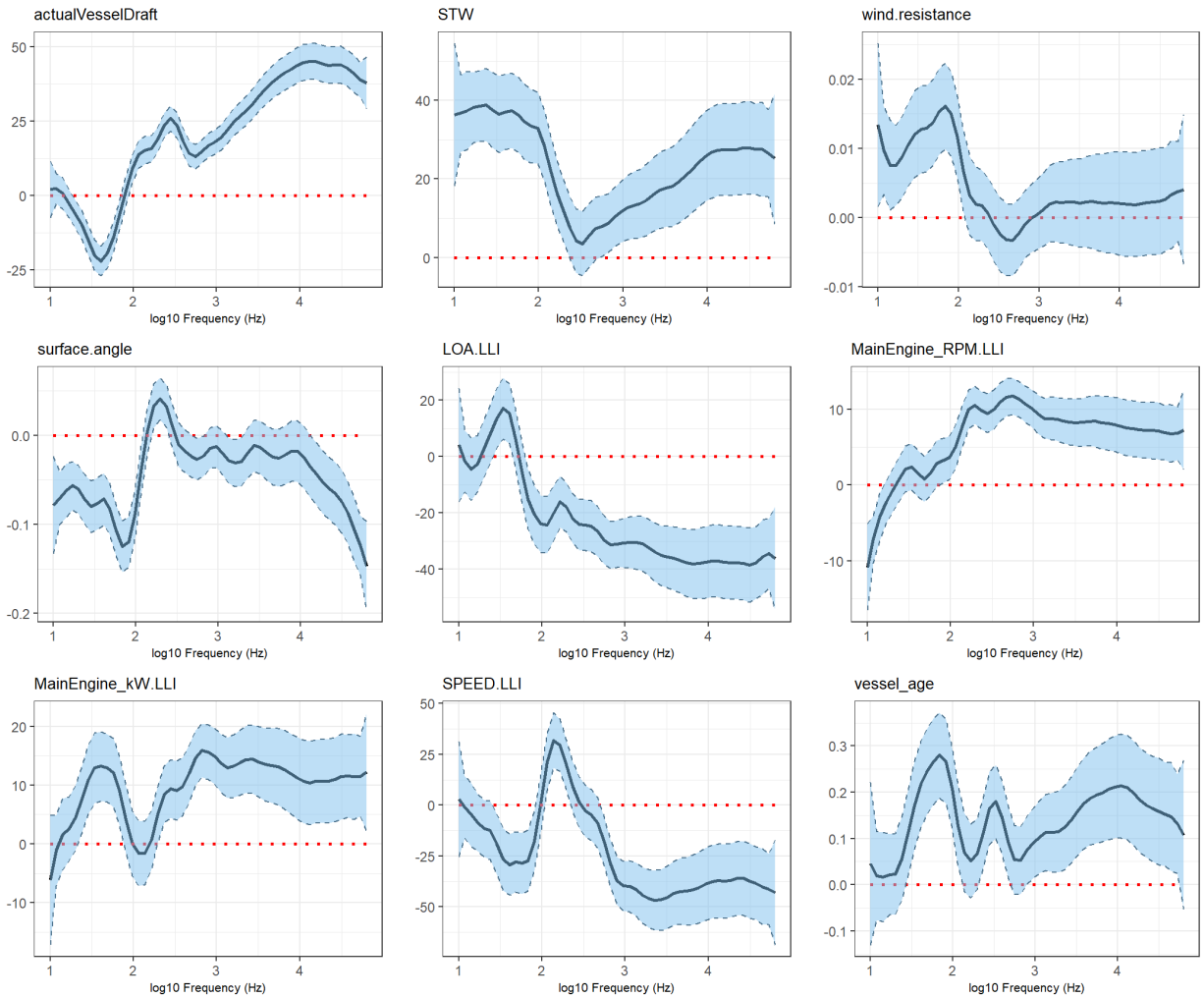

C.2.4.2. RNL

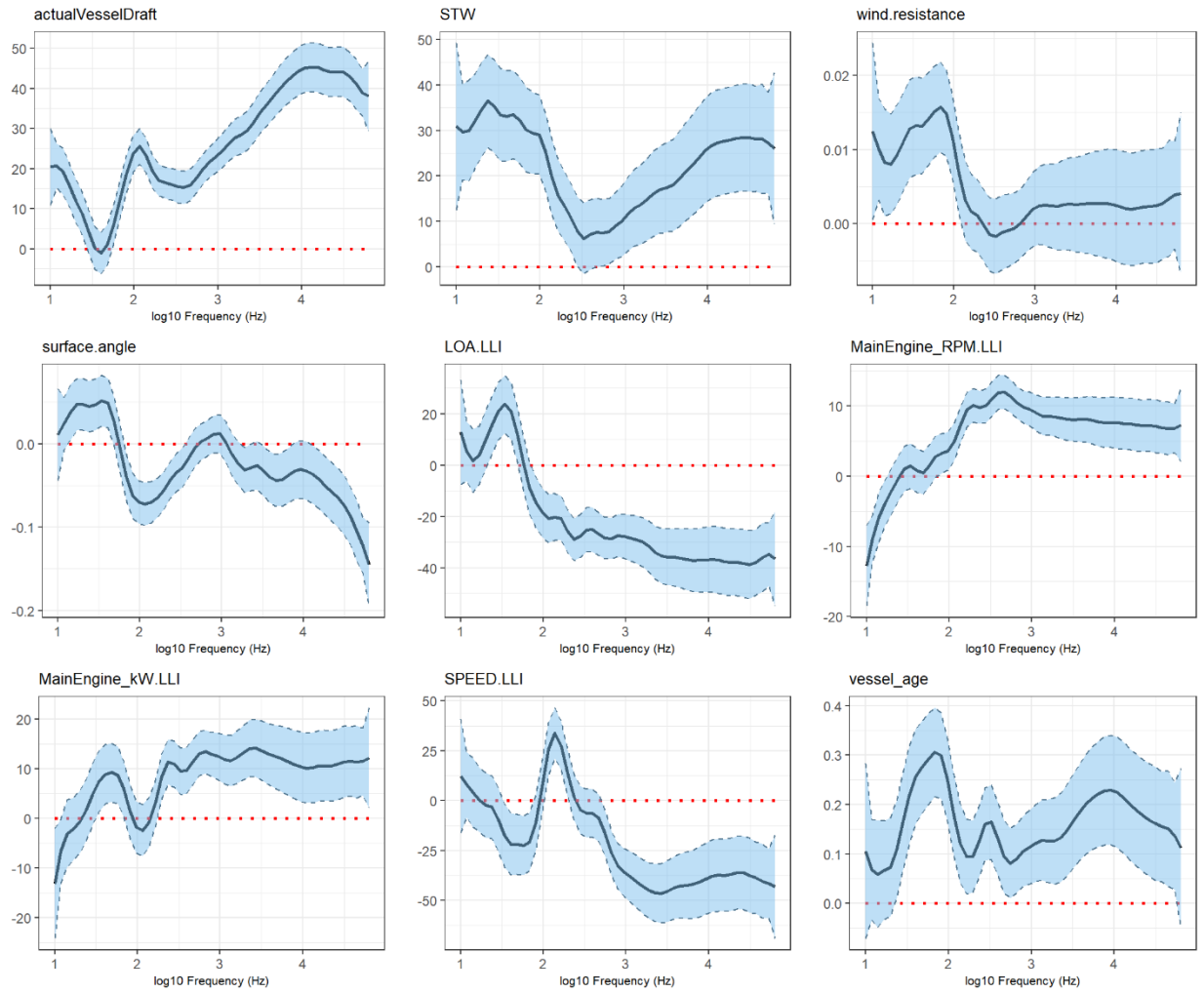
actualVesselDraft
STW
wind.resistance
surface.angle
LOA.LLI
MainEngine_RPM.LLI
MainEngine_kW.LLI
SPEED.LLI
vessel_age
log10 Frequency (Hz)

C.2.5. Tugs

C.2.5.1. MSL

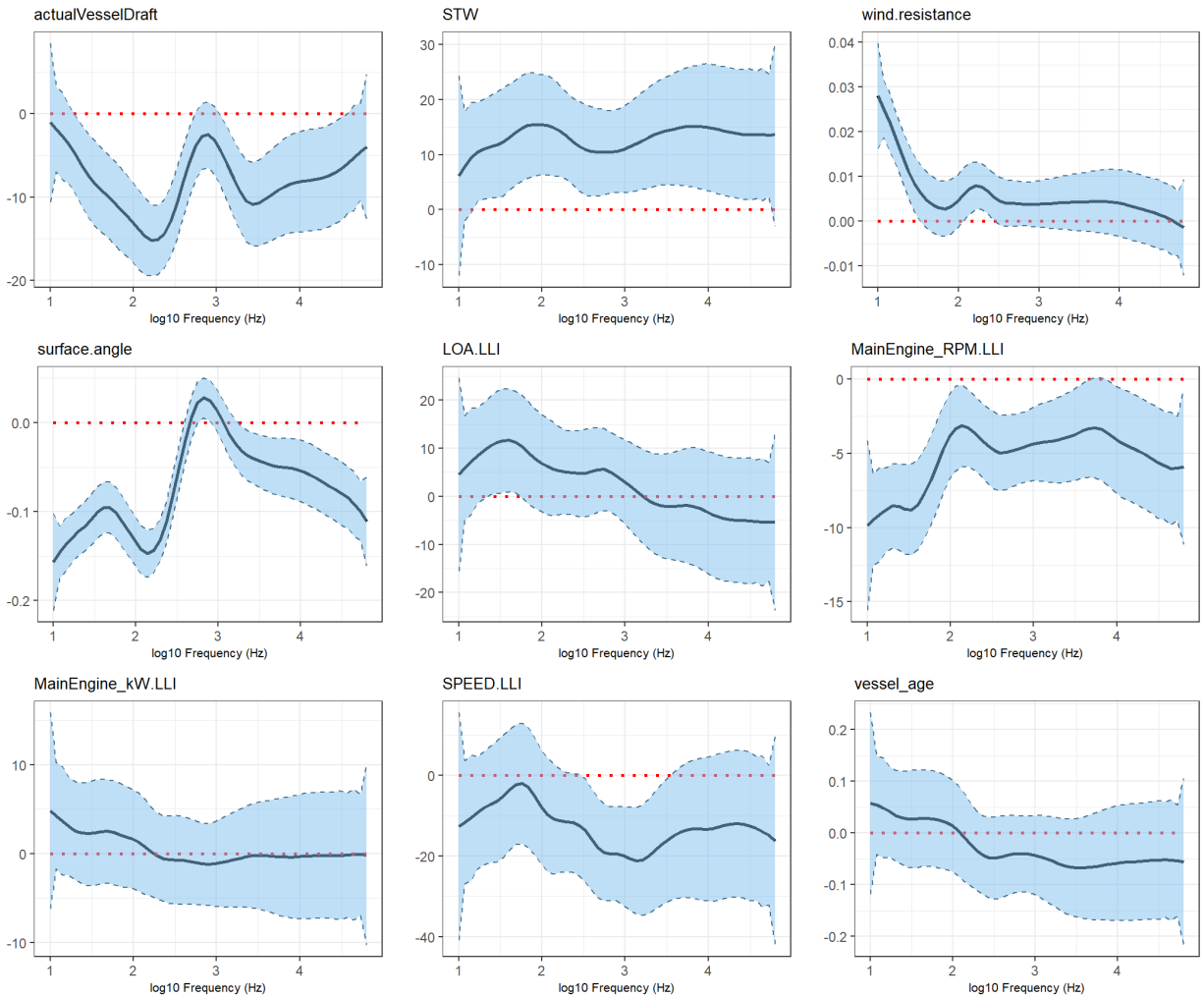

C.2.5.2. RNL

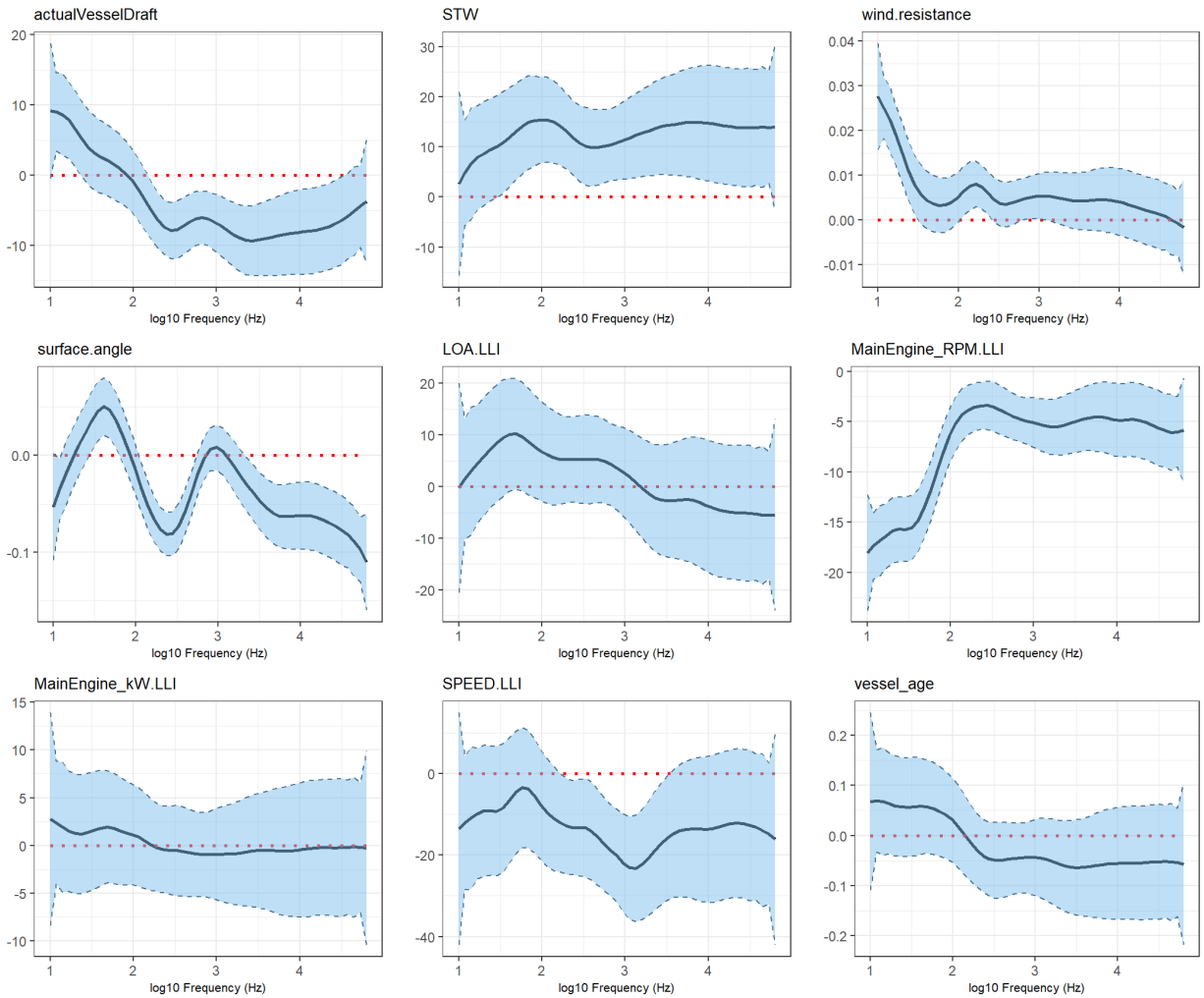
actualVesselDraft
STW
wind.resistance
surface.angle
LOA.LLI
MainEngine_RPM.LLI
MainEngine_kW.LLI
SPEED.LLI
vessel_age
log10 Frequency (Hz)

C.2.6. Vehicle Carriers

C.2.6.1. MSL

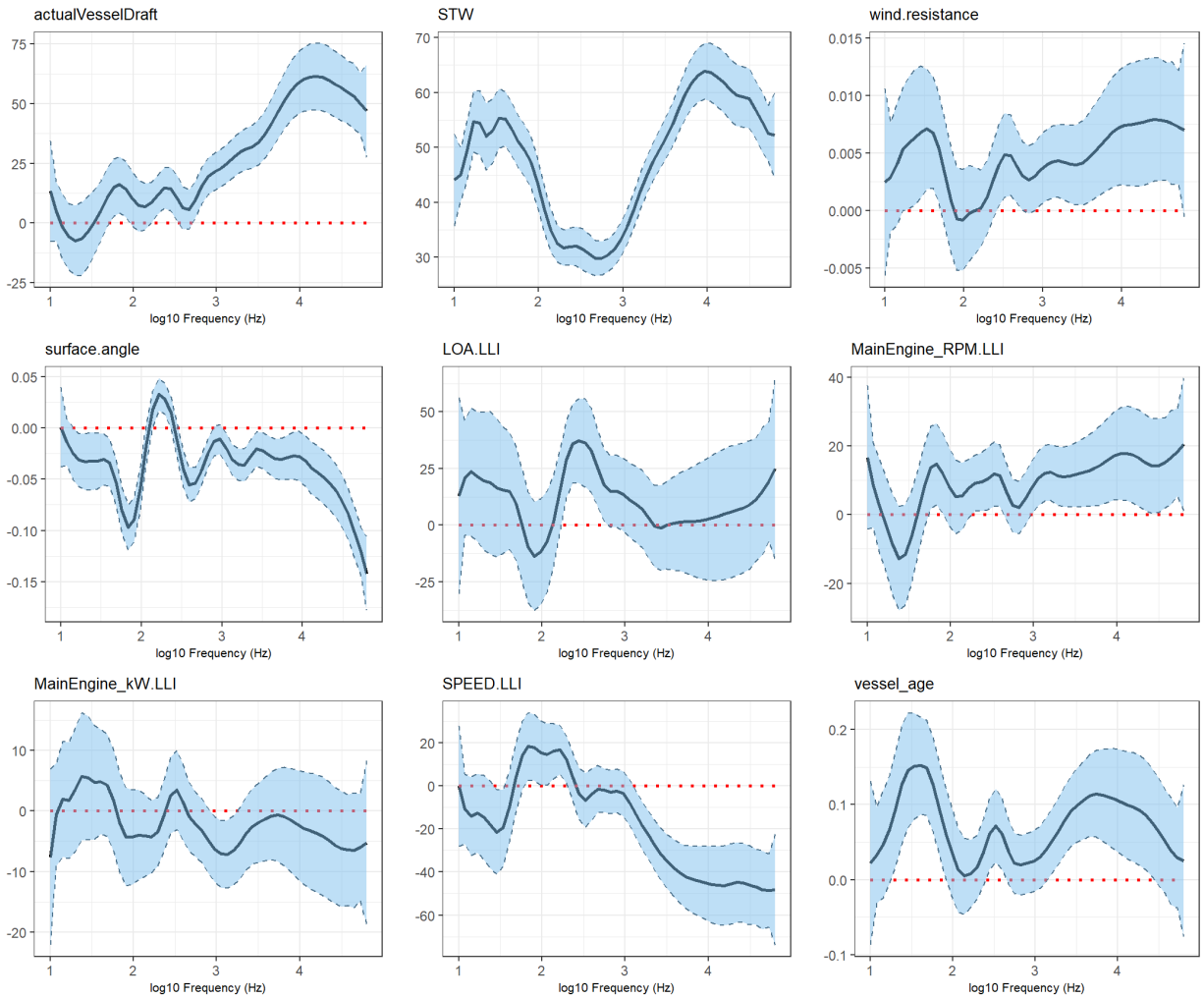

C.2.6.2. RNL

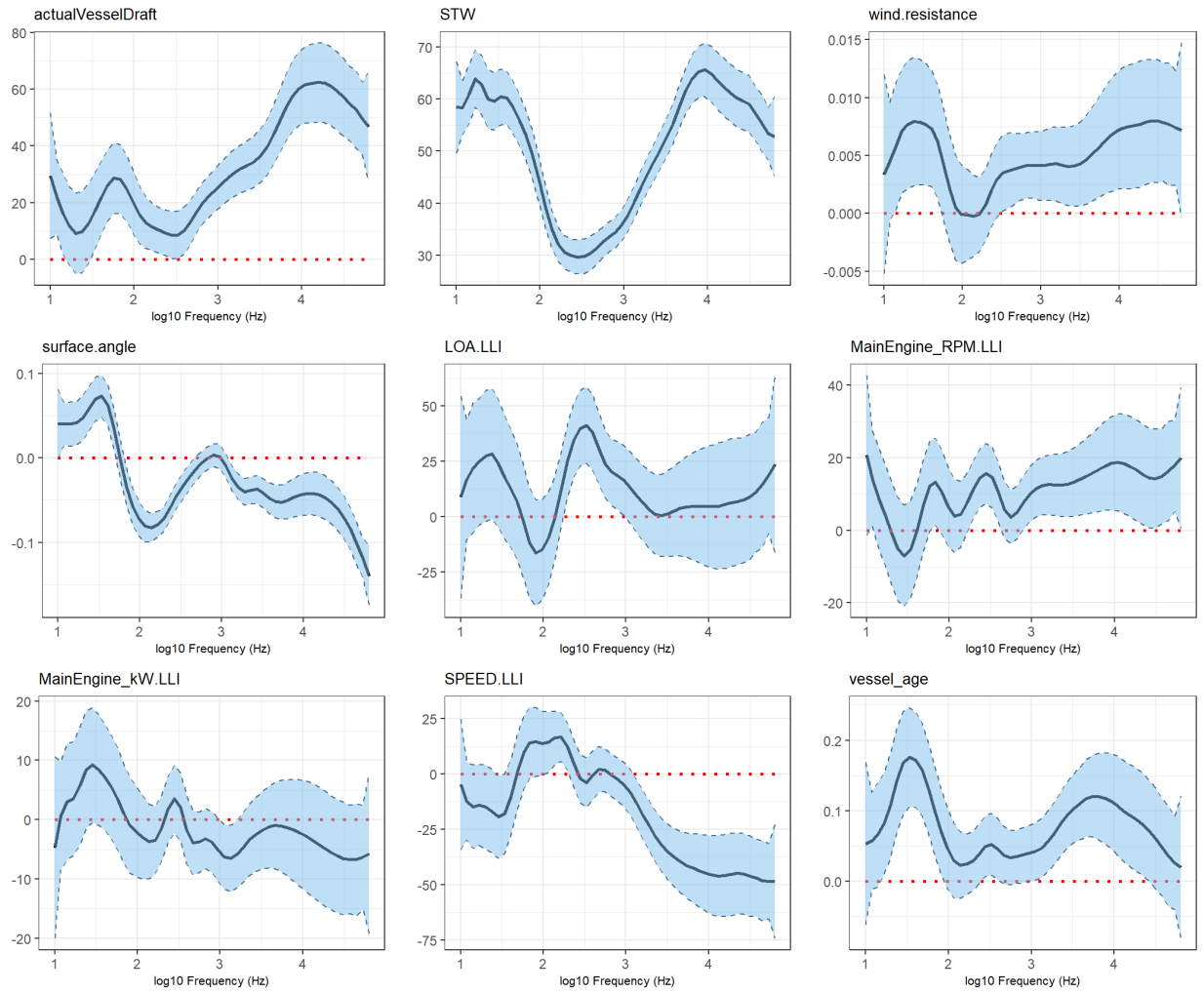
actualVesselDraft
STW
wind.resistance
surface.angle
LOA.LLI
MainEngine_RPM.LLI
MainEngine_kW.LLI
SPEED.LLI
vessel_age
log10 Frequency (Hz)

C.3. Influence Plots

Plots in this appendix show the influence of individual predictors on source levels (dB re 1 µPa m) of an average vessel in each group. Each panel shows the effect of varying a different predictor in the model, while keeping the other predictors constant. The curves show the predicted deviation from the mean source level obtained by varying the predictor value over the range indicated by the colour bar. The colour of each curve corresponds to the associated predictor value. For covariates having more than 200 possible values in the data, 200 values were randomly selected, as well as the minimum and maximum value. Narrow groups of lines correspond to cases where there was very little variation with a given predictor.

C.3.1. Bulkers

C.3.1.1. MSL

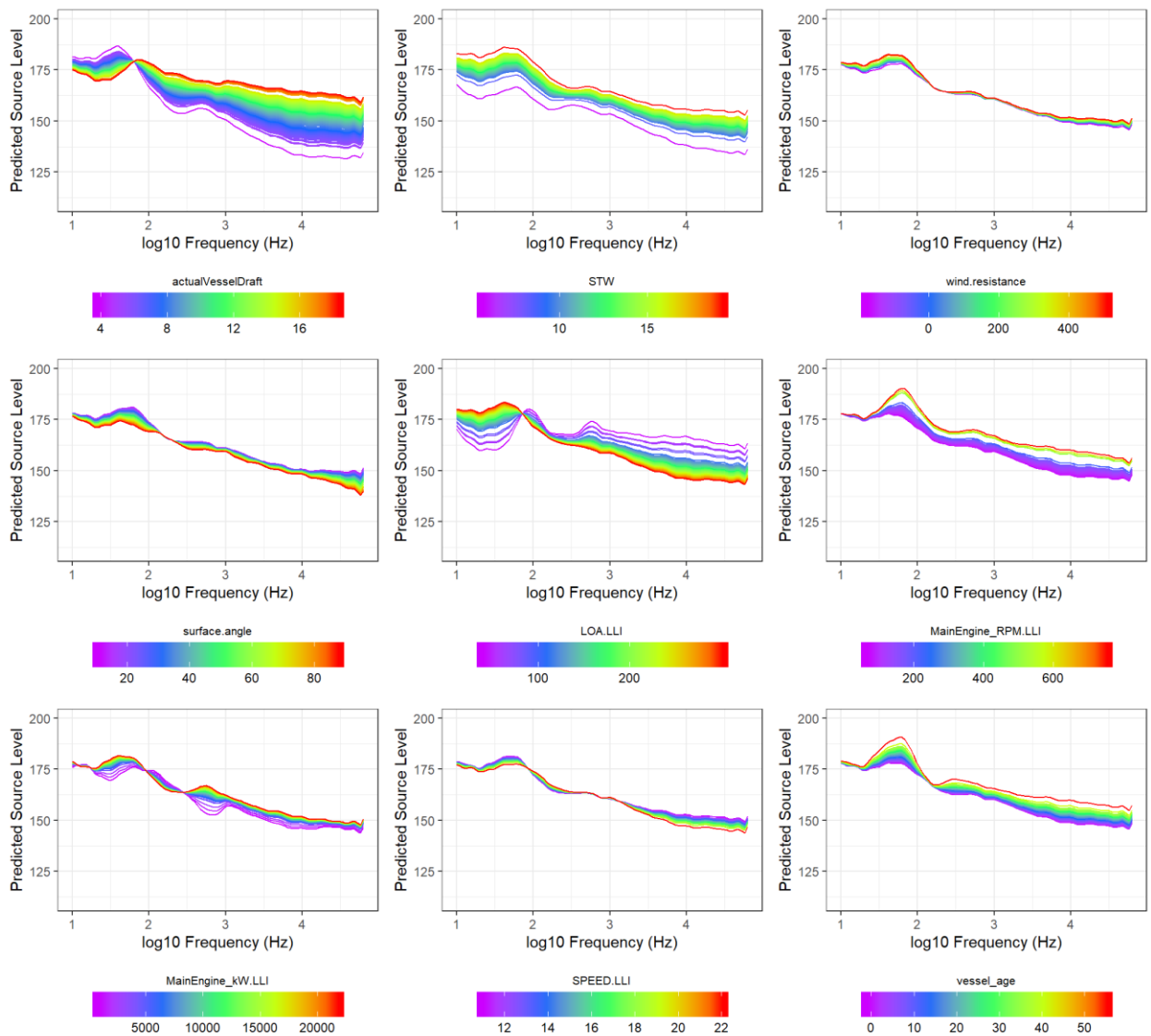

C.3.1.2. RNL

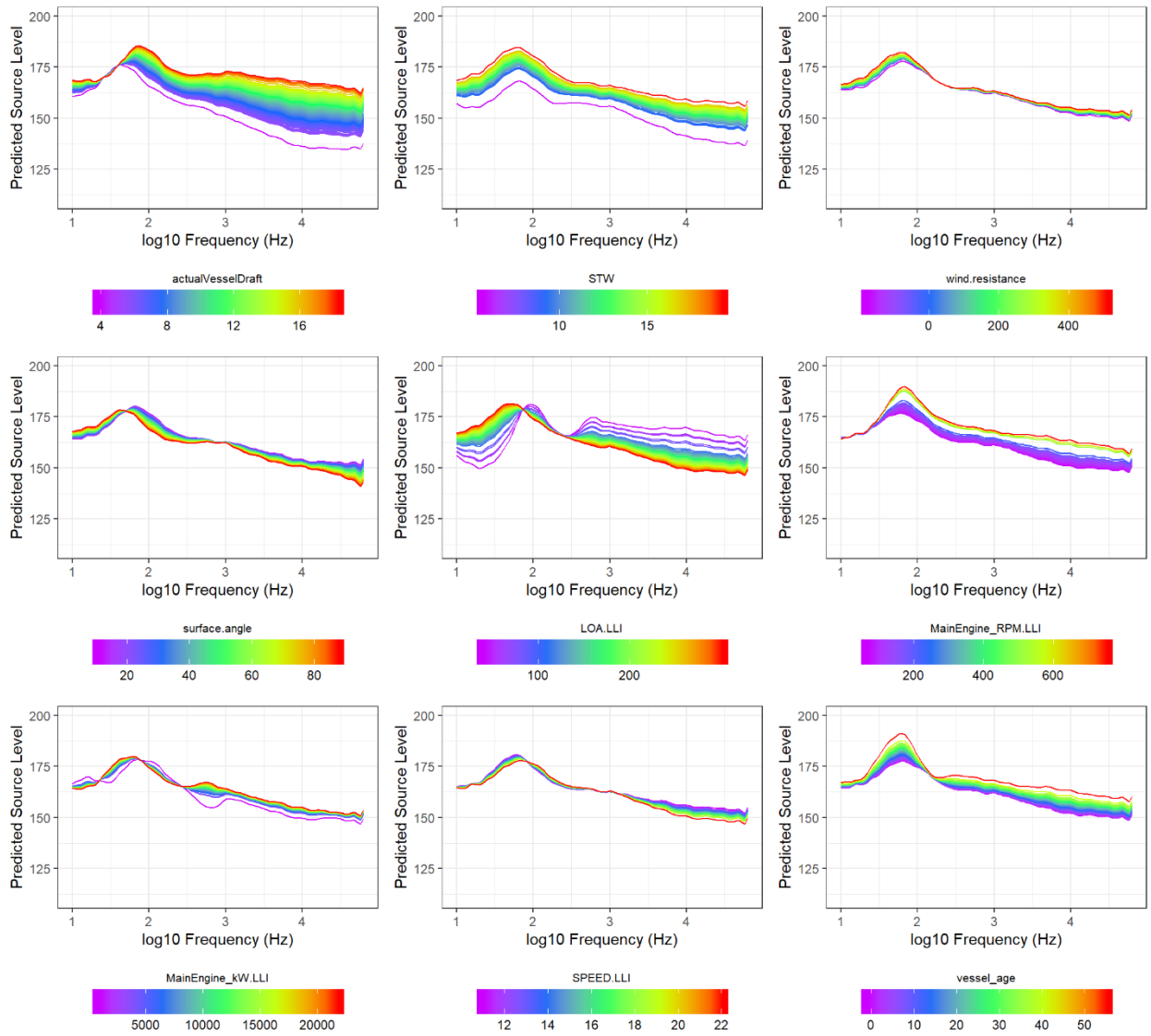
Predicted Source Level
log10 Frequency (Hz)
actualVesselDraft
STW
wind.resistance
surface.angle
LOA.LLI
MainEngine_RPM.LLI
MainEngine_kW.LLI
SPEED.LLI
vessel_age

C.3.2. Containers

C.3.2.1. MSL

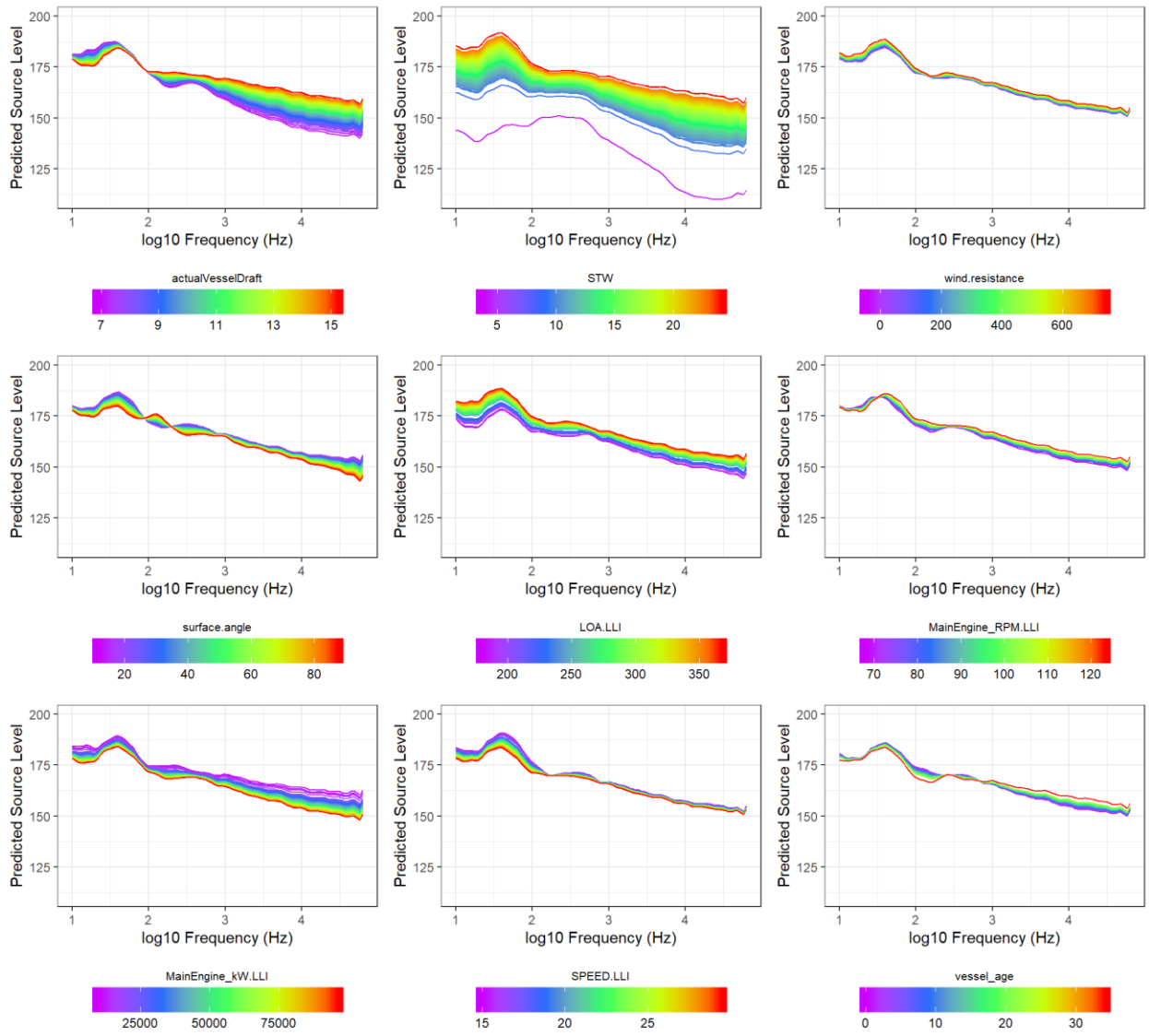

C.3.2.2. RNL

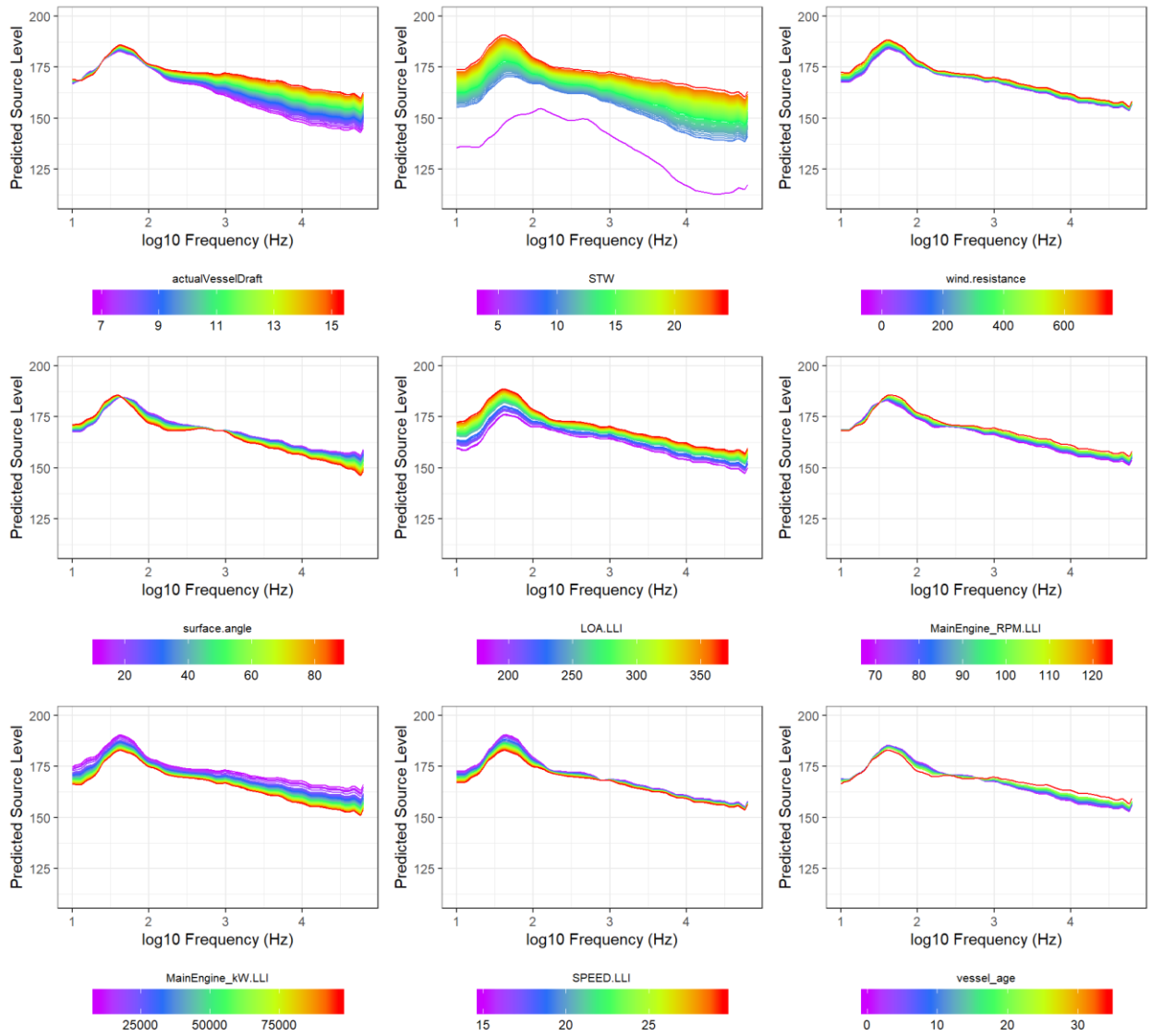
Predicted Source Level
log10 Frequency (Hz)
actualVesselDraft
7 9 11 13 15
STW
5 10 15 20
wind.resistance
0 200 400 600
surface.angle
20 40 60 80
LOA.LLI
200 250 300 350
MainEngine_RPM.LLI
70 80 90 100 110 120
MainEngine_kW.LLI
25000 50000 75000
SPEED.LLI
15 20 25
vessel_age
0 10 20 30

C.3.3. Cruise

C.3.3.1. MSL

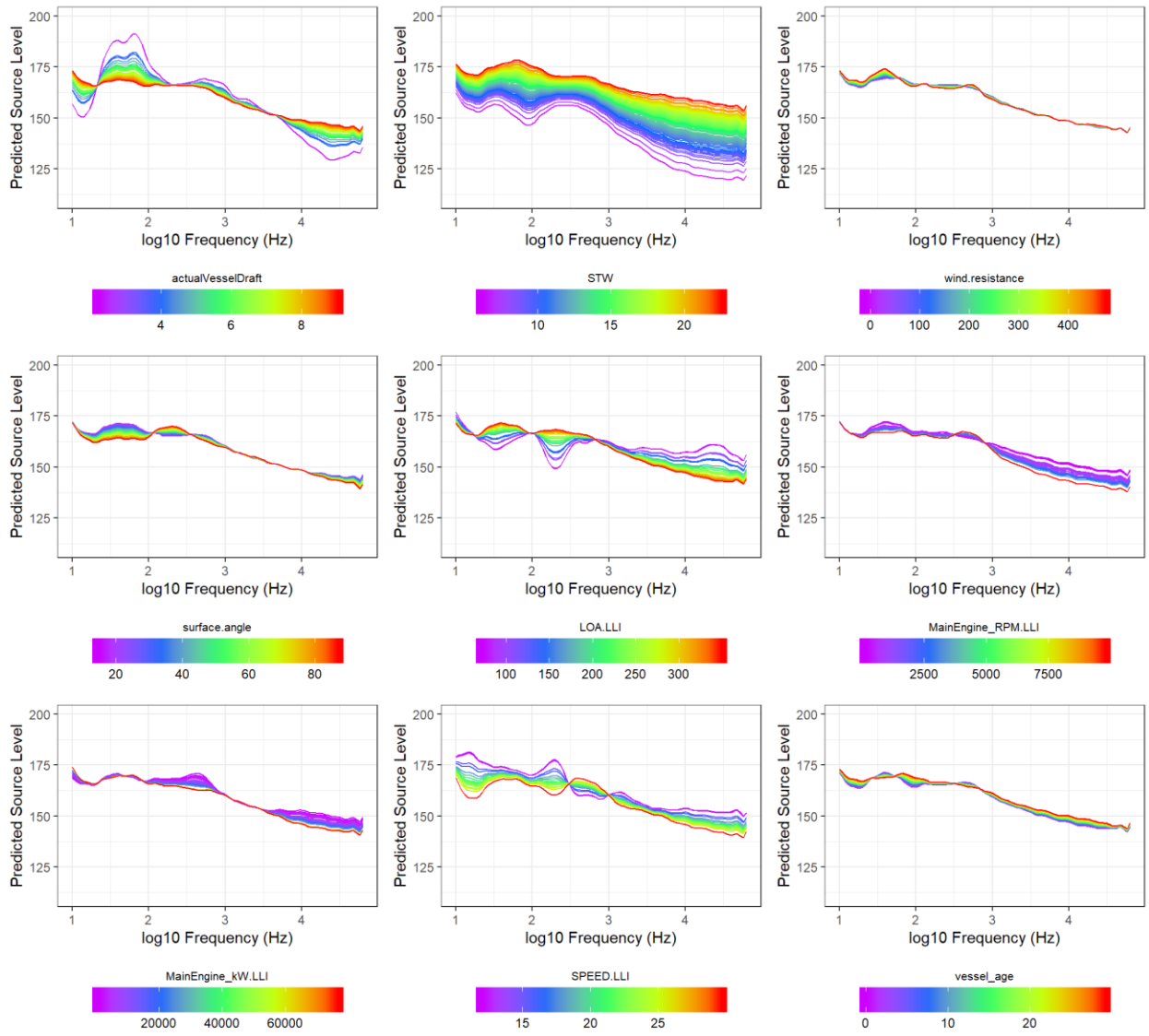

C.3.3.2. RNL

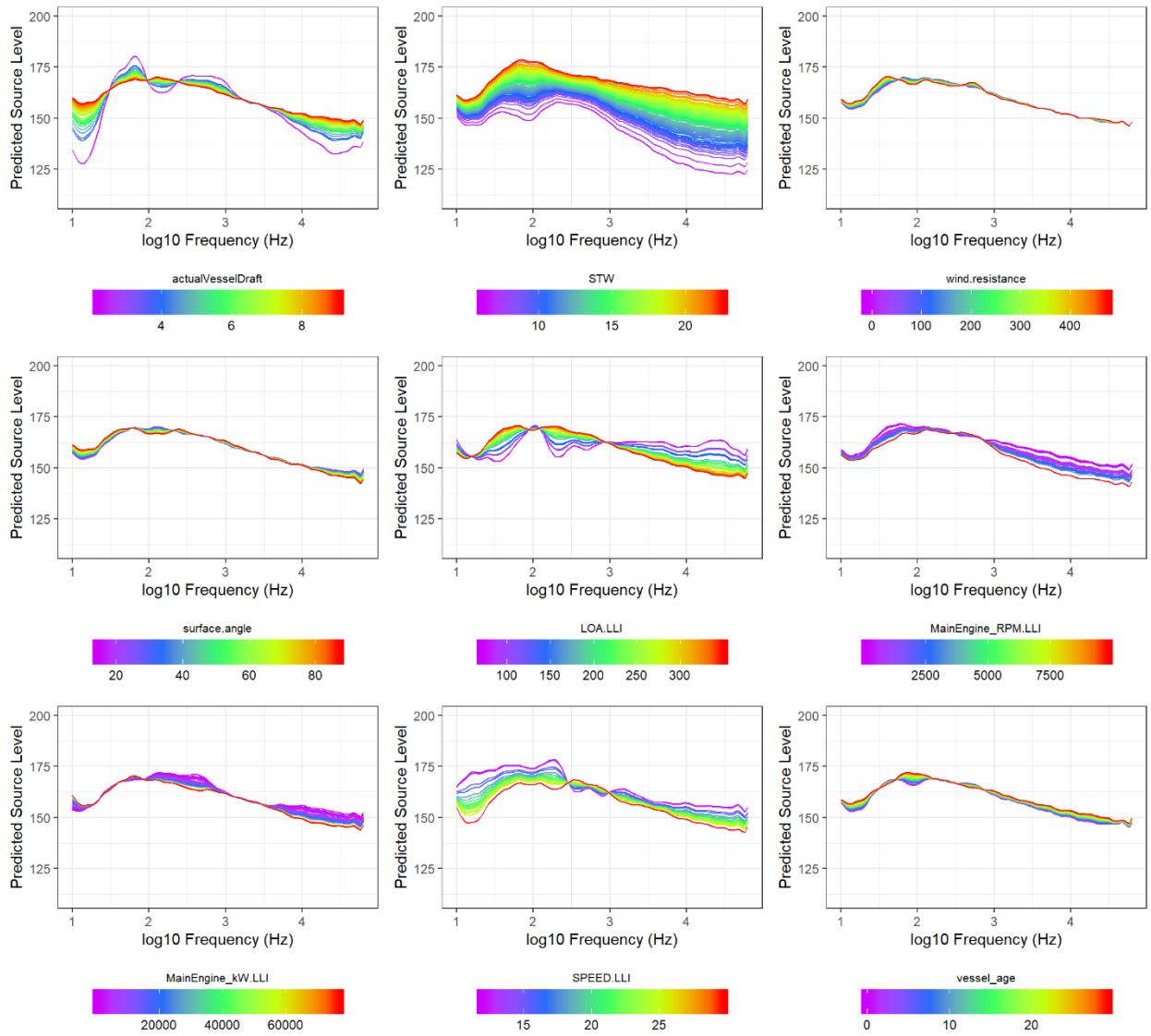
Predicted Source Level
log10 Frequency (Hz)
actualVesselDraft
STW
wind.resistance
surface.angle
LOA.LLI
MainEngine_RPM.LLI
MainEngine_kW.LLI
SPEED.LLI
vessel_age

C.3.4. Tanker

C.3.4.1. MSL

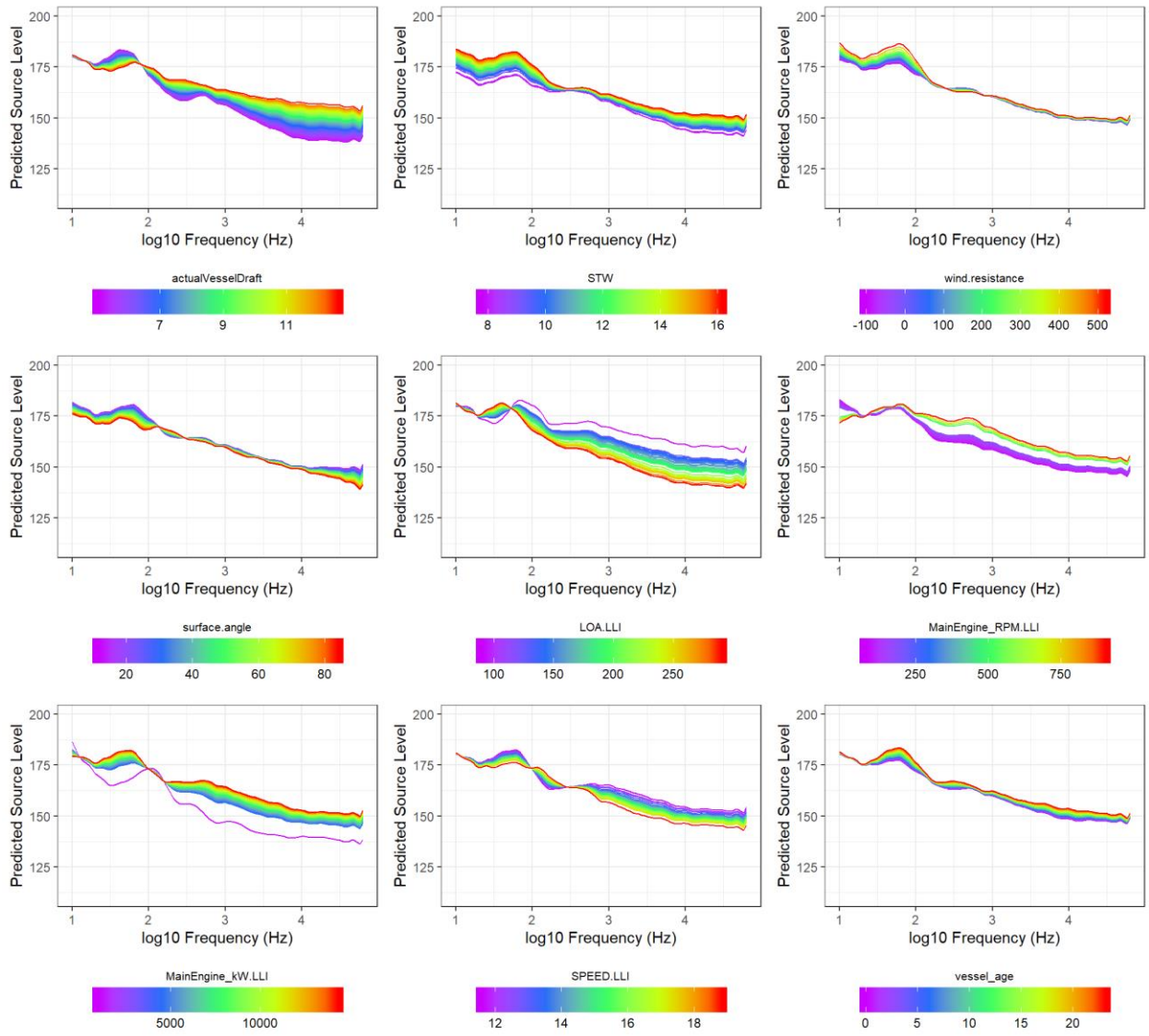

C.3.4.2. RNL

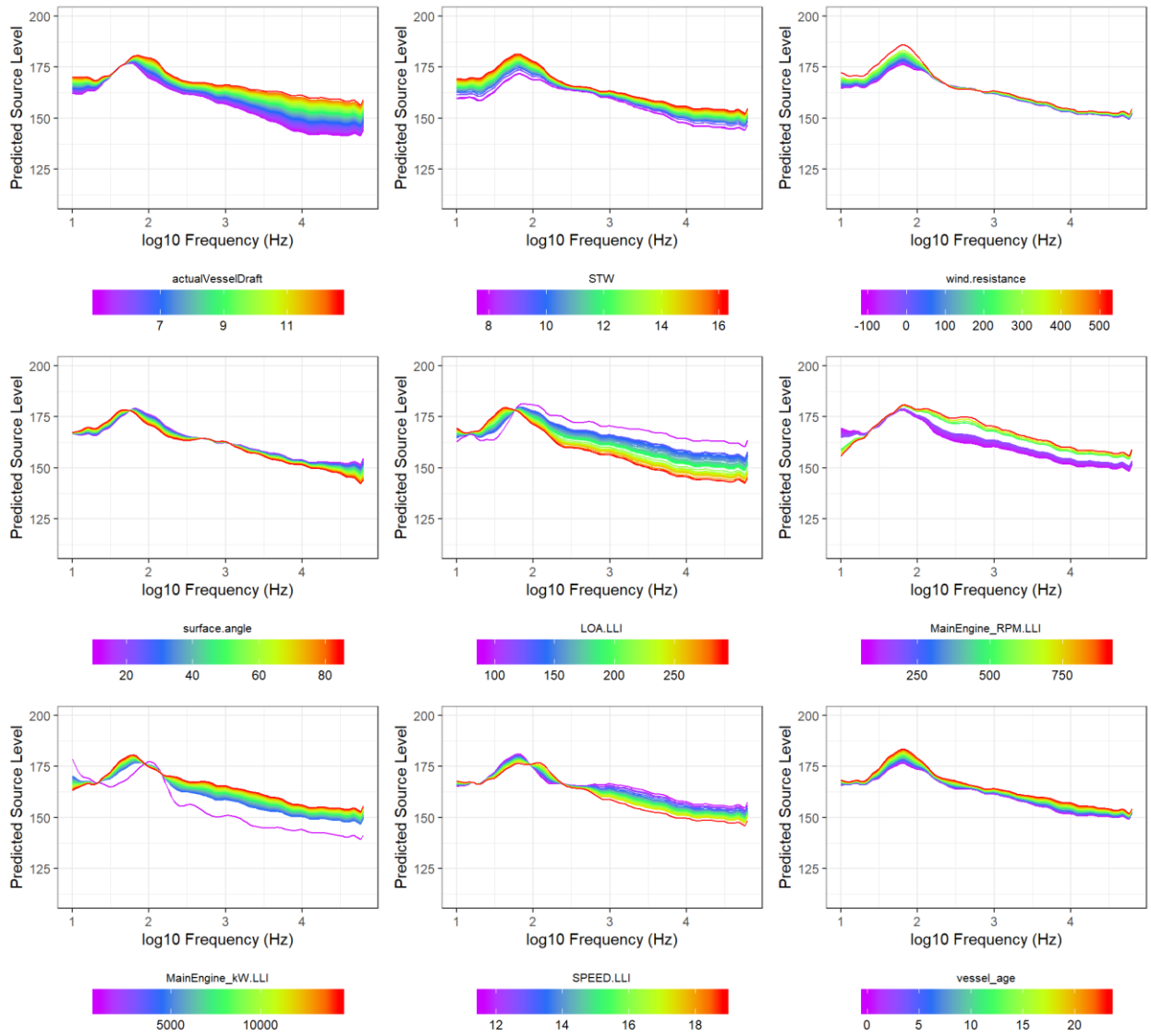
Predicted Source Level
log10 Frequency (Hz)
actualVesselDraft
7 9 11
STW
8 10 12 14 16
wind.resistance
-100 0 100 200 300 400 500
surface.angle
20 40 60 80
LOA.LLI
100 150 200 250
MainEngine_RPM.LLI
250 500 750
MainEngine_kW.LLI
5000 10000
SPEED.LLI
12 14 16 18
vessel_age
0 5 10 15 20

C.3.5. Tugs

C.3.5.1. MSL

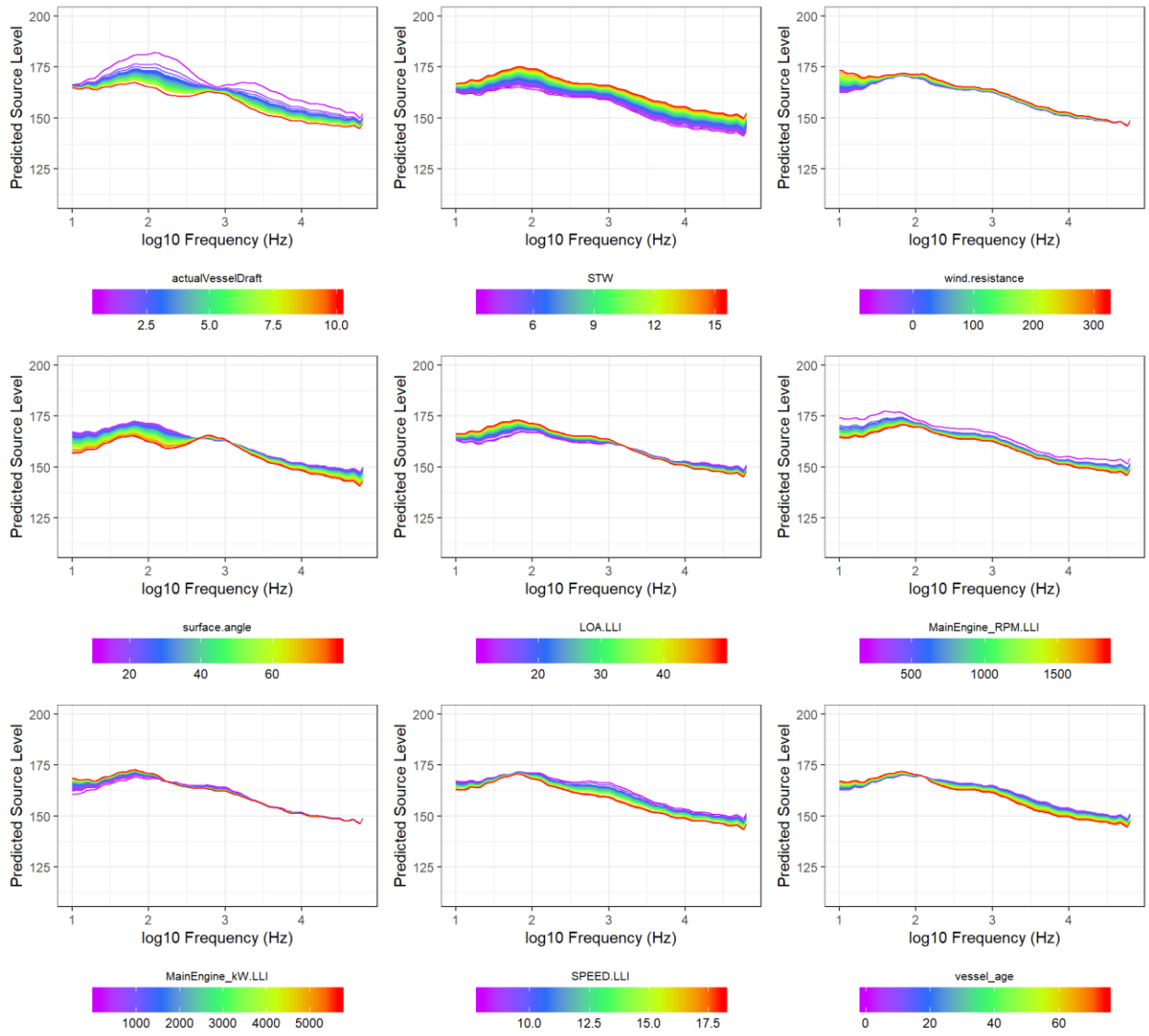

C.3.5.2. RNL

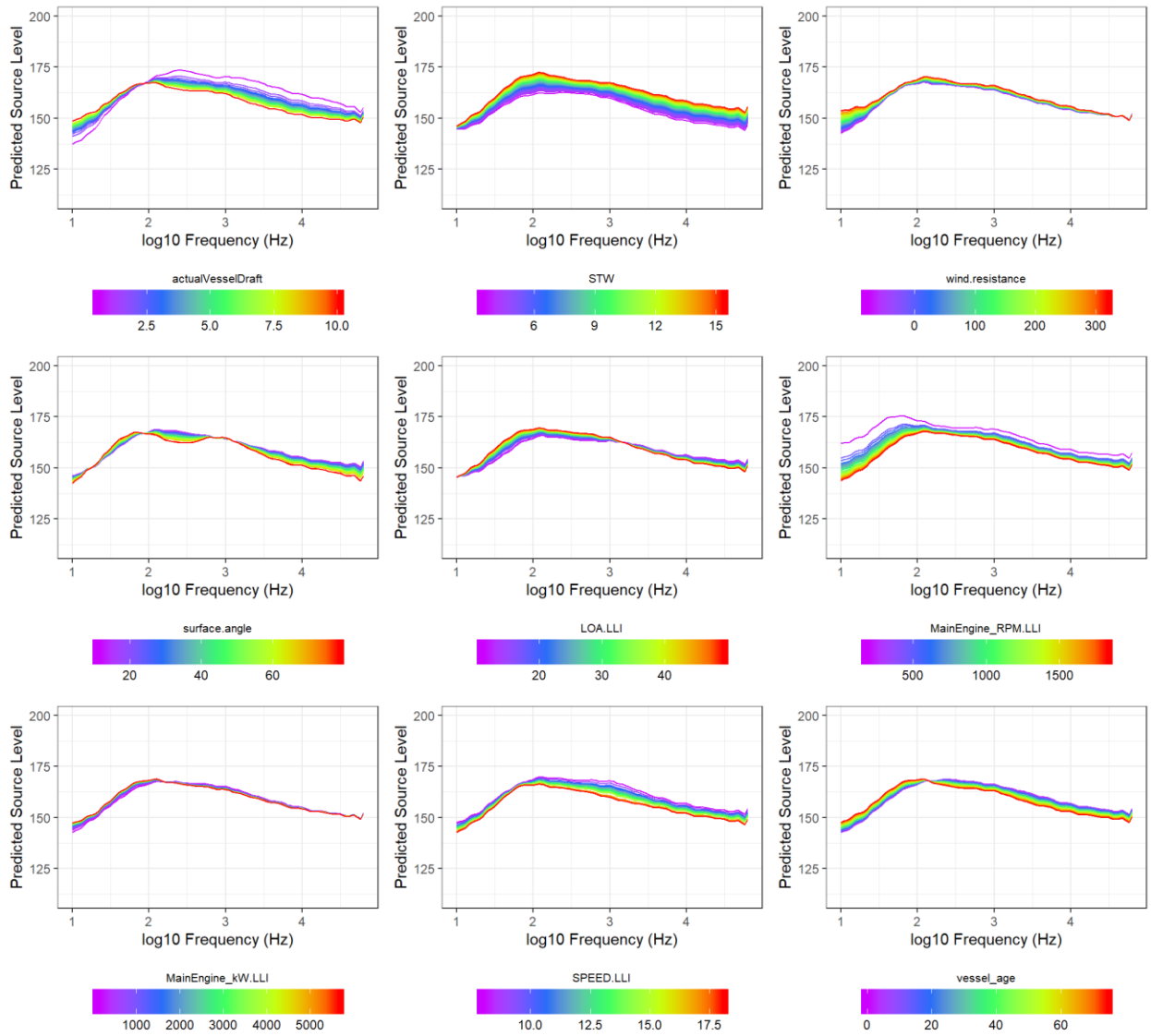
Predicted Source Level
log10 Frequency (Hz)
actualVesselDraft
2.5 5.0 7.5 10.0
STW
6 9 12 15
wind.resistance
0 100 200 300
surface.angle
20 40 60
LOA.LLI
20 30 40
MainEngine_RPM.LLI
500 1000 1500
MainEngine_kW.LLI
1000 2000 3000 4000 5000
SPEED.LLI
10.0 12.5 15.0 17.5
vessel_age
0 20 40 60

C.3.6. Vehicle Carriers

C.3.6.1. MSL

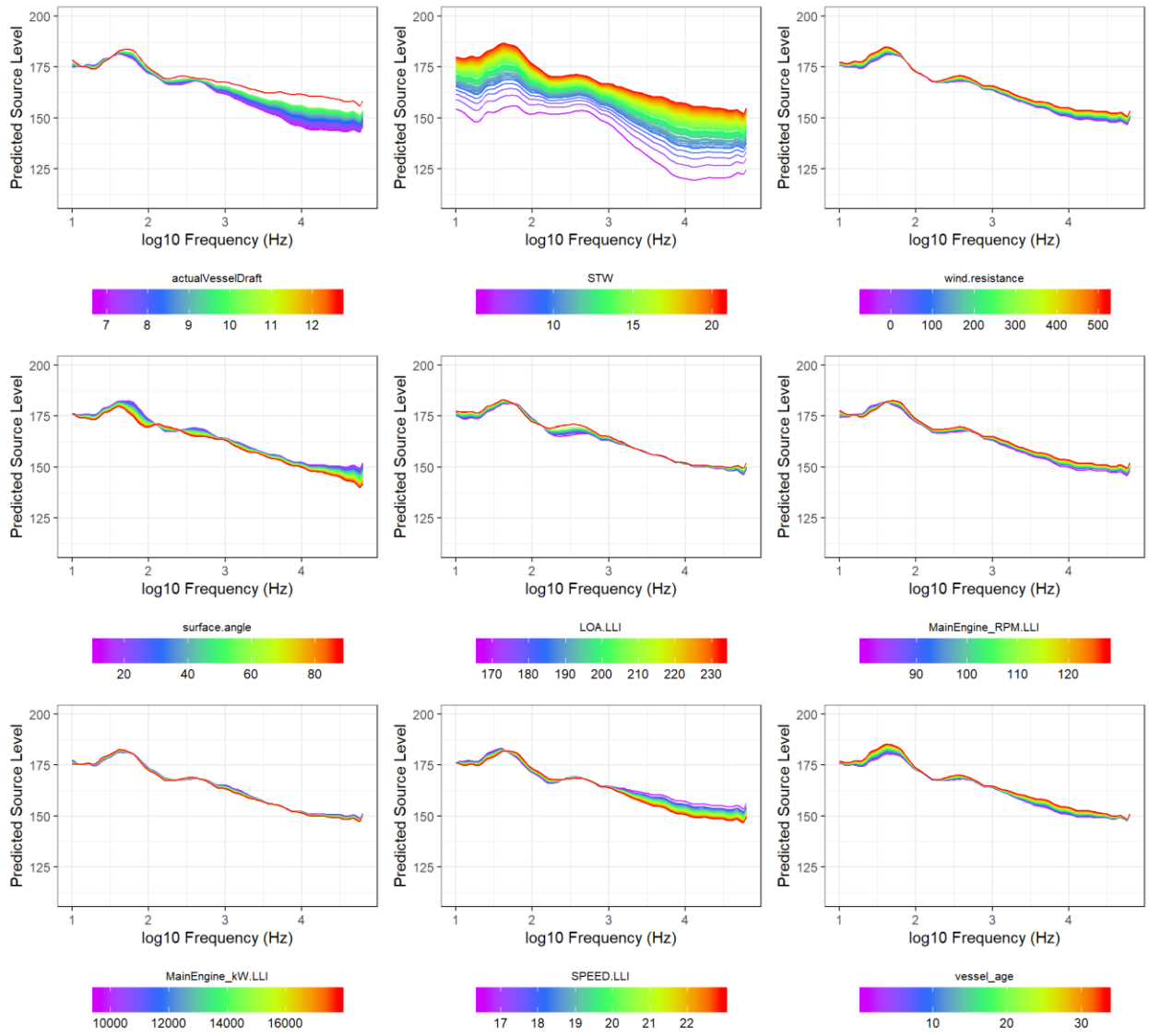

C.3.6.2. RNL

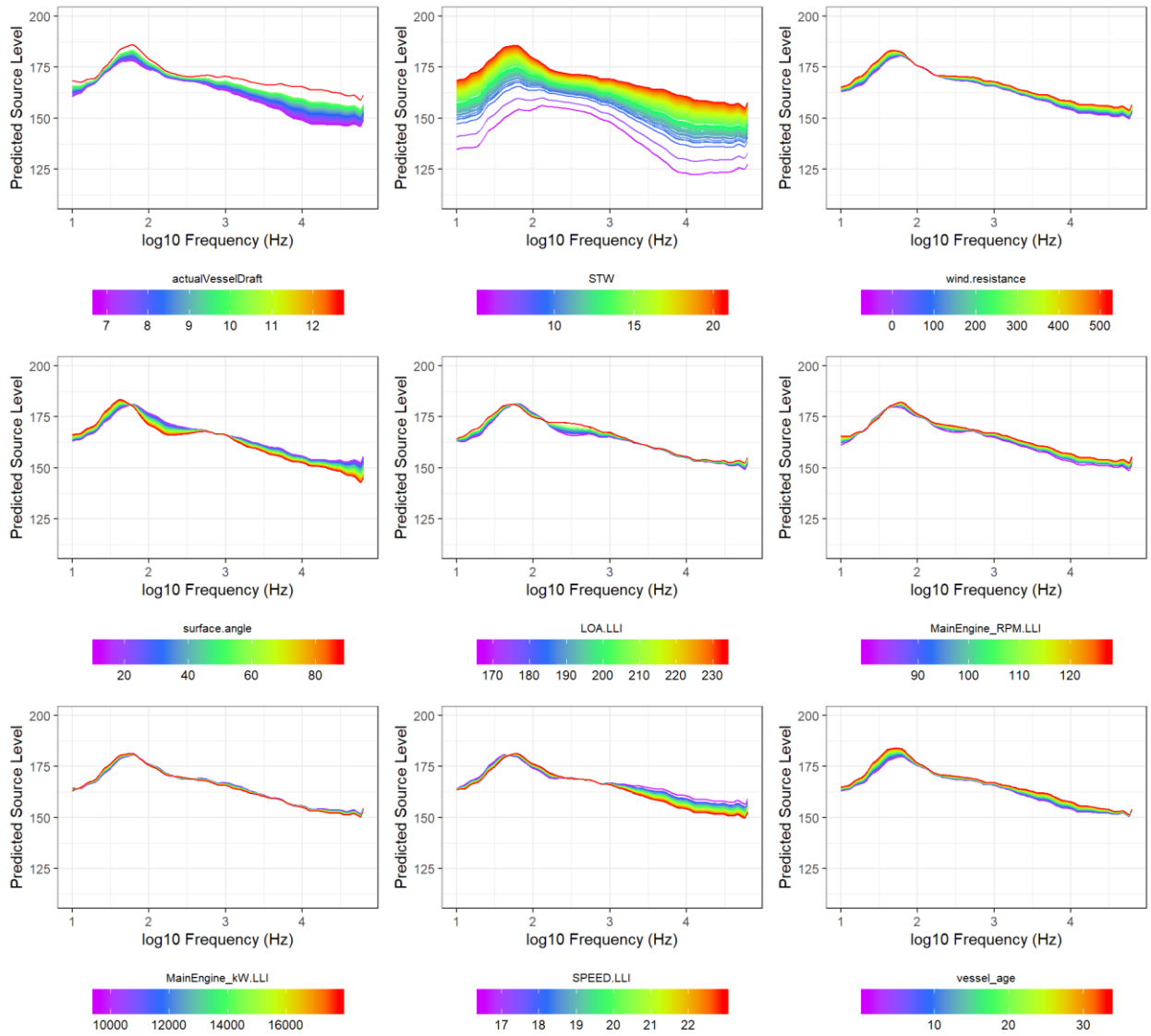
Predicted Source Level
log10 Frequency (Hz)
actualVesselDraft
7 8 9 10 11 12
STW
10 15 20
wind.resistance
0 100 200 300 400 500
surface.angle
20 40 60 80
LOA.LLI
170 180 190 200 210 220 230
MainEngine_RPM.LLI
90 100 110 120
MainEngine_kW.LLI
10000 12000 14000 16000
SPEED.LLI
17 18 19 20 21 22
vessel_age
10 20 30

Appendix D. EVDI Correlations

The following plots show correlations between underwater radiated noise and GHG emissions for each vessel category using the combined Phases 1 and 2 data sets, as follows:

- Left panels are scatter plots of adjusted decade-band RNL versus EVDI (grams CO_2 per tonne nautical mile). The blue lines indicate the best-fit linear trend for the data.
- Right panels are violin plots of adjusted decade-band RNL versus GHG rating (ranked from A-G). The width of the swath indicates the distribution of the data and interior boxes indicate the 25th, 50th, and 75th percentiles of the data (dots indicate outliers).

The measured RNL values have been adjusted for operating speed and draft of the vessels at time of measurement.

D.1. Bulkers

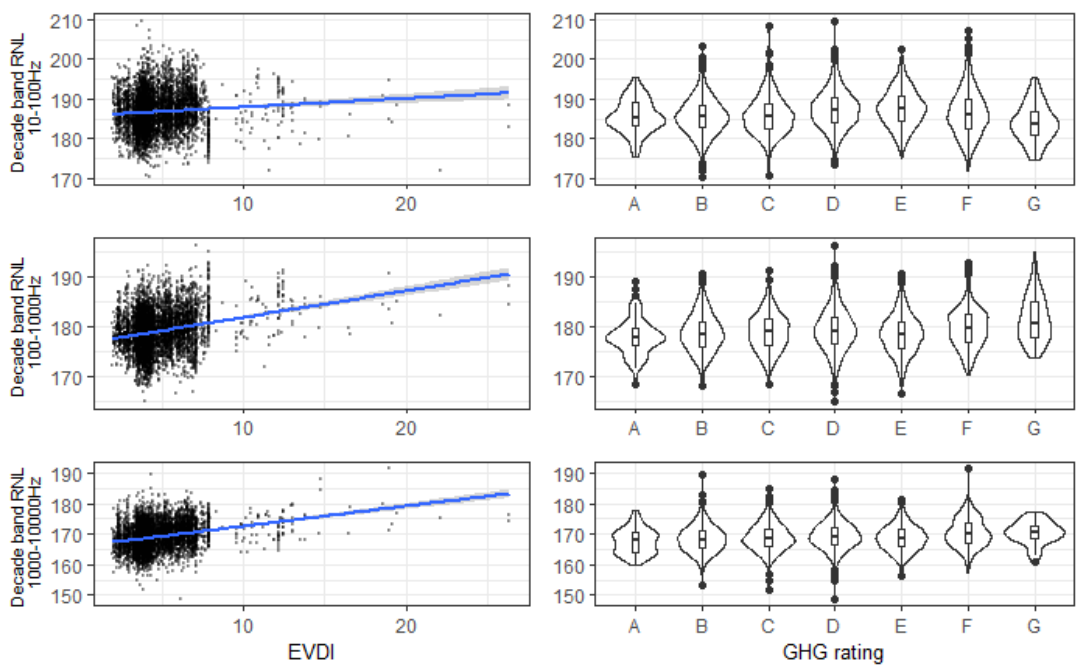

D.2. Containers

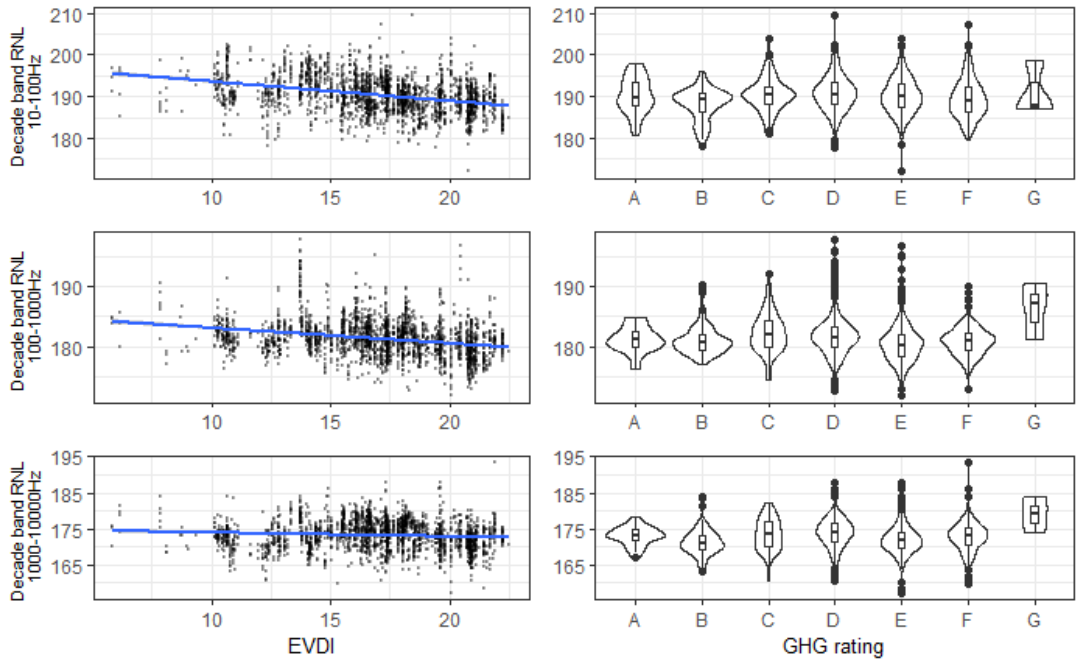

D.3. Tankers

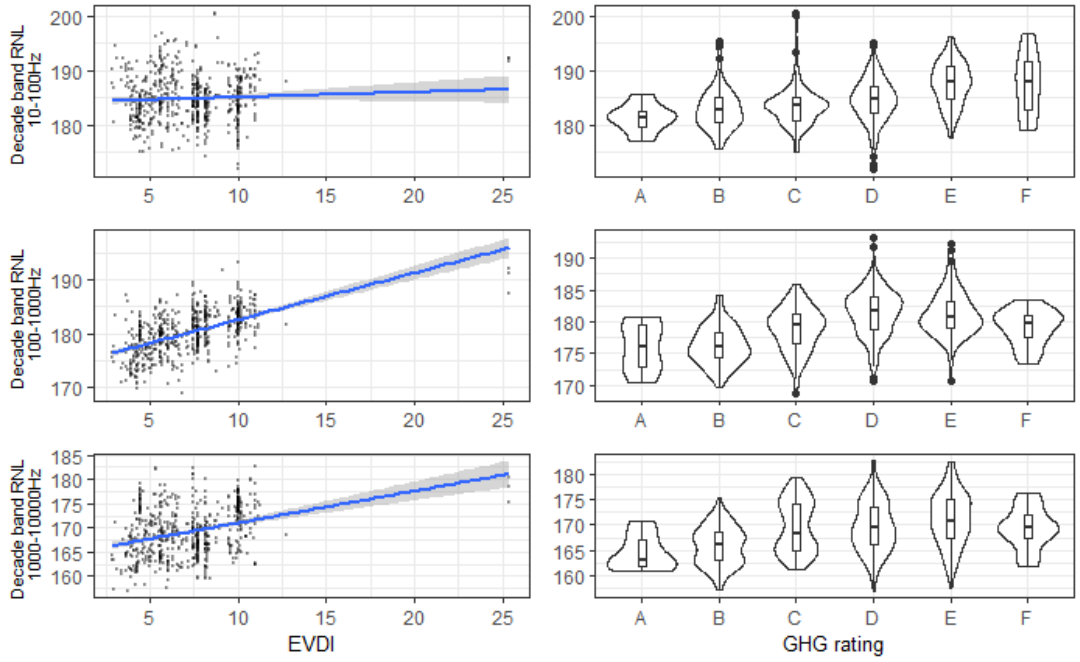

D.4. Vehicle Carriers

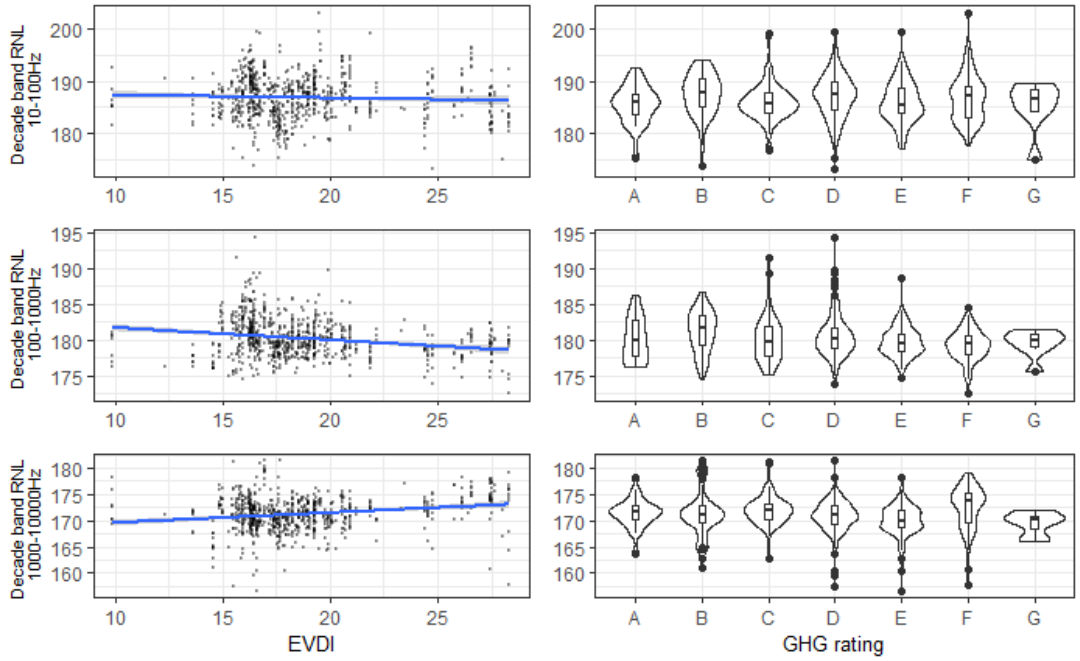

Appendix E. Single-vessel Correlations

E.1. Correlation Matrices

Correlation matrix plots in this appendix show correlations between pairs of variables in different vessel categories for the selected Task 3 vessels. The coloured circles indicate the strength and magnitude of the correlation (blue = positive, red = negative, correlations along the diagonal are r=1). The “?” indicates where the correlation cannot be computed between two variables (usually due to missing values, but sometimes due to a variable having a constant value).

E.1.1. Bulk Carrier A

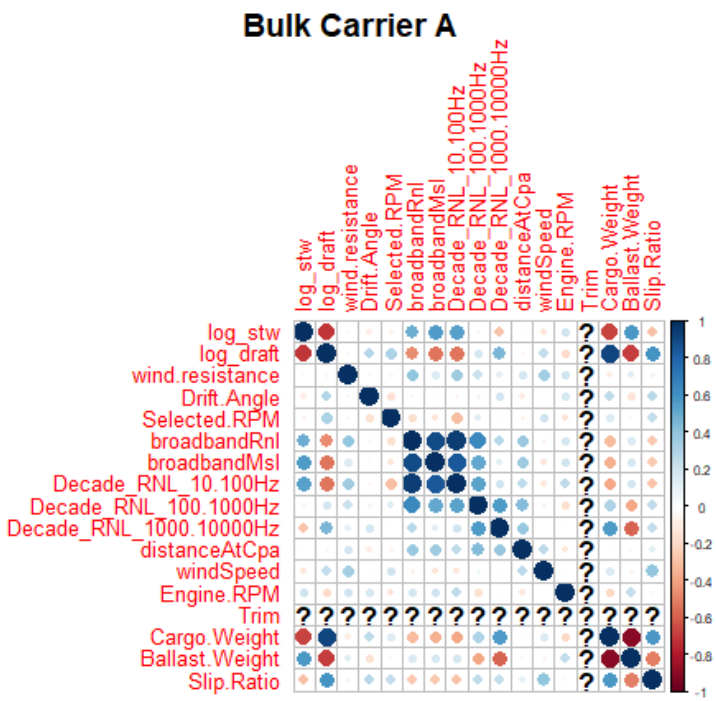

E.1.2. Container Ship A

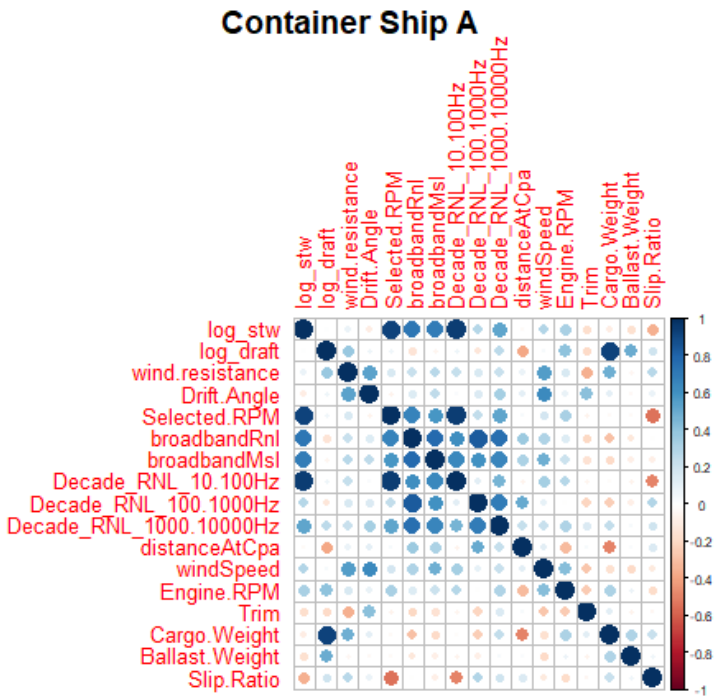

E.1.3. General Cargo Vessel A

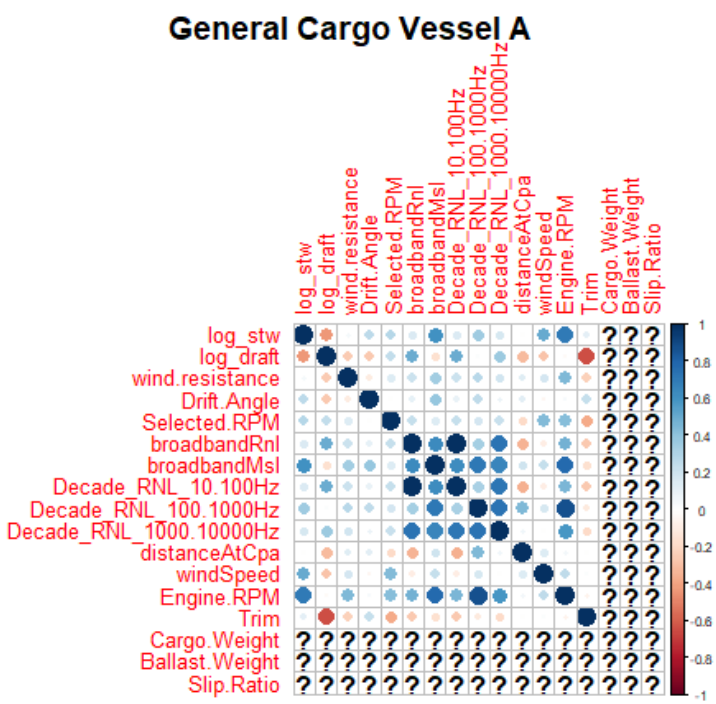

E.1.4. General Cargo Vessel B

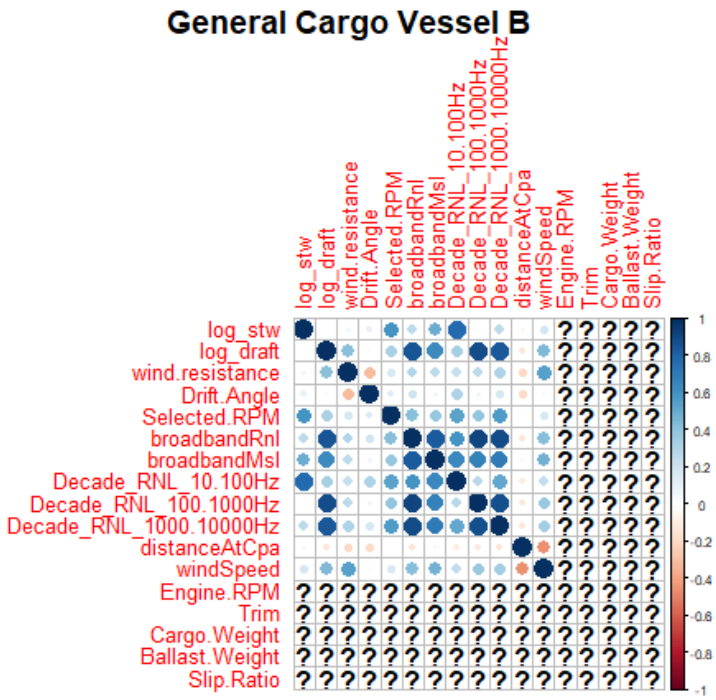

E.2. Decidecade Band Correlations

The plots below show decidecade band correlations of logged operating parameters with RNL. Each line shows the correlation coefficient (*r*) with a single operating parameter versus frequency. Correlation of decidecade band RNL with broadband RNL is also shown for reference. Positive *r*-values indicate that an increase in the parameter was associated with an increase in RNL, whereas a negative *r*-value indicates an increase in the parameter was associated with a decrease in RNL. Dashed horizontal lines indicate standard statistical thresholds for strong ($|r| \geq 0.8$) and moderate ($0.8 > |r| \geq 0.5$) correlations.

E.2.1. Bulk Carrier A

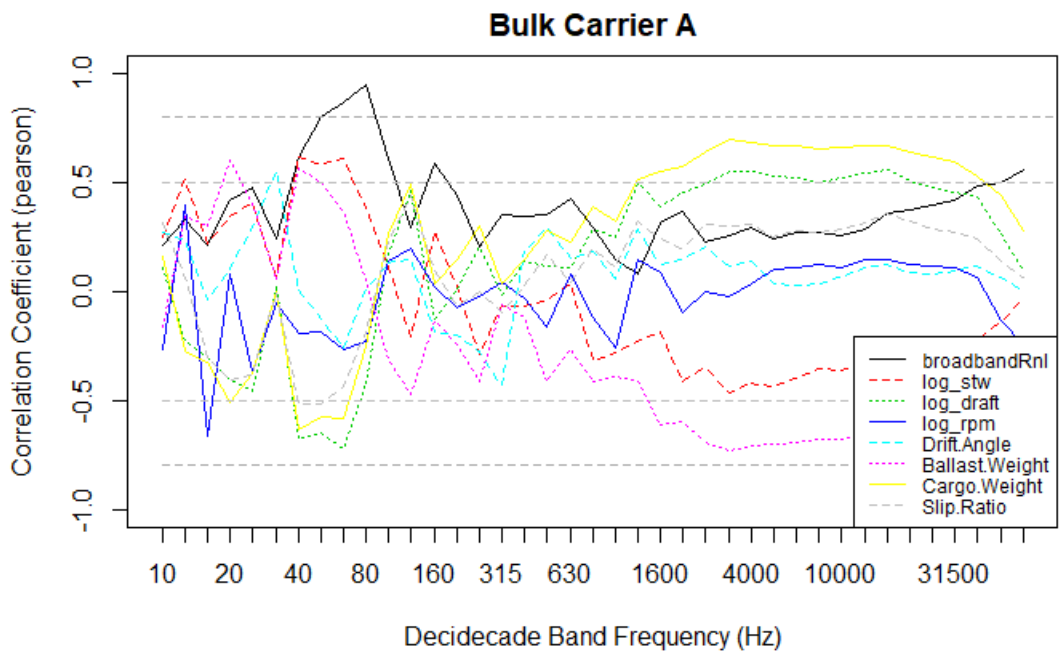

E.2.2. Container Ship A

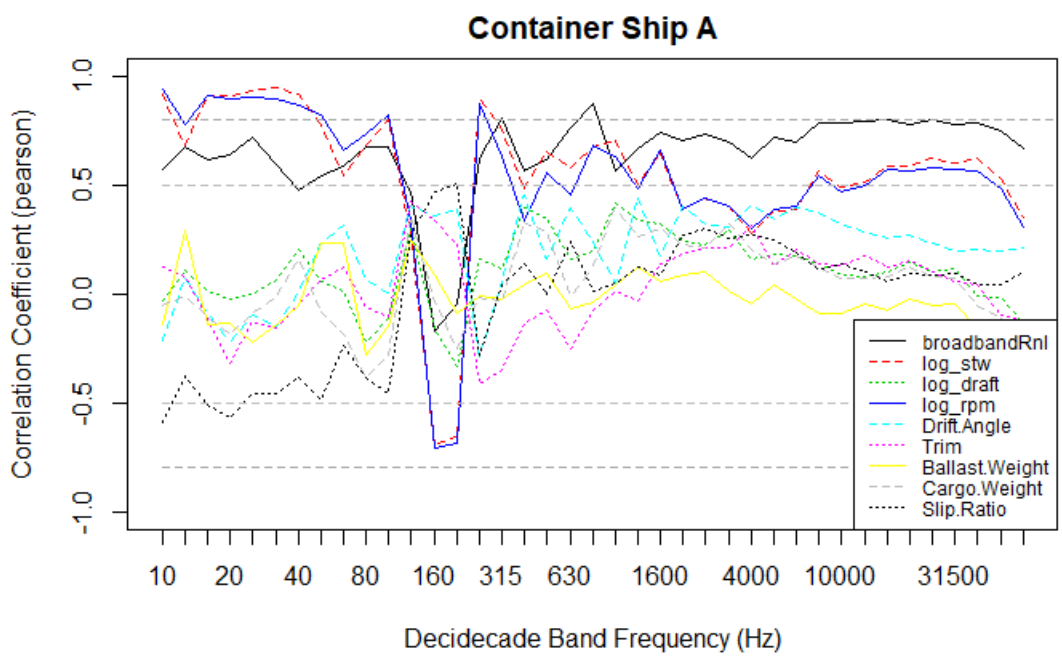

E.2.3. General Cargo Vessel A

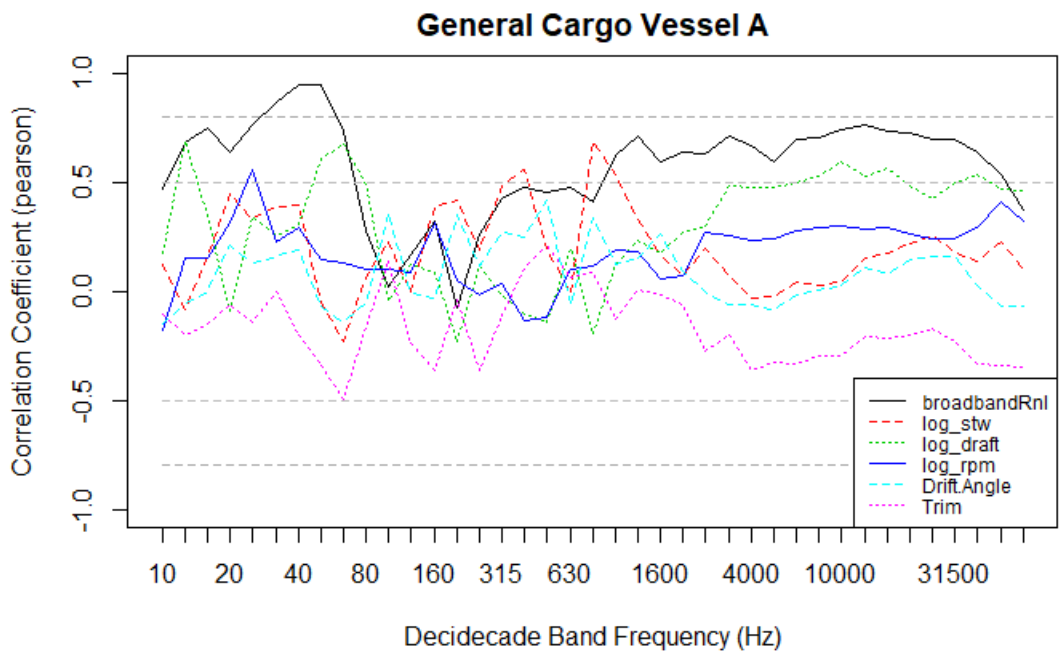

E.2.4. General Cargo Vessel B